THE UNIVERSITY OF QUEENSLAND

AUSTRALIA

Discovery and characterization of Na_V modulatory venom peptides

Joshua Seth Wingerd

B.Sc. of Molecular Biology

A thesis submitted for the degree of Doctor of Philosophy at

The University of Queensland in 2013

Institute for Molecular Biosciences

Abstract

Voltage-gated sodium channels (Na_V) are integral membrane proteins that are responsible for the increase in sodium permeability that initiates and propagates the rising phase of action potentials, carrying electrical signals along nerve fibers and through excitable cells. Na_V channels play a diverse role in neurophysiology and neurotransmission, as well as serving as molecular targets for several groups of neurotoxins that bind to different receptor sites and alter voltage-dependent activation, inactivation and conductance. There are nine Na_V channel isoforms so far discovered, each of which display distinct functional profiles and tissue-specific expression patterns. The modulation of specific isoforms for therapeutic purposes has become an important research objective for the treatment of conductance diseases exhibiting phenotypes of chronic pain, epilepsy, myotonia, seizure, and cardiac arrhythmia. However, because of the high sequence similarity and structural homology between Na_V channel isoforms, many current therapeutics that target Na_V channels – the vast majority of which are small molecules – lack specificity between isoforms, or even other voltage-gated ion channels. The current push for greater selectivity while maintaining a relevant degree of potency has led the focus away from small molecules and towards the discovery and development of peptidic ligands for therapeutic use. Venom derived peptides have proven to be naturally potent and selective bioactive molecules, exhibiting inherent secondary structures that add stability through the formation of disulfide bonds. Organisms such as cone snails and spiders have evolved venom for the purpose of prey capture and defense, therefore many of the components exhibit paralytic qualities and specifically target Na_V channels. Much of the discovery process has focused on screening crude venoms for a particular function and then isolating the molecule responsible for that function using assay guided purification.

The first section of this thesis describes the development of a cell-based, high-throughput functional assay for the detection of Na_V modulating venom peptides in crude venom. This assay was successfully implemented and resulted in the isolation and sequencing of MVIA from *Conus magus*. Initial results and sequence similarity placed MVIA into the δ-conotoxin family, a poorly described class of peptides that inhibits fast inactivation. However, multiple solid-phase synthesis and bacterial recombinant expression methods were unsuccessful in producing enough of the extremely hydrophobic δ-MVIA for further characterization. As no more *C. magus* crude venom was available, this project was left until optimized methods of production for highly hydrophobic peptides could be developed.

An optimized method of bacterial recombinant expression was successful in producing large yields of another venom peptide, β/δ-TRTX-Pre1a, isolated from the spider *Psalmopoeus reduncus*. The same recombinant expression method was also used to produce uniformly labeled $^{13}C/^{15}N$-peptide for determination of a heteronuclear NMR solution structure. Pre1a was revealed to be a sub-micromolar inhibitor of both $Na_V1.2$ and $Na_V1.7$ peak currents, yet demonstrated potent inhibition of fast inactivation of $Na_V1.3$. This dual mode of action on different Na_V isoforms had not yet been reported for any known venom peptide. Further, Pre1a exhibited structural heterogeneity as determined by analysis of rpHPLC and NMR ^{15}N-HSQC, which was traced to the contribution of residues making up the all aromatic, hydrophobic face of the peptide.

The high sequence similarity of Pre1a to previously discovered spider venom peptides allowed comparative functional analysis and the identification of key residues contributing to Na_V isoform selectivity. Mutagenesis focusing on both structural and functional aspects of Pre1a was performed incorporating both alanine and non-alanine substitutions. Through a single mutation a residue critical for the observed conformational heterogeneity was identified. This mutation served as a model for the obtainment of a high-resolution solution structure for comparison with the active Pre1a. Lastly, we identified a single residue on the C-terminus critical for Na_V channel isoform selectivity. Substitution with amino acids exhibiting different properties of charge, polarity, and size could modify selectivity and in the process create a highly selective inhibitor of $Na_V1.2$. This study not only revealed a unique mode of action for a venom peptide, but also demonstrated novelty as a proof-of-concept for the rational design and engineering of venom peptides using available information and non-standard methods of selective mutagenesis.

Declaration by author

This thesis is composed of my original work, and contains no material previously published or written by another person except where due reference has been made in the text. I have clearly stated the contribution by others to jointly-authored works that I have included in my thesis.

I have clearly stated the contribution of others to my thesis as a whole, including statistical assistance, survey design, data analysis, significant technical procedures, professional editorial advice, and any other original research work used or reported in my thesis. The content of my thesis is the result of work I have carried out since the commencement of my research higher degree candidature and does not include a substantial part of work that has been submitted to qualify for the award of any other degree or diploma in any university or other tertiary institution. I have clearly stated which parts of my thesis, if any, have been submitted to qualify for another award.

I acknowledge that an electronic copy of my thesis must be lodged with the University Library and, subject to the General Award Rules of The University of Queensland, immediately made available for research and study in accordance with the *Copyright Act 1968*.

I acknowledge that copyright of all material contained in my thesis resides with the copyright holder(s) of that material. Where appropriate I have obtained copyright permission from the copyright holder to reproduce material in this thesis.

Publications during candidature

Peer-reviewed publications

Vetter, I., Mozar, C.A., Durek, T., **Wingerd, J.S.**, Alewood, P.F., Christie, M.J., Lewis, R.J. Characterisation of Na_V types endogenously expressed in human SH-SY5Y neuroblastoma cells (2012) *Biochemical Pharmacology* 83 (11) , pp. 1562-1571

Muttenthaler, M., Dutertre, S., **Wingerd, J.S.**, Aini, J.W., Walton, H., Alewood, P., Lewis, R. Abundance and diversity of Conus species (Gastropoda: Conidae) at the northern tip of New Ireland province of Papua New Guinea (2012) *The Nautilus* 126 (2), pp.47-56

Book Chapters

Wingerd, J.S., Vetter, I. and Lewis, R.J. (2012) Voltage-Gated Sodium Channels as Therapeutic Targets, in Therapeutic Targets: Modulation, Inhibition, and Activation (eds L. M. Botana and M. Loza), John Wiley & Sons, Inc., Hoboken, NJ, USA. doi: 10.1002/9781118185537.ch3

Posters/Abstracts

Wingerd, J.S., Vetter, I. Rash, L. and Lewis, R. (2011, May 15-20) *Exploring the Na_v Activity of ICK Venom Peptides Using TRTX-Pre1a and δ-MVIA as Models.* Poster at the Fourth Conference on Venoms to Drugs, Heron Island, QLD, Australia.

Wingerd, J.S. (2011, Mar 23) *TRTX Pre1a: A Tale of Two Pharmacologies.* Poster #P2J20-1 at The 11th Southeast Asian Western Pacific Regional Meeting of Pharmacologists, Yokohama, Japan.

Publications included in this thesis

No publications included.

Contributions by others to the thesis

Significant input regarding design, development, and implementation for fluorescent based assays in Chapter II was given by Dr. Irina Vetter, especially regarding the development of FLIPR methods in section 2.8 and 2.9 and the primer design for the cell line characterization for section 2.1.

The initial isolation, sequencing, and some activity on $Na_V1.3$ and $Na_V1.7$ for TRTX-Pre1a were completed by Dr. Lachlan Rash. Dr. Rash also contributed significantly to the experimental design of Chapters III and IV, training in the use of TEVC oocyte electrophysiology, and interpretation of the e-phys results. Dr. Rash was also instrumental in the critical review and revision of Chapters III, IV and V of this thesis.

NMR instrumentation was handled and experiments were run by Dr. Mehdi Mobli. Significant input regarding interpretation of the NMR results, as well as critical revision of relevant sections of Chapters III and IV of the thesis, was also done by Dr. Mobli.

Patient training in the use of Sparky NMR analysis software was provided by Dr. Yanni Chin. Dr. Chin also gave her support regarding data interpretation, running TALOS statistics, and the development of the ^{15}N-HSQC overlay figures, Figure 41, Figure 42, and Figure 64.

The pLIC shuttle vector was originally designed by Dr. Natalie Saez.

Statement of parts of the thesis submitted to qualify for the award of another degree

None

Acknowledgements

This thesis is a compilation of years of work that could not have been possible without the personal and professional support of family, friends, and colleagues. First and foremost I would like to thank my parents, Mala and Bruce, for their constant support in all realms and undying positive reinforcement. Although there have been no shortage of hard times, their love and encouragement has helped me to succeed through it all.

I would also like to thank my supervisor, Prof. Richard Lewis for his continual support during the entirety of my PhD studies at the Institute for Molecular Bioscience. Not only has Richard allowed me to study in an amazing lab, but he has opened up many opportunities outside the lab and in the field. I would also like to thank my co-supervisor Dr. Irina Vetter for her wisdom, advice and friendship from the onset of this degree.

Many thanks go to Dr. Lachlan Rash, who gave his support as a co-supervisor and a mentor for the final half of this degree. Lachlan has been an excellent teacher and motivator, sharing his knowledge in the lab, injecting his passion for science, and sharing his many excellent ideas for the progression of the Pre1a project and beyond. Not only has Lachlan been professionally encouraging, but he has been a great friend. I am in debt to his support. Thanks go to Dr. Mehdi Mobli for his patience and guidance teaching the fundamentals of a difficult but extremely interesting subject, NMR. You've not only made yourself available for professional help, but you have also been a great friend. Here's hoping for more titanium in the future. And to Dr. Yanni Chin, thank you for all your help and patient support with structural elucidation.

Many thanks to all my friends and colleagues along the way, here in Brisbane and back in San Diego, and all the memorable times we shared on islands, boats, and beaches. A big final thank you to the IMB's biggest asset Amanda Carozzi, who went above and beyond what was necessary to ensure success.

Dedicated to my brother Ryan (1984-2012). You are deeply missed.

Keywords

Spider and cone snail venom toxins, sodium channels (Na_V), inhibitory cysteine knot, recombinant expression, structure activity relationships, assay development, two electrode voltage clamp

Australian and New Zealand Standard Research Classifications (ANZSRC)

ANZSRC code: 060112, Structural Biology (incl. Macromolecular Modeling), 30%

ANZSRC code: 111501, Basic Pharmacology, 50%

ANZSRC code: 110106, Medical Biochemistry: Proteins and Peptides (incl. Medical Proteomics), 20%

Fields of Research (FoR) Classification

FoR code: 0601, Biochemistry and Cell Biology, 45%

FoR code: 1115, Pharmacology and Pharmaceutical Sciences, 45%

FoR code: 1101, Medical Biochemistry and Metabolomics, 10%

Table of Contents

List of Tables

List of Figures

List of Abbreviations

5-HT$_3$	5-hydroxytryptamine
Amp^R	Ampicillin resistant
ANOVA	Analysis of variance
ATP	Adenosine triphosphate
BTX	Batrachotoxin
CAM	Cell adhesion molecule
cAMP	Cyclic adenosine monophosphate
Ca$_V$	Voltage-gated calcium channel
CIP	Congenital insensitivity to pain
CNG	Cyclic nucleotide-gated [ion channel]
CNS	Central nervous system
DDH	Disulfide-directed β-hairpin
DMEM	Dulbecco's modified Eagle medium
EDTA	Ethylenediaminetetraacetic acid
hERG	human Ether-à-go-go-related gene
ERK	Extracellular signal-regulated kinases
FBS	Foetal bovine serum
FLIPR	Fluorometric imaging plate reader
GDNF	Glial cell-derived neurotrophic factor
HSQC	Heteronuclear single quantum correlation
HTS	High-throughput screening
IEM	Inherited erythromelalgia
Ig	Immunoglobulin
IMAC	Immobilized metal-ion affinity chromatography
IPTG	Isopropyl β-D-1-thiogalactopyranoside
I_{Na}	Inward sodium ion current
K$_V$	Voltage-gated potassium channel
LC/MS	Liquid chromatography/mass spectroscopy
MALDI-TOF	Matrix-assisted laser desorption/ionization–time-of-flight
MTT	3-(4,5-dimethylthiazol-2-yl)-2,5-diphenyl tetrazolium bromide

NADPH	Nicotinamide adenine dinucleotide phosphate
NGF	Neuron (Nerve) growth factor
Na_V	Voltage-gated sodium channel
NMR	Nuclear magnetic resonance
O/V	Ouabain/veratridine
PBS	Phosphate buffered saline
PbTX	Brevetoxin
PCR	Polymerase chain reaction
P-CTX	Pacific ciguatoxin
PEG	Polyethylene glycol
PEPD	Paroxysmal extreme pain disorder
PNS	Peripheral nervous system
PSS	Physiologic salt solution
PTM	Post-translational modificaiton
RMSD	Root-mean-square deviation
rpHPLC	Reverse-phase high-performance liquid chromatography
SAR	Structure/Activity relationship
SEM	Standard error of the mean
SPPS	Solid-phase peptide synthesis
STX	Saxitoxin
TEV	Tobacco etch virus
TRP	Transient receptor potential [ion channel]
TTX(r/s)	Tetrodotoxin (resistant/sensitive)

Chapter I: Introduction

The use of plant and animal remedies to knowingly cure and treat disease predates written human history[1]. Although herbal remedies are arguably the most widely known examples of natural medicine throughout ancient history, treatments derived from animal venoms have been in use for thousands of years[2]. Venom is a complex mixture of molecular components that is administered via bite or sting for the purpose of prey capture and defense. Low molecular mass peptides make up the primary bioactive component of venoms. Millions of years of evolutionary selection have honed these peptides to maximize effectiveness for prey capture and defense[3].

Many venom peptides work together as a *cabal* to immobilize prey through selectively targeting ion channels, either by inhibiting conductance or altering gating kinetics[4]. It is this action that has led researchers to explore individual venom components as potential therapeutic leads for the discovery of new molecules to treat neurological disorders, such as chronic pain. Two organisms – the marine gastropods *Conus spp.* and spiders – have served as a rich source for the discovery of highly potent, selective, neurologically bioactive peptides, and are the focus of this thesis.

This thesis outlines structure-function relationships of peptides isolated from two venomous organisms, the piscivorous *Conus magus* and a single species of old-world spider in the family Theraphosidae. The peptides isolated and characterized within represent molecules that – although from different organisms – share a similar structural motif and target mammalian voltage-gated sodium channels, which are ion channels associated with nerve signal transmission.

1 Voltage-gated sodium channels

Voltage-gated sodium (Na_V) channels are integral membrane proteins which form gated pores that conduct Na^+ ions passively across the cell membrane, via an electrochemical gradient[5]. This electrochemical gradient is maintained through the active transport by Na^+/K^+-ATPases as well as various potassium channels, imparting a negative resting potential – or resting state – of around -70 to -90 mV for most neurons[6]. Na_V are activated through cell membrane depolarization events – which

is a positive shift in the membrane potential past threshold – triggered by a variety of external stimuli, typically involving ligand-gated, mechano- or chemo-receptors[6].

Na_V channel depolarization is responsible for the initiation and propagation of the rising phase (or positive shift) of action potentials, which carry electro-chemical signals through nerve fibers and excitable cells (Figure 1). However, Na_V channels are found on the surface of a wide range of cell types, both excitable and non-excitable[7]. Because of their ubiquitous role in driving signal conduction throughout the entire nervous system, Na_V channels make excellent therapeutic targets for a variety of neuropathic disorders.

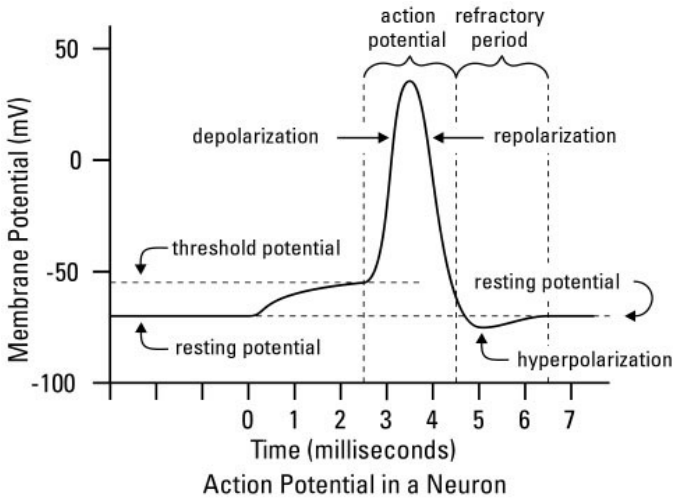

Figure 1: An "ideal" action potential.

Na_V channels contribute to the "upward" depolarization – or a shift to more positive potential – of the cell membrane after a threshold is reached. Potassium channels are activated in response to depolarization and help to "reset" the resting membrane potential through repolarization.

1.1 The mammalian Na_V family

Mammalian Na_V channels are part of the superfamily of voltage-gated ion channels, which is the largest subgroup of ion channels[6]. Other members of this superfamily include voltage-gated calcium channels (Ca_V) and voltage-gated potassium channels (K_V). Several other ion channel families share structural and functional homology to these primary members of the voltage-gated ion channels, however they lack the strong cation selectivity of their cousins. The cyclic nucleotide-gated (CNG) ion channels and some members of the transient receptor potential (TRP) family ion channels are weakly voltage dependent and retain voltage sensor domains with a few positive charges[8, 9]. The CNG channels have been showed to be involved with vertebrate phototransduction, olfaction[8], and smooth muscle contraction[10]. The TRP family has diverse functions, including invertebrate phototransduction[11] as well as vertebrate thermal-, mechano- and somatosensation[9].

Members of the voltage-gated ion channel superfamily share a tertiary structural homology composed of four homologous domains (DI-DIV). Each domain is composed of six transmembrane segments (S1-S6)[6, 12], which fold into a voltage sensing region (S1-S4) and a pore forming region (S5-S6)[13]. The quaternary structure of these proteins is typically functionally expressed in association with a variety of auxiliary subunits that modify function and expression, such as the β-subunits in association with Na_V channels.

1.2 Evolution of mammalian Na_V channels

Mammalian Na_V channels have evolutionary roots dating back to the earliest metazoans, with ancestral Na_V genes detected in eukaryotic organisms without a nervous system, including a placazoan and a single-celled choanoflagellate[6, 14]. Human voltage-gated channels are believed to have derived from whole-gene duplication events that occurred early in the vertebrate lineage. The 2R hypothesis suggests two early whole genome duplication events in vertebrates led to four ancestral Na_V genes in teleosts, which further evolved into the current set of mammalian channels[15-17]. Using electrophysiological recording, biochemical purification, and molecular cloning techniques, nine mammalian Na_V α-subunits – officially designated $Na_V1.1$-1.9 – have been identified and functionally characterized (Table 1). Further reference to Na_V channels will be in regards to mammalian isoforms, unless otherwise specified. The gene sequence homology between the nine Na_V α-subunits – encoded by the *SCNA* genes – are all greater than 50% in the transmembrane and extracellular regions, enough that all nine isoforms are classed in the same Na_V family[18]. By comparison, members of the Ca_V and K_V channels can be grouped into distinct subfamilies with greater than 50% gene variation between each other, but a much higher relative sequence similarity within the subfamilies[19].

Differentiating between mammalian Na_V isoforms has been aided with the discovery of subtype selective neurotoxins such as tetrodotoxin (TTX), a key natural product that helped early researchers divide Na_V channels into either TTX-sensitive (TTXs) or TTX-resistant (TTXr) classes[20] (Table 1). Studies of Na_V isoform expression have shown unique patterns of temporal and spatial expression throughout different tissues, with some localized to specific regions such as cardiac ($Na_V1.5$) or skeletal muscle ($Na_V1.4$) tissue. Many of the neuronal isoforms exhibit differential regulation after mechanical[21] or inflammatory[22] stress, as well as preferential expression to pre-natal versus post-

natal tissue[23]. Further, splice variants of multiple isoforms have recently been discovered, expanding the potential for therapeutic targeting[24].

Table 1: Mammalian Na_V channel family.

Red indicates Na_V channels contributing to pain transmission[18].

Voltage-gated sodium channel family				
Channel Name	Gene	TTX sensitivity	Preferential Expression	Attributes
$Na_V1.1$	*SCN1A*	TTXs (10 nM)	CNS, cardiac	KO perinatal lethal
$Na_V1.2$	*SCN2A*	TTXs (10 nM)	CNS, peripheral	Defects implicated w/ seizure and epilepsy
$Na_V1.3$	*SCN3A*	TTXs (1.8-4 nM)	Embryonic CNS DRG, sympathetic neurons Cardiac myocyte	Rapid repriming Amplifies depolarizing inputs ↑regulation after injury LoF attenuates pain
$Na_V1.4$	*SCN4A*	TTXs (5 nM)	Skeletal muscle	Skeletal muscle function
$Na_V1.5$	*SCN5A*	TTXr (1.8 μM)	Cardiac myocyte, CNS	Cardiac pacemaker
$Na_V1.6$	*SCN8A*	TTXs (1 nM)	Nodes of Ranvier DRG, dendrites Synapses, glia	Ubiquitous. Mutations lead to muscular, neuro, and nocicepti dysfunction
$Na_V1.7$	*SCN9A*	TTXs (4-25 nM)	DRG, sympathetic neurons, dorsal horn Sciatic nerve Schwann cells	Slow repriming, amplifies GoF results in IEM, PEPD LoF results in CIPD ↑reg postinflammation
$Na_V1.8$	*SCN10A*	TTXr (40-60 μM)	DRG	Rapid repriming, supports repetitive firing ↑reg after injury, inflammation
$Na_V1.9$	*SCN11A*	TTXr (40 μM)	Small diameter DRG	Slow activation, Ultra-slow inactivation, amplifies Hyperpolarized voltage-dependance of activation

Although there has been some variation in the determination of Na_V phylogeny in mammals, the most recent research supports a general consensus in agreement with the 2R hypothesis[25]. The entire Na_V channel family is thought to be a product of pre-mammalian whole genome duplication events, with recent evidence suggesting evolution predating the development of the nervous system (Figure 2)[26, 27]. This relatively high homology between members of the ion channel superfamily contributes to making the search for selective modulators quite difficult.

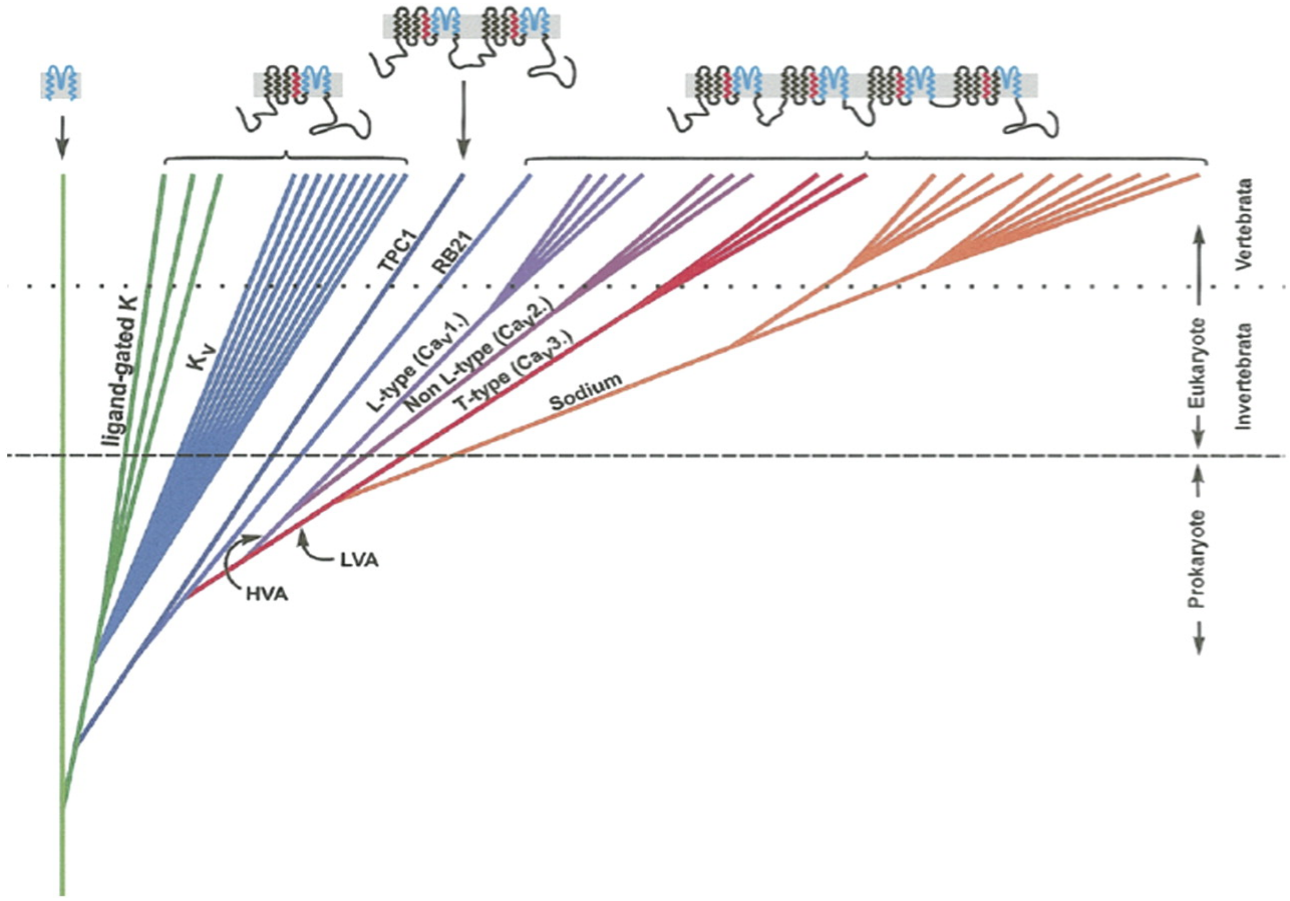

Figure 2: Evolutionary relationships among key members of the ion channel superfamily.
The top of the figure shows the structures of the channels. Moving from left to right: a linear leak K^+ channel that is composed of two membrane-spanning helices and a pore (blue); a 6 transmembrane (TM) channel with a single voltage sensor (red); and 4 domain x 6TM channels with four voltage sensors. There is uncertainty about the origin of the 4x6TM family, which more likely evolved in eukaryotes than prokaryotes, as indicated in this figure. Figure used without permission from Zakon H.H. PNAS 2012[27]

The latest phylogenetic tree for the human Nav family used a method of maximum parsimony to compared aligned sequences for relatedness by measuring the number of nucleotide changes required for the change in codon at each position[19]. By this method $Na_V1.1$, $Na_V1.2$, $Na_V1.3$, and $Na_V1.7$ have been determined to be the most genetically related, with all four encoding genes occurring on human chromosome 2q23-24. All four channels are also strongly TTX-sensitive and widely expressed in neurons[15]. $Na_V1.5$, $Na_V1.8$, and $Na_V1.9$ also have close phylogenic homology, with encoding genes found on human chromosome 3p21-24. These sodium channels are TTXr to varying degrees due to changes in amino acid sequence at a single position on the pore forming region[28]. $Na_V1.4$ and $Na_V1.6$ are the most phylogenetically distinct TTXs subtypes, occurring on human chromosomes 17q23-25 and 12q13, respectively.

1.3 Na_V channel structure

The voltage sensitivity and Na^+ ion selectivity of the Na_V α-subunit allows these membrane proteins to play an essential role in initiation and propagation of action potentials in neurons and other excitable cells[6]. Na_V channels are defined by their activation through membrane depolarization events, allowing Na^+ ions to flow passively along a gradient[6]. However, channel state and kinetics can be affected by various ligands – including toxins – as well as membrane potential, which will be discussed later. Understanding the structure of the Na_V channel and how ligands can interact with different regions is fundamental to developing better regulatory therapeutics.

1.3.1 The Na_V α-subunit

The α-subunit of the Na_v channel is arranged from four homologous domains (DI-DIV), each containing six highly conserved, hydrophobic, α-helical transmembrane segments (S1-S6) that form a protein approximately 260 kDa in size[29-32]. The transmembrane regions are connected by intra- and extracellular loops (Figure 3). The outer vestibule and ion selectivity filter of the Na_V channel is formed by an extracellular "P-loop" on each domain that re-enters the membrane between S5 and S6, making up the pore forming region[33]. S4 is traditionally referenced at the voltage sensor, although the entire S1-S4 region has been referred to as the voltage sensor domain[34]. Co-expression with a β-subunit is usually required for the α-subunit to exhibit the endogenous kinetics and voltage-dependence

of native Na_V channels, as well as regulating channel expression[35]. However, the α-subunit is fully functional as a voltage-mediated ion pore on its own.

The predicted structure of the outer vestibule and selectivity filter were both discerned using the guanidinium toxins TTX and saxitoxin (STX). These small molecule toxins have similar structural properties, overlapping binding sites, and are highly selective for Na_V channels. A number of interaction sites between the toxins and the Na_V channel were determined through point mutation studies of the channel[36-39], then spatially arranged by Lipkind and Fozzard to produce a working model of the extracellular pore region[33]. An unexpected outcome of the model was the visualization of a narrowing in the pore caused by four conserved caboxylate amino acids – DEKA – that form an inner ring necessary for conveying Na^+ ion selectivity to the P-loop. This precise region was initially proposed by Heinemann et al[40] to be a candidate for the selectivity filter after mutations to the DEKA amino acids were observed to cause a pronounced alteration of ion selectivity. Later studies demonstrated the importance of an additional outer ring composed of the carboxylate amino acids EE(M/D)D[39, 41, 42].

These studies succeeded in linking critical toxin binding sites along the outer vestibule to residues controlling ion permeation that help define the first pharmacologically relevant site on the Na_V channel, "Site 1". An updated structural model for the Na_V channel TTX-binding region within the outer vestibule has since been published, taking into account an additional 15 years of work and using the crystal structure of the bacterial KcsA channel as a template[43]. A structural model for the anticonvulsant binding site within the inner pore has also been published[44]. While these models have limitations as they are based on relatively low homology templates and a rigid conformation for ligand interactions, they remain useful for visualizing Na_V channel residues important for drug interactions.

Recently, a groundbreaking accomplishment was made utilizing a bacterial Na_V channel from *Arcobacter butzleri* (Na_VAb) to elucidate the first full crystal structure of a Na_V channel[46]. This was quickly followed up with structures in potentially two inactivated states[45]. These detailed snapshots into the conformational changes of the Na_V structure have great potential for understanding the complexities of how ligands bind and interact with the Na_V channel, which is critical for the development of selective therapeutics.

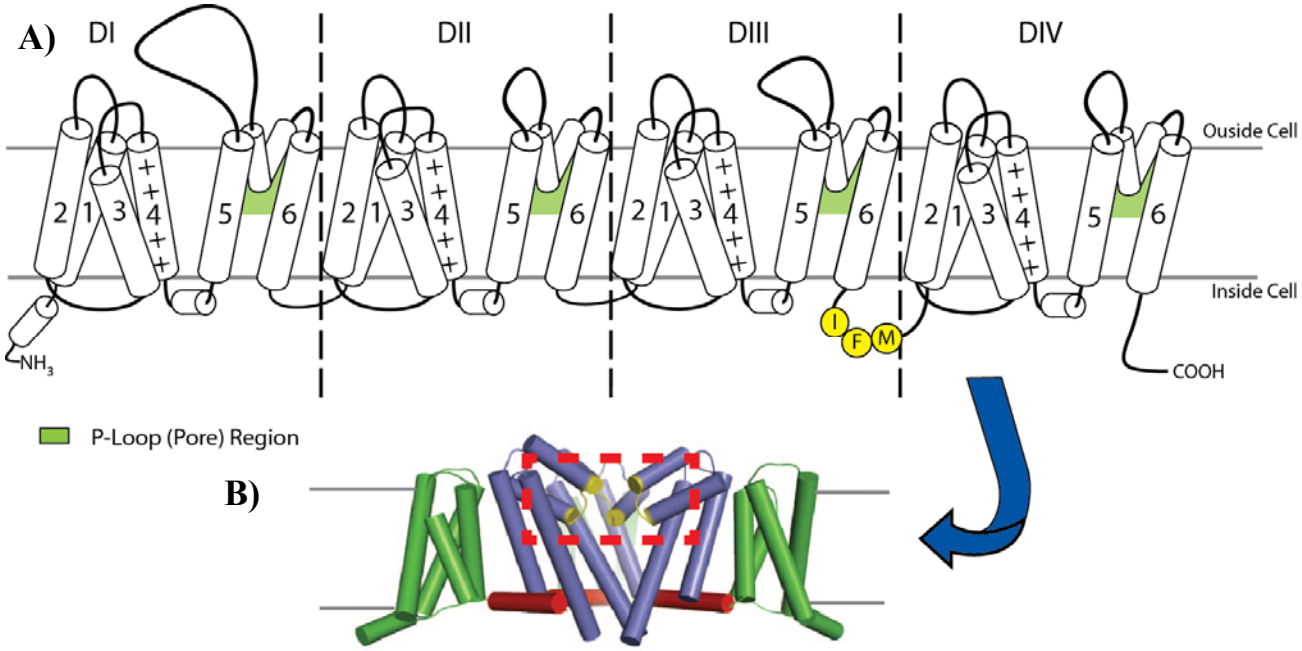

Figure 3: Na_V channel structure.

A) Flat cartoon of general Na_V structure based off crystal structure arrangement. Individual segments are numbered (1-6). Domains are labeled (I-IV). The S4 voltage sensor is labeled with (+) and the inactivation gate is labeled with IFM. The pore forming region is highlighted in green. B) Folded conformation of Na_V channel based off crystal structure of Na_VAb[45]. Green = voltage sensing region. Purple = pore forming region, boxed region = selectivity filter. Red = linker regions connecting the activation gate.

1.3.2 Na_V physiological states

Electrophysiological experiments conducted over the past four decades have demonstrated three primary physiological states directly related to observed Na^+ permeability, which can be further broken down mathematically into eight kinetic states[6]. The three primary states include: activated (open state), inactivated (closed state), and resting (primed closed state). These physiological states are dictated by conformational changes occurring within the Na_V α-subunit. It wasn't until 2005 when the first structural template of the mammalian $K_V1.2$ (Shaker) channel was elucidated in an "activated-open state" by X-ray crystallography[47]. This allowed the development of molecular dynamics simulations of the lipid membrane embedded $K_V1.2$ receptor to characterize structural details[48-50], which later led to a series of more defined models detailing the "resting-closed state) as well as

transitional states [51-53]. This data culminated in a mechanistic model of voltage-dependant gating for the entire voltage gated cation channel superfamily[54].

In 2011, the elucidation of a bacterial Na_V α-subunit X-ray crystal structure from *Arcobacter butzleri*, Na_VAb, was resolved at 2.7 Å[46]. This structure featured a closed PD and the four VSDs seemingly activated. The latter was interpreted as representative of the pre-open state of the channel or, in other words, a metastable (intermediate) structure along the pathway connecting the resting-closed state to the activated-open state. Consistently, recent MD simulations of the channel embedded in a lipid membrane have shown structural stability on timescales of ~100 ns[55]. Importantly, the Na_VAb structure provides a high-resolution template for enhancing our knowledge on Na^+ and related Ca^{2+} channels, for which much less is known. However, there remains a pressing need to relate the reported Na_VAb X-ray structure to specific functional states of the channel. Given the significant degree of structural similarity shared by members of the VGCC family, more extensive studies on K_V channels are a resource for providing insight into this issue.

The details of how the Na_V channel conforms to each state is critical to understanding how ligands interact, as the different physiological states are able to preferentially bind small molecule and peptide ligands in what is known as "state-dependence". The information gathered through molecular dynamics simulations and, more importantly, X-ray crystal structures, is instrumental in forming a unified model of voltage-dependant gating through a complete cycle. What is known will be summarize

When in the resting state the Na_V channel is closed and non-conducting, but primed for activation. Activation of the Na_V channel occurs when membrane depolarization causes a conformation change of the voltage sensor region - specifically with the S4 helices - opening the outer pore to allow Na^+ ions to flow down an electrical gradient. After activation of the Na_V channel, an inward flow of Na^+ ions (I_{Na}) occurs within milliseconds, immediately followed by decay in I_{Na} during the depolarization phase. This decay is due to inactivation of the channel by an intracellular gating motif and is a closed conformation state that is distinct from the resting state. The physiological role of the inactivated state is to stop ion conductance during prolonged depolarization, allowing the channel to reset to a fully closed (resting) conformational state. Na_V channel inactivation is typically described as either fast or slow, with slow inactivation encompassing both ultraslow and intermediate modes[56].

The primary role for fast inactivation is to aid in repolarization of the cell after firing of an action potential. In mammalian Na_V channels, fast inactivation is well described and has been attributed to a highly conserved intracellular linker region between DIII-DIV of the α-subunit (Figure 3). Deletion of the linker[57] followed by targeted inactivation of the region using antibodies[58] provided the first experimental results pinpointing this region as the inactivation gate. Further point mutations of the DIII-DIV linker identified a cluster of three highly conserved hydrophobic amino acids – labeled the IFM motif – that is critical for inactivation[59]. To confirm the role of the IFM motif in inactivation, introduction of the peptide KIFMK via intracellular expression was shown to recover the function of inactivation on channels with deleted IFM motifs through open-state dependent block[60]. The first hi-resolution NMR solution structure of the inactivation gate was published a year later[61], revealing an α-helical core with a flexible hinge-like N-terminal turn, which includes the IFM motif. This linker region was shown to be stabilized in the inactivated state through interactions with the C-terminal section of the Na_V channel, which will be discussed in more detail below[62]. The IFM motif demonstrates precedence for the potential of intracellular Na_V pore block.

Slow inactivation has been shown to be a distinct process from fast inactivation, differing spatially, structurally, and pharmacologically - although the process is still not completely understood[63, 64]. Slow inactivation is a critical component of recovery from depolarization, controlling membrane excitability, firing properties, and spike frequency[65]. Abnormalities in slow inactivation have been linked to the neuromuscular disorders hyperkalemic periodic paralysis and myotonia[66], epilepsy[67], as well as several cardiac arrhythmia disorders such as Brugada syndrome[68], atrioventricular conduction block[69], and long-QT syndrome[70]. These associations underscore the physiological importance of this process. Slow inactivation is common to all mammalian Na_V channels, although not as pronounced in the cardiac $Na_V1.5$ isoform compared to nerve and skeletal muscle isoforms[71].

This functional difference between $Na_V1.5$ and skeletal $Na_V1.4$ was exploited in attempts to isolate the structural components of slow inactivation[72]. A comprehensive study utilizing chimeras of $hNa_V1.4$ and $hNa_V1.5$, as well as differential expression of an associated β1-subunit, resulted in two important observations involving the regulation of slow inactivation: (i) that P-loops are structural determinants of slow inactivation and (ii) that the β1-subunit modulates this process in $hNa_V1.4$ but not $hNa_V1.5$ through a possible interaction with the P-loops[73]. P-loop association was further confirmed with mutational and modeling studies directed at the outer selectivity ring EEDD motif, which was shown to

play a crucial role in modulating slow inactivation[74]. This information was pieced together using a model of the TTX-bound channel to give the most comprehensive ionic model of slow inactivation to date, and in the process elucidated the binding of many state-dependant drugs that modulate slow inactivation[75]. This model suggested that slow inactivation involves disordering of the outer pore region rather than direct plugging, which may explain the different kinetic states of slow inactivation. However, there is much that remains unanswered, including the suggested involvement of the S4 voltage sensor. The recent availability of a Na_V crystal structure will help to address many of these questions.

1.3.3 Voltage sensor

The mechanism of voltage dependent gating is directly linked to changes in the membrane potential of the cell. A candidate for the voltage sensor, the S4 transmembrane helix, had already been suggested at the time of the first Na_V channel cloning due its location within the membrane electric field and strong inherent positively charged residues[76]. This positive charge is due a polybasic region composed of arginine and lysine at every third position of the S4 helix. The S4 regions of each domain have subsequently been shown to be critical for voltage dependence through site-directed mutagenesis studies that targeted these key charged residues[57]. However, the voltage sensors in DI-DIII have been shown to be critical for channel gating, while the DIV voltage sensor is more closely associated with fast inactivation[77, 78]. This association has been demonstrated further with the use of gating modifier toxins, which interact directly with the voltage sensor region of S1-S4[79, 80].

The classical voltage sensor model suggests that in response to a change in the membrane's electric field due to an influx of positive charge, the voltage sensors will undergo a conformational change, moving towards the extracellular space and opening the pore[81, 82]. Continuing research on the voltage sensor is revealing that voltage dependant gating is a much more intricate process, involving ion pair interactions between multiple segments after physical movement of the voltage sensor during depolarization of the membrane[83]. These interactions include a process described as "disulfide locking" of the S4 after activation, which is shown to contribute to slow inactivation[84, 85] and demonstrates that activation and inactivation are not completely independent processes[86].

1.4 β-subunits

The four known mammalian Na_V channel β-subunits, β1-β4, are between 33-36 kDa in size and encoded by the genes *SCN1B-SCN4B*[87, 88]. *SCN1B* has been shown to produce species-specific splice variants, with humans expressing the variant β1B[89]. All four β-subunits share a similar structure, composed of an N-terminal extracellular immunoglobulin (Ig) domain, an alpha-helical transmembrane segment, and a short intracellular C-terminal region. All of the β-subunits belong to the Ig superfamily of cell adhesion molecules (CAMs)[90]. The Na_V β-subunits are known to co-localize with Na_V α-subunits, with β1 and β3 forming non-covalent bonds while β2 and β4 are covalently linked through disulfide bonding, although the residues responsible have not yet been identified[30, 91-93]. These interactions with Na_V α-subunits have been shown to be multifunctional, affecting not only receptor excitability, but also cell adhesion, neuronal migration[94], neurite outgrowth[95], transcriptional regulation, and metastatic activity in cancer[96]. Through their interactions with Na_V α-subunits, β-subunits canact as regulators of both temporal and spatial expression of the α-subunits through the formation of macromolecular complexes [89].

Because of their association with and regulation of Na_V α-subunits, β-subunits have the potential to make useful therapeutic targets. However, their multifunctional role as CAMs may be a complication as well as a benefit. Using domains of the subunits to elicit a physiologic effect has already been demonstrated *in vitro*. For example, the Ig domain of β1 can promote neurite outgrowth on its own[95], which opens up the potential for designing peptide drugs based off of active regions of these subunits. Monitoring mutations of β-subunits can be a useful diagnostic tool to help identify the most appropriate treatments for variety of ailments such as cardiac arrhythmias[97], multiple forms of epilepsy[98, 99], and potentially even some cancers. Manipulating the expression or interaction with α-subunits has the potential to lead to multiple downstream signaling effects *in vivo* and has been shown to play an important role in affecting channel kinetics *in vitro* [90, 100]. However, the *in vivo* spatio-temporal relationships between β-subunits and associated α-subunits are yet to be fully understood.

2. Therapeutic relevance of Na_V channels: Role in pain pathophysiology

Na_V channels play a diverse physiological role and function in many aspects of neurotransmission, such as nociception, as well as participating in the modulation of various cellular processes. Deleterious genetic defects can occur in domains that affect expression or function, such as the voltage sensor, N- and C-terminal domains, or loop regions that act to bind regulatory proteins. Amino acid substitutions, deletions, or additions also occur in regions of the channel responsible for voltage sensing, inactivation and ion selectivity, resulting in a wide array of conductance diseases, some of which will be discussed in detail. Na_V isoforms are each expressed selectively in multiple tissues and cell types throughout the body, including both excitable and non-excitable cells, immune cells, myocytes, and nerve tissue. Therefore, defects among members of this family of voltage conducting channels can be attributed to numerous disease states involving electrical conductance throughout the body, including pain and inflammation pathways[101], neurodegeneration[102], cardiology[103], neurology[104], and even cancer[105]. This ability of Na_V channels to contribute to a wide range of physiologic roles supports the advance of greater isoform selective targeting for therapeutic development, which has been lacking to date. This thesis primarily focuses on targeting the TTXs $Na_V1.3$ and $Na_V1.7$ channels, which are known to be involved in pain transmission and nociception. However, since selectivity is of the utmost importance for research and therapeutic purposes, all available Na_V isoforms will be screened for activity. Of these, a few key selections will be discussed for their therapeutic relevance.

2.1 Pain and inflammation

Primary afferent nociceptors of the peripheral nervous system are responsible for detecting high threshold environmental input from thermal, mechanical, or chemical sources, and converting this stimulus into electrochemical signals [106]. These peripheral nerves can be divided based on morphology and function into three classes. Large diameter myelinated Aα/β-fibers have a low threshold for activation and mainly conduct information about innocuous touch. Both the fast conducting, lightly myelinated, medium diameter Aδ-fibers and the small, slow conducting, unmyelinated C-fibers contribute to nociception from noxious stimuli [107]. Because of their different conductance, it is thought that Aδ-fibers mediate the first rapid, acute response while C-fibers contribute to the second delayed, throbbing pain.

At the transition between the peripheral and the central spinal nervous system lie bundles of afferent nerve cell bodies (soma) called dorsal root ganglion (DRG). DRGs are located along the vertebral column along the spine just outside the CNS, where the afferent dendritic fibers interface with the soma and transition into axon. These ganglia are responsible for transmitting afferent signal from external thermo-, mechano-, or chemo-sensory input from the periphery to the spinal cord and on to the brain for processing. The channels and receptors responsible for transmission of peripheral nociception are expressed in DRGs, including an array of Na_V channels that provide the inward current necessary for formation and propagation of action potentials[108]. Because of their function and composition, DRG neurons have provided researchers with a native cell type to identify the receptors involved in pain transmission at the periphery, as well as the mechanisms for neurite outgrowth.

Early electrophysiology studies have demonstrated that after neuronal injury, DRG neurons become hyperexcitable, giving rise to the spontaneous action potentials and bursting that contribute to neuropathic chronic pain [109-111]. There is substantial evidence linking this hyperexcitability to a differential expression of a few key Na_V isoforms [112]. In addition, an array of clinical and experimental observations using Na_V channel inhibitors has demonstrated a link between Na_V hyperexcitability and the propagation of neuropathic pain [113-115]. The contribution of two TTXs Na_V channels to neuropathic pain will be discussed.

2.1.1 $Na_V1.3$

$Na_V1.3$, encoded by the *SCN2A* gene, is the most questionable in relation to its contribution to neuropathic pain. $Na_V1.3$ mediates TTXs, fast-activating and fast-inactivating Na^+ current. It is developmentally regulated, with lower expression in adult compared to embryonic rodents[116]. In addition, studies using animal models for physical pain from injury – such as sciatic nerve axotomy or spinal nerve ligation – have shown marked increases in expression of $Na_V1.3$ around injured nerve regions[117-120]. This isoform seems to be the only Na_V consistently upregulated after nerve injury based on mRNA analysis, RT-PCR and electrophysiology experiments, which determine both functional and transcriptional expression[117, 120-122].

This data points to $Na_V1.3$ being an important contributor to the TTXs component apparent in the spontaneous, rapid repriming current seen in inflammatory and neuropathic pain. However, more

recent data has contradicted this hypothesis. Antisense oligonucleotides to knockdown expression of $Na_V1.3$ after peripheral nerve injury reduced $Na_V1.3$ expression by 50% in DRG neurons[123]. Yet this reduction failed to yield a therapeutic benefit by attenuating mechanical and thermal allodynia. In addition, the upregulation of $Na_V1.3$ was shown to be non-specific to injured DRG. However, this study was contrary to previous results, again using oligonucleotides targeting $Na_V1.3$, which showed that knockdown of mRNA and protein did attenuate hyperexcitability and allodynia[21]. In a pivotal study, normal levels of neuropathic pain were recorded in two conditional $Na_V1.3$ knockout mice strains and hyperexcitability seen in neuropathic pain states was unaffected[122]. Thus, despite robust upregulation of $Na_V1.3$ after nerve injury, its role in the development of neuropathic pain remains unclear[124].

In recent years, $Na_V1.3$ has also received attention for its putative involvement in epilepsy. Although rodent $Na_V1.3$ is down-regulated postnatally, adult human brain expresses significant levels of the $Na_V1.3$ isoform, with mutations found in patients with cryptogenic pediatric partial epilepsy[125]. These mutations were found to enhance both the persistent and ramp currents of $Na_V1.3$, and increase excitability in hippocampal neurons, a finding consistent with upregulation of $Na_V1.3$ in spontaneously epileptic rats[126]. However, the precise contribution of $Na_V1.3$ to various forms of epilepsy remains to be determined. Similarly, while specific site mutations have not been identified to date, recent data from animal models of epilepsy suggest an involvement of $Na_V1.6$ in certain forms of epilepsy, including absence seizures. These data suggest that subtype-specific pharmacological modulators might emerge as useful treatments for multiple epileptic disease states.

2.1.2 $Na_V1.7$

$Na_V1.7$ is encoded by the *SCN9A* gene and preferentially expressed in both nociceptive DRG and sympathetic ganglion neurons[127, 128]. This channel also mediates a TTXs fast-activating, fast-inactivating current, however it is slow to recover from inactivation as compared to other Na_V channels[129-131]. $Na_V1.7$ also exhibits slow inactivation from the closed-state, which allows the channel to generate a current in response to a small, slow ramp depolarization. This action helps set a gain by amplifying sub-threshold conductance that contribute to hyperexcitability[132, 133]. The ability of this channel to boost sub-threshold stimuli ultimately increases the total probability that a

neuron will reach its threshold to fire an action potential. This functional role has been observed in recent studies linking $Na_V1.7$ to heat hypersensitivity after burn injury[134].

Originally detected in somatosensory and sympathetic ganglion neurons, $Na_V1.7$ has since been reported in myenteric neurons[135], olfactory sensory neurons[136, 137], visceral sensory neurons[138] and vascular myocytes[139]. $Na_V1.7$ expression is also well characterized in both the large diameter, myelinated aδ-fibers and small diameter, unmyelinated C-fibers[140]. Expression of $Na_V1.7$ within free nerve endings in the epidermis is consistent with its proposed role of amplifying weak stimuli[134, 141]. $Na_V1.7$ has also been detected in a variety of non-excitable cells, including prostate and breast tumor cells[105, 142], human erythroid progenitor cells[143] and immune cells[144]. However, there has been no evidence of CNS expression, except for within the superficial lamina of the dorsal horn in the spinal cord [128, 145].

$Na_V1.7$ potentially represents one of the best validated pain targets for the development of therapeutics. The role for $Na_V1.7$ in human acute and chronic neuropathic pain has been demonstrated through observations of human familial mutations, which are responsible for three pain syndromes. The two gain-of-function disorders, inherited erythromelalgia (IEM) and paroxysmal extreme pain disorder (PEPD), are dominantly-inherited mutations causing hyperexcitability and increased pain perception[146, 147]. Congenital insensitivity to pain (CIP) is a recessive loss-of-function disorder, with mutations inactivating the $Na_V1.7$ channel[148]. CIP patients typically experience a complete loss of pain sensation, even after burns, fractures, or puncture wounds. The only other sensory deficit observed is a partial or global loss of olfaction. This loss of smell was determined to be the cause of prenatal mouse *SCN9A*-knockout lethality, since blind, prenatal mice require a sense of smell in order to feed, with no other deficit in sensory, motor or cognitive functions observed[149]. These mutations highlight the distinct role of $Na_V1.7$ in nociception in humans. The reader is directed to a recent comprehensive review highlighting all known human mutations of $Na_V1.7$[150].

Initial studies seeking to confirm the role of $Na_V1.7$ in pain using $Na_V1.7$ knockout animals were hampered due to the perinatal lethality of the global $Na_V1.7$ null mutant. While this was originally attributed to decreased gut motility due to the presence of $Na_V1.7$ in the gut, a more likely cause has been traced to loss of olfactory sensation, as is seen in human loss-of-function mutations, resulting in postnatal starvation as a consequence of loss of $Na_V1.7$ in olfactory neurons. Conditional knock-out

and knock-down of $Na_V1.7$ in animal models of pain have demonstrated that $Na_V1.7$ plays a significant role in the development of acute and inflammatory pain, probably attributed to an upregulation of the channel caused by inflammatory cytokines[151, 152]. Thus, $Na_V1.7$ has attracted considerable attention as a putative therapeutic target for the treatment of extreme pain conditions [153] with one lead compound, CNV1014802, already in Phase II clinical trials with Convergence Pharmaceuticals (a spinoff of GSK)[154]. Xenon Pharmaceuticals is currently working on its own lead compound, XEN402, which blocks $Na_V1.7$-mediated pain associated with post-herpetic neuralgia [155]. Other major pharmaceutical companies contributing research into small molecule $Na_V1.7$ inhibitors include Merck[156, 157], Pfizer, Amgen [158], and AstraZeneca[159], to name a few.

2.2 Muscle channelopathies

The human gene *SCN4A* encodes $Na_V1.4$, which plays a critical role in affecting skeletal muscle excitability and maintaining resting membrane potential. Muscle channelopathies can be characterized by their affects on excitability by causing conditions associated with either nondystrophic myotonia (hyperexcitability) or periodic paralysis (nonexcitability) through a variety of ion channel mutations. Nondystrophic myotonia conditions are characterized by phenotypes of extreme muscle stiffness caused by prolonged relaxation of skeletal muscle after voluntary contraction or external mechanical stimulation. Periodic paralysis conditions are characterized by episodes of muscle weakness associated with variations in serum K^+ concentrations and may be also involve symptoms of myotonia[160].

Missense mutations specifically affecting *SCN4A* are known to be responsible for a variety of human myotonia and periodic paralysis conditions. Hyperkalemic periodic paralysis and paramyotonia congenita (Eulenburg's disease) are conditions resulting from gain-of-function mutations in *SCN4A* that impair inactivation, leading to persistent Na^+ current and mild membrane depolarization[160]. $Na_V1.4$ blockers are able to correct the associated myotonia, but are not very effective in preventing muscle weakness or frequency of attacks in these two conditions[161]. Potassium-aggravated myotonias include myotonia fluctuans, myotonia permanens, and acetazolamide-sensitive myotonia, are caused by various *SCN4A* mutations and aggravated by K^+ ingestion[162, 163]. Thus, $Na_V1.4$ is a promising therapeutic target for a variety of skeletal muscle disorders, although $Na_V1.4$-specific antagonists are lacking, with the exception of certain μ-conotoxins.

2.3 Cardiac arrhythmias

The fast-inactivating cardiac-specific $Na_V1.5$ is encoded by the gene *SCN5A* and is essential for normal cardiac function. $Na_V1.5$ directly contributes to phase 1 of the cardiac action potential, which is the depolarization phase caused by the rapid influx of Na^+ ions (I_{Na}) into the cell, initiating and propagating Na^+ current. $Na_V1.5$ also contributes to setting the resting membrane potential[103]. Multiple disease states result from defects in I_{Na} conduction, typically resulting from point mutations on the *SCN5A* gene. Since the first identification of a mutation on the gene *SCN5A* that was attributed to long-QT syndrome (LQTS)[164], close to 200 mutations have been identified. $Na_V1.5$ mutations have since been implicated in Brugada syndrome, progressive cardiac conduction defect, dilated cardiomyopathy, atrial fibrillation, and sick sinus node syndrome[103]. The numerous mutations implicated in the multiple cardiac rhythm disease states can aid the clinical diagnosis and help determine both latent risk factors and clinical severity.

Reduced Na_V availability due to diminished peak I_{Na} amplitude or negative shift in the inactivation profile is associated with loss-of-function phenotypes such as Brugada and sick sinus node syndrome[165, 166]. The impairment of conduction can act through different mechanisms, such as reduced membrane channel density, a voltage-dependant shift in the steady-state inactivation and activation profiles, or an increased onset of inactivation. These phenotypes are not pharmacologically treated by Na_V channel blockers, although increasing $Na_V1.5$ activity through subtype selective activators could be a potential treatment strategy.

In contrast, mutations that cause increased late I_{Na} augment the depolarizing impact on cardiac myocytes and thereby prolong the action potential duration, as seen in LQTS[167]. This latter type of arrhythmias can be treated with Class I Na_V channel blockers[168, 169]. Current antiarrhythmic drugs have low target specificity and potential for serious side effects[170]. Current antiarrhythmic drugs were developed at a time when the underlying molecular mechanisms of the pathology were little understood, so molecular target selectivity was not a factor. That said, there are currently no selective $Na_V1.5$ drugs available on the market.

2.4 Epilepsy

As one of the world's most prevalent neurological disorders, epilepsy encompasses a group of diseases with a wide range of clinical features and causes, all sharing the similar phenotype of seizure. Monogenetically inherited epileptic syndromes are typically associated with mutations in genes encoding for ion channels. In the case of Na_V channels, over 300 mutations on the *SCN1A* gene that encodes $Na_V1.1$ have been discovered to date[171, 172]. Gene mutations and functional disturbances causally linked to the development of both inherited and acquired epilepsy have also been reported for *SCN2A*/$Na_V1.2$, *SCN3A*/$Na_V1.3$[125, 173] and *SCN8A*/$Na_V1.6$[174]. It is interesting to note that $Na_V1.1$, $Na_V1.2$ and $Na_V1.6$ are all highly expressed in the adult mammalian brain and their genes *SCN1A*, *SCN2A*, and *SCN3A* are all located on the same chromosomal cluster.

Na_V mutations have been correlated with multiple epileptic disease states [175], with $Na_V1.1$ linked primarily to severe myoclonic epilepsy of infancy and generalized epilepsy with febrile seizures plus syndrome, while $Na_V1.2$ has been linked to benign familial neonatal-infantile seizures. Reduced expression and mutations of the β1-, β2-, and β3-subunits have all been shown to contribute to seizure activity through modulation of Na_V voltage-dependence towards a more increased level of persistent current, most likely by affecting expression patterns of associated Na_V α-subunits[100, 176]. Intriguingly, loss of function mutations in $Na_V1.1$, which intuitively would lead to decreased neuronal excitability, are also associated with the development of epilepsy. The majority of *SCN1A* mutations result in localized high-frequency repetitive firing and hyperexcitability through hyperpolarized shifts in voltage-dependence, persistent inward current, or inhibition of inactivation. The reason for this seeming discrepancy presumably arises from predominant expression of this Na_V isoform in inhibitory interneurons, whose loss of Na_V currents leads to increased excitability overall [177]. Compensatory inhibition of $Na_V1.6$ has been suggested to partially correct the neuronal hyperexcitability resulting from loss-of-function mutations in $Na_V1.1$[178]. Thus, inhibition of Na_V activity remains a possible treatment strategy, even for types of epilepsy based on loss-of-function mutations.

In recent years, $Na_V1.3$ has also received attention for its putative involvement in epilepsy. While rodent $Na_V1.3$ is downregulated postnatally, human brain expresses significant levels of $Na_V1.3$, and mutations in $Na_V1.3$ were found in patients with cryptogenic pediatric partial epilepsy[125]. These mutations were found to enhance both the persistent and ramp currents of $Na_V1.3$, and increase excitability in hippocampal neurons, a finding consistent with upregulation of $Na_V1.3$ in spontaneously

epileptic rats[126]. However, the precise contribution of $Na_V1.3$ to various forms of epilepsy remains to be determined. Similarly, while specific site mutations have not been identified to date, recent data from animal models of epilepsy suggest an involvement of $Na_V1.6$ in certain forms of epilepsy, including absence seizures. These data suggest that subtype-specific pharmacological modulators might emerge as useful treatments for multiple epileptic disease states.

The antiepileptic drugs (AEDs) currently in use are not known to be Na_V subtype selective[179]. However, they do act as use-dependent modulators, blocking the high-frequency repetitive firing that is believed to occur during seizures. AEDs preferentially block depolarized channels in a mechanism that resembles fast-inactivation. The current AED drugs on the market are all known to bind to a common site, the local anesthetic (LA) binding site, located within the pore of the Na_V channel[180]. However, the slow onset of activity distinguishes AEDs from LAs. This slow binding is important because it highlights the requirement of repetitive depolarization events, as seen in epileptic seizures versus normal synaptic transmission. There is also evidence that current AEDs can inhibit persistent current, which contributes to the initiation and propagation of seizure-like current. $Na_V1.6$ is the most abundantly expressed Na_V channel in the nervous system and plays a significant role in promoting repetitive firing and enhanced excitability seen in persistent current[174, 181]. The specificity of AEDs to Na_V isoforms including $Na_V1.1$ and $Na_V1.6$ is not yet known, although such experiments may prove enlightening.

2.5 Summary

The contribution of Na_V channels to many other pathological conditions have been identified and are discussed in greater detail within the book chapter from which this was adapted[182]. This further demonstrates the relevance of Na_V channel modulators as potential therapeutics. The broad spectrum of physiologic conductance roles also highlights the need to develop subtype specific modulators, which is something current small molecule therapeutics are lacking.

3. Na_V channel neurotoxin receptor sites

As a significant member of the ion channel superfamily, NaV channels act as unique molecular targets for several groups of naturally derived neurotoxins. Early pharmacological studies identified four neurotoxin receptor sites on mammalian NaV channels, primarily affecting ion conductance and voltage-dependent gating[183]. Later studies provided evidence for sites 5[184, 185] and 6[186] (Figure 4). Binding to these sites can influence gating kinetics by inducing conformational changes to the NaV channel or simply act as a plug, blocking the flow of ions and therefore the transmission of current.

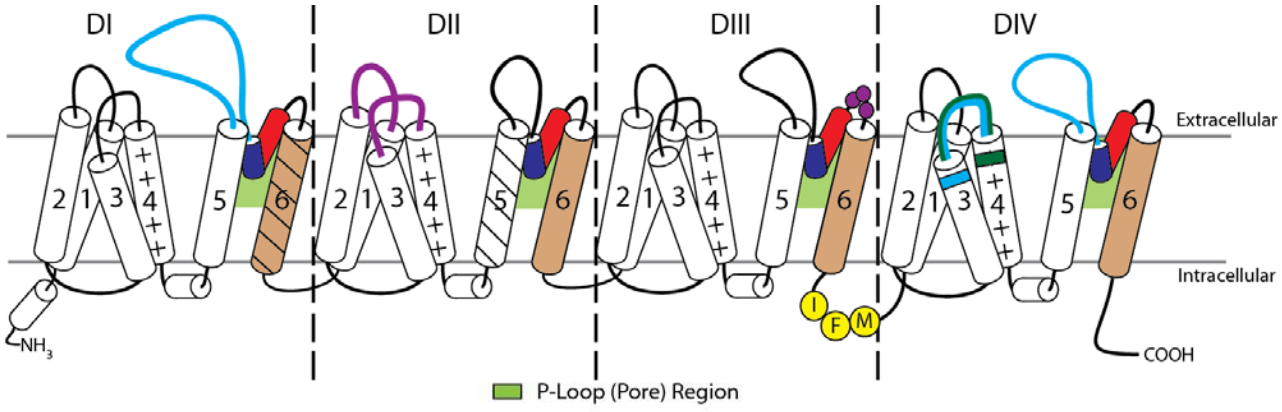

Binding Site	Neurotoxin	Function
Site 1	TTX, STX	Pore block
Site 1	μ-conotoxin	
Site 2	Batrachotoxin Veratridine Aconotine Grayanotoxins	Enhance activation via hyperpolarized shift Reduced I_{Na} (peak current) Reduced ion selectivity Inhibition of inactivation
Site 3	α-scorpion toxins Anemone toxins Spider F2, F4, F12	Voltage-dependent inhibition of inactivation

Binding Site	Neurotoxin	Function
Site 4 *	β-scorpion toxins Spider F1, F3 F5, F7	Enhance activation via hyperpolarized shift Reduced I_{Na}
	μO-conotoxin	* Inhibition via trapping
Site 5	Brevetoxin Ciguatoxin	Enhance activation via hyperpolarized shift Inhibition of inactivation
Site 6	δ-conotoxin	Inhibition of inactivation

Figure 4: Na_V channel neurotoxin binding sites.

Neurotoxin binding sites are color coded where toxins are known to interact with mammalian Na_V channels and cover broad regions of the extracellular loop domains and transmembrane helical regions. The S4 voltage sensor is labeled with (+) and the inactivation gate is labeled with IFM.

These sites have been determined primarily through a series of site-directed mutagenesis studies focusing on different regions of the NaV channels, used in combination with electrophysiology, isotopic ion permeability and radioligand competitive binding assays to assess the regions role in activity[187]. Similar neurotoxin binding sites exist on insect Na_V channels, with some venom peptides demonstrating activity for both insect and mammalian Na_V channels[188-190]. However, insect Na_V channels will not be discussed in this thesis for the sake of brevity.

Because of their natural high affinity and specificity to individual sites on the Na_V channel, several groups of neurotoxins have been instrumental tools for structure-function studies[191, 192]. Binding to these sites strongly modulate channel function by altering permeation and gating properties. There have been three proposed molecular mechanisms of action for neurotoxin modulation of Na_V channels; pore block, indirect allosteric modulation of gating, and voltage sensor trapping[192]. These mechanisms will be explained in greater detail in the next section.

3.1 Site 1 - Pore blockers

Site 1 one the Na_V channel is composed of residues that make up the re-entrant P-loop between S5 and S6 on all four domains. Binding to this site results in extracellular pore block and inhibition of I_{Na} conductance[193]. TTX and STX are both water-soluble heterocyclic guanidines that fall into the first class of neurotoxins known to interact with Na_V channels[194]. As previously mentioned, these toxins have been fundamental tools in studies dissecting Na_V channel structure and function[39, 195]. The peptidic μ-conotoxins have been isolated from marine cone snails and interact competitively with TTX and STX[196, 197] (Figure 4). However, certain mutations of the Na_V pore forming region have been found to affect TTX affinity without altering μ-conotoxin binding, suggesting these toxins share only a partially overlapping binding site[198, 199]. More recent experiments have demonstrated synergistic inhibition of I_{Na} with both μ-KIIIA and TTX forming a ternary complex with the Na_V channel pore region[200]. μ-KIIIA alone allows a small but measurable leak of I_{Na}, while the addition of TTX results in complete inhibition. Although the inhibition effect was more complete when both toxins were combined, kinetic effects for both toxins appeared competitive. The presence of prebound TTX accelerates the off rate of μ-KIIIA after subsequent addition, while the presence of prebound μ-KIIIA slows the on rate of TTX after subsequent addition. However, it was noted that the same ternary complex forms regardless of the order of ligand addition. TTX also appears to reduce the K_{on} of μ-

KIIIA The authors explained these effects as being caused by differential binding on site-1 "microsites", dependent on the order of ligand binding. As μ-KIIIA binds closer to the vestibule, it would slow the K_{on} of TTX through partial physical occlusion of the inner binding site. Likewise, the presence of TTX would limit the affinity of subsequent μ-KIIIA binding. These results give hints towards the development of a peptide that could either i) act as a stronger inhibitor of Na_V channels through the addition of guanidine side chains, or ii) bind strongly to the outer pore in a way to limit TTX binding while still allowing enough leak current to maintain a functional channel. This latter method could be developed as an effective treatment for paralytic shellfish poisoning.

3.2 Site 2

Toxins that bind to the transmembrane site 2 on the Na_V channel are lipid soluble, small molecule, allosteric modulators, causing persistent activation as either full or partial agonists[192, 201-203] (Figure 4). However, these toxins are derived from a variety of organisms and are diverse in structure. Plant derived toxins include the diterpene grayanotoxins from the *Ericaceae* family[204], and the alkaloids aconotine from *Aconitum*[205] and veratridine from the *Lilaceae* family[206]. The alkaloidal steroid batrachotoxin (BTX) is found in frog, bird, and insect species and has served as a primary tool for determining site 2 functional roles in Na_V channels[207]. Antillatoxin and hoiamide are two structurally unique Na_V agonists isolated from marine cyanobacteria[208, 209]. Both molecules were found to partially displace [^{3}H]BTX, but the precise site of binding remains undefined.

Site 2 toxins share the characteristic of preferential binding to open-state Na_V channels and are able to modulate several functional Na_V properties. BTX has been used as a primary tool to study many functional roles of site 2 modulation as well as map residues composing the site 2 region. Site 2 modulation results in a hyperpolarizing shift in the voltage-dependence of activation, resulting in activation at resting potential[210]; slowed or inhibited inactivation, resulting in sustained, non-inactivating currents[137]; reduced I_{Na} conductance[211]; and modification of the selectivity filter, resulting in reduced selectivity for permeating ion[212].

Photoreactive BTX was initially used to determine an interaction site at DIS6[213]. Site-directed mutagenesis studies of $Na_V1.4$ confirmed residues along DIS6 were necessary for toxin binding as well as demonstrating overlapping regions in DIVS6 that were common to both BTX and grayanotoxin[207,

214]. Accumulating evidence from computer modeling and molecular docking experiments suggests that BTX and veratridine – as well as potentially other site 2 agonists – interact with all four S6 segments near the DEKA selectivity filter in a way that stabilizes the open-state of the Na_V channel, as well as limiting fast inactivation through S6 interactions[212, 215, 216]. BTX has been shown to bind towards the cytosolic end of the pore region in an open-state dependent, irreversible manner[217]. Grayanotoxin has been shown to bind an overlapping but not identical region in the pore in a reversible manner[207]. The close interactions with the selectivity filter region helps explain observed changes to ion permeability. The modeling experiments demonstrating pore binding also helps explain the decrease in peak current, as well as the observation that close analogues to some site 2 agonists are able to act as Na_V inhibitors[218, 219].

The mode of binding has been less studied for veratridine, although classical electrophysiology studies measuring whole tissue currents have been completed. Veratridine is known to have a reversible effect on $Na_V1.1$-$Na_V1.7$ and exhibits similar functional alterations of Na_V channels[18, 220]. An interesting functional quality of veratridine is a lack of state-dependent binding in nerve tissue[221] while exhibiting state-dependence in muscle tissue[222-224]. Interestingly, in many of these same studies veratridine was also shown to have differential effects on peak amplitude in a tissue specific manner. Differences between cardiac myocytes, smooth muscle, and nerve tissue hint that the effect is most likely dependant on the Na_V isoforms preferentially expressed in corresponding tissue. A more recent study on $Na_V1.6$ in mouse vas deferens myocytes demonstrated a bell-shaped curve for peak amplitude in relation to veratridine concentration. Peak amplitude was enhanced until a concentration of 10 μM was reached, whereas higher concentrations reduced I_{Na}[225]. No change in ion selectivity was noted. The effect is likely due to partial pore obstruction caused by toxin binding.

3.3 Site 3 and Site 4

Toxins that bind to both site 3 and site 4 are gating modifier toxins that have evolved voltage sensor trapping mechanisms. They typically exhibit hydrophilic properties and therefore likely do not interact directly with the transmembrane segments, but instead exert their actions on the S4 voltage sensor through binding to extracellular loop domains[192]. Site 3 and site 4 were described for the first time as two distinct sites on rat brain synaptosomes while assessing competitive binding of the scorpion toxins AaH II (*Androctonus australis* Hector) and Css II (*Centruroides suffusus suffusus*) [226, 227]. The lack

of competition between these two toxins, which bound to distinct sites and exhibit different pharmacological profiles, led to the classification of α- and β-scorpion toxins, of which AaH II and Css II belong respectively[226, 227].

Several classes of peptide toxins have been found to interact with site 3 through electrophysiological and competitive binding experiments, including α-scorpion toxins, sea anemone toxins, and the spider toxin families 2, 4, and 12[228-230]. This group of toxins work by preventing the outward movement of the DIVS4 transmembrane segment, thereby inhibiting conformational changes necessary for fast inactivation[231]. An important feature of these toxins is their voltage-dependent binding, which decreases in affinity as prolonged depolarization forces the outward movement of the S4 region, even causing voltage-dependant displacement of the ligand[229, 232]. Initial antibody mapping using photoaffinity labeling with α-scorpion and sea anemone toxins suggested the extracellular transmembrane segments S5-S6 in both DI and DIV, as well as part of the DIS5-S6 P-loop, comprised at least part of the site 3 binding domain[233, 234]. Experiments suggested that these extracellular loops are in close proximity and form a single binding space when the Na_V channel is viewed in its tertiary structure. Further experiments revealed the additional contribution to α-scorpion toxin binding of the S3-S4 extracellular loop in DIV[231]. Research into Na_V isoform selectivity using chimeras of DIVS3-S4 demonstrated only a few residues were critical for α-scorpion toxin binding and selectivity, demonstrating regions of importance that can be exploited when attempting to design specific ligands to Na_V subtypes[235].

Site 3 neurotoxins function through the mechanism of voltage sensor trapping, where binding to the extracellular DIVS3-S4 loop is thought to slow or inhibit inactivation by preventing the normal outward movement of the DIVS4 transmembrane segment during channel gating. Site-specific fluorescent labeling of the S4 segment of $Na_V1.4$ demonstrated the effect of stabilizing S4 of DI and DIV through α-scorpion toxin binding[236]. Both sea anemone and α-scorpion toxins have been shown to enhance the recovery of inactivation[232, 237]. As the S4 region is responsible for voltage-dependant gating, toxins that interact with this region are referred to as gating modifier toxins.

Venom peptides from two organisms have been instrumental in studying the mammalian Na_V neurotoxin site 4: the β-scorpion toxins and spider Na_V toxin families 1, 3, 5, and 7[226, 227, 238, 239]. Unlike site 3 neurotoxins that inhibit inactivation, site 4 neurotoxins enhance activation by

trapping the voltage sensor region in its resting state, subsequently shifting the voltage-dependence of activation to a more hyperpolarized potential, as well as reducing peak current[240-242]. Site 4 neurotoxins bind preferentially to resting state channels in a concentration-dependent manner. However, some more recently discovered spider venom peptides have redefined the original role for site 4 modulation, which will be discussed later[243-246].

In order to initially determine the site 4 region of interaction and learn more about voltage sensor function, the β-scorpion toxin TiTxγ (*Tityus serrulatus*) was tested against chimeras of $Na_V1.4$ (skeletal) and $Na_V1.5$ (cardiac) domains. This research determined TiTxγ interacts preferentially with the $Na_V1.4$ isoform at DII, which was necessary for the negative shift in the voltage-dependence of activation to occur[247]. A more detailed chimeric study using domains of $Na_V1.5$ and the CNS expressed $Na_V1.2$ with the highly potent β-scorpion toxin Css4 (*Centruroides suffusus suffusus*) confirmed DII, localized to the extracellular loops between DIIS1-S2 and DIIS3-S4. It was proposed that as the DIIS4 moves outward during depolarization, toxins will bind to newly accessible residues on the DIIS3-S4 loop, subsequently trapping the voltage sensor (S4) in an outward, activated position [248, 249]. The study also demonstrated that a single residue change of G845N is primarily responsible for the lack of affinity of $Na_V1.5$ as compared to $Na_V1.2$, giving further insight into the potential precision with which toxins interact with their receptors[242]. The β-scorpion toxin Tz1 (*Tityus zulianus*) helped resolve an additional interaction site on the Na_V channel as well as determine specificity for different mammalian Na_V isoforms[250]. Tz1 had the highest affinity for $Na_V1.4$, followed by the neuronal $Na_V1.2$ and $Na_V1.6$, while $Na_V1.5$ and $Na_V1.7$ had little to no effect. Through chimeric studies with $Na_V1.2$ and $Na_V1.4$, the additional site 4 binding region of DIII was narrowed down to three residues on the C-terminal pore loop. The DIII region is critical for the observed Na_V subtype specificity, which may be of interest when attempting to design specific Na_V channel modulators[250].

Four Na_V modulating spider toxin families are known to interact with mammalian neurotoxin site 4 (Figure 4), all of which conform to an inhibitory cysteine knot (ICK) secondary structure and are thought to act as gating modifiers[251, 252]. Mg1a (Magi-5), isolated from *Macrothele gigas*, was the first spider venom to show affinity towards the mammalian site 4 through displacement of the β-scorpion toxin, CssIV (*Centruroides suffusus suffusus*), using rat brain synaptosomes[188]. The electrophysiological properties of site 4 neurotoxins as defined by the β-scorpion toxins and Mg1a

exhibit a shift in the voltage-dependence of activation to a hyperpolarized potential, resulting in hyperexcitability through activation at sub-threshold potentials[188, 253, 254].

Multiple other spider venom peptides have since been discovered with critical binding domains located on the site 4 DIIS3-S4 loop[239](Figure 4), as determined by either mutagenesis of key residues on this region of the Na_V channel[243, 245, 255] or competitive assay with β-scorpion toxins[244]. However, many of these spider venom peptides exhibit a distinct functional profile to the β-scorpion toxins, whereby the peptide traps the DIIS4 voltage sensor in the closed state resulting in an inhibition of peak current [245, 255, 256]. Although a few of the jingzhaotoxins (*Chilobrachys jingzhao*) so far discovered have been shown to inhibit Na_V current by acting as gating modifiers[244, 257-259], only one – β/κ-TRTX-Cj1a (jingzhaotoxin-III) – has so far demonstrated direct binding to the site 4 DIIS3-S4 loop[245]. Two other spider venom peptides that have been shown to bind the DIIS3-S4 linker through mutational analysis include μ-TRTX-Hh2a (huwentoxin-IV isolated from *Ornithoctonus huwena*)[243] and μ-TRTX-Hhn2a (hainantoxin-III isolated from *Ornithoctonus hainana*)[255]. Both of these toxins also inhibit Na_V current by interacting with the DIIS3-S4 linker and trapping the voltage sensor in the closed conformation. These Na_V inhibitory spider venom peptides acting as gating modulators conform to a similar ICK secondary structure but exhibit highly variable Na_V isoform selectivity profiles and promiscuous activity, affecting both Ca_V and K_V channels[257, 259, 260]. This promiscuity across members of the voltage-gated ion channel superfamily could be attributed to partial binding in the vicinity of the highly conserved voltage sensor domain (S4) as many of these venom peptides have been shown to bind to S3-S4 linkers of the highly homologous voltage-gated ion channel family[261]. This should be taken into consideration when assessing the selectivity profiles of similar venom peptides.

In addition to the spider venom peptides just mentioned, a single family of conotoxins, labeled μO, have been found to bind to a similar, overlapping region of site 4, also resulting in inhibition of current. Through Na_V channel chimeric studies using $Na_V1.2$ and $Na_V1.4$, the μO-conotoxin MrVIA has been reported to interact with the C-terminal pore loop in DIII to inhibit activation[262]. Further, neutralization of the charged residues on the S4 segments of each domain demonstrated affinity to DII[263]. This same study also demonstrated functional competition between MrVIA and the β-scorpion toxin Ts1a (*Tityus serrulatus*), suggesting μO conotoxins are site 4 modulators[263]. The inhibitory effects of these toxins can be reversed by strong, long-lasting positive voltage pulses, which

drive the voltage sensor back into its activated conformation[246]. Only five μO-conotoxins have been isolated to date, most varying only slightly in sequence homology[263-266].

The discovery of structurally related peptides that can exhibit two modes of voltage sensor trapping on the same receptor site demonstrates the unique ability of venom combinatorial libraries to exploit potential modulatory niches with only slight modifications in amino acid sequence. These small changes can be exploited to identify the functional necessity of charge, hydrophobicity, or chemical space for optimal interaction with the receptor. It also highlights the importance of continuing research into the discovery of venom peptides that might yet determine new functional roles or regulatory domains of the Na_V channel.

3.4 Site 5

Marine dinoflagellates produce two classes of highly lipophilic, cyclic polyether compounds that interact with Na_V neurotoxin site 5: brevetoxins (PbTX), produced by *Karenia brevis* and ciguatoxins (CTX), produced by *Gambierdiscus toxicus*[185, 267, 268]. Both classes of toxins bind preferentially to open-state, activated channels and result in a negative, hyperpolarized shift in the voltage-dependence of activation, with some derivatives producing inhibition of fast inactivation[192]. Competitive Na_V channel binding experiments demonstrated both toxins allosterically enhance [^{3}H]batrachotoxin activation while they compete against each other for a unique binding site, subsequently labeled neurotoxin receptor site 5[269]. Photoaffinity labeling experiments using PbTX identified critical residues along DIS6 and DIVS5 that may form a binding pocket, as they would be located in close proximity in the native folded Na_V channel[270] .

To date, thirteen natural derivatives of PbTX and twenty-nine natural derivatives of Pacific (P)-CTX have been identified[271, 272]. However, most research has focused on synthetic studies of these molecules and has neglected a more in-depth look into Na_V channel pharmacology, such as selectivity profiles or defined site 5 residues.

3.5 Site 6

Site 6 on the Na_V channel was originally identified through characterization of δ-conotoxin TxVIA, isolated from the cone snail *C. textile*[186, 273]. However, the first group of δ-conotoxins discovered was mollusk-specific and, although able to bind, had no effect on mammalian Na_V channels. The isolation of δ-AM2766 from *C. amadis* was the first δ-conotoxin discovered to modulate mammalian Na_V channels[274]. This discovery was quickly followed up by δ-EVIA from *C. ermineus*, which was found to be the first conotoxin selective for neuronal Na_V isoforms – although activity was very low – with no effect on $Na_V1.4$ or $Na_V1.5$[275]. NMR solution structures for both toxins confirmed a common ICK motif for this class of peptide as well as visualizing the large hydrophobic surface area also common for the δ-conotoxins[276, 277].

The δ-conotoxins have been shown to interact with Na_V channels in a state-dependent manner, trapping the voltage sensor in the outward, activated position and resulting in an inhibition of fast inactivation, with sustained depolarization leading to toxin dissociation. Although the mechanism is extremely similar to site 3 modulation, δ-conotoxins so far discovered do not seem to exhibit voltage-dependence[273, 275, 278]. The most in depth work to date on δ-conotoxins used δ-SVIE from *C. striatus* as a tool to discern the molecular mechanisms of interaction with Na_V channel site 3, using two representative α-Lqh scorpion toxins in conjunction[279]. Mutagenesis of the $Na_V1.4$ channel site 3 DIVS3-S4 loop resolved a highly conserved triad of residues (Y_{1433}-F_{1434}-V_{1435}) critical for δ-SVIE activity. Mutation of these residues also affected the function of α-Lqh-2 while doing nothing to α-Lqh-3. This result was used to demonstrate functional competition with α-Lqh-2 and synergistic cooperative binding with α-Lqh-3 through mutual stabilization [279]. This work helped further define site 6, while maintaining strong overlapping effects between site 3 and site. However, site 6 still remains largely undefined and could simply be a natural extension of site 3, or could include residues completely unique to site 6. The discovery of novel δ-conotoxins is needed to further elucidate the structural interactions and functional roles this class has with Na_V channels.

3.6 Regarding toxin "sites"

The classical nomenclature of neurotoxin sites has been essential in defining and classifying molecular interactions with the Na_V channel. With the elucidation of a Na_V channel crystal structure, more insight into how ligands interact with the various regions of the Na_V channels can be explored in 3-

dimensional space[45]. Computer aided modeling and co-crystallization studies can compliment traditional functional studies, which typically involve mutagenesis of key residues on either the ligand, receptor, or both. Macromolecular polypeptides most likely form complex interactions with multiple interaction sites across the Na_V channel, such as what has been observed with sites 3, site 4, and site 6 modulators. There still remains great potential for stronger definitions of binding regions. The classical definition of neurotoxin receptor sites as viewed on a planar map will likely shift to a more 3-dimensional perspective as more ligands are discovered and receptor binding surfaces materialize. Furthermore, multiple regulatory roles for existing sites – such as in the dual modes of voltage sensor trapping apparent at site 4 – may yet to be determined. This is promising for structural bioengineering of ligands with greater selectivity profiles, among other functional properties.

4. *Conus* and spider venom peptides targeting Na_V channels

Venoms represent a virtually untapped resource of novel pharmacologically active molecules[280]. In addition to potent drug leads, these highly specific peptides are also important tools to probe the structure and function of their receptor and ion channel targets[3]. Each venom producing species yields its own distinct natural combinatorial library of target selective molecules to be explored[281, 282]. Of all the venom producing organisms, spiders and cone snails are of particular interest in the search for Na_V channel modulators[283]. The majority of active peptides from these organisms are relatively small and contain multiple disulfide bonds, imparting a stable secondary structure[284].

The genes encoding venom peptides are under intense selective pressure and have been shown to undergo rapid hypermutation, imparting target selectivity to individual peptides in a continual, generational predator-prey arms race[285]. These hypermutation events from ancestral genes have created venom peptide families with high sequence similarity as well as similar genetic precursors[239, 285]. As sequencing technology becomes more accessible, this information can be used in the search for novel venom peptides at the transcribed gene level. This is accomplished through mRNA sequencing of venom producing tissue in a quickly arising offshoot of transcriptomics, dubbed venomics[286, 287].

Further, as the number of new gene sequences and novel isolations from crude venom increases, methods for producing these toxins in a complimentary manner to solid phase peptide synthesis (SPPS) need to be developed. Recombinant expression has the ability to compliment SPPS and can be adaptable to both eukaryotic (yeast) and prokaryotic (bacterial) systems[288, 289]. By current measures, bacterial recombinant expression is by far the most cost-effective and straightforward means to express peptides and proteins. Issues such as solubility, folding, and purification can usually be overcome through the addition of a fusion protein, co-expression with chaperones, or the addition of molecular tags for directed expression or affinity chromatography. High-resolution structural elucidation has been improved through utilizing $^{15}N/^{13}C$-labeling of peptides in combination with improved automated multidimensional NMR methods, requiring a fraction of the time of previously used methods, including crystallography[290]. Recombinant expression allows the fast labeling of peptides through simple media changes, at a fraction of the cost of SPPS[291].

4.1 Peptides as therapeutics

Compared to small molecules, which can be developed and produced at low cost, orally bioactive, membrane-permeable, and generally stable, peptides are at a disadvantage[292, 293]. Nevertheless, venom peptides have become a source of novel ligands with potential therapeutic value. The rich diversity of venom peptides is a result of remarkable genetic hypervariability and accompanying post-translational modifications (PTMs) which in turn generates species specific libraries of hundreds to thousands of primary structures[294-296]. Their high natural selectivity and potency towards key receptors, channels, transporters or enzymes of crucial biochemical signalling pathways involved in organism homeostasis make venom peptides an unrivalled and unexplored source of leads for the development of molecules with therapeutic potential.

Many properties of venom peptides set them apart from the traditional limitations of peptides as therapeutics. Despite their variable size, averaging between 10–90 amino acids, most venom peptides have a high cysteine content which enables them to form specific disulfide bonds that provide them with a high level of thermodynamic stability as well as resistance to proteases. Conserved cysteine patterns and disulfide-bond connectivities with defined folds are found among the venom peptides of several thousands of different venomous animal species and in many cases are examples of either convergent or divergent evolution[296-298]. Coupled with secondary structure, many synthetic

methods are being developed to improve oral bioavailability and plasma/thermostability of peptides[299]. Some of these include cyclization[300, 301], substitution of cysteine with selenium[302], and the creation of peptidemimetics[303, 304].

Although peptide therapeutics are not historically well represented in the market compared to small molecules, the number of NCEs for peptide based drugs has grown by 27% at the turn of the century compared to the 1980s[305]. Methods of production and synthesis have increased in efficiency and ability, leading to a sharp increase in the number of new chemical entities. Six peptide drugs were approved in 2013 alone, with only one of those administered intravenously[306]. The clinical pipeline as of 2013 is composed of 128 peptide therapeutics under evaluation for a wide variety of ailments, with 40 in Phase I studies and 74 that have advanced to Phase I/II or Phase II studies[306]. The current increase in peptides approved for therapeutic use is a promising sign of future developments in the search for new drug entities.

4.2 The inhibitory cysteine knot

Despite the apparent sequence diversity among individual species, venom peptides appear to have evolved from a relatively small number of structural frameworks that are particularly well suited to addressing the crucial issues of potency, selectivity, and stability[280]. One of these structural motifs – the inhibitory cysteine knot (ICK) – is present in peptides and proteins from a variety of species, including both spider and cone snails[307]. The ICK motif is comprised of a two distinct structural features: i) a triple-banded antiparallel β-sheet and ii) a ring formed by two disulfide bonds and their connecting backbone segments, which is threaded by a third disulfide bond forming a "knot"[308] (Figure 5). Many ICK spider peptides lack a third β-strand, exhibiting a double-banded antiparallel β-sheet[309].

It was previously suggested that the three-disulfide ICK motif is an elaboration of a simpler, ancestral two-disulfide fold coined the disulfide-directed β-hairpin (DDH)[310]. The discovery of DDH folded peptides in the venoms of both spiders (HWTX-II/Hh1a) and scorpions (Lw1a) lend support for the hypothesis that the DDH motif is an evolutionary precursor of the ICK[311].

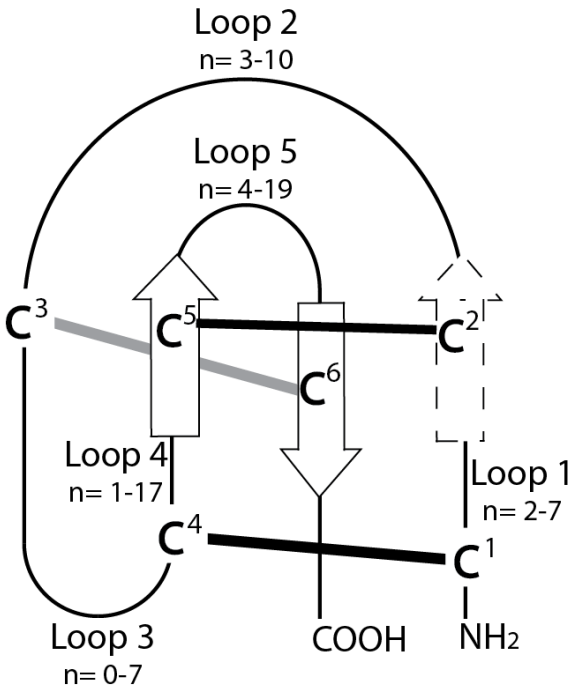

Figure 5: Inhibitory cysteine knot (ICK).

A common structural motif adopted by many Na_V modulating spider and cone snail peptides. Cysteines are labeled 1-6 and follow a connectivity pattern of I-IV; II-V; III-VI. Arrows represent β-strands. The 5 possible loops are variable regions of the peptide sequence, with n equating to the range of amino acids known to occur in different peptides.

The most important aspect of ICK peptides is their inherent structural stability imparted by the knot motif. The term "knot" is actually a misnomer, as the ICK motif does not actually fold a true knot in the mathematical sense of the word, unlike its closed-loop cyclotide relative the cyclotide cysteine knot (CCK)[312, 313]. The ICK structure can be unfolded without the need for breaking any bonds whereas the CCK cannot[314]. Regardless of this discrepancy, ICK peptides still maintain a relatively high level of structural, thermal and biological stability, lending themselves as well-defined molecular scaffolds for drug design[315]. As ICK peptides do not require cyclization, they can be recombinantly expressed in single-celled organisms such as bacteria and yeast, which lack the enzymes necessary to catalyze such a reaction[289]. ICK peptides can also be converted to CCK peptides through chemical synthesis, which has been shown to increase gastric stability, leading to an orally active peptide[316].

4.3 Conotoxins

Cone snails are marine venomous predators of the genus *Conus*. *Conus* is the largest known genus of marine invertebrates, with over 700 extant species described[317]. Cone snails are found in tropical marine environments and are particularly prominent around coral reefs and other shallow-water tropical marine habitats[318, 319]. They are prey specialists that include vermivorous, molluscivorous, and piscivorous species. The piscivorous species are expected to produce the most pharmacologically

interesting peptides to human health, since they have evolved to target chordates[320, 321]. The molecular diversity and enhanced target selectivity of individual peptides across each *Conus spp.* venom is thought to arise from the specificity of prey between different species[322]. Selective pressures forcing gene duplication events over millions of years of evolution have given rise to a vast resource of potent scaffolds, specific for a multitude of ion channel targets. The molecular targets of individual conotoxins are functionally diverse yet appear to act simultaneously in what has been termed *cabals*[4].

A relatively rapid radiation of the *Conus* lineage has resulted in over 500 different species, with the venom of individual *Conus* species estimated to contain a unique compliment of over 200 peptide components[323, 324]. However, a more recent mass spectrometry analysis suggests the number of conopeptides per species could surpass 1000 unique peptides[325]. The majority of conotoxins so far discovered range in size from 12-35 amino acids and contain between 2 to 5 disulfide bonds between cysteine residues. Each *Conus* peptide gene encodes a precursor that typically has an N-terminal signal sequence of about 25 amino acids, an intervening "pro" region of 20-40 amino acids and a mature toxin sequence at the C-terminal end[326, 327]. The correlation between the conservation of both the disulfide framework and the "pre-pro" signal regions has allowed a definition of superfamilies based on both the pre-pro region and disulfide framework[4, 328]. Genome mining using these highly conserved signal sequences has allowed the discovery of new members belonging to defined superfamilies, as well as the discovery of completely novel superfamilies[329-332]. It is of interest to note the extremely high conservation of signal sequences is in direct conflict with the hypermutational variability of the mature toxin region, which is responsible for the amazing biodiversity of conotoxins[328]. These superfamilies were further subdivided into families based on molecular targets – represented by Greek nomenclature – with four of these families targeting Na_V channels[322, 333].

The ι-conotoxins are the most recently discovered family of Na_V modulating peptides isolated from cone snails and have helped to define the I-superfamily[334, 335]. Eighteen paralogs were found within a single genome of *C. radiatus*, five of which demonstrated excitatory neuronal activity[334]. One interesting aspect of this class of peptides is the appearance of a D-epimerized amino acid at the C-terminus, such as the D-Phe at position 44 of ι-RXIA[336]. To assess the functional role of ι-conotoxins, ι-RXIA was used as a tool[335]. Results demonstrated ι-RXIA shifted the voltage-dependence of activation to a more hyperpolarized potential, with some parallels made with the

mechanism of action to β-scorpion toxins. Some selectivity between Na_V channel isoforms was observed. However, unlike β-scorpion toxins there were minimal effects on the voltage-dependence of inactivation or the kinetics of I_{Na} currents. The L-analog of ι-RXIA[L-Phe44] demonstrated severely decreased affinity and efficacy[335]. No binding site has been determined for this family of conopeptides.

The μ-conotoxin family was previously mentioned for its ability to inhibit Na_V current through site 1 pore block in a manner complimentary to small molecule guanidinium toxins, like TTX. The μ-conotoxins belong to the M-superfamily of conotoxins. They are small peptides ranging in size from 16-30 amino acids, three disulfide bonds, and a highly conserved C-terminal helical region[337]. Recurring features include an Arg crucial for activity on the loop 2 region of the peptide, C-terminal amidation, and a hydroxylated Pro that seems to aid proper folding but is not always present[338].

The first μ-conotoxin isolated and characterized was μ-GIIIA from *C. geographus*. μ-GIIIA was shown to be a potent and selective inhibitor of the skeletal muscle $Na_V1.4$, setting a precedence for the ability of conotoxins to possess inherent selectivity[339, 340]. Another $Na_V1.4$ selective conotoxin, μ-PIIIA from *C. purpurascens*, demonstrated similar preference for $Na_V1.4$, yet also affected some neuronal Na_V isoforms, just with much lower potency[341]. Since those first discoveries, numerous μ-conotoxins have been discovered through genomic analysis or activity-guided isolation from crude venom and have demonstrated a wide range of activity and selectivity profiles for Na_V channels[342-344]. Solution structures and mutagenesis studies of a few select μ-conotoxins have begun to reveal key residues, loop regions, and even backbone lengths necessary to impart selectivity between different Na_V channel isoforms[337, 338, 342, 345]. The μ-conotoxins have been a focus for the development of novel analgesics targeting single-target Na_V isoforms that contribute to nociception. Both μ-KIIIA (*C. kinoshitai*) and μ-SIIIA (*C. striatus*) have been shown to have analgesic properties in mouse inflammatory pain assays[338, 346]. The μ-conotoxins small size, high affinity and diverse selectivity of inhibition for TTXs and TTXr Na_V channels make them strong prospective therapeutic agents.

The Na_V channel selective μO- and δ-conotoxins both belong to the O-superfamily and have been discussed in great detail in an earlier section regarding their interactions to Na_V neurotoxin sites. Both are unusually hydrophobic peptides with the same disulfide scaffold that imparts an inhibitory cysteine knot (ICK) secondary structure, which is discussed in detail later[4]. This ICK fold mirrors that of the

spider toxins and imparts very high structural rigidity to these peptide classes. The μO-conotoxins inhibit activation of Na_V current through voltage sensor trapping of the Na_V channel in its resting state[263]. Peptides of this class can block both TTXs current and the $Na_V1.8$ TTXr current by binding to the C-terminal section of the pore loop in DIII in a mechanism different to TTX[262]. Although the δ-conotoxins also act as gating modifiers, they exhibit a much different pharmacologic profile through trapping the voltage sensor in the activated state, resulting in inhibition of inactivation and channel hyperexcitability[279, 347]. The mechanism of action is very similar to α-scorpion toxins, with both toxin classes trapping the DIVS4 voltage sensor in an inward, more depolarized position. Research into this mechanism of action has demonstrated that δ-conotoxins bind to a region slightly overlapping from site 3 on the S3-S4 loop of DIV, which has been defined as the Na_V neurotoxin receptor site 6[279]. An interesting feature of the δ-conotoxins that has not yet been addressed or explored is the reoccurrence of hydroxyprolines, an Arg on or around position 14, and C-terminal amidation; all of which are structural features seen repeated in the μ-conotoxin family of Na_V channel inhibitors. These close structural characteristics could help predict binding regions of the δ-conotoxins or could simply be a vestigial feature evolutionary divergence. These questions remain to be answered and could serve as critical pieces of information for ligand design.

To date, one conotoxin – the N-type calcium channel blocker MVIIA isolated from *C. magus* – has been approved in the US as an antinociceptive, marketed by Elan Pharmaceuticals under the name Prialt[328]. There are a handful of other conopeptides currently undergoing pre-clinical or clinical trials for treatment of various neuropathic disorders but presently these don't include any Na_V channel inhibitors[285, 348].

4.4 Spider venom

There are over 43,000 spider species within 110 families currently catalogued, with many more expected to be discovered[349]. Mass spectrometry analysis of the composition of different spider venoms determined the presence of between 500 and 1000 peptide components per sample, suggesting a potentially enormous total pool of bioactive peptides to be explored[350, 351]. Recently, in an attempt to categorize the ever increasing number of new peptides discovered, groups of known Na_V-active spider venom peptides (NaSpTx) have been assigned to twelve families based solely on sequence homology[239]. Those NaSpTxs specifically affecting mammalian Na_V channels average

between 31 to 41 amino acids in length and are cross-linked with 3 or 4 disulfide bonds, which impart a secondary structure commonly exhibiting an ICK motif[352]. Rational nomenclature for spider venoms has also been adopted – loosely based on the conventions of conotoxin naming – where a Greek symbol denotes activity and is followed by a letter/number code describing the source organism and relation to similar toxins[353]. This nomenclature is extensively used throughout this thesis.

Although many of these spider venom toxins demonstrate activity across ion channel targets, with a significant portion purely selective for insect receptors, only those active on mammalian Na_V channels are of concern to this thesis. These families of toxins have already been discussed in detail regarding their classification and how they relate to Na_V channel function through neurotoxin site-specific binding and the mechanism of voltage sensor trapping.

5. Project summary

Modulation of Na_V channels has been applied as a therapeutic strategy for many years towards roles in local anesthesia, cardiac arrhythmia and epilepsy. Clinically available Na_V channel modulators have also increasingly found applications in conditions ranging from neuropathic pain, migraine, bipolar disorder and Alzheimer's disease to myotonia[354, 355]. In addition, new off-label applications for Na_V channel modulators are being investigated for neurodegenerative disorders such as Parkinson's disease and multiple sclerosis, neuropsychiatric disorders such as bulimia nervosa and obsessive compulsive disorder, and cancers[354-357].

The usefulness of the limited number of clinically available small molecule compounds in such a diverse range of therapeutic areas most likely arises from their relatively poor ion channel and subtype selectivity, giving these molecules functional diversity. However, this same lack of selectivity contributes to the significant toxicity and side-effect profiles seen for these compounds, as well as their often narrow therapeutic index. The poor subtype selectivity of many these compounds is offset at least partially by their state-dependence, or preferential binding to either the open- or inactivated-state of its target receptor[358]. Thus, even poorly subtype-selective Na_V channel inhibitors are able to somewhat selectively modulate excitability in hyperexcitable states and tissues.

As our understanding of the biology of Na_V channels and their affiliations with disease states expands, so does their therapeutic potential for treating these various diseases through the development of selective Na_V modulators. The identification of novel, subtype-selective Na_V modulators would represent significant therapeutic advance in this regard. Unfortunately, little progress has been made towards this goal in recent years. This can be partially attributed to the high sequence homology of the different Na_V subtypes, particularly in the region constituting the local anesthetic binding site in the channel pore. For the last few decades, the focus of drug research has been primarily focused on small molecules, which tend to occupy a smaller chemical space and lend themselves to receptor cross-talk[359]. However, an increasing number of subtype-selective peptidic Na_V modulators are being isolated and characterized from natural venom sources[239, 348].

This thesis attempts to describe research into the design and development of new methods to identify Na_V modulators from venom peptides using whole-cell high-throughput technology and electrophysiology. Then, using information available from known peptides of related class, attempt to study variations of structure of a single peptide through mutagenesis to determine how it relates to function. This will benefit towards gaining a better understanding of Na_V channel modulation by peptidic ligands, as well as potentially improve upon a natural ligand through guided mutagensis.

The primary aims of the thesis were as follows:

1) Develop a high throughput, cell-based assay for the screening of crude venoms for the purpose of isolating Na_V channel modulators.

2) Develop recombinant methods of production for venom peptides.

2) Characterize the function and structure of TRTX-Pre1a, a Na_V channel modulator isolated from spider venom with a unique pharmacologic profile.

3) Develop mutants of Pre1a, targeting specific residues determined as important through comparative sequence homology to known, related peptides.

4) Test the function of these mutants to determine if they enhance Na_V isoform selectivity or function, then solve the solution structure of a single mutant to compare physical attributes with functional changes.

Chapter II: Development of whole-cell microtiter plate assays to discover Na_V modulating venom peptides

1. Introduction

As mentioned previously, voltage-gated sodium (Na_V) channels are integral membrane proteins that play an essential role in the initiation and propagation of action potentials in excitable cells, making them excellent therapeutic targets for a variety of neuropathies involving conductance[6]. The study of Na_V channel structure and function has been aided by using peptide components isolated from paralytic venoms from a variety of organisms, including cone snails and spiders. The individual venom peptides possess unique selectivity and affinity profiles that allow researchers to explore novel ligand binding domains and different modes of modulation, such as voltage sensor trapping. Less than 0.1% of naturally produced venom peptides are thought to have been discovered over the past few decades[3]. This estimate doesn't even take into account the venomous organisms yet to be discovered or studied.

A number of discovery techniques have evolved over the years to keep up with the ever-growing number of naturally produced bioactive compounds. One of those techniques heavily employed is assay-guided fractionation, which is the systematic isolation and characterization of bioactives from the mixture of peptides, proteins, small molecules, and salts present in venoms. The basic requirements of a functional assay include high sensitivity, accuracy, and reproducibility. This is especially important when dealing with unknown mixtures of crude venoms or partially purified fractions. A growing range of potential methods for functional assay are becoming more widely available. However, effective initial screens are still needed that are general enough discover an activity of interest (e.g., modulation of excitability) yet specific enough to discern a functional target (e.g., Na_V channels).

The purpose of this chapter was to develop a cell-based assay to search for Na_V channel modulators, capable of meeting all the basic requirements of a functional assay, including having enough capacity and throughput to handle large volumes of crude or fractionated venoms over short time scales. The first aim was to identify potential cell lines demonstrating expression of neuronal Na_V isoforms. After choosing three cell lines, they were carried forward for testing with two functional platforms using either absorbance or fluorescence detection, each measuring a different end-point demonstrating Na_V

channel function. Each assay shared a common theme of requiring an agonist control to elicit a Na_V response, which in turn could either be potentiated or inhibited upon addition to an unknown Na_V modulator within crude venom. The absorbance assay was based on an end-point of cell survival measured with the color changing metabolite, MTT. Reversal of induced cell death through inhibition of I_{Na} resulted in "rescuing" or reversal of Na^+ toxicity. The fluorescence based assays incorporated two fluorescent dyes: Fluo4 measured I_{Ca} as a product of Na_V depolarization while the other measured direct changed to membrane depolarization. The details of all assays are discussed at the end of the chapter.

Using assay methods developed herein, a previously unisolated δ-conotoxin was discovered, purified and sequenced.

2. Methods

2.1 Reagents

Veratridine was obtained from Ascent Scientific (Bristol, UK), tetrodotoxin (TTX) was from Enzo Life Sciences (Farmingdale, NY, USA). P-CTX-1 (Pacific ciguatoxin 1) was isolated and purified by members of the Lewis laboratory[360]. All other reagents including MTT, unless otherwise stated, were obtained from Sigma–Aldrich (Castle Hill, NSW, Australia). MTT stock solutions were made by dissolving the powder in PBS to 5 mg/ml. TTX, veratridine, deltamethrin, P-CTX-1, and all peptide toxins were routinely diluted in 0.3–0.5% bovine serum albumin (BSA) solution to avoid adsorption to plastic surfaces.

Dulbecco's Modified Eagle Medium (DMEM), RPMI Medium, Ham's F12 Medium, phosphate buffered saline (PBS), sodium pyruvate, and 0.25% trypsin/EDTA were obtained from Invitrogen (Australia). Fetal Bovine Serum (FBS) was obtained from Invivo Medical (NSW, Aus).

2.2 Cell culture

SH-SY5Y human neuroblastoma cells were a kind gift from Victor Diaz (Max Planck Institute for Experimental Medicine, Goettingen, Germany). Cells were routinely maintained in RPMI medium (Invitrogen, 22400) supplemented with 15% FBS and L-glutamine.

The Neuro2a rat neuroblastoma (ATCC-CCL131), F11 hybridoma of mouse neuroblastoma (N18TG-2) with embryonic rat DRG (ATCC-HB11761), NG108 hybridoma of a mouse neuroblastoma with a rat glioma (HB12317), and PC12 rat pheochromocytoma (ATCC-CRL1721) cell lines were obtained from the American Type Culture Collection (USA). Neuro2a and Ng108 cells were maintained in DMEM (Invitrogen, 11995) supplemented with 10% FBS. PC12 cells were maintained in Ham's F12 (Invitrogen, 11765) supplemented with 15% horse serum, 2.5% FBS, and 20 mM HEPES. F11 cells were maintained in Ham's F12 supplemented with 10% FBS and HAT.

The 50B11 rat immortalized DRG was a kind gift from Dr. Ahmet Höke (School of Medicine, Johns Hopkins University, MD, USA). Cell were routinely maintained in DMEM/F12 medium (Invitrogen, Carlsbad, CA) supplemented with 10% FBS, 0.5 mM L-Glutamine and 1x B-27 supplement (Invitrogen).

The ND7/23 hybridoma of mouse neuroblastoma (N18TG-2) with rat DRG and the ND7/23-rNa_V1.8 stably transfected cell line were kindly donated by Dr. Tony Priestley (Department of Chemical Research, Schering-Plough Research Institute, NJ, USA) [361]. Cells were routinely maintained in DMEM medium supplemented with 10% FBS. ND7/23-rNa_V1.8 cells were additionally cultured with 200 μg/mL Geneticin-G418 to maintain selection (Invitrogen).

All mammalian cell lines were passaged every 3-5 days at between 70-90% confluency using 0.25% trypsin/EDTA. Cells were incubated in a temperature, humidity, and CO_2 controlled incubator set to 37°C with 5% CO_2.

2.3 Semi-quantitative PCR methods

Primer pairs were designed with PrimerX (http://www.bioinformatics.org) using Na_V sequences acquired through BLAST (http://blast.ncbi.nlm.nih.gov) (Table 2**)**. Oligos were ordered through Sigma

(Australia)**.** Cells were cultured as previously described. Total RNA was isolated from cells using the Qiagen RNeasy Plus Mini Kit (Qiagen) according to the manufacturer's instructions with on-column DNA digestion. The Omniscript Reverse Transcription Kit (Qiagen) was used to reverse transcribe 1 µg of RNA, as determined by spectrophotometric absorbance at 260 nm, and 20 ng of the resulting cDNA was amplified using the Platinum® Pfx kit (Invitrogen). PCR reactions additionally contained final concentrations of 2× amplification buffer, 0.3 mM dNTP, 1 mM $MgCl_2$, 0.4 µM primers and 1 U Pfx polymerase in a volume of 50 µl and were amplified under the following conditions: 94°C for 5 min, 30 cycles of 94 for 15 s, 60-64 for 30 s, 68 for 1 min and a final extension at 68 for 10 min. Rodent Na_V primers were designed using Primer BLAST (Table 2). 100 ng of plasmid encoding for each $Na_V1.1$-1.8 verified amplification of the correct products for each subtype. All reaction products were analyzed on 2% agarose gels.

Table 2: Primer sets for murine Na_V channels

Target	Accession number	Primer pair sequence	Tm °	GC%	PCR product (bp)	Location (bp)
Nav1.1	NM_030875.1	5'-TCCTCAGAAGGAAGCACAGT-3' 5'-TCTGCACACAGCCTTCAGTG-3'	52.35 54.75	50.00% 55.00%	112	3702- 3813
Nav1.2	NM_012647.1	5'-GCCTGATTTGGGACTGTTGT-3' 5'-CCAAGCCGAGTTCCATTAAA-3'	52.54 50.26	50.00% 45.00%	315	2261-2575
Nav1.3	NM_013119.1	5'-GATTCGCGGGACGTCAAACT-3' 5'-GCAGAAACTCCCCAGTGAAG-3'	55.33 52.7	55.00% 55.00%	442	4548-4989
Nav1.4	NM_013178.1	5'-GCCTGAGGATATCAAGAAGC-3' 5'-TCAGAGTAGCCCAGCCAGTT-3'	49.96 54.57	50.00% 55.00%	525	3266-3790
Nav1.5	NM_013125.2	5'-ACAGGAATCCCAAGTTGTGT-3' 5'-ATCAGGAAGTCCAGCCAGCA-3'	51.02 55.22	45.00% 55.00%	606	3431- 4036
Nav1.6	NM_019266.2	5'-GGAGTGTCACCCCTACTGGA-3' 5'-TCAGAAGCAAGGCCAGGAAT-3'	54.29 53.34	60.00% 50.00%	734	2361-3094
Nav1.7	NM_133289.1	5'-CAACGCACTCATAGGAGCAA-3' 5'-GAATGTTGCAACTTGAAGCA-3'	52.55 49.71	50.00% 40.00%	283	3927-4209
Nav1.8	NM_017247.1	5'-CTGGCTGGACTTCAGTGTCA-3' 5'-GGAACACACTGCCGTGGCTA-3'	53.77 56.91	55.00% 60.00%	944	605-1548

2.4 Specimen collection

Conus spp. were collected from various locations throughout the Great Barrier Reef on the East coast of Australia and on the New Ireland Island group, Papua New Guinea [319]. *C. magus* was collected from intertidal zones on Lizard Island, Australia.

Specimens were transported to the lab either on ice to be frozen whole at -80°C for dissection or kept alive in seawater for milking and genomic analysis.

2.5 Venom extraction

Two separate rounds of venom extraction were each performed on single species of *C. magus*. Crude venom duct contents were extracted with 30% acetonitrile/water acidified with 0.1% trifluoroacetic acid and centrifuged at 13,000 rpm for 20 minutes. The pellets were washed several times and re-centrifuged under identical conditions. Soluble material was lyophilized and stored at -20°C prior to use. Crude venom pellets were stored separately at -20°C. After venom was removed from the duct sheath manually the remaining duct and bulb were stored at -80°C in RNAlater (Qiagen).

2.6 Reversed phase high-performance liquid chromatography (rpHPLC)

rpHPLC was performed on 200 μg of a 500 μg crude *C. magus* venom sample using a Dionex Ultimate 3000 instrument and fitted with a Vydac C18 column (218TP54; 4.6 × 250 mm; 5 μm particle diameter; 300 Å pore size) with automated fraction collection. Peptides were eluted with a flow rate of 0.7 mL/min using a 1.5% B/min linear gradient buffer exchange over 60 min using buffers A (H20, 0.1% FA) and B (90% ACN, 10% H20, 0.1% FA). Further peptide purification was carried out by second rpHPLC run of fractions under equivalent conditions with slight variations to the gradient. rpHPLC fractions were collected at 1 min intervals by a 96-well autosampler. After purification, all samples were lyophilized and resuspended in 30% acetonitrile/water for storage at -20°C and further analysis.

2.7 Mass and sequence determination

Toxin masses were confirmed by matrix-assisted laser desorption ionization–time-of-flight mass spectrometry (MALDI-TOF MS) using a model 4700 Proteomics Bioanalyser (Applied Biosystems, Foster City, CA). rpHPLC fractions were mixed [1:1 (v/v)] with α-cyano-4-hydroxy-cinnamic acid matrix (7.5 mg/ml in 70/30 acetonitrile/H2O) and MALDI-TOF spectra were collected in positive reflector mode. The mass range was set to *m/z* 800-8000 with a focus mass of 4500 Da. Shots were collected using manual acquisition control and close external calibration. The calculated molecular weights were obtained using Data Explorer (Applied Biosystems, CA). All masses given are for the monoisotopic $M+H^+$ ions unless otherwise stated.

The sequence of purified peptide was determined by Edman degradation at the Australian Proteome Research Facility. In brief, the peptide was dissolved in urea (4 M) in ammonium bicarbonate (50 mM) and reduced with dithiothreitol (100 mM) at 56 °C for 1 h under argon. The sample was then alkylated using acrylamide (220 mM) for 0.5 h in the dark. The reaction was quenched by the addition of excess dithiothreitol. After desalting by rpHPLC, the collected fraction was loaded onto pre-cycled bioprene discs and subjected to 35 cycles of Edman N-terminal sequencing using an Applied Biosystems 494 Procise Protein Sequencing System.

2.8 Na^+ induced toxicity and measurement of survival by MTT

Neuro2a and ND7/23 cells were plated at a density of 30-50 x 10^3 cells/well on 96-well clear imaging plates (Corning) 24 h prior to assay. SH-SY5Y cells were plated at a density of 120 x 10^3 cells/well on 96-well black-walled imaging plates (Corning) 48 h prior to assay. All cells plated in 90 µl standard growth media in 96-well flat bottom microtiter plates (Corning). Cells were treated after 24 h incubation to allow settling, attachment, and the start of normal cell division. Ouabain, veratridine, and control toxins were all added at this step with no pre-incubation. Unlike the FLIPR assay, which measures fast responses to compound addition, the long compound incubation times inherent to cell survival assays meant that pre-incubation of a control agonist/antagonist would not likely influence the end point measurement of cell survival in a meaningful way, as the lethal effect of Na^+ toxicity takes up to 24 h to observe. Ouabain and veratridine were diluted in unsupplemented DMEM to a single 10x stock. Samples to be tested, including all positive and negative controls, were diluted to a 5x working

concentration in unsupplemented DMEM. In the absence of control toxins, unsupplemented DMEM with appropriate buffer controls was added.

To determine the maximum survival for each experiment, 60 µl of unsupplemented DMEM was added to a minimum of 4 wells per plate. To determine a maximal effect of control compounds on survivability, 30 µl of unsupplemented DMEM was added along with ouabain and veratridine to a minimum of 4 wells per plate.

Treated microtiter plates were incubated with reagents for 48 h at 37°C with 5% CO_2. After incubation, media was removed from microtiter plates and 60 µl of MTT was added to each well. Prior to addition, MTT was diluted 1:6 in unsupplemented DMEM. Plates were then incubated for 30 min at 37°C with 5% CO_2. After 30 min incubation, MTT solution was gently removed from each well and cells were solubilized with 60 µl DMSO. Absorbance at 580 nm was measured by the PerkinElmer Envision 2104 microtiter plate reader.

2.9 Fluorescence measurement of membrane potential changes

To assess changes in membrane potential, SH-SY5Y cells were loaded with the red membrane potential dye (Molecular Devices, Sunnyvale, CA) according to the manufacturer's instructions. In brief, red membrane potential dye (proprietary composition) was reconstituted with a volume of physiological salt solution (PSS; composition in mM: NaCl 140, glucose 11.5, KCl 5.9, $MgCl_2$ 1.4, NaH_2PO_4 1.2, $NaHCO_3$ 5, $CaCl_2$ 1.8, HEPES 10) as specified in the manufacturer's instructions and after a wash with PSS, cells were incubated with 100 µl of the membrane potential solution at 37˚C for 30 min. The cells were then transferred to the FLIPR^{TETRA} fluorescent plate reader and changes in fluorescence (excitation 510–545 nm; emission 565–625 nm) in response to addition of agonists was measured every second for 300 s.

2.10 Fluorescence measurement of calcium responses

SH-SY5Y cells were loaded with the fluorescent calcium dye Fluo-4 acetoxymethyl ester (AM) by incubating the cells in PSS containing 0.3% bovine serum albumin and 4 mM Fluo-4-AM (Invitrogen) for 30 min at 37°C. To remove extracellular dye and facilitate dye hydrolysis, cells were washed with

PSS for 5–15 min prior to loading of plates into the FLIPR^{TETRA+} (Molecular Devices, Sunnyvale, CA) fluorescent plate reader. Fluorescence (excitation 470–495 nm; emission 515–575 nm) was measured using a cooled charge-coupled device (CCD) camera with camera gain and excitation intensity adjusted for each plate to yield an average baseline fluorescence value of 1000 AFU. After 10 baseline reads, buffer or control antagonists were added and the fluorescence response was measured every second for 300 reads, followed by addition of agonists and fluorescence measurements every second for a further 300 s. Raw fluorescence readings were converted to response over baseline using the analysis tool of Screenworks 3.1.1.4 (Molecular Devices) and were expressed relative to the maximum increase in fluorescence of control responses.

2.11 Z' factor determination of assay robustness

The Z' factor, a quantitative representation of assay quality, was determined as previously described[362], with 48 replicates of a negative control (PSS) and 48 replicates of positive controls (50 μM veratridine) per plate. Mean and standard deviation for positive and negative controls were determined using GraphPad Prism v4.0 (San Diego, California) and the Z' factor for each plate determined according to the following equation:

$$Z' = 1 - ((3SD_{positive} + 3SD_{negative})/(mean_{positive} - mean_{negative}))$$

2.12 Data analysis

Unless otherwise stated, all data are expressed as the mean ± standard error of the mean (SEM) determined from at least $n = 3$ experimental replicates, with 2-4 replicates per plate. To establish concentration-response curves, responses after addition of compounds were plotted against agonist concentration and a 4-parameter Hill equation with variable Hill slope or a two-site model was fitted to the data using GraphPad Prism v4.0. Potency of agonists and antagonists are reported as the mean ± SEM of 3-4 separate experiments. Statistical significance was determined using an ANOVA analysis with statistical significance defined as $p < 0.05$ unless otherwise stated.

Unless otherwise stated, all data are expressed as the mean ± standard error of the mean (SEM) determined from at least $n = 3$experimental replicates, with 2-4 replicates per plate. Positive absorbance as compared to the treated control is attributed to cell survival, or the ability of a Na_V channel inhibitor

to reverse the induced toxic effect. The percent recovery from ouabain and veratridine (O/V) treatment was calculated by the following equation:

$$\% \text{ Recovery} = \frac{\text{(avg. test wells treated with O/V) - (avg. cont. wells treated with O/V)}}{\text{(avg. untreated cont. wells) - (avg. cont. wells treated with O/V)}}$$

Additive cell death as compared to the control is indicative of a possible Na_V channel agonist and is measured by a decrease in absorbance. This was calculated by the following equation:

$$\% \text{ Inhibition} = \frac{\text{(avg. test wells treated with O/V) - (avg. cont. wells treated with O/V)}}{\text{(avg. cont. wells treated w/ O/V)}}$$

All above calculations including standard error from the mean (SEM) were performed using GraphPad Prism 4.0. To establish concentration-response curves, responses after addition of compounds were plotted against the log of sample concentrations and a least squares fit 4-parameter Hill equation with variable Hill slope fit to the data using GraphPad Prism 4.0. Statistical significance was determined using an ANOVA analysis with statistical significance defined as $p < 0.05$ unless otherwise stated.

3. Results

3.1 Expression profiles of commonly used neuronal cell lines

Seven neuronal derived cell lines were characterized by an initial PCR screen using primers designed to specific regions of the rat Na_V isoform of interest. SH-SY5Y was also tested along with this pool of cells with the knowledge that it is a human derived cell line and would need specific primers developed, which was completed and published in a collaborative follow-up project[363].

PCR results suggested prevalent expression of $Na_V1.2$ in all cell lines tested, with only a slight band apparent for 50B11 cells (Figure 6). $Na_V1.6$ and $Na_V1.7$ demonstrated a similar expression profile to each other, with bands for both isoforms apparent in the same cell lines. However, there did not seem to be correlation between cell line origin and expression pattern. There was a surprising lack of $Na_V1.8$

expression, which is found prevalently in DRG neurons. The centrally expressed $Na_V1.1$, peripherally expressed $Na_V1.3$, and skeletal muscle isoform $Na_V1.4$ were also absent in all experiments. $Na_V1.5$ appeared to be expressed in three cell lines. All results were replicated with at least three separate experiments. However, the PCR was not performed in a quantitative manner, so not further conclusions on relative expression or receptor density could be made.

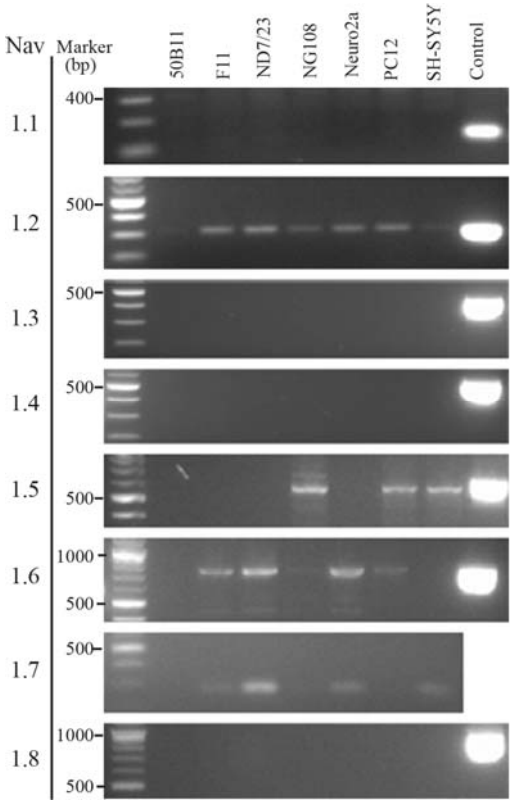

Figure 6: Agarose gel of Na_V channel PCR. *Control lanes use 1 ng of pcDNA3.1 vector containing the Na_V gene of interest. No $Na_V1.7$ control vector was available at the time of the experiment.*

3.2 MTT Results for ND7/23-$Na_V1.8$

The MTT survival assay platform was tested on the stably transfected ND7/23-r$Na_V1.8$ cell line. Veratridine does not affect TTXr Na_V channels, which includes $Na_V1.8$. However, the pyrethroid deltamethrin has been shown to inhibit inactivation of $Na_V1.8$, causing sustained activation similar to veratridine [364, 365]. Therefore, deltamethrin was used in place of veratridine in the presence of 1 μM TTX, to block the contribution of TTXs sodium channels[366, 367].

Deltamethrin showed no toxicity at concentrations tested up to 30 μM (Figure 7). The LD_{50} of deltamethrin in the presence of 300 μM ouabain was 4.8 ± 2.8 μM, with a 100-fold drop in potency in the presence of 300 nM ouabain, suggesting a Na^+ induced toxicity (Figure 7). The addition of 100 nM TTX did not affect the results of the deltamethrin induced toxicity in the presence of 300 μM ouabain (Figure 8). This confirms TTXs Na_V channels are not contributing to the observed toxic effect. Non-transfected ND7/23 cells were tested under similar conditions and were unaffected by treatment up to

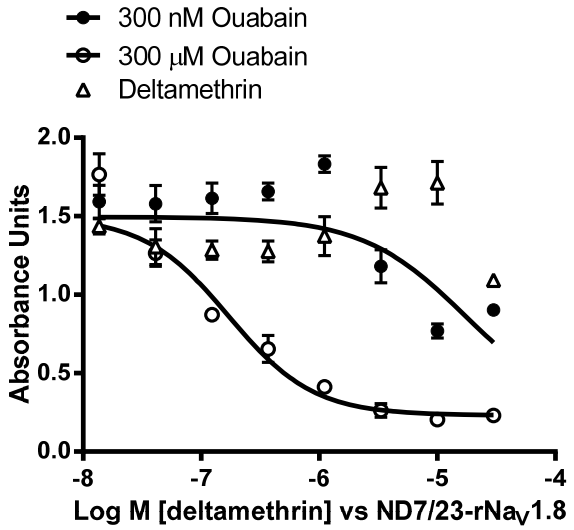

Figure 7: Deltamethrin concentration response on ND7/23-rNa$_V$1.8 cell line.

Deltamethrin alone (black) did not induce lethality. Deltamethrin in the presence of 300 μM ouabain (○) *induced lethality in a concentration dependant manner. Reducing ouabain to 300 nM* (●) *resulted in a 100-fold shift to the right in deltamethrin toxicity.*

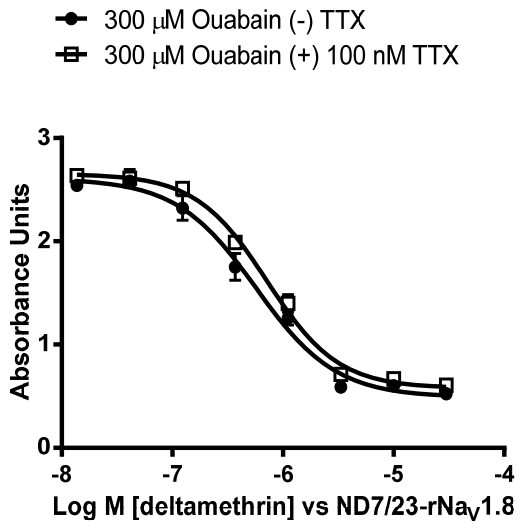

Figure 8: Concentration response of deltamethrin on ND7/23-rNa$_V$1.8 with TTX.

300μM ouabain is present. There is a lack of contribution to TTXs Na$_V$ channels to deltamethrin induced lethality.

30 μM deltamethrin, suggesting that the Na$_V$1.8 channel is playing a significant role in cell death from Na^+ toxicity (Figure 9).

P-CTX1 was also tested as an agonist in place of deltamethrin on the ND7/23-rNa$_V$1.8 cell line in the presence of TTX (Figure 10). Not only was an attempt made to look at different agonist mechanisms on cell toxicity, but results suggest P-CTX1 may activate Na$_V$1.8[368]. However, our results suggested that toxicity increased with higher levels of ouabain in combination with P-CTX1 without a concentration dependant effect of P-CTX1, which suggested a non-Na$_V$ induced mechanism of toxicity as well as no observable effect for Na$_V$1.8 induced toxicity.

In order to test for reversal of induced toxicity, concentrations of 300 μM ouabain and 30 μM deltamethrin were chosen. In order to recover the cells from Na^+ induced toxicity, two $Na_V1.8$ inhibitors were used at pharmacologically relevant concentrations. Lidocaine is a use-dependant inhibitor of $Na_V1.8$ and works by shifting the steady-state activation toward more depolarized potentials[369]. The same ND7/23-r$Na_V1.8$ cell line was previously used to determine the use dependence of lidocaine, further justifying its use as a control inhibitor[370]. Additionally, the μO conotoxin MrVIB has been shown to inhibit $Na_V1.8$ current with IC_{50} values of 100 nM[371]. This conopeptide represents a major and consistent component of *C. marmoreus* venom, with a distinctive peak that elutes consistently and yields an identifiable mass signature via MALDI MS. MrVIB was discovered through use of a bioassay, exhibiting the most potent Na_V modulating activity apparent within the crude venom of *C. marmoreus*[372, 373]. Due to the extreme hydrophobicity of MrVIB, up

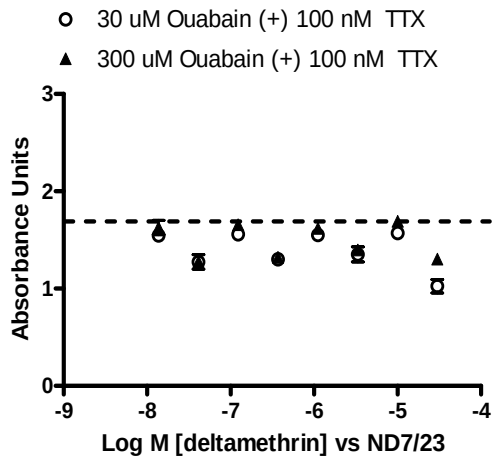

Figure 9: Untransfected ND7/23 cells.
Tested under equivalent conditions to ND7/23-r$Na_V1.8$, these cells demonstrated no significant effect on survival, suggesting $Na_V1.8$ is the sole Na_V contributor to the observed lethality.

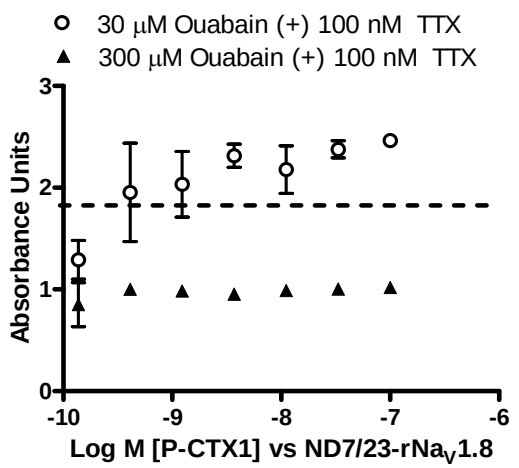

Figure 10: Concentration response of P-CTX on ND7/23-r$Na_V1.8$ cells.
P-CTX in combination with ouabain resulted in no measurable lethality, suggesting this molecule does not affect $Na_V1.8$ at the conditions used. Dotted line represents the average absorbance of untreated controls.

to 80% of the expected mass is lost upon purification from crude venom. As no synthetic material and only a small amount of crude venom was available at the time of this experiment, it was decided to use a known active concentration of the whole venom. Therefore, 5 μg of crude *C. marmoreus* venom was used to test inhibition of $Na_V1.8$ in the presence of 100 nM TTX (Figure 11).

Neither lidocaine nor *C. marmoreus* crude venom resulted in cell death on their own (Figure 11). As lidocaine was incubated for 48 h, it is unlikely that the lack of effect seen was due to slow onset. Use-dependence could be a factor in limiting activity. However, evidence has demonstrated in a similar

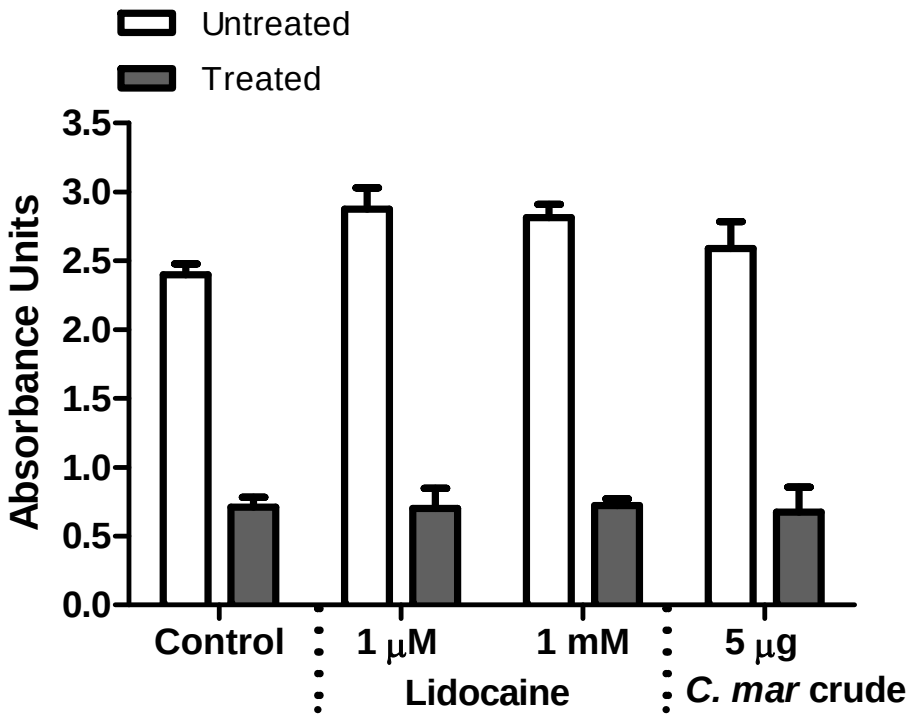

Figure 11: Reversal of induced Na^+ tox on ND7/23-r$Na_V1.8$ cells.

Control represents maximum survival for untreated (light) and treated cells (dark). The addition of lidocaine at 1 μM and 1 mM does not affect cell survival when added alone (light). However, lidocaine does not result in a reversal of induced Na^+ toxicity (dark). The addition of 5 μg of C. marmoreus crude venom containing MrVIB also does not result in reversal of induced Na^+ toxicity.

assay that compounds bind to the Na_V channel in a manner comparable to the inactivated state, which exhibits an open conformation at the pore[374]. As lidocaine preferentially binds to a depolarized Na_V channel (closer to the open state)[375, 376], then is can be inferred that the use-dependence of lidocaine was not a factor in its lack of activity for this assay.

There was also no recovery from induced toxicity by treatment with either lidocaine or MrVIB, both known to block $Na_V1.8$ channels (Figure 11). The question remains why there was no recovery from agonist induced toxicity by known $Na_V1.8$ blockers. It is possible that deltamethrin binds competitively and preferentially versus both lidocaine and MrVIB. The results could also be attributed to off target effects, as deltamethrin and lidocaine are non-selective ligands, as will be discussed.

3.3 MTT results for Neuro2a and SH-SY5Y

The Neuro2a rat neuroblastoma cell line was chosen as a model for this assay due to its successful use on a similar assay platform[377]. Basic PCR analysis also suggested expression of $Na_V1.2$, $Na_V1.6$ and $Na_V1.7$, of which $Na_V1.7$ is currently a pursued target for the treatment of neuropathic pain.

Methods described previously incorporating both ouabain and veratridine were used to assess viability and responsiveness to the drug combination for Neuro2a cells. A concentration dependent lethality was observed with veratridine in the presence of ouabain at 100 µM and 300 µM (Figure 12). Although both concentrations of ouabain allowed a comparable veratridine IC_{50}, 300 µM ouabain resulted in a decrease of cell survival by 50%. This in turn lowers the effective window by an equivalent amount.

Concentrations of 100 µM veratridine and 100 µM ouabain were used to test the effect of the Na_V channel inhibitor TTX on preventing induced Na^+ toxicity. Recovery from induced Na^+ toxicity was observed with 30 nM concentrations of TTX (Figure 13A). TTXs Na_V channels exhibit an IC_{50} of around 10 nM[18]. To observe agonist synergy with control toxins, the concentration of veratridine was lowered to 30 µM in order to stimulate a lowered but measurable lethality. The Na_V neurotoxin site 5 agonist brevetoxin (PbTX1) was used as a positive Na_V agonist control[378]. PbTX1 was tested on its own and induced no lethality up to 1 nM. However, this same concentration induced an apparent synergistic lethality when tested in combination with ouabain and veratridine, demonstrating synergistic agonist induction of Na^+ toxicity (Figure 13B).

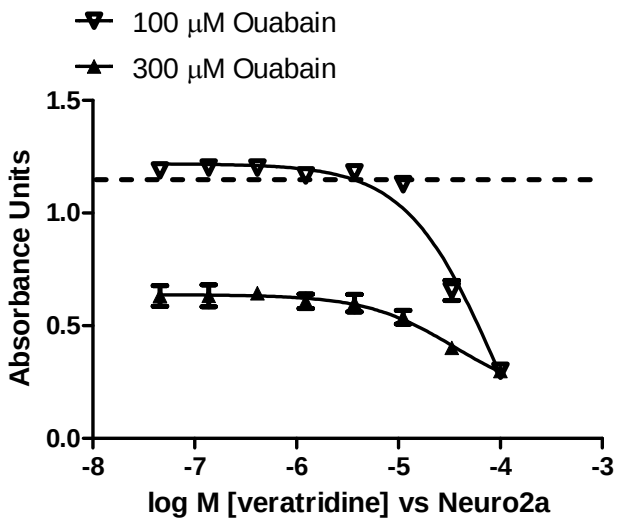

Figure 12: Concentration response of veratridine on Neuro2a cells.

A concentration response of veratridine was tested over both 300 μM and 100 μM ouabain. Although both concentrations of ouabain allowed a similar IC_{50}, 300 μM ouabain decreased cell survival by approximately 50%.

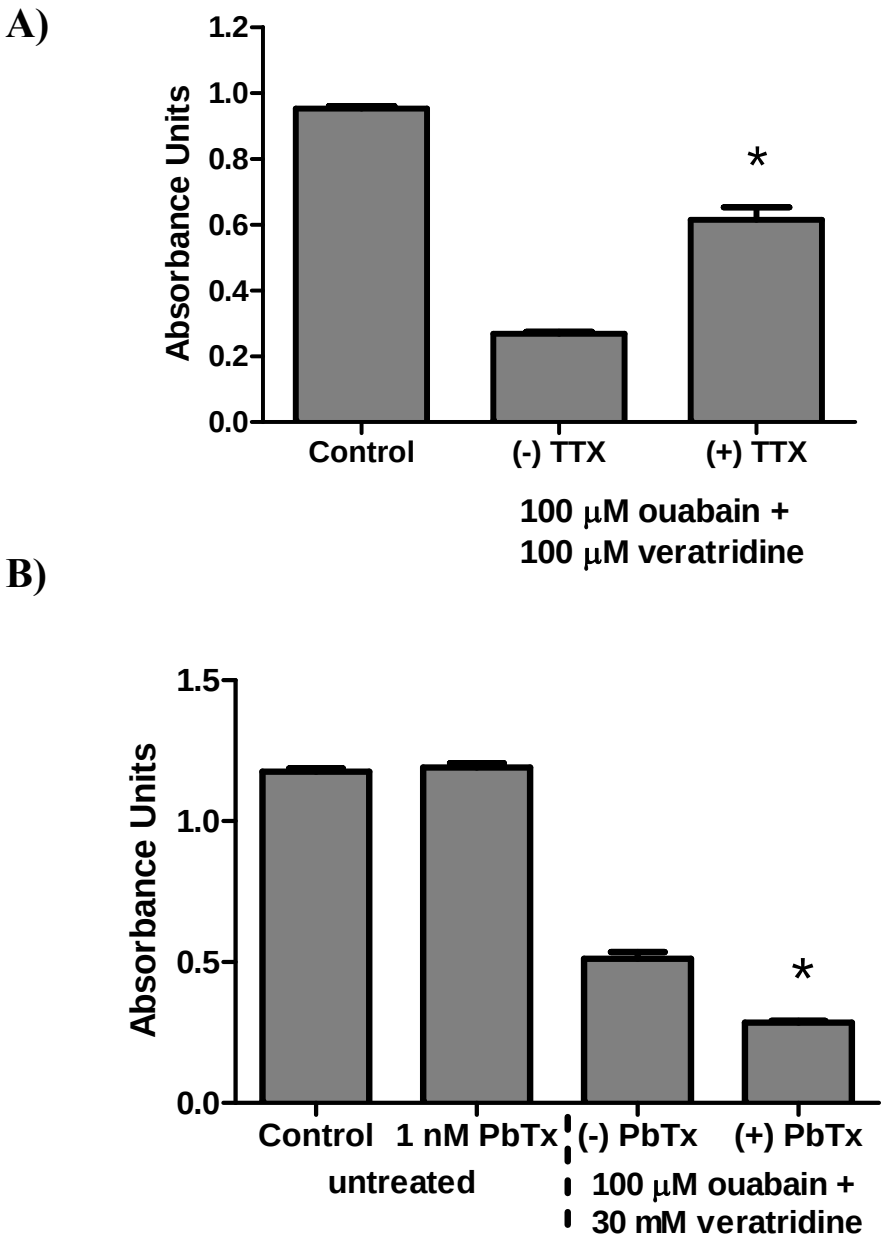

Figure 13: Neuro2a MTT assay validation.

A) The addition of 30 nM TTX inhibits the lethal combination of 100 μM veratridine and 100 μM ouabain. B) 1 nM PbTX does not affect cell survival on untreated cells. However, in combination with 30 μM veratridine and 100 μM ouabain, 1 nM PbTX decreased cell survival by an additional 20%, demonstrating a possible synergistic effect. Asterisk indicates significance as compared to ouabain and veratridine treated wells ($p < 0.05$).

The SH-SY5Y human neuroblastoma cell line was also chosen as a model for this assay because of the expression profile of Na_V channels relevant to pain transmission as well as this cell lines human origin, which is important when screening for human therapeutic relevance. In depth analysis of this cell line was performed using human specific PCR primers, functional characterization, and immunohistochemistry and results were subsequently published[363].

Assay conditions were described previously. Ouabain induced lethality at concentrations above 100 nM (Figure 15). However, lower concentrations of ouabain were not used as the effect on the Na^+/K^+-ATPase reverses at low nM concentrations. A concentration dependent lethality was observed with veratridine in the presence of 300 nM ouabain (Figure 14).

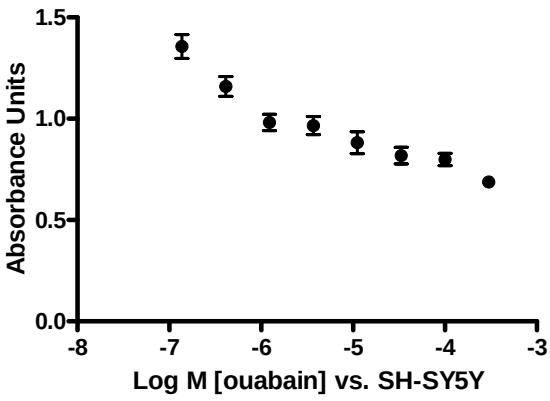

Figure 15: Lethal concentration response of ouabain on SH-SY5Y cells.

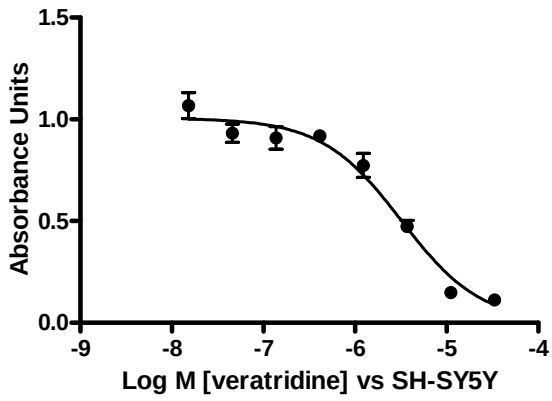

Figure 14: Lethal concentration response of veratridine on SH-SY5Y cells.

Response measure with addition of 300 nM ouabain. The LD_{50} for veratridine over a background of 300 nM ouabain was 3 ± 0.4 μM; n = 3.

To test the reversal of the induced toxic effect of ouabain and veratridine, two Na_V channel inhibitors were used at pharmacologically relevant concentrations (Figure 16). In the presence of 20 μM veratridine and 300 nM ouabain, cell survival decreased by approximately 80%. The addition of 10 mM lidocaine or 1 μM TTX both inhibited the toxic effect by almost 50%, demonstrating the ability of this assay to detect Na_V channel inhibitors. The MTT based assay using Neuro2a and SH-SY5Y has not been used to screen crude venom in a high throughput manner. However, this assay has the potential to serve as another screening platform to guide identification of novel peptides.

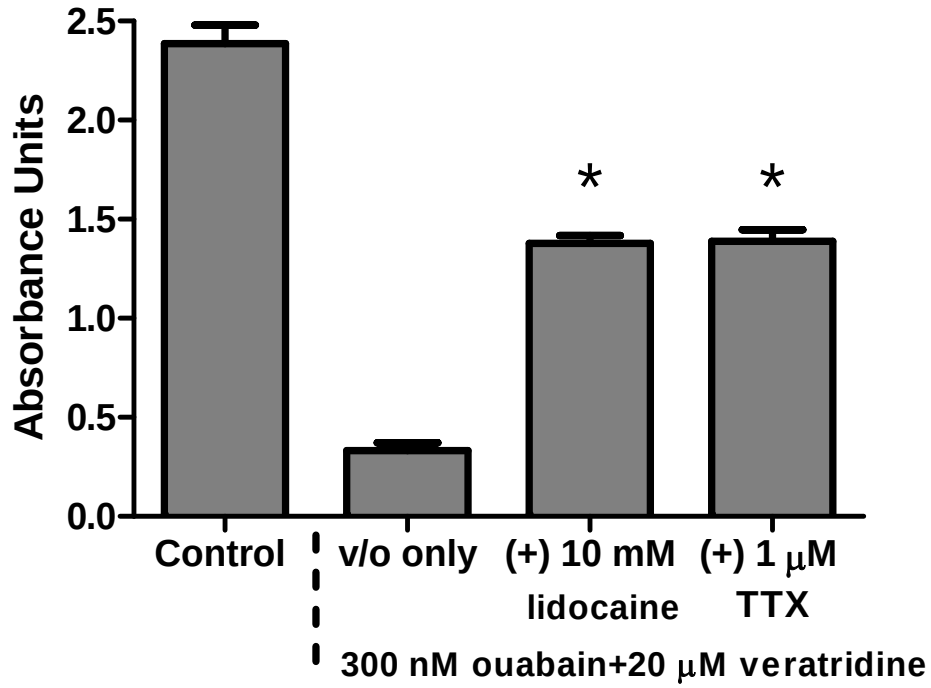

Figure 16: SH-SY5Y recovery from induce Na^+ toxicity.

Control represents maximum survival for untreated SH-SH5Y cells. 200 μM of veratridine with 300 nM ouabain resulted in a decrease in survival by approximately 90% compared to control. The addition of 10 μM lidocaine or 1 μM TTX in combination with ouabain and veratridine resulted in inhibition of induced Na^+ toxicity. Asterisks indicate significant recovery from ouabain/veratridine induced toxicity ($p < 0.05$)

3.4 FLIPR assay results and assay validation

The Neuro2a, ND7/23, and SH-SY5Y immortalized cell lines adapted for the MTT assay format were tested for total agonist-induced fluorescent response with two fluorescent dyes: Fluo4 AM (Figure 17A), which monitors Ca+ flux as an endpoint; and the Molecular Devices Membrane Potential Assay Kit (MP-kit) (Figure 17B), which measures ionic changes in a cells resting membrane potential. 1 mM veratridine was used as a control agonist for all experiments. Neuro2a cells did not yield a significant response upon addition of veratridine when loaded with Fluo4. However, these cells did result in a small but measurable response with the MP-kit, which was inhibited in the presence of 100 nM TTX. ND7/23 cells loaded both Fluo4 and the MP-kit and elicited a TTXs veratridine response, but with total responses lower than the positive response for Neuro2a. SH-SY5Y cells demonstrated an ability to load both Fluo4 and the Membrane Potential dye, as well as yield the largest total response of all cells tested to veratridine stimulation. The SH-SY5Y fluorescent response for the Membrane Potential dye was approximately half that of Fluo4. Overall, it was determined that SH-SY5Y cells yielded the greatest overall veratridine induced fluorescence response, which is directly applicable to the observable window of efficacy, or Z-score, for determining activity of unknowns. Veratridine was also able to elicit a concentration-dependent response from SH-SY5Y cells loaded with Fluo4 (Figure 18). This data resulted in SH-SY5Y cells being subjected to further, in depth characterization of Na_V α- and β-subunits as well as validating this cell line for use in a FLIPR-based Fluo4 assay with a number of control compounds[363].

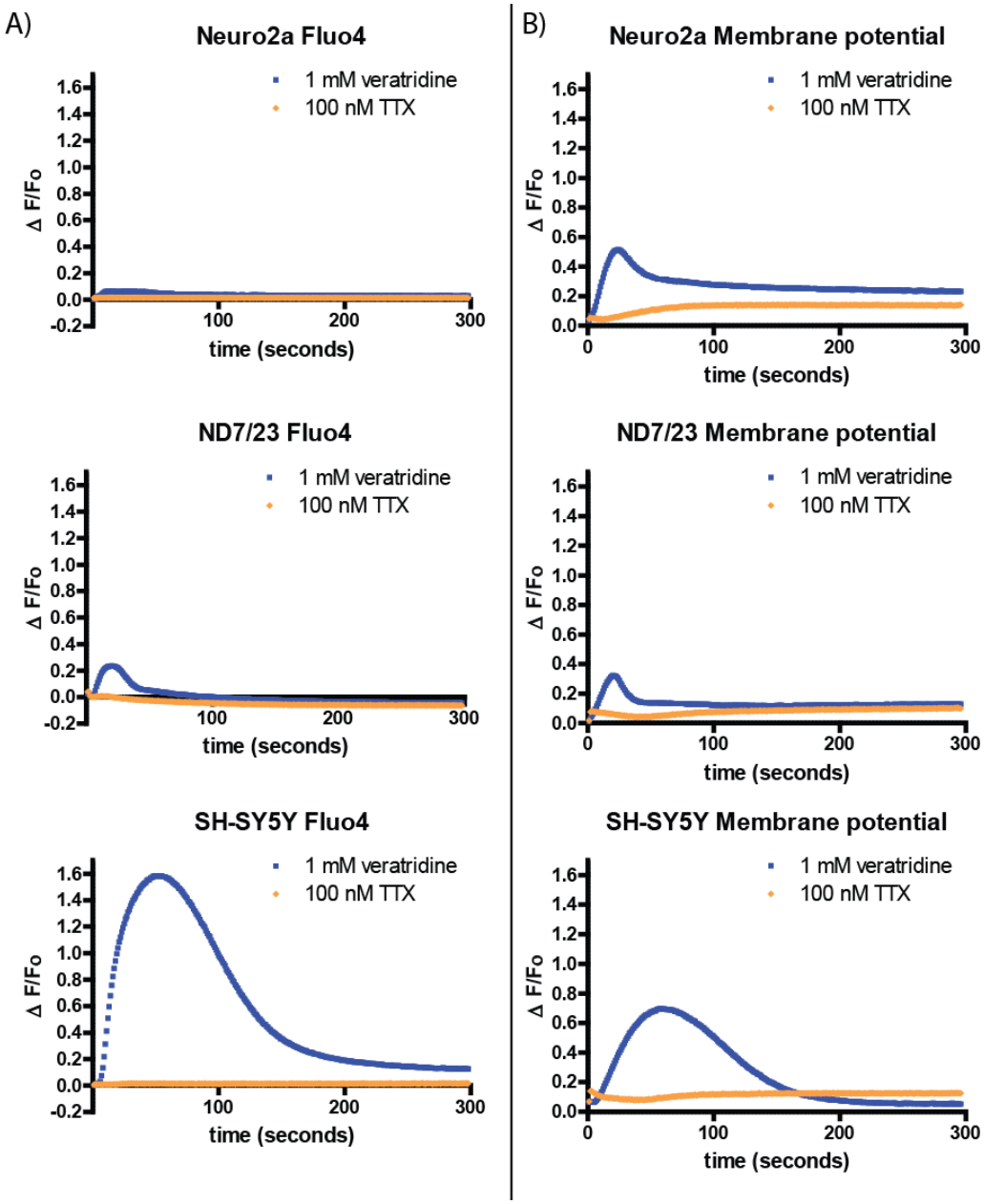

Figure 17: Cell line comparison of veratridine response with two fluorescent dyes.

Three cell lines were loaded with either A) Fluo4 or B) the Membrane Potential Kit. Maximal response was elicited with 1 mM veratridine. The presence of 100 nM TTX demonstrates a Na_V mediated response.

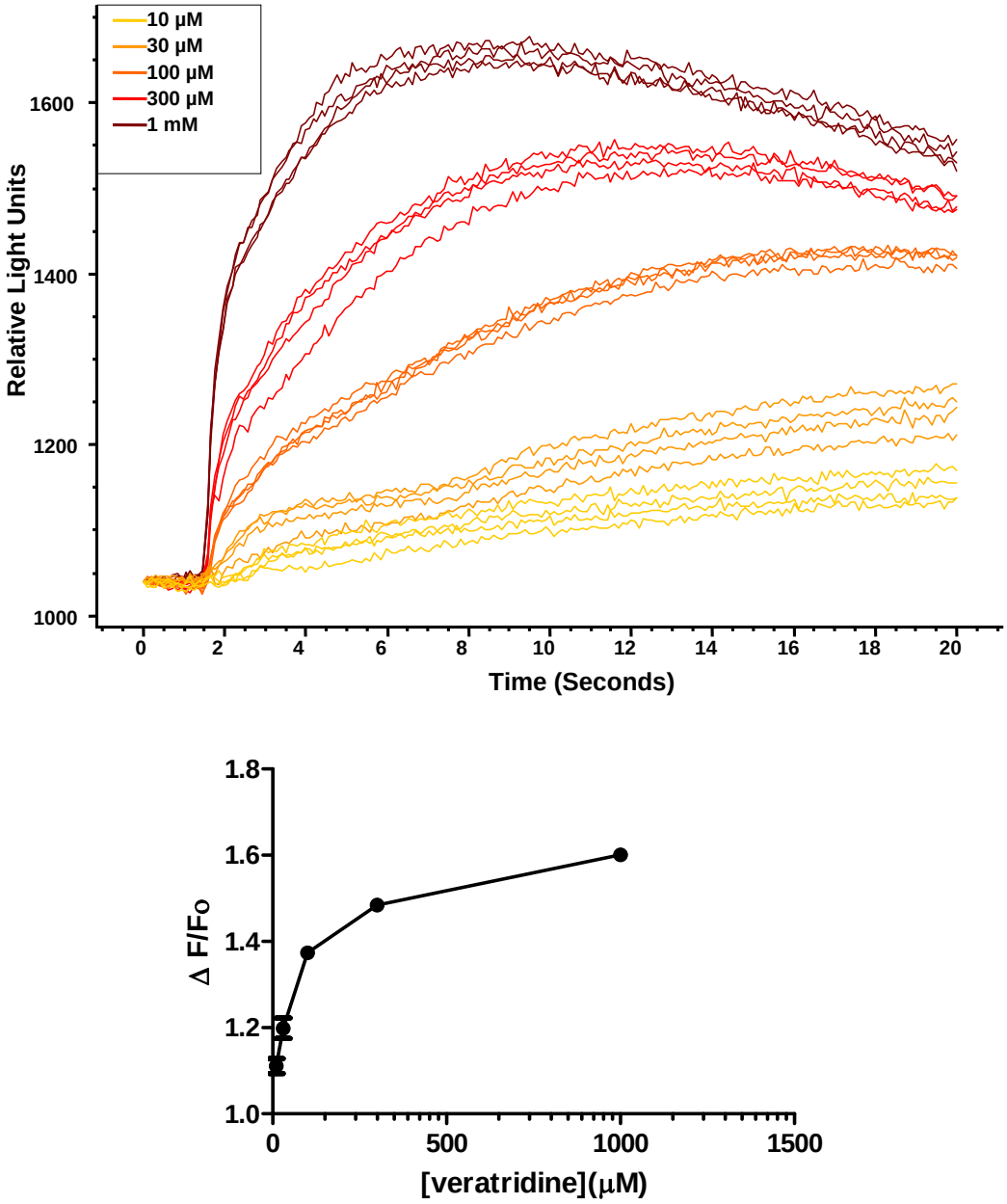

Figure 18: Veratridine concentration response using SH-SY5Y cells loaded with Fluo4.

Maximal response could be elicited with 1 mM veratridine.

3.5 Activity guided isolation of δ-MVIA

A FLIPR screen of *Conus* crude venoms tested in duplicate was conducted using SH-SY5Y cells with Fluo4. The wells containing C. magus demonstrated both excitation and potentiation of the veratridine control response (Figure 19). Initial analysis of *C. magus* crude venom demonstrated concentration dependant agonist activity when tested against SH-SY5Y cells loaded with Fluo4 (Figure 20). Potentiation of the fluorescent response for both agonists controls, veratridine and ciguatoxin (P-CTX1), was also observed. This response was inhibited with the addition of 1 µM TTX, demonstrating a Na_V channel mediated response.

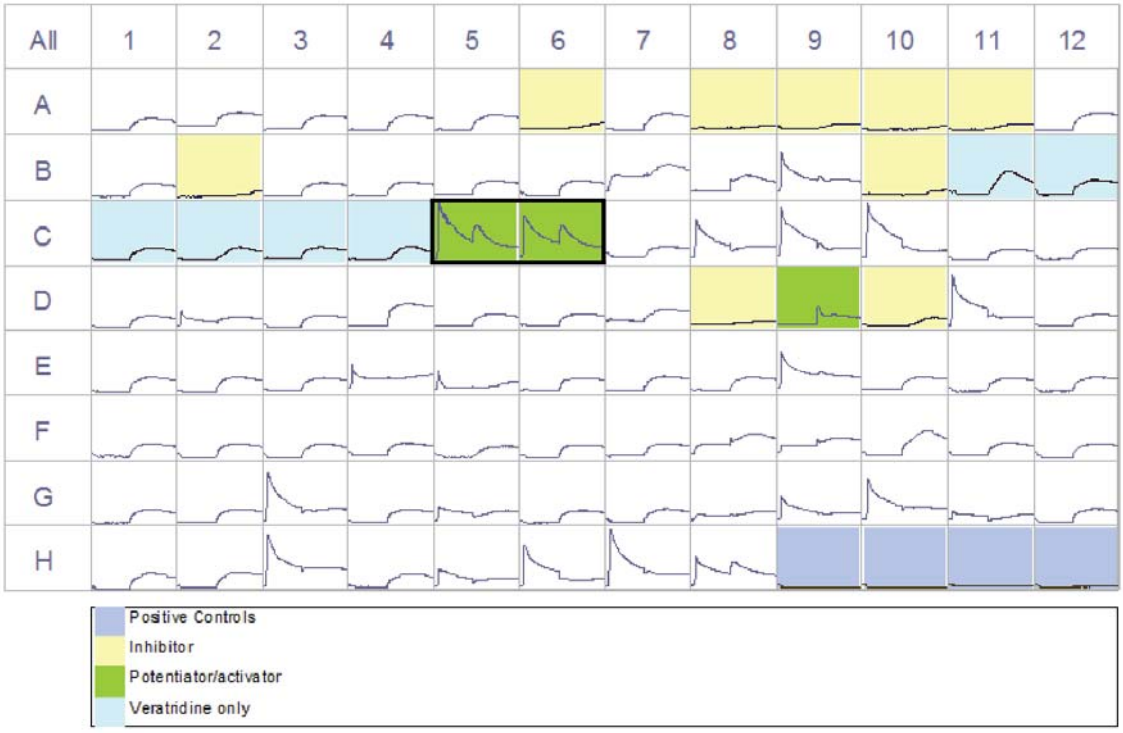

Figure 19: FLIPR screen of Conus crude venoms. *C. magus is outlined in black.*

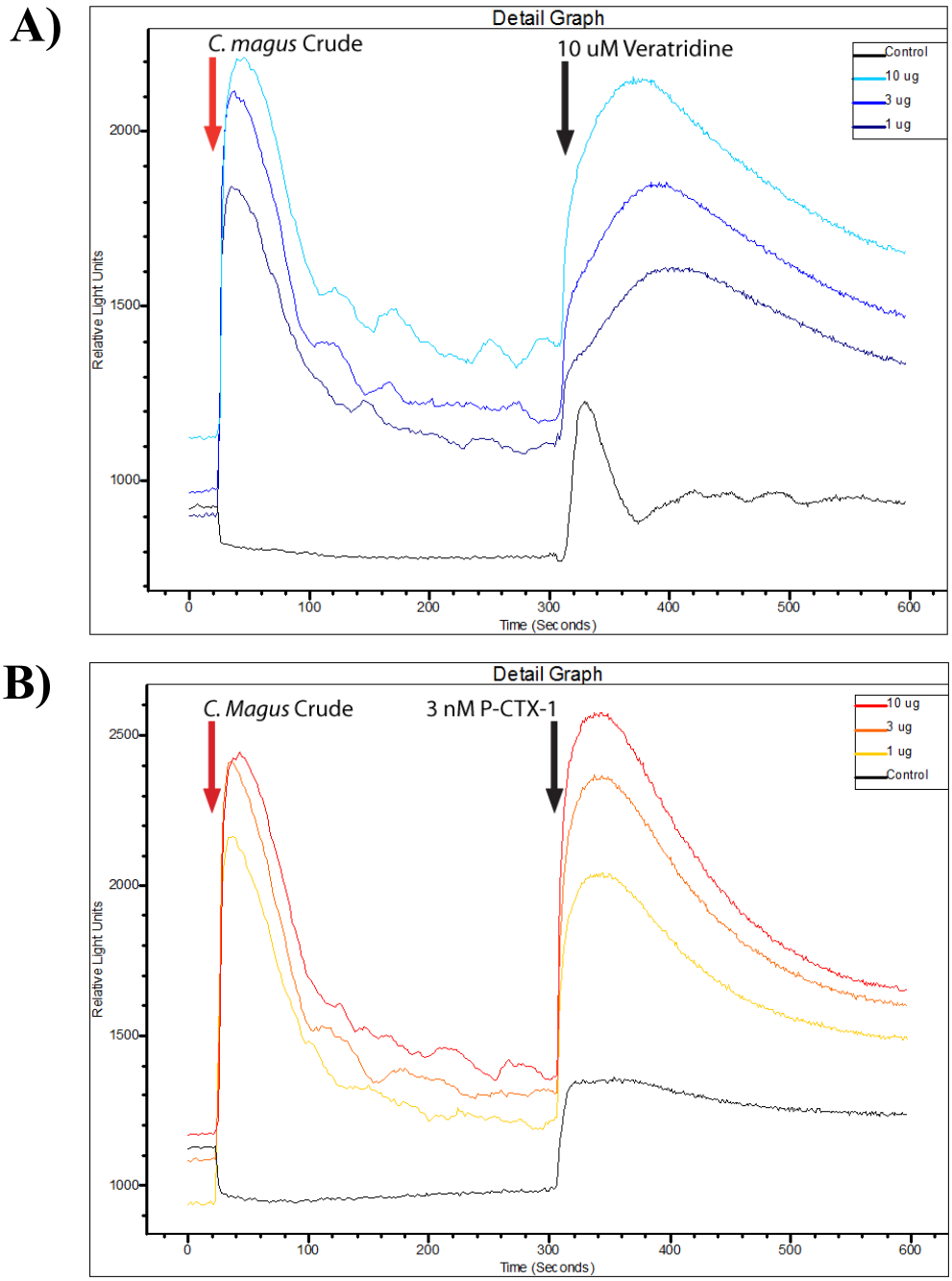

Figure 20: Concentration dependence of *C. magus* crude venom on SH-SY5Y cells.

Measured on the FLIPR with Fluo4. Crude venom was added at the solid red arrow. The dotted arrow represents the 2nd addition of agonist control A) veratridine or B) P-CTX1.

The crude venom was subject to analytical rpHPLC with fractions collected by autosampler, lyophilized, and resuspended at an equivalent volume of 100 µL. 10% volume of each fraction was tested for activity after reconstitution in PSS (composition in mM: NaCl 140, glucose 11.5, KCl 5.9, $MgCl_2$ 1.4, NaH_2PO_4 1.2, $NaHCO_3$ 5, $CaCl_2$ 1.8, HEPES 10). Fractions were added as a primary addition to corresponding wells of a 96-well microtiter cell plate containing SH-SY5Y cells. The FLIPR^{TETRA} assay was carried out as previously described. Late eluting fractions demonstrated activity along consecutive wells corresponding to minute 45-50 (Figure 21). The discrepancy of well number and time was caused by a noted 7 minute early startup of the fraction collector plus a standard one minute lag due to travel from the detector to the collector. The active fractions from wells 55 and 56 were pooled, freeze dried, and resuspended in 30% B.

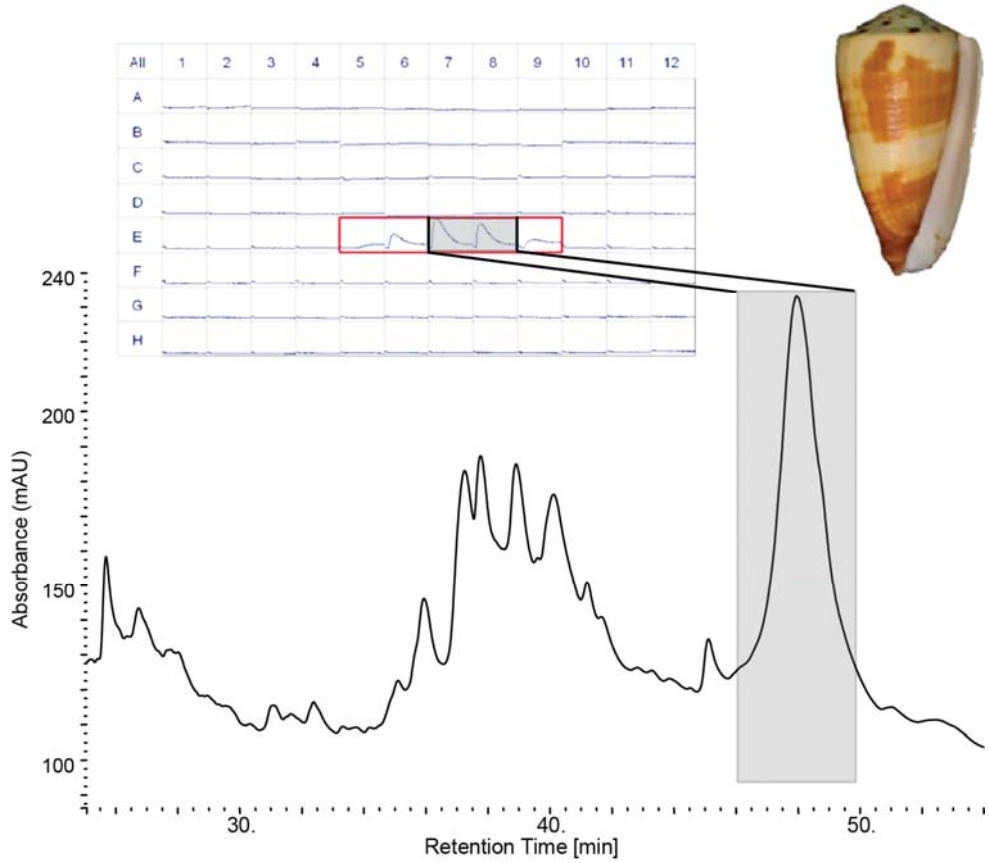

Figure 21: Activity guided fractionation of *C. magus* crude.*rpHPLC of C. magus crude venom with active peak highlighted. Insert shows FLIPR assay plate with active wells 53-57, corresponding to the marked HPLC peak. Bell-shaped response is suggestive of one active constituent across fractions.*

Approximately 0.05% of the pooled active peak from the primary fractionation was loaded onto a MALDI plate with a 1:1 ratio of 5 mg/mL CHCA matrix to yield a single strong $M+H^+$ peak of 3536.5, corresponding to a molecular weight of 3535.5 Da (Figure 22). This mass did not match any known *Conus* peptides in public databases, including ConoServer[379]. The pooled sample was reduced and alkylated before being submitted for N-terminal Edman degradation (Australian Proteome Analysis Facility), which yielded the following sequence (Figure 23):

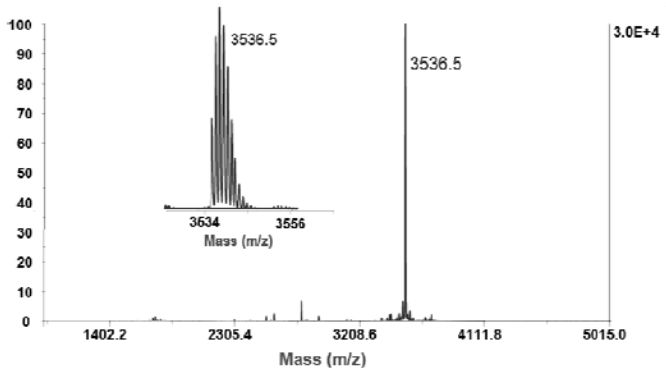

Figure 22: MALDI-TOF analysis of *C. magus* pooled fractions 55 and 56.

A strong, dominant mass signature of $M+H^+$ of 3536.5 was detected.

1)	**DGCYNAGTFCGIRPGLCCSEFCFLWCITFVDS**		**3526.5**
	16	=	hydroxylation of proline
	-6	=	3 disulfide bonds
	-1	=	C-terminal amidation
2)	**DGCYNAGTFCGIROGLCCSEFCFLWCITFVDS***		**3535.5**

Figure 23: δ-MVIA sequence.

*1) As isolated by cDNA analysis with predicted PTMs[380]. 2) Experimentally determined mass of δ-MVIA, which matches sequence mass + predicted PTMs. O=hydroxyproline; *=C-terminal amidation*

The determined peptide sequence was found to be previously discovered through cDNA analysis[380]. The methods to isolate the cDNA sequence for δ-MVIA used specific primers to pre/pro-toxin regions designed for ω- and δ-conotoxins and named the resulting peptide for which the sequence encodes, δ-MVIA. C-terminal amidation and a position 14-hydroxyproline were predicted post-translational

modifications (PTMs) due to sequence homology to other known δ-conotoxins. Based on current nomenclature convention, the original discovery should have been named "m6a" to represent a gene-based discovery. This work represents the first known isolation of the δ-MVIA peptide from venom.

The previous discovery helped to explain the observed discrepancy between the molecular mass of the determined sequence versus the experimental results. The mass detected experimentally for native δ-MVIA corresponded to an oxidized peptide sequence containing three disulfide bonds and the original prediction of two PTMs: C-terminal amidation and 14P hydroxyproline.

4. Discussion

4.1 Assay development

In order to quickly and efficiently screen a large number of crude venoms for Na_V activity, high-throughput methods of detection are needed. However, the discovery process has been hindered by a lack of effective, high throughput assays sensitive enough to detect active molecules from crude venoms, but accessible enough for use outside of the biotech industry[381, 382]. Ideally, assays should display high sensitivity and specificity, high-throughput and information content, high robustness and flexibility as well as high physiological and ideally pathological relevance, all at a relative low cost[383]. The ability of cell based multi-well microtiter detection assays to be developed into high-throughput methods is well characterized [384, 385]. Many neuronal mammalian cell lines express endogenous Na_V channels equivalent to the tissue isolated, such as cortex or DRG. Endogenously expressed receptors have greater pharmacologic relevance due to their expression in a native system, containing necessary auxiliary subunits and expression cofactors/enzymes, as opposed to being transfected into a non-neuronal host-cell. A variety of cell-based functional assays have been employed to guide the identification and characterization of novel, subtype-selective Na_V modulators. Two such assay platforms include fluorescence-based and survival endpoint assays and have been commonly used for screening a variety of receptor targets, including both voltage-gated and ligand-gated ion channels.

Fluorescence-based assays are widely used for high-throughput screening[386]. A high-throughput assay platform particularly well suited to the primary identification of novel drug leads is the FLIPR^{Tetra} (Molecular Devices). This sophisticated technology consists of a fluorescence detection platform in combination with advanced robotics which enable multiple user-defined compound addition protocols and simultaneous fluorescent readings from 96-, 384- or 1536-well plates[387]. The FLIPR was designed for high-throughput Ca^{2+} flux assays and is rightly the industry leader in this application. However, this has limited the availability of different excitation and emission wavelengths. Na^+ dyes with fluorescence spectra similar to calcium dyes, such as CoroNa Green, Sodium Green, or more recently Asante NAtrium, are commercially available. However, most of the single wavelength Na^+ dyes amenable to high throughput FLIPR assays are relatively weakly fluorescent, a problem that is further compounded by the relatively shallow Na^+ gradient that exists across cell membranes. The concentration difference of intracellular versus extracellular Na^+ is roughly 10 fold, whereas the difference in Ca^{2+} is over 30 000 fold[388]. This results in a generally poor signal to noise ratio for fluorescent measurement of the movement of Na^+ ions and makes these Na^+ dyes poorly suited for drug discovery of Na_V modulators.

In contrast, membrane potential dyes measure changes in the electrical potential of the membrane, with significantly improved sensitivity to Na^+ specific dyes[383, 389, 390]. Although this provides some functional and indirect kinetic data, the steady-state changes that are measured are neither specific nor precise enough for detecting compounds that modulate state-dependent Na_V function[383, 390-392]. Experimental evidence has suggested that the MP dye, when used in combination with veratridine as a control agonist, correlates well with the inactivated state binding constant, obtained through electrophysiological experiments[374]. This suggests that the assay measures a single physiological state of Na_V channels and potentially would not differentiate the state dependence of a compound. In addition, membrane potential dyes are particularly prone to artifacts arising from dye-compound interactions as well as non-specific effects of compounds on cell viability and membrane integrity and require specialized filter sets[383, 390].

Another assay platform that has been less widely used is based off a standard colorimetric cytotoxicity assay. Sustained, persistent I_{Na} leads to sufficiently high intracellular Na^+ concentrations and is toxic to many cells. This principle is adapted for cytotoxicity assays, which measure cell survival after activation of Na_V, usually through incorporation of dyes that are metabolically converted to

colorimetric end-products, such as the case with MTT or XTT[377, 393]. Exposure of cells to Na_V activators – such as veratridine – causes increased I_{Na} and subsequent cell death, which can be reversed through Na_V inhibitors[393]. These assays frequently require the need to incorporate ouabain, a potent cardiac glycoside that blocks the action of the Na^+/K^+-ATPase, shutting down the Na^+ efflux pathway and aiding in accumulating toxic levels of $[Na^+]_i$ to increase the signal window[393]. Moderate throughput can be achieved with these assays. They are also relatively inexpensive, both in regards to equipment needed (absorbance UV plate reader) and total reagent costs.

A major drawback to survival endpoint assays is the requirement of both Na_V agonists and ouabain for effective cell death to occur. The lack of selective agonists limits the use of this assay for primary screening, unless a heterologously expressing single-channel cell line is used. Using two control compounds may also complicate the interpretation of results, especially when testing crude venoms, as the action may be the result of inhibiting either receptor. This assay also provides no information on kinetics or state dependence of inhibition as channel activity is not directly measured. If this assay is adapted for agonist detection through a synergistic response with the control, false positives would be expected frequently, as inhibition of growth or proliferation would yield an equivalent result to cytotoxocity. Lastly, general toxicity – even minor – would mask potential reversal of I_{Na} induced toxicity through Na_V inhibition, decreasing potential hits. The major drawback for fluorescence-based assays is that Na_V channel gating modifiers, such as veratridine, deltamethrin or batrachotoxin, are required to elicit Na_V responses in absence of electrical stimulation[389]. However, compared to the two compounds necessary for the cytotoxicity assay, this is an improvement. Kinetics and state dependence are also not available, as the fluorescent measurements are of downstream effects of Na_V regulation. It has also been suggested that fluorescence-based assays – while providing the highest throughput by far – may be biased towards detection of pore blockers and results using these technologies will need to be interpreted carefully[394]. However, with these negatives addressed, the assays used are for general purpose primary discovery screening of crude venoms and many of these issues, once understood, can be addressed[384, 395]. The absolute goal of a cost-effective, reproducible assay with a large enough window to discern activity from a crude venom sample remains.

To specifically address the SH-SY5Y MTT assay, although a higher concentration of TTX (1 μM) was used, the ability of TTX to fully inhibit the effects of ouabain and veratridine could be due to the endogenous expression of the TTXr $Na_V1.5$[363], which has a reported IC_{50} of around 1 μM[396].

Lidocaine is a known inhibitor of $Na_V1.5$, as well as a range of TTXs Na_V channels, although a complete inhibitory profile has not been performed [397, 398]. A similar explanation to TTX can be given for lidocaine, as the lack of full "recovery" after the addition of 1 μM lidocaine may not fully inhibit certain Na_V channels expressed in SH-SY5Y cells at the concentration used. Additionally, it is apparent when looking at Figs. 14 and 15 that ouabain on its own is able to induce a lethal effect. This lethal effect could be influencing cell survival, thereby limiting the maximum amount of "recovery" upon addition of a Na_V channel inhibitor. The mechanism of lethality of ouabain alone is not known.

For the development of a whole cell, high-throughput, microtiter plate-based assay, much relies on the cell line used. Immortalized cell lines have been instrumental in the development of a wide variety of detection assays[399]. Immortalized cells are no longer subject to the Hayflick limit, which describes the number of times a cell population will divide before senescence, due to telomere shortening[400, 401]. These cell lines are typically derived from cancerous cells, which already possess mechanisms for sustained division. However, immortalized cell lines can also be generated from "normal" cells through methods such as insertion of oncogenes[402] or induction of key proteins such as telomerase[403] or viral T protein[404]. Aside from their ability to divide for prolonged periods of time, immortalized cell lines have an added benefit of expressing endogenous receptors relevant to the tissue derived. Therefore, neuronal cell lines would preferentially express key neuronal ion channels and theoretically have a similar functional pharmacology to primary tissue as opposed to heterologously expressed channels. This has been apparent in previous experiments where a splice variant of $Na_V1.7$ demonstrated abnormalities when expressed in neurons that were not seen when expressed in non-neuronal HEK cells[405]. However, the Na_V expression profiles of many commercially available immortalized cell lines remain to be characterized. The initial investigation of this thesis focused on determining Na_V α-subunit expression profiles for a select group of these neuronal cell lines, which included rat neuroblastomas, rat/mouse hybridomas of neuronally derived cells, and the human neuroblastoma SH-SY5Y. The expression of endogenous Na_V α-subunits was assessed using PCR or, in the case of SH-SY5Y, immunohistochemistry and channel function via electrophysiology.

4.2 Cell line characterization and adaptation for assay

Seven commercially available neuronal cell lines were used in the development of a Na_V channel assay. Comprehensive research into the Na_V expression of most of these cell lines had not yet been completed

or submitted to the public domain. The cells that have been studied serve as controls. The initial goal of this project was to determine one or more effective cell lines to be used in a general primary screen for Na_V channel activity. Optimally, expression of $Na_V1.3$ and $Na_V1.7$ with minimal expression of the other channels was desired as these two subunits represent high-interest targets for the treatment of pain, as described previously. Each cell line was chosen for its mammalian neuronal origins, having been isolated from rat, mouse, or human sources. Most have been extensively used as research models for neuronal differentiation and neurite growth, with some cell lines developed for use with various assays such as Fluo4 or MTT.

SH-SY5Y is a dopaminergic cell line developed from a human neuroblastoma parental line, SK-N-SH, isolated from a metastatic bone tumor biopsy[406]. The parental SK-N-SH cell line was subcloned three times; first to SH-SY, then to SH-SY5, and finally to SH-SY5Y, then submitted to the ATCC cell bank in 1970 for public use[406]. Various research has demonstrated that undifferentiated SH-SY5Y cells express nACHr[407] such as α7[408], Kir2.1, $K_V1.4$, $K_V2.1$, $K_V4.2$, $K_V7.1$, [409], $K_V3.1$ [410], $Ca_V2.2$[411], $Ca_V1.3$[411], various ASICs [412], $Na_V1.1$ [413] and $Na_V1.7$ [409, 414]. Conductance changes attributed to both Na_V and Ca_V channels such as increased peak current and slower inactivation were observed after differentiation[415] [416]. SH-SY5Y cells have served as hosts for transfecting a number of receptors and ion channels, including TRP channels[417] and $Na_V1.8$[367]. Both native and transfected cells have been extensively used for a variety of assays measuring neurotoxicity and cell survival[418-421] as well as being used with Fluo4 to measure Ca^{2+} flux triggered by activation of ion channels or GPCRs[422, 423].

Neuro2a is a CNS derived mouse neuroblastoma and has been extensively used to monitor Na_V channel modulation by paralytic shellfish toxins[377, 424] with measurable Na_V channel expression detected in a number of experiments[425-427]. A comprehensive study of Na_V α- and β-subunits using RT-PCR demonstrated the endogenous expression of $Na_V1.2$, $Na_V1.3$, $Na_V1.4$, $Na_V1.7$ and the β1- and β3-subunits, with the predominant α-subunit being $Na_V1.7$[428]. A number of other receptors and ion channels have been detected, including Cl^- channels[429], angiotensin II receptor subtypes AT_{1A}, AT_{1B}, and AT_2[430], purinergic receptors[431, 432], somatostatin receptors[433], and the K_V channels $K_V1.1$, $K_V1.4$, and $K_V2.1$. Low level Ca_V expression was observed in cAMP differentiated cells using the Ca^{2+} sensitive dye fura-2[434]. Further, these cells have successfully been adapted for use with MTT[377, 424].

PC12 is another cell line derived from a CNS, isolated from a pheochromocytoma of rat adrenal medulla[435]. Differentiation has been shown to increase the number or responsiveness of several kinds of ion channels and receptors, such as nicotinic and muscarinic acetylcholine[436, 437], opiate [438], bradykinin[439, 440], 5-HT_3[441], and both $Ca_V1.2$ and $Ca_V2.2$[442-444]. More recently ASICs[445] and O_2-sensitive K_V channels[446] have been found in undifferentiated PC12 cells. Undifferentiated PC12 cells have very low Na_V conductance and expression that can be upregulated through differentiation with NGF or cAMP [447-449]. Through mRNA hybridization analysis, $Na_V1.2$ and $Na_V1.7$ were shown to be the primary Na_V channels present in undifferentiated PC12 cells[450].

50B11 is a PNS derived cell line recently created from immortalize rat DRG[451]. The authors performed detailed electrophysiological analysis to demonstrate no difference between differentiated and undifferentiated cells at resting membrane potentials with no spontaneous activity reported. Depolarizing IV-stimulation of undifferentiated cells also did not induce action potentials. However, action potentials were observed under depolarizing conditions with differentiated cells, suggesting upregulation of Na_V expression after neuronal differentiation[451]. Interestingly, real-time RT-PCR experiments of undifferentiated 50B11 cells confirmed $Na_V1.4$ and $Na_V1.7$ expression at high levels, while $Na_V1.8$ was expressed at low levels. Differentiation in the presence of forskolin and NGF upregulated the expression of $Na_V1.4$ and $Na_V1.8$ alone, but differentiation in the presence of GDNF and forskolin had no significant effect[451]. This data suggests the presence of mRNA with limited to no active protein expression of Na_V channels in undifferentiated cells. A comprehensive analysis of Na_V channels has not been completed.

The last three cell lines described are hybridomas of a mouse neuroblastoma (N18TG2) with either embryonic rat DRG for F11, adult rat DRG for ND7/23[452] or an immortalized rat glioma cell line (C6-BU-1) for Ng108. All three exhibit many properties of neuronal cells after differentiation, including neuronal response to bradykinin, expression of neuropeptides, and extensive neurite-like processes characteristic of DRG neurons, but with distinct electrophysiological profiles[452-456].

F11 cells can differentiate in the presence of cAMP into neurons with increased expression of ion channels and receptors for bradykinin, opioids[457], volume-sensitive Cl^- channels, KCNQ channels[458], and Ca_V channels, showing a similar functionally in many regards to DRG sensory

neurons[459-461]. Undifferentiated cells were shown to have only TTXs current[462]. However, no comprehensive study on Na_V expression has been completed to date. F11 cells have also been validated for Fluo3 assay[463]. ND7/23 cells exhibit TTXs current similar to DRGs with no endogenous TTXr current and expression of both the β1- and β3-subunits[464]. These cells have been successfully used to recombinantly express ion channels, specifically multiple Na_V isoforms[465-468]. The NG108 cell line was originally named 108CC15[469]. Undifferentiated cells have been found to express β-adrenergic receptors [470], 5-HT_3[471], delayed rectifier K^+ channel[472], K_V3.1[473], ERG[474], bradykinin receptors[475]. Neuronal differentiation causes upregulation of Na_V and Ca_V current [476] with upregulation of Na_V current due partially to increase in Na_V1.7 expression[477]. However, apparent change of Na_V current only occurred after 15 days of differentiation[478]. A comprehensive analysis of Ca_V channels was recently completed in by Liu et. al., where the Ca_V1, Ca_V2, and Ca_V3 families of Ca_V channels were all observed. However, it was noted that changes in Ca_V mRNA, expression, and current were all strongly subject to time-dependence of differentiation[479].

This project did not include differentiated cell lines as terminally differentiated cells do not undergo cell division[480], require expensive reagents, and take days to weeks to undergo total differentiation. Additionally, the regulation of receptors and ion channels by differentiation is dependent on a variety of factors, including reagent used and time of incubation. This would be extremely limiting when attempting to develop and maintain reproducible, multi-well, high-throughput, functional assays. An initial PCR characterization of seven neuronal cell lines was completed using primers designed for specific regions of rat Na_V channel isoforms. PCR results suggested prevalent expression of Na_V1.2 in all cell lines tested, with only a slight band apparent for 50B11 cells. This is not a surprising result, as Na_V1.2 was previously detected in Neuro2a cells[428] and is the most abundant α-subunit expressed in the CNS, contributing up to 70% of total Na_V expression in rat brain[481]. All cell lines used, with the exception of the immortalized DRG line 50B11, are either fully or partially derived from CNS tissue.

Na_V1.6 and Na_V1.7 demonstrated a similar expression profile with bands for both isoforms appearing in the same cell lines, although there did not seem to be correlation between cell line origin and expression pattern. Na_V1.6 is the predominant Na_V isoform found at the Nodes of Ranvier on small diameter, myelinated Aδ-fibers, and is also expressed on dendrites and synapses[482]. Na_V1.7 expression is more widely distributed and appears in the somata of all small diameter neurons as well as the central and peripheral terminal processes of small diameter DRG neurons[145]. Both Na_V1.7 and

$Na_V1.6$ at Nodes of Ranvier in small diameter Aδ-fibers occurring throughout the dorsal root and sciatic nerve had a 90% coincident of expression. This observation could help explain the concurrent expression seen in the cell lines. However, although all cell lines have been shown to express $Na_V1.7$ in the literature, 50B11, Ng108, and PC12 did not in this experiment. Ng108 could be explained by its lack of differentiation resulting in decreased expression of the channel [477]. However, the discrepancy with PC12 cannot be explained, as previous experiments observed the presence of mRNA for undifferentiated cells [450, 451]. The lack of $Na_V1.3$ and $Na_V1.4$ mRNA was also a discrepancy from previous published results for Neuro2a [428] and 50B11[451]. In the case of murine derived Neuro2a, the primers were designed for rat specificity and may be binding to an area of the Na_V channel that is not conserved for murine Na_V isoforms. Finally, $Na_V1.8$ was not detected in 50B11 or any other DRG hybridoma. The discrepancy with 50B11 is apparent as no Na_V primers detected mRNA for each subunit tested. This was most likely due to an error in RNA extraction and cDNA production for this individual cell line. The expression profile for $Na_V1.7$ shown here was very similar to that performed with human isoform-specific primers, with the only discrepancy being that of $Na_V1.3$ shown to be expressed using human isoform specific primers [363].

It is recognized that a more complete characterization would include a follow-up sequencing of each band to conclude with more confidence that each band correlates to the expected gene fragment, antibody detection of each α-subunit via Western, and electrophysiological characterization of Na_V function. At the time, only a superficial characterization was required, as other phenotypic methods of determining viability of each cell line were used. Cell lines were judged on their ability to grow without treated plates, the time it takes to reach confluency within flasks or plates, and the ability of the cells to metabolize MTT efficiently or respond to a given fluorescent dye. Further characterization was reserved for the best performing cell lines.

Most of the cell lines were determined to be deficient for assay use in an HTS format required for this project. The majority of cell lines tested require the presence of cAMP or growth factor for differentiation into a neuronal-type cell. Additional to the prohibitive affects of differentiation mentioned previously, without differentiation the cells tested either do not express the necessary Na_V or Ca_V channels or express them at significantly reduced levels. Individually, the PC12 cell line is known to exhibit loss of proliferation after routine passage, with significant changes to phenotype observed[483]. This loss of proliferation and a change in phenotype to favor non-adherence was

observed after moderate use (approximately 5 passages). Optimally, a cell line that can withstand multiple passages while maintaining an equivalent phenotype is preferred, as changes in phenotype could signify changes within the genome that can affect expression profiles and, in turn, results. Both PC12 and NG108 cell lines grow optimally on the presence of poly-D-lysine or collagen I[484, 485]. Their lack of innate adherence could be overcome with the addition of an extracellular matrix. However, all assay formats tested require plate washing steps that can mechanically dissociate loosely attached cells. This greatly affects reproducibility and is a limiting factor. F11 cells exhibited slow proliferation and a suboptimal expression profile of Na_V channels. The phenotypic traits described were all considered undesirable for our purposes of developing a cost-efficient, robust, and high-throughput primary Na_V channel screen. The cell lines that did demonstrate robust growth, adherence to microtiter plate plastic, and a reasonable level of expression for a Na_V isoforms without differentiation were carried through for evaluation with the survival based MTT assay and, finally, a fluorescence based assay. These included the Neuro2a, SH-SHY5Y, and ND7/23 cell lines. Once an optimal cell line was determined – in this case SH-SY5Y – a combination of semi-quantitative PCR, electrophysiology, and immunohistochemistry was used for a more detailed characterization of functional expression before a validated assay was finally developed. The methods and results for the validated assay have been published[363].

4.3 MTT

The purpose of the MTT assay platform was to develop a method that can stand alone as a Na_V primary screen, yet inexpensive, easily accessible, and robust enough to identify new Na_V regulators through assay-guided fractionation. The ability to adapt the assay for testing agonist activity was also explored. The attempt was made to use this assay with both stable and transiently transfected cell lines to probe single and pan Na_V isoform activity. The stable cell line used was ND7/23-rNa_V1.8, kindly donated by Dr. Tony Priestly.

The MTT assay is a colorimetric, endpoint survival assay that measures the ability of cytosolic enzymes in viable cells to metabolize the yellow, soluble tetrazolium salt 3-(4,5-dimethylthiazol-2-yl)-2,5-diphenyl tetrazolium bromide (MTT) to a deep purple, insoluble formazan dye[486] (Figure 24). The reduction of tetrazolium is dependent on NADPH-dependent oxidoreductase enzymes and increases with cellular metabolic activity due to elevated NADPH[487]. It is interesting to note that

viable resting cells that are metabolically quiet reduce very little MTT. In contrast, rapidly dividing cells exhibit high rates of MTT reduction. Changing assay conditions can alter metabolic activity and thus tetrazolium dye reduction without affecting cell viability.

The concept of inducing cell death by forcing an influx of Na^+ was originally used to screen STX-like paralytic shellfish toxins using MTT to measure a survival endpoint[377, 424]. The method uses a combination of two small molecule toxins, the alkaloidal site-2 agonist veratridine and the glycoside ouabain, the latter of which inhibits Na^+ excretion through deactivation of the Na^+/K^+-ATPase. The synergistic action of these two molecules effectively promotes cell death through Na^+ toxicity. It is important to note that the working concentration of ouabain is around 100 µM for inhibition of the Na^+/K^+-ATPase[488, 489]. However, low nM concentrations of ouabain have been shown to reverse the effect and stimulate Na^+/K^+-ATPase activity, as well as trigger multiple downstream signaling cascades involving the enhancement of ERK1/2 phosphorylation and reduction of cellular ATP[490-492]. Further, when testing unknown samples it is not known for certain whether the recovery effect was caused by Na_V channel block or an off-target effect. This could include chelation or disruption of ouabain or veratridine directly, reversal of ATPase inhibition, or another mechanism entirely. As this is a primary screen, this information can be assessed in greater detail during secondary screening or upon isolation and production of the active component.

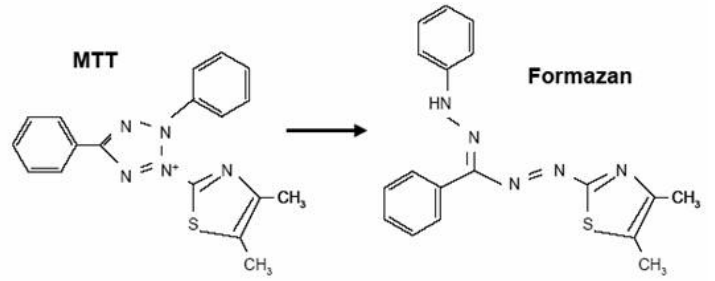

Figure 24: Chemical structure of MTT and its metabolized formazan product.

In the presence of a Na_V channel inhibitor, the influx of Na^+ ceases and the cell is saved from apoptosis. TTX or other known Na_V channel inhibitors can act as a control for Na_V cell recovery. Theoretically, this assay format should be transferrable to different Na_V expressing cell lines - either transiently, stably, or endogenously – as long as the cells are able metabolize MTT. This assay format has the potential to serve as a primary screen for general Na_V inhibitory activity in crude venoms or, in the case of single-channel expressing cell lines, could contribute to selectivity screening. Further, this assay format can potentially be adapted for discovering Na_V channel agonists by adjusting ouabain and

veratridine concentrations to elicit a minimally significant (20-30%) decrease in survival as compared to untreated controls. The addition of a Na_V agonist should theoretically result in an additive decrease in survival as compared to control. It is possible to use other Na_V channel activators, such as ciguatoxin or deltamethrin, as controls in place of veratridine. The time point of 48 h was necessary for two complimentary reasons: a) The cells were plated at a density where they were only partially confluent. The 48 h allowed cells enough time to grow to confluency; b) The 48 h incubation resulted in an exposure time sufficient enough to monitor both cell death and growth inhibition, both of which can result from Na^+ overload at the cellular level [377, 493, 494]. Limited death from Na^+ overload can be seen before 24 h. Longer exposure time increases the window (z-score) of apparent cell death.

A variant of the ND7/23 cell line was obtained that expressed the TTXr $Na_V1.8$. This cell line was tested in place of ND7/23 for its ability to serve as a potential screen of $Na_V1.8$. The contribution of $Na_V1.8$ can be isolated from other Na_V channels endogenously expressed in ND7/23 with the addition of 1 mM TTX. ND7/23-r$Na_V1.8$ cell line demonstrated the potential to serve as a model to screen for $Na_V1.8$ activity with the MTT assay format. Initial results indicated a robust lethal response with a combination of ouabain and deltamethrin. This was unaffected with the combined addition of TTX, suggesting the response was defined by TTXr Na_V channels. However, the lethal response elicited from ouabain and deltamethrin was not affected by the addition of the known $Na_V1.8$ inhibitor lidocaine or a significant volume of *C. marmoreus* crude venom containing the potent $Na_V1.8$ inhibitor MrVIB. A number of factors could be responsible for this occurrence. Ouabain appeared to have no lethal effect with the concentrations used. This was apparent in Figure 10, where the addition of P-CTX resulted in no significant change from baseline survival. This suggests that the induced toxicity could have been affected by the presence of the deltamethrin.

Deltamethrin is a synthetic pyrethroid, which is a class of small molecules based of the naturally occurring pyrethrins from genus *Chrysanthemum*[495]. Because of their observed selectivity towards insect Na_V channels and improved UV tolerance, these chemical were first synthesized during the 1970s for use as commercial insecticides. They modulate Na_V channel activity by shifting the voltage-dependence of activation to a more hyperpolarized potential, resulting in persistent current. However, it was quickly demonstrated that pyrethrins cause acute toxicity in rats through a variety of mechanisms. Although these molecules bind preferentially to $Na_V1.3$, $Na_V1.6$ and $Na_V1.8$, modulation of Ca_V, voltage-gated chloride channels, GABA, glutamate, and acetylcholine receptors have all been

reported[496]. This high receptor promiscuity, often seen with small molecule ion channel modulators, is most likely contributing to induced toxicity through other ion channel or ligand gated channel mechanism, which was not explored in this thesis. For example, acetylcholine receptors are permeable to Na^+, therefore activation of this channel with deltamethrin would result in increased I_{Na} and cell lethality[6, 497]. This would help to explain the inability of both TTX and lidocaine to reverse Na_V induced toxicity, although more experiments would have to be done in order to prove this theory, including characterization of multiple ion channel and ligand-gated receptors present in the ND7/23 cell line. As the focus of this thesis was Na_V channels, the project moved on to more promising cell lines.

The Neuro2a and SH-SY5Y cell lines both resulted in MTT assay methods that could be used to screen for general Na_V channel inhibitors for the endogenous Na_V channels expressed in each cell line. Further, Neuro2a cells were able to be adapted to screen for Na_V channel agonists. Each 96-well microtiter plate is able to screen up to 40 crude venoms with replicates. A fluorescence-based assay was also developed in parallel to the MTT assay. The ND7/23, Neuro2a, and SH-SY5Y cell lines were all attempted in order to determine the best method available for efficiently screening for Na_V modulators.

4.4 Fluorescence-based assays

The Fluorometric Imaging Plate Reader Tetra [FLIPR^{Tetra} (Molecular Devices)] is a 96- or 384-well capable microtiter plate reader capable of simultaneous whole-plate addition of one or two rounds of test compound with continuous whole plate reads. This allows detection of inhibitors by pre-incubating with unknowns followed by addition of a control agonist. Likewise, agonists can be detected within the same assay.

The FLIPR^{Tetra} was used to quantitate an induced fluorescent response via two mechanisms. Fluo-4 acetoxymethyl ester [AM (Invitrogen)] is a small molecule calcium chelator, which is taken up by the cell where the acetoxymethyl ester group is cleaved, internalizing the fluorophore. External Fluo-4 is removed to enable the monitoring of calcium mobilization into the cell, in our case after a depolarization event. Fluo-4 excites at 488 nm upon binding with a Ca^{2+} ion[498] (Figure 25) and requires a moderate to high level of Ca_V channel expression to elicit a measurable response. The

contribution of Na_V channels to the observed response can be tested with a follow up experiment in the presence of TTX or other known Na_V blocking agents.

A proprietary FLIPR^{Tetra} Membrane Potential Assay kit (Molecular Devices; R8126) was also used to determine Na_V channel activity. This kit incorporates a no wash fluorophore in combination with a background quencher. Both chemicals bind to the outer lipid membrane of the cell (Figure 26). Membrane depolarization causes the fluorophore to dissociate from its quencher in the outer membrane by following the flow of cations into the cell. The dissociation results in a relative increase in the fluorescence response, which is measured by a fluorescent detector. The actions are similar to a FRET-based assay.

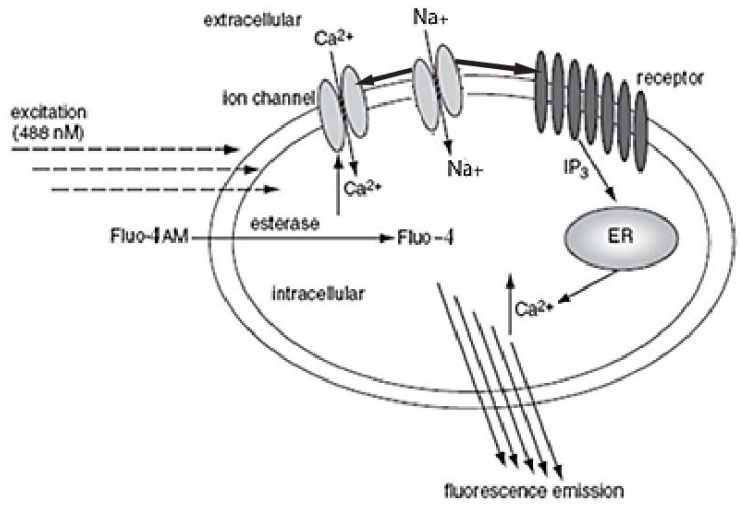

Figure 25: Diagram of Fluo4 AM mode of action through Na_V channel signaling.

Na_V activation results in Ca^{2+} entering the cytoplasm through two linked pathways: external entrance via activation of Ca_V channels and release of internal Ca^{2+} stored through GPCR pathways. Cytoplasmic Ca^{2+} then binds Fluo4, resulting in fluorescence.

Initial experiments tested the fluorescent response of ND7/23, Neuro2a and SH-SY5Y cells with both Fluo4 and the MP-kit. All cell lines displayed a fluorescence response to depolarization invoked upon the addition of 1 mM veratridine using the MP-kit. This response was blocked with TTX, signifying a Na_V specific response. Neuro2a cells did not respond with Fluo4, indicating a potential lack or limited availability of Ca_V channels to mediate entry of Ca^{2+} after Na_V depolarization. ND7/23 cells yielded an equivalent fluorescence response with both Fluo4 and the MP-kit. This suggests a minimal depolarizing

effect from the addition of veratridine as well as potentially a limited availability of Ca_V channels for Fluo4 detection. SH-SY5Y cells demonstrated the largest comparative fluorescent response using both Fluo4 and the MP-kit.

After initial experiments comparing cell lines available, the SH-SY5Y cell line was deemed the most applicable to the FLIPR^{Tetra} assay format. This was due to its robust nature, ability to load multiple fluorescent dyes efficiently, and endogenous expression of human Ca_V and Na_V channels necessary for detection by fluorescence response[499, 500]. Ca_V channel expression in SH-SY5Y cells was determined separately[422]. Another large determining factor in choosing the SH-SY5Y cell line was the apparent endogenous expression of both human isoforms of $Na_V1.3$ and $Na_V1.7$[363].

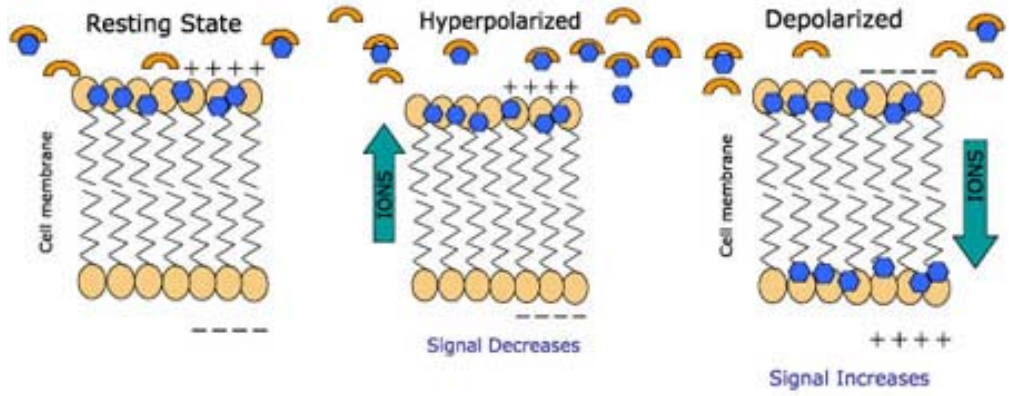

Figure 26: Diagram of Molecular Devices Membrane Potential dye mode of action.
Blue circles represent the charged fluorescent dye that moves in response to ionic flow across a membrane caused by depolarization events.
From: http://www.moleculardevices.com

Because of the large fluorescent response, ability to respond using both Fluo4 and the MP-kit, and robust nature, human neuroblastoma cell line was adopted for primary use. The need for only one control compound coupled with the high-throughput, quick turn-around time and 384-well potential resulted in the FLIPR^{Tetra} assay platform as the lead choice for primary screening of crude venoms. The SH-SY5Y in conjunction with the FLIPR^{Tetra} fluorescent assay platform resulted in the most widely used cell-based method for in-house primary HTS of crude venoms[266]. Proof-of-concept for this assay was demonstrated after a 96-well crude venom screen of *Conus* venoms yielded multiple active

hits. One of those hits, from *C. magus*, resulted in the isolation and sequencing of a previously undiscovered δ-conotoxin.

4.5 Discovery of δ-MVIA

Using the Fluo4 assay format previously described, initial screening of cone snail crude venoms revealed multiple active hits. One of the most potent hits was an agonist of the Fluo4 response, which also demonstrated veratridine potentiation of the fluorescent control response. The active peptide was purified, sequenced, and found to be a previously unisolated member of the δ-conotoxin family. However, the sequence of this conotoxin had already been identified through transcriptome analysis and named δ-MVIA[380].

The δ-conotoxins represent a poorly classified family of toxins with a unique mode of action. To date, only a small handful of mammalian selective δ-conotoxins have been isolated, with two solution structures resolved. They embody the only toxins that interact with the neurotoxin receptor site 6 of Na_V channels. However, the precise site 6 residues of interaction remain to be determined. Molluscan selective δ-conotoxins have been shown to act as both competitive inhibitors and synergistic agonists with site 3 scorpion toxins, sharing overlapping but not identical binding regions[501]. Also similar to site 3 toxins the δ-conotoxins inhibit inactivation. However, δ-conotoxins also shift the voltage-dependence of activation and steady-state inactivation to more hyperpolarized potentials, resulting in hyperexcitability[347]. Because of their unique interaction with Na_V channels, δ-conotoxins have a high potential for use as tools to discern the site 6 binding region as well as further elucidate interactions with site 3 ligands. Further, as gating modifier toxins, it is possible that these peptides can be engineered to act as Na_V inhibitors, similar to the variation that occurs with site 4 peptides derived from spider venom.

The initially observed properties of δ-MVIA were consistent with the δ-family of conotoxins in function and structure. Like other δ-conotoxins discovered, δ-MVIA exhibits a cysteine arrangement typical of peptides that conform to the ICK structural motif. The ability to elicit depolarization on its own as well as act in synergy with both veratridine and P-CTX suggests binding to a different site on the Na_V channel. However, the very small amount of isolated crude venom with no other source to obtain more limited initial experiments. Therefore, a method of production was needed before

pharmacologic characterization could be performed. The extremely high hydrophobicity of δ-conotoxins can result in complications with solid-phase peptide synthesis, as has been seen with the similarly hydrophobic μO-conotoxins. This was the case with δ-MVIA as both BOC and FMOC solid-solid phase synthesis were attempted but failed in yielding a soluble product. Recombinant expression methods have been tested in multiple systems and have proven to be successful means of producing conotoxins[265, 502]. However, recombinant expression with two fusion constructs failed to produce soluble, mature protein. One system for recombinant expression was developed in association with work completed in the following chapters utilizing an MBP fusion protein. Results and methods for δ-MVIA expression can be found in Appendix A. Although expression was possible, the product was insoluble as a fusion protein. Methods to resolubilize were unsuccessful. The general methods for expressing an MBP fusion construct were successfully used in the following chapters and will be explained in depth.

Chapter III: Characterization of Na_V modulating TRTX-Pre1a: Pharmacology and structure

1. Introduction

As previously discussed in the introduction, $Na_V1.7$ has emerged as a leading target for the development of pain therapeutics. Studies involving animal pain models, localization, and functional excitability in neurons have demonstrated the contribution of $Na_V1.7$ to pain pathophysiology[139, 503]. However, it was clinical and genetic observations of $Na_V1.7$'s role in familial inherited human pain disorders that has solidified this ion channel as a key molecular target for the treatment of pain. $Na_V1.7$ is primarily expressed in somatosensory, peripheral nerve fibers. Gain-of-function mutations on the $Na_V1.7$ encoding *SCN9A* gene develop into paroxysmal extreme pain disorder (PEPD) or primary erythromelalgia[146, 504]. By contrast, a different series of mutations that result in loss of channel function have been shown to contribute to a rare genetic disorder, congenital insensitivity to pain (CIP)[148]. Patients with CIP experience a complete loss of all forms of pain with no deficits to motor, cognitive, sympathetic and gastrointestinal function, or loss of any other sensory modality with the exception of some instances of impaired olfaction, detected in both rats and humans[149, 505]. The functional validation of $Na_V1.7$ as a therapeutic target has initiated a huge research effort towards the discovery and development of selective and potent modulators. The majority of pharmaceutical research has historically been directed towards small molecule discovery platforms[506, 507]. However, over the past decade, venom peptides have proven to be a source of novel, selective, and potent modulators of ion channels, leading to an increasing interest in these molecules for therapeutic development[508].

Spiders are by far the most successful venomous predators on the planet with over 43,000 species so far described[349]. Individual species can produce a unique assemblage of up to 1000 peptide components, yielding a total bioactive compound library in the tens of millions, with less than 0.1% so far described[350, 509]. Given that the purpose of spider venom is rapid immobilization of prey, it is not surprising that one of their dominant pharmacological actions includes the modulation of Na_V channels. Not only are spider venom peptides able to target Na_V channels selectively, they have demonstrated an

ability to functionally differentiate between individual isoforms while still maintaining a high level of potency[252, 510]. The ability to selectively modulate Na_V isoforms is related to these peptides ability to exhibit unique modes of modulatory action, interacting with the voltage sensor domain in order to trap the channel in different conformational states and shifting the voltage-dependence of gating. Unfortunately, much of this functional information has only been acquired over the past decade, with many questions regarding both receptor and ligand left unanswered.

Recently, a unique peptide was isolated from the venom of the tarantula, *Psalmopoeus reduncus*. Named TRTX-Pre1a, this peptide demonstrated the ability to functionally regulate multiple Na_V isoforms with two different mechanisms of action. Further, TRTX-Pre1a demonstrated structural heterogeneity, appearing to take on multiple conformational states in solution at room temperature. This chapter described the production, functional, and structural aspects of a new peptide isolated from spider venom via a $Na_V1.7$ functional screen using two-electrode voltage clamp (TEVC) methods.

The primary aims of this chapter were as follows:

1) Produce correctly folded and isotopically labeled TRTX-Pre1a using a recombinant expression system.

2) Characterize the Na_V isoform activity through a combination of electrophysiology and cell-based assay.

3) Determine the solution structure of TRTX-Pre1a through heteronuclear NMR.

2. Methods

2.1 Expression vector design

A synthetic gene encoding TRTX-Pre1a was codon optimized for expression in *E. coli* and cloned into a variant of the pLIC-MBP expression vector by GeneArt (Germany)[511] (Figure 27). This vector encodes a *MalE* signal sequence for periplasmic export, a His_6 affinity tag for purification, a maltose binding protein (MBP) fusion tag to aid solubility, and a tobacco etch virus (TEV) protease recognition site directly preceding the TRTX-Pre1a sequence. This expression vector produces the native toxin with an additional N-terminal serine residue, a vestige of the TEV protease cleavage site. A T7 promoter with a *lac* operon allows for inducible expression upon the addition of IPTG (Invitrogen). The pLIC vector also encodes for ampicillin resistance (Amp^R).

A)

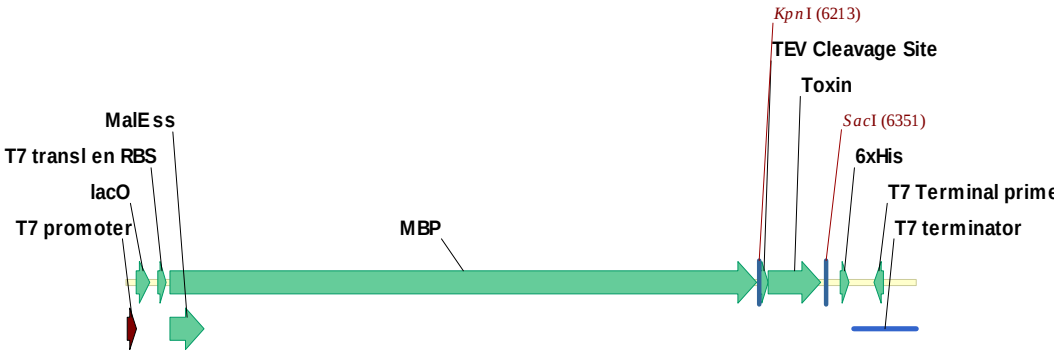

B)

rPre1a: SEDCLGWFSRCSPKNDKCCPNYKCSSKDLWCKYKIW 4314.9

Figure 27: Gene encoding recombinant Pre1a.

A) Gene segment of pLIC expression vector which encodes for the mature fusion protein. B) Sequence of recombinant Pre1a with a N-terminal Ser residue that remains after TEV cleavage.

2.2 Bacterial recombinant expression

The pLIC vector containing the synthesized expression gene was transformed into BL21(ΔE3) chemically competent *E.coli* (Invitrogen, CA) by heat shock (60 s at 42°C) for recombinant toxin production. Cultures were started in 100 mL of Luria-Bertani (LB) medium inoculated from a glycerol stock. Starter cultures were grown overnight at 37°C with shaking at 200 rpm under ampicillin (Amp) selection. For test expressions, 10% of the starter culture was used to inoculate fresh 100 mL batches of LB + Amp and grown to an OD_{600} of 0.7 to 1.0 before induction with a final concentration of 1 mM IPTG (Invitrogen). Several incubation conditions were tested varying both temperature and time. Expression was terminated by centrifugation for 15 min at 6000 × *g*, 4°C. Cells were lysed by sonication on ice at 4°C. To check for solubility, the whole cell lysate was centrifuged at 18 000 × *g* for 30 min at 4°C and the supernatant was collected for analysis on SDS PAGE.

For large scale expression, 50 mL of starter cultures were added to fresh 2 L batches of LB medium and grown at 16°C with shaking at 150 rpm under Amp selection. Expression of the toxin gene was induced with 1 mM IPTG at an OD_{600} of 0.7 to 1.0 and expression was allowed to proceed at 37°C or 16°C with 150 rpm shaking. Expression was terminated 18-20 h (16°C) or 3 h (37°C) later by centrifugation for 15 min at 6000 × *g* at 4°C. For production of uniformly $^{13}C/^{15}N$-labeled TRTX-Pre1a, cultures were grown as previously described in LB medium. Once an OD_{600} of 0.7 to 1.0 was reached in a 2 L culture, the entire culture was centrifuged at 3000 × *g* and the LB medium was removed. The pellet was washed once with unsupplemented minimal medium and then gently resuspended in 500 mL complete minimal medium supplemented with $^{13}C_6$-glucose and $^{15}NH_4Cl$ as the sole carbon and nitrogen sources, respectively. Expression was allowed to continue at 16°C as previously described.

2.3 Lysis and IMAC purification

After removal of medium, the bacterial cell pellets were resuspended in 20 mL chilled TN buffer (40 mM Tris, 400 mM NaCl, pH 8.0) per gram. TN buffer was supplemented with complete protease inhibitor cocktail (Roche) and DNaseI (Roche) then the His_6-MBP-toxin fusion protein was extracted from the bacterial periplasm by continuous flow cell disruption (TS Series Benchtop System, Constant Systems Ltd, Northants, UK) at a constant pressure of 30 kPa. The resulting lysate was centrifuged for

30 min at 18000 × *g* at 4°C to collect the soluble protein. Upon confirmation that the fusion protein was in the soluble fraction, the insoluble pellet was discarded.

The His_6-MBP-toxin fusion protein was captured by passing the whole cell lysate over Ni-NTA Superflow resin (QIAGEN, Valencia, CA) followed by washing with 15 mM imidazole in TN buffer to remove nonspecific binders. The fusion protein was then eluted with 250 mM imidazole in lysis buffer. The buffer was exchanged with pure TN buffer by centrifugal filtration to remove imidazole (Amicon Ultra, Millipore). Reduced and oxidized glutathione were added to 3 and 0.3 mM, respectively, to activate TEV protease. TEV protease was made recombinantly in-house according to published methods[512]. Approximately 50 µg of His_6-tagged TEV protease was added per mg of recombinant TRTX-Pre1a, and the cleavage reaction was allowed to proceed at 30°C for 3 h.

2.4 Reversed-phase high performance liquid chromatography

Semi-preparative rpHPLC was performed on a Shimadzu LC-20AT system with a SPD-10A dual wavelength UV/VIS detector. For purification of recombinantly expressed TRTX-Pre1a, the instrument was equipped with a Vydac C_8 column (208TP1022; 50 × 250 mm; 5 µm particle diameter; 300 Å pore size) using a flow rate of 10 ml/min and a linear gradient of 15 to 60%. solvent B (0.1% trifluoroacetic acid in 90% acetonitrile) in solvent A (0.1% trifluoroacetic acid in water) over 30 min. Secondary purification was followed up on a Thermo Hypersil GOLD C_{18} (10 × 250 mm; 5 µm particle diameter; 300 Å pore size) using a flow rate of 3 ml/min.

Analytical rpHPLC was performed on a Shimadzu LC-20AT Prominence system equipped with SIL-20AHT autosampler, SPD-20A dual 214/280 nm UV/VIS detector and CTO-20A column oven. An Onyx C18 monolithic column (Phenomenex; 2 × 100 mm; 130 Å pore size) was used for final purification (if needed) and analyzing purity of all samples.

2.5 Determination of peptide concentration

Peptide concentrations were calculated using the molar extinction coefficient and the absorbance at λ = 280 nm. Absorbance was measured against a buffer blank on a NanoDrop (Thermo)

spectrophotometer. The extinction coefficient was calculated based on the methods of Gill and von Hippel[513] using the following equation:

$$\varepsilon_{peptide} = (nW \times \varepsilon W)+(nY \times \varepsilon Y)+(nC \times \varepsilon C)$$

Where $\varepsilon W = 5500$; $\varepsilon Y = 1490$; and $\varepsilon C = 125$[514]

The absorbance reading at 280 nm was then used to calculate molarity (M) of the peptide in solution using the calculated ε-value with a derivation of the Beer-Lambert Law:

$$M_{peptide} = A_{280} / \varepsilon_{peptide}$$

2.6 MALDI-TOF mass spectrometry

Toxin masses were confirmed by matrix-assisted laser desorption ionization–time-of-flight mass spectrometry (MALDI-TOF MS) using a model 4700 Proteomics Bioanalyser (Applied Biosystems, Foster City, CA). rpHPLC fractions were mixed [1:1 (v/v)] with α-cyano-4-hydroxy-cinnamic acid matrix (7.5 mg/ml in 70/30 acetonitrile/H_2O) were collected in positive reflector mode. The mass range was set to *m/z* 800-8000 with a focus mass of 4500 Da. Shots were collected using manual acquisition control and close external calibration. All masses given are for the monoisotopic $M+H^+$ ions unless otherwise stated.

2.7 Peptide sequence determination

Prior to sequencing, approx. 2-3 µg of the peptide was dissolved in 5 µl of 100 mM ammonium acetate (pH 4.5) and reduced by adding 10 µl of 100 mM TCEP (1 hour, 37°C). Alkylation was carried out by adding 20 µl of 100 mM maleimide (made up in 10 % acetonitrile) and incubating for 1 hour at 37°C. The reaction was quenched by adding 100 µl of 0.1% TFA and desalted using rpHPLC (Prosphere C4 column, 3x150 mm, 15-35% B in 18 mins). The mass of the reduced/alkylated peptide was determined using an API2000 mass spectrometer. The sequence of purified, reduced/alkylated peptide was determined by Edman degradation at the Australian Proteome Research Facility using an Applied Biosystems 494 Procise Protein Sequencing System.

2.8 TEVC methods

Toxin activity was assessed using two-electrode voltage clamp experiments performed on *Xenopus laevis* oocytes expressing rat or human Na_V channels. Oocytes were surgically removed from mature *X. laevis* frogs anesthetized by submersion in 0.13% tricaine methanesulfonate (MS-222). Stage V–VI oocytes were prepared for injection by dissociation in Ca^{2+}-free solution containing the following: 96 mM NaCl, 2 mM KCl, 2 mM $MgCl_2$, 5 mM HEPES (pH 7.4), plus 1 mg/ml collagenase (Sigma, type I) for 1.5 h at room temperature. Oocytes were maintained in ND96 solution containing 96 mM NaCl, 2 mM KCl, 1 mM $CaCl_2$, 2 mM $MgCl_2$, 5 mM HEPES, 5 mM pyruvate, 50 μg/ml gentamicin (pH 7.4) and 2.5% horse serum. cRNA of Na_V 1.2 (100 ng/μL), Na_V1.3 (660 ng/μL), Na_V1.4 (100 ng/μL), Na_V1.5 (100 ng/μL), and Na_V1.7 (250 ng/μL) were injected using a precision injector (Nanoliter 2000) and incubated at 18°C for 2-4 days. cRNA was made using an Ambion mMessage mMachine kit (Invitrogen) with linearized pcDNA3.1 plasmid containing the Na_V expression gene of interest.

Voltage and current electrodes filled with 3M KCl had a final resistance of 0.5–2.0 MΩ. Stimulation, data acquisition, and analysis were performed using pCLAMP 10.0 software (Molecular Devices, CA, USA) using an Axoclamp 900A voltage clamp amplifier (Molecular Devices). All experiments were performed at room temperature (20–22 °C). Serial dilutions of stock peptide solution (100 μM in H_2O) were made in ND96 solution containing 0.1% fatty acid free BSA (Sigma) to prevent adsorption to tubing. Current-voltage (I-V) relationship curves were evoked by depolarizations to 0 mV in 5 mV increments from a holding potential of -80 mV. The amount of toxin-induced block was measured at -20 mV with the exception of Na_V1.5, measured at -30 mV due this channels hyperpolarized shift in activation potential. I-V curves were taken both before addition of compound and after reaching steady-state activity (see Appendix B for example I-T plots). All toxins were tested on at least $n = 3$ individual oocytes.

The linear membrane capacitative and leak currents were subtracted using a -P/4 pulse protocol. Membrane currents were sampled at 20 kHz and filtered at 2 kHz. Oocytes showing <15% change in peak current amplitude over a 5 min incubation period were used in these studies to avoid effects associated with current run down. Perfusion was stopped, and cumulative additions of toxin were added to a Perspex chamber (0.1 ml volume) to achieve rapid mixing. Activity of peptide was assessed by monitoring the change in either peak current or late current over time, until equilibrium was reached

(Appendix B). An I-V protocol was performed before and after addition of peptide by holding the membrane potential at -80 mV and depolarizing for 20 ms in 5 or 10 mV steps, from -60 to +40 mV (Appendix C). Nonlinear regression and statistics calculations (means ± S.E; $n \geq 3$) were performed using GraphPad Prism software 5.0 (San Diego, CA).

2.9 Cell culture and FLIPR assay

CHO-K1-hNa_V1.4 cells were purchased from Chantest (USA; CT4005). HEK-rNa_V1.6-TTXr and HEK-rNa_V1.7-TTXr cell lines were a kind gift from Dr. Steven Waxman. All three cell lines were maintained in DMEM medium supplemented with 10% fetal bovine serum. All mammalian cell lines were passaged every 3-5 days using 0.25% trypsin/ EDTA and incubated in a temperature, humidity, and CO_2 controlled incubator set to 37°C with 5% CO_2. For assay, all three cell lines were plated at a density of 120-140 × 10^3 cells per well in a 96-well, black-walled imaging plate (Corning) 48 h prior to assay.

The FLIPR assay was run as previously described in Chapter II, Section 2.8 for the Molecular Devices No-Wash Membrane Potential Kit, with the exception of using the above described single-channel expressing, stably transfected cell lines in place of SH-SY5Y cells.

2.10 Data analysis

FLIPR

Unless otherwise stated, all data are expressed as the mean ± standard error of the mean (SEM) determined from at least $n = 3$ experimental replicates, with 2-4 replicates per plate. To establish concentration-response curves, responses after addition of compounds were plotted against agonist concentration and a 4-parameter Hill equation with variable Hill slope or a two-site model was fitted to the data using GraphPad Prism (Version 4.00, San Diego, California). Potency of agonists and antagonists are reported as the mean ± SEM of 3-4 separate experiments. Statistical significance was determined using an unpaired student's *t*-test with statistical significance defined as $p < 0.05$ unless otherwise stated.

TEVC

Data were analyzed using pCLAMP 10.0 (Molecular Devices, CA, USA) and GraphPad Prism 5.0 software programs. All data points are shown as mean ± S.E. where *n* is presented as the number of the separate experiments.

To establish concentration-response curves, responses after addition of compounds were plotted against the log of sample concentrations and a least squares fit 4-parameter Hill equation with variable Hill slope fitted to the data using GraphPad Prism 5.0. Statistical significance was determined using an unpaired student's *t*-test with statistical significance minimally defined as $p < 0.05$ unless otherwise stated.

2.11 NMR methods and homology modeling

Lyophilized $^{13}C/^{15}N$ labeled recombinant TRTX-Pre1a was resuspended at a final concentration of 300 µM in 300 µl 10 mM sodium phosphate buffer, pH 6.0, constituted in 95% H_2O / 5% D_2O. An additional sample was prepared by lyophilizing the above sample and resuspending it into 100% D_2O. These samples were both added to susceptibility-matched 5-mm outer diameter microtubes (Shigemi Inc., Japan).

Data were acquired at 298 K using a 900 MHz NMR spectrometer (Bruker BioSpin GmbH, Rheinstetten, Germany) equipped with a cryogenically cooled triple resonance probe. Sequence specific backbone resonance assignments were obtained using 3D CBCA(CO)NH, 3D HNCACB, 3D HNCO, 3D H(CCCO)NH-TOCSY, 3D (H)CC(CO)NH-TOCSY, and 2D ^{1}H-^{15}N HSQC spectra, which were all acquired using non-uniform sampling and transformed using maximum entropy reconstruction with the Rowland NMR Toolkit (http://www.rowland.org/rnmrtk/toolkit.html) as described previously[515]. HSQC-NOESY (^{15}N in H_2O and ^{13}C in D_2O) spectra were obtained for assignment of disulfide bonds, using a mixing time of 250 ms. Secondary structure elements were predicted using TALOS+ chemical shift analysis [516]. NOESY spectra were manually peak picked and integrated using Sparky NMR analysis software[517]. The peak lists were then automatically assigned, distance restraints extracted, and an ensemble of structures calculated using the torsion angle dynamics package CYANA[518]. The tolerances used for CYANA were 0.03 ppm in the direct ^{1}H dimension, 0.01 ppm in the indirect ^{1}H dimension, and 0.4 ppm for the heteronucleus ($^{13}C/^{15}N$). During the automated

NOESY assignment/structure calculation process, CYANA assigned 90.1% of all NOESY cross-peaks (829of 920).

TRTX-Pre1a was modeled against the solution structure of β-TRTX-Ps1a (phrixotoxin-3) using Modeler v9.8[519]. The solution structure data for β-TRTX-Ps1a was obtained from Prof. Glenn King and used with permission.

3. Results

3.1 Discovery background

Initial analysis of crude venom from *P. reduncus* – a tarantula from the family Theraphosidae – using two-electrode voltage clamp (TEVC) electrophysiology demonstrated that it potently inhibited $hNa_V1.7$ channels expressed in *X. laevis* oocytes. The initial separation step showed that fraction 18 contained the desired $hNa_V1.7$ inhibitory activity (Figure 28). Two subsequent steps of activity-guided rpHPLC purifications resulted in the identification of a major peak exhibiting inhibitory $hNa_V1.7$ activity (Figure 28). The pure peptide also interacted with the rat isoform of $Na_V1.3$. However, instead of inhibiting current, as was seen with $hNa_V1.7$, TRTX-Pre1a inhibits the fast inactivation of $rNa_V1.3$ as evidenced by the increase in late current (Figure 28 insert). Mass analysis via MALDI-TOF MS revealed an $M+H^+$ of 4227.5 (or MW of 4226.5 Da). The mass of the fully reduced/alkylated peptide was found to be 588 Da (6 × 98, the MW of maleimide) higher than the native peptide, indicating the presence of six cysteines, thus the three disulfide bonds. Edman degradation of the reduced/alkylated peptide resulted in complete sequence determination and revealed a previously undiscovered spider venom peptide, highly similar to Na_V modulating spider Family 1 toxins. This novel peptide was found to be 35 amino acids in length with six cysteine residues with spacing indicative of an ICK motif, commonly observed with spider venom peptides[239]. The peptide was named as TRTX-Pre1a according to standard rational nomenclature proposed by King et al. [520]. Table 3 highlights the sequence similarity of TRTX-Pre1a with multiple other spider toxin peptides and their known molecular targets.

Reverse-phase HPLC analysis of pure TRTX-Pre1a revealed a leading tail and earlier eluting minor peak, as shown in the inset of Figure 28 B. The initial assumption that the lack of symmetry of the

peptide was due to the presence of an impurity was put into question when these regions revealed the presence of an equivalent mass to the major peak, suggesting there is potential structural heterogeneity of TRTX-Pre1a.

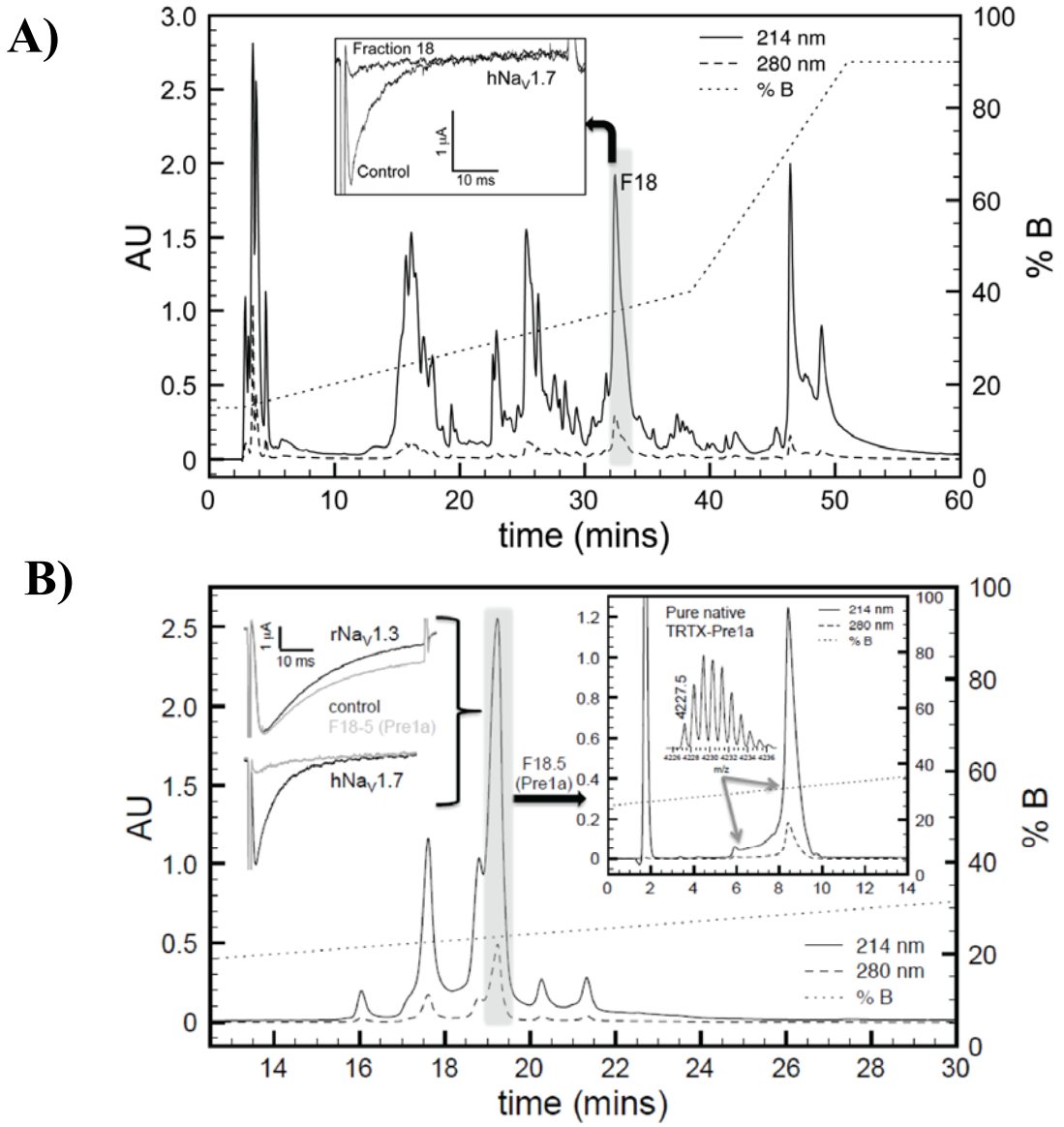

Figure 28: rpHPLC purification of *P. reduncus* crude venom.

A) Fraction F18 inhibited $Na_V1.7$, as shown in the insert. B) Secondary purification of F18 demonstrated $Na_V1.7$ inhibition and $Na_V1.3$ inhibition of fast inactivation. Tertiary purification yielded a dominant peak with a leading tail, both with a $M+H^+$ of 4227.5 (B; insert).

Table 3: Sequence alignment of TRTX-Pre1a and related Theraphotoxins.

Numbering and % similarity are relative to TRTX-Pre1a. U = unknown assignment.

Systematic name	Target	Sequence	aa	%sim
		1 5 10 15 20 25 30 35		
U-TRTX-Pre1a	Na_V	EDCLGWFSRCSPKNDKCC--PNYKCSSKDLWCKYKIW	35	
β-TRTX-Ps1a*	Na_V	-DCLGFLWKCNPSNDKCCR-PNLVCSRKDKWCKYQI-	34	77.1
κ-TRTX-Tb1b	K_V	DDCLGMFSSCDPKNDKCC--PNRVCRSRDQWCKYKLW	35	82.9
β-TRTX-Cm1a	Na_V	-DCLGWFKSCDPKNDKCC--KNYTCSRRDRWCKYDL-	33	71.4
β-TRTX-Cm1b	Na_V	-DCLGWFKSCDPKNDKCC--KNYTCSRRDRWCKYYL-	33	71.4
κ-TRTX-Tb1c	K_V	DDCLGMFSSCDPNNDKCC--PNRVCRVRDQWCKYKLW	35	80.0
κ-TRTX-Tb1a	K_V	AACLGMFESCDPNNDKCC--PNRECNRKHKWCKYKLW	35	71.4
μ-TRTX-Hhn1a	Na_V	-ECLGFGKGCNPSNDQCCKSANLVCSRKHRWCKYEI-	35	65.7
μ-TRTX-Hh2a	Na_V	-ECLEIFKACNPSNDQCCKSSKLVCSRKTRWCKYQI-	35	65.7
μ-TRTX-Hhn1b	Na_V	-ECLGFGKGCNPSNDQCCKSSNLVCSRKHRWCKYEI-	35	62.9
μ/ω-TRTX-Hh1a	Na_V/Ca_V	-ACKGVFDACTPGKNECC--PNRVCSDKHKWCKWKL-	33	62.9
μ-TRTX-Hhn2a	Na_V	-GCKGFGDSCTPGKNECC--PNYACSSKHKWCKVYL-	33	60.0
μ-TRTX-Hhn2b	Na_V	-ECKGFGKSCVPGKNECC--SGYACNSRDKWCKVLL-	33	60.0
		---loop-1--- ---loop-2--- ---loop-3--- ---loop-4---		

3.2 Structural heterogeneity of TRTX-Pre1a as studied by rpHPLC

It was a possibility that the apparent conformers were a result of *cis-trans* isomerization about the amide bonds, typically occurring around Pro residues but apparent in non-proline peptide bonds, as well (Figure 29). C*is-trans* isomerization of a peptide bond can result in equilibrium between a *cis*- and *trans*-isomer as seen for the scorpion toxin BmKαIT01[521] and BmK M7[522].

The peptide bond has two stabilized resonance forms, which results in a partial double bond character and *cis-trans* isomerization. Normally peptide bonds adopt the energetically favorable *trans*-conformation[523]. But in some instances a peptide bond can adopt *cis*-configuration as seen for the peptide bond Asp_9-Tyr_{10} in the α-scorpion toxin BmK-IT01[521]. An Asn-Tyr bond is also present in TRTX-Pre1a so it is possible, that *cis-trans* isomerization around such a non-Pro peptide bond results in the two peaks in Figure 30. Isomerization of the peptide bond between Ser or Cys and Pro in TRTX-Pre1a is also a possibility, as *cis*-isomers of peptide bonds between a random amino acid and Pro occurs at higher frequency than non-Pro peptide bonds[522].

In order to test whether the leading tail and minor peak seen with purified TRTX-Pre1a was an impurity, misfolded protein, or conformational isomer, a simple rpHPLC experiment based on methods developed by Swartz and Mackinnon was implemented[524]. Two fractions were collected covering

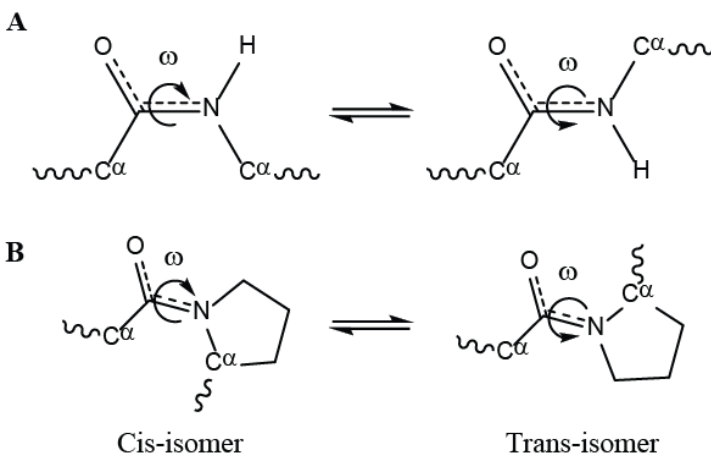

Figure 29: Schematic representation of *cis-trans* isomerization of a peptide bond.

Rotation around the dihedral angle ω of the partial double bond allows the isomerization. A) cis-trans isomerization of a non-Pro peptide bond and B) a Pro peptide bond.

sections of the dominant peak of TRTX-Pre1a (Figure 30). These fractions were reinjected and a similar chromatographic profile with the minor peak and leading tail was evident. This experiment was repeated with recombinant TRTX-Pre1a with equivalent results. If the leading tail was an impurity or misfolded protein, it should not appear in the major peak. Therefore, reinjection of fractions collected from only the major peak would result in the absence of a minor peak and leading tail, yielding a single sharp peak. However, if the structure of TRTX-Pre1a has properties that lend it towards conformational instability, then the minor peak could represent a correctly folded conformational isomer. At room temperature, peptide isomerization around the amide bond tends to be a slow process[525, 526]. This could help explain the leading tail between the two visible peaks as transitional states between isomers. However, more experiments were necessary to test this hypothesis, as well as the possible contribution of one or both of the Pro residues.

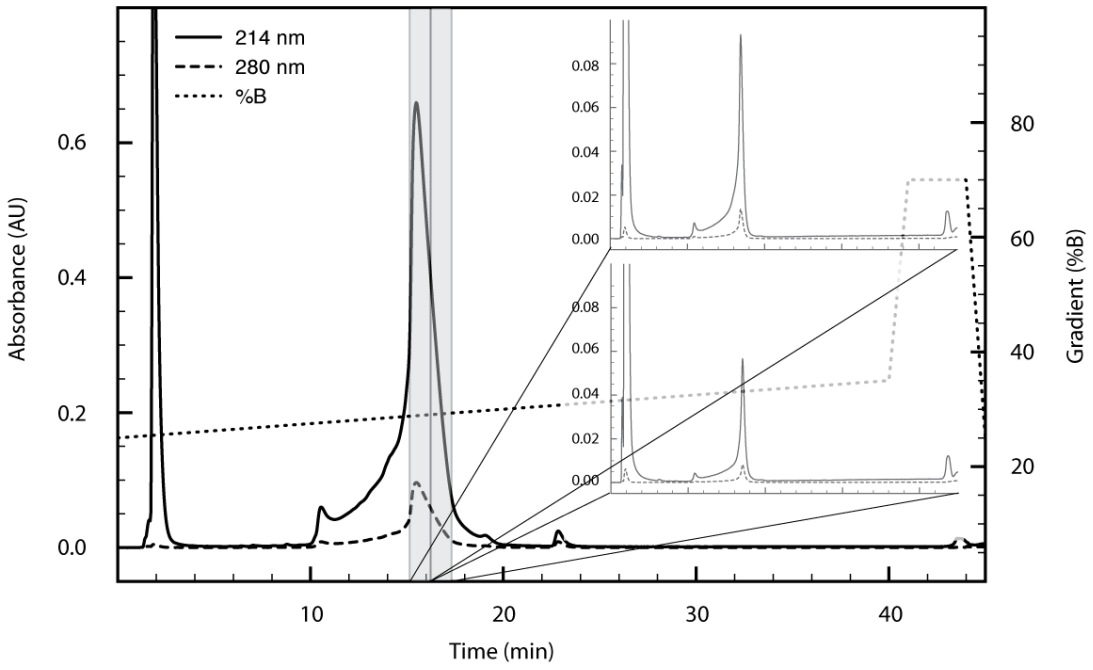

Figure 30: Chromatographic profile of folded purified TRTX-Pre1a and reinjection of major peak.

rpHPLC analysis of folded TRTX-Pre1a on an analytical C_{18} column with a 1 mL/min flow rate and linear gradient (0.25%/min, 25-35 %B) depicted by the dotted line. The grey bars indicate the fractions collected after initial injection. Inserts show rpHPLC analysis of the two reinjected fractions using the exact same parameters for analysis.

3.3 TRTX-Pre1a homology model

More information was required to explain the possible conformational heterogeneity seen with the rpHPLC chromatogram. In the absence of a solution structure of TRTX-Pre1a, a homology model was created based on the template of a previously isolated spider venom peptide with high sequence and structural homology. A sequence comparison of β-TRTX-Ps1a with TRTX-Pre1a shows strong homology between many of the loop regions, with some variation occurring over a four residue stretch of Loop 1 (Table 3). Isolated from the Chilean spider *Paraphysa scrofa*, β-TRTX-Ps1a is a non-selective inhibitor of Na_V channels that inhibits current through the mechanism of voltage sensor trapping[251]. The NMR solution structure of a β-TRTX-Ps1a has been solved by our close collaborator Professor Glenn King, although not yet in the public domain. The structure of β-TRTX-

Ps1a was consequently used with permission as a template to create a homology model of TRTX-Pre1a (Figure 31).

The model of TRTX-Pre1a revealed a hydrophobic face composed of five aromatic residues, W_7, F_8, Y_{22}, W_{30} and Y_{32}. Both W_7 and F_8 appeared to be towards the center of the hydrophobic stack on adjacent residues and may therefore result in steric clashes leading to energetically strained structural arrangement. Further, their sequence position followed directly after the G_6 residue. Gly is known to contribute to a loss of structural rigidity due to its lack of a sterically hindering carbon side chain, resulting in increased flexibility and rotational capacity around this region[527, 528]. Interestingly, the highly homologous β-TRTX-Ps1a contains a Gly in a comparable position, but is structurally stable while maintaining nanomolar activity[251]. This stability could be attributed to the F_5 and W_7 residues of β-TRTX-Ps1a being separated by a non-aromatic Leu, resulting in a more stable arrangement of the F_5, L_6, W_{30}, and Y_{33}, while W_7 is oriented towards the opposite face (Figure 31). The features described for Loop 1 of TRTX-rPre1a and its possible contribution to conformational heterogeneity will be explained in more detail in the discussion.

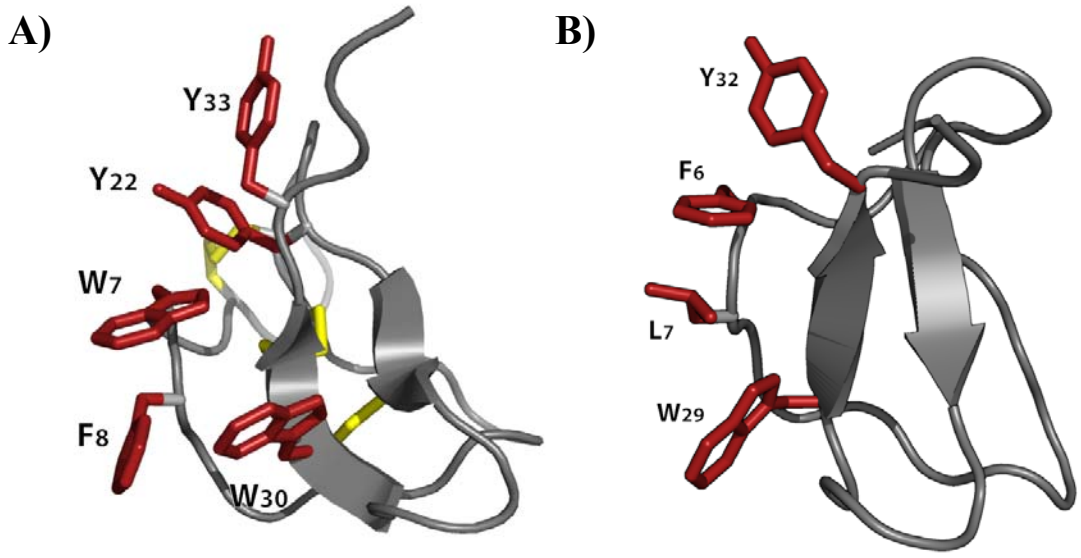

Figure 31: Homology model of TRTX-rPre1a compared to β-TRTX-Ps1a.

A) TRTX-Pre1a, with hydrophobic face residues highlighted in red, disulfide bonds in yellow. B) β-TRTX-Ps1a solution structure with comparative features highlighted.

The homology model resolved structural features of note, specifically involving the close interactions between aromatic residues that make up the hydrophobic face and could contribute to aromatic stacking. However, as the actual structure of TRTX-Pre1a is likely to differ from the model, unanswered questions remain regarding the conformational stability of Loop 1. Therefore, a NMR solution structure of $^{13}C/^{15}N$-labeled recombinantly expressed TRTX-rPre1a was solved and will be discussed in this chapter.

3.4 Bacterial recombinant expression

Further studies required the production of TRTX-Pre1a for pharmacological characterization as well as isotopic labeling for heteronuclear NMR experiments. In order to quickly and efficiently produce labeled and properly folded disulfide rich protein a method of recombinant expression developed in-house[529]. TRTX-Pre1a was successfully expressed recombinantly in *E. coli* as an MBP fusion protein. Before scale-up expression to 2 L LB, a 100 mL test expression was carried out with two temperature conditions with multiple time points. No observable difference in the level of inducible expression was seen between temperatures or time points tested when assessed by SDS-PAGE (Figure 32). The optimal growing temperature for *E. coli* is 37°C, which results in a shorter window for logarithmic growth and therefore faster induced expression of the peptide product[530].

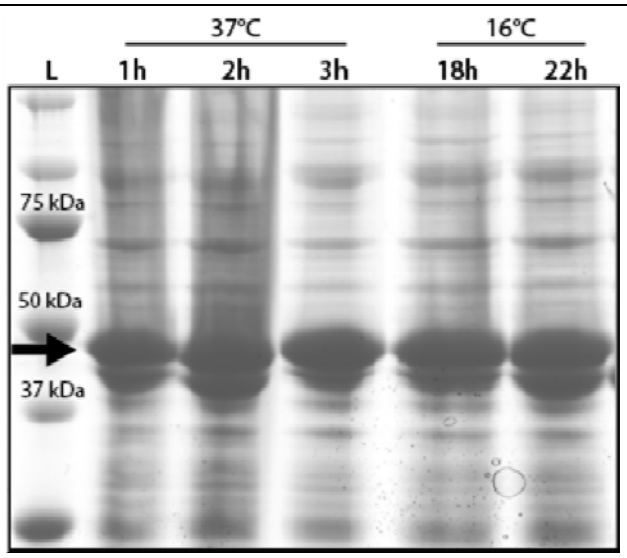

Figure 32: SDS-PAGE Coomassie stain of test expression for rPre1a.

Time 0 refers to before addition of IPTG. All other times are hours after induction. Induction was observed to be equivalent for all time points measured. Fusion protein mass = MW of [MBP (~42 kDa) + His_6 (~600 Da) + peptide (~4.3 kDa)] = ~47 kDa, indicated by arrow.

These results prompted an initial 2 L expression at 37°C for 3 h. After IMAC and rpHPLC purification, multiple peaks of equivalent size were seen in the region of expected mature toxin elution (~40% solvent B, minute 25) with no clear dominant peak (Figure 33). These results could be indicative of either disulfide shuffling due to exposure of glutathione during TEV protease cleavage or improper folding occurring *in vivo*. The latter hypothesis could be tested by optimizing the expression protocol. Reducing the temperature of induced expression to 16°C has been proven effective for enhancing the expression of soluble protein, limiting protein aggregation, and ensuring proper folding[531]. Therefore, a second 2 L expression was carried out with an overnight induction period of 16°C.

Equivalent protocols for IMAC purification and cleavage by TEV protease were performed as described previously (Figure 34). The entire cleavage reaction was separated by rpHPLC and a single

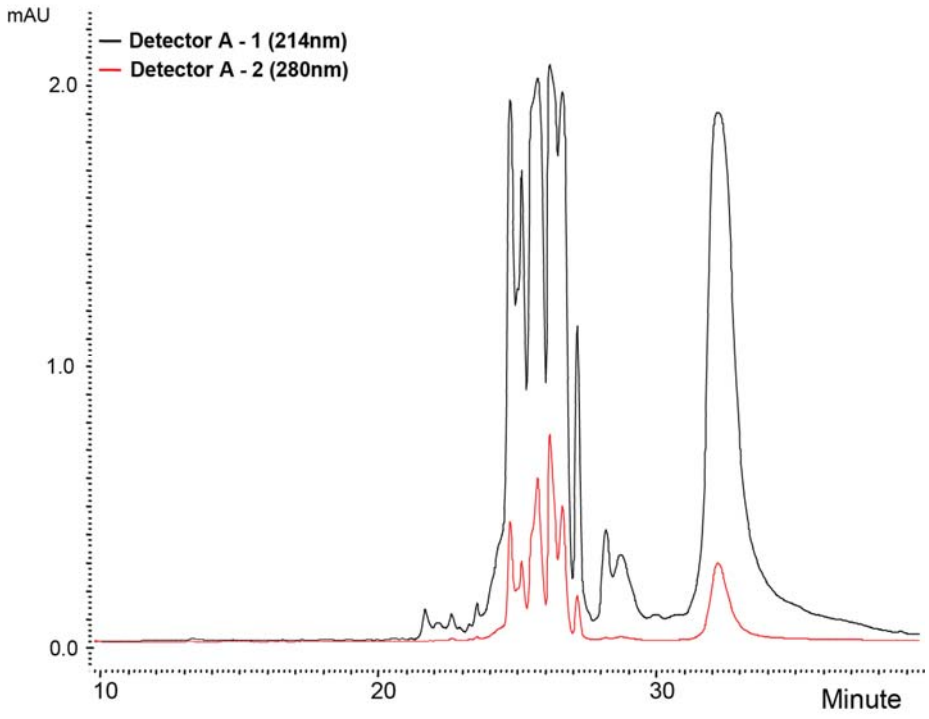

Figure 33: rpHPLC trace of rPre1a 2L expression at 37°C post TEV cleavage.

Cleaved MBP can be seen at minute 34.

dominant peak was observed (Figure 35A). This result was indicative of proper *in vivo* folding. The peak was identified by MALDI-TOF MS as containing the correct mass for recombinant (r)Pre1a, 4314.5. The theoretical mass of rPre1a was determined by adding the molecular weight of native Pre1a to that of Ser, equating to 4314.93 (Figure 35B). Despite the addition of an N-terminal Ser residue, recombinant Pre1a also eluted at the same retention time as the synthetic, properly folded Pre1a (Figure 36). The fraction was lyophilized and resuspended in pure H_2O for further analysis and functional testing. 10 µM stocks of purified TRTX-rPre1a were made and stored individually at -20°C to limit freeze-thawing of primary stock.

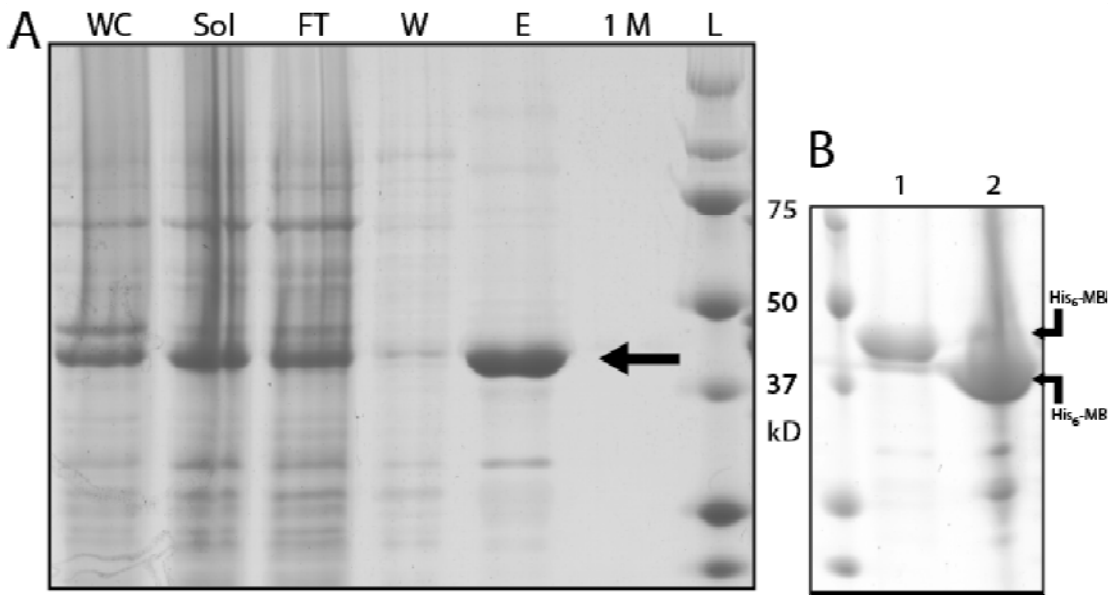

Figure 34: SDS-PAGE Coomassie stain of NiNTA purification of rPre1a lysate.
A) Purification of lysate by NiNTA IMAC. WC=whole cell lysate; Sol=Soluble lysate; FT=initial flow through; W=15 mM imidazole wash; E=250 mM imidazole elution; 1M=1 M final imidazole wash; L= molecular weight marker. B) Before (1) and after (2) TEV cleavage of fusion protein.

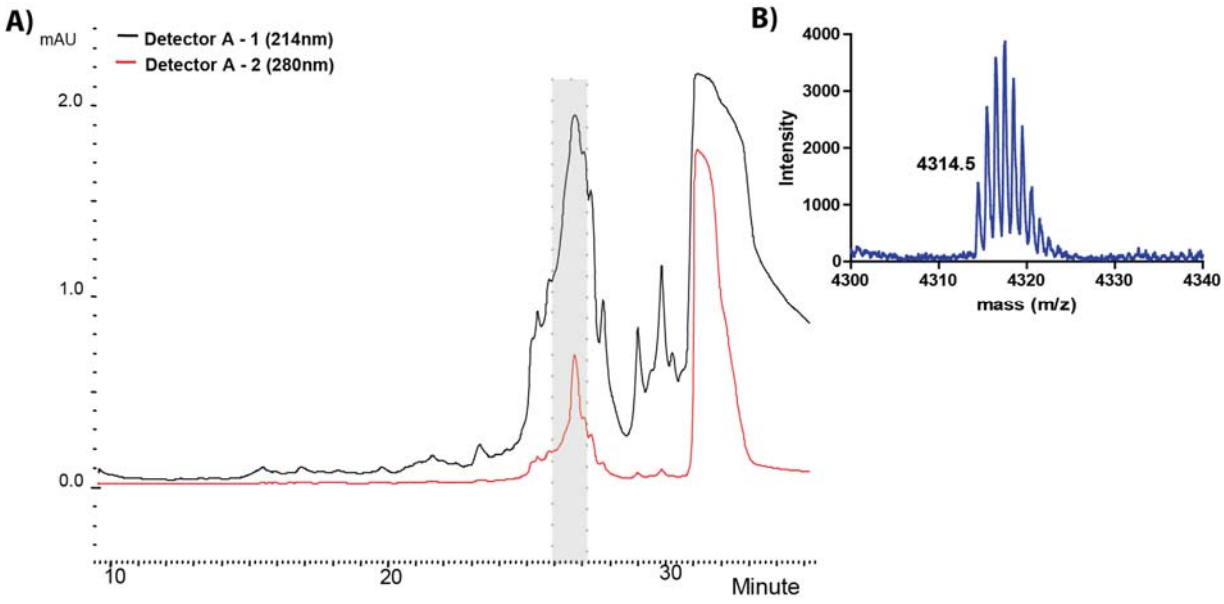

Figure 35: rpHPLC purification of rPre1a.

A) rpHPLC trace of rPre1a 2L expression at 16°C post TEV cleavage. A dominant peak is visible at minute 25-27, suggesting one dominant fold. B) MALDI-TOF MS confirmed a M+H$^+$ of 4314.5.

3.5 Na_V channel activity of TRTX-rPre1a

TRTX-rPre1a was tested on *X. laevis* oocytes injected with rat (r) or human (h) Na_V channel RNA and measured with two-electrode voltage clamp (TEVC) methods. Initial testing with 1 µM concentrations across all available isoforms of Na_V channels was performed to obtain a general selectivity profile, followed by concentration response curves for the more active isoforms. All available Na_V channel constructs were tested, which included the centrally expressed neuronal rNa_V1.2, the peripherally expressed neuronal rNa_V1.3 and hNa_V1.7, the skeletal muscle rNa_V1.4, and the

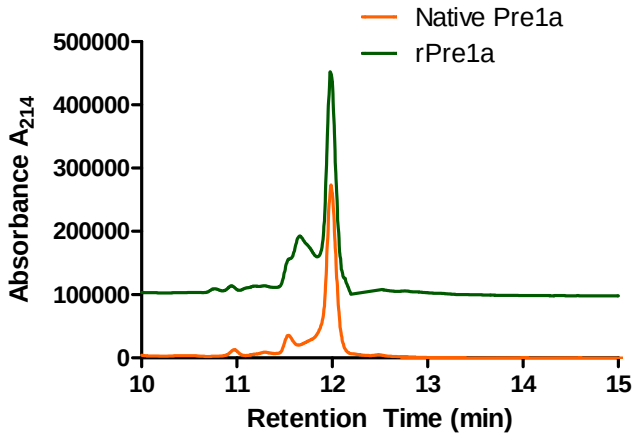

Figure 36: Comparison of elution time of rPre1a with native Pre1a

cardiac hNa$_V$1.5.

The observed effect of TRTX-rPre1a on rNa$_V$1.3 expressed in oocytes was consistent with previous results indicating inhibition of inactivation (Figure 37). Inhibition of fast inactivation can be viewed as a prolongation of late current, or a failure of the channel to conform to the inactivated state during a depolarizing stimulus. A slight potentiation of peak current was also detectable at 1 µM concentrations.

For all other Na$_V$ channels tested, TRTX-rPre1a exhibited either inhibition of current or resulted in no significant activity (Figure 38). TRTX-rPre1a had the greatest effect on the neuronally expressed rNa$_V$1.2 and hNa$_V$1.7, with 1 µM resulting in an approximate 70% reduction in peak current. Concentrations of 1 µM TRTX-rPre1a also inhibited rNa$_V$1.4 to a lesser extent, resulting in approximately 15% reduction in peak current. The functional effect of TRTX-rPre1a on hNa$_V$1.5 was negligible at a concentration of 1 µM. It is of interest to note that these initial results suggested neuronal selectivity over both skeletal and cardiac isoforms.

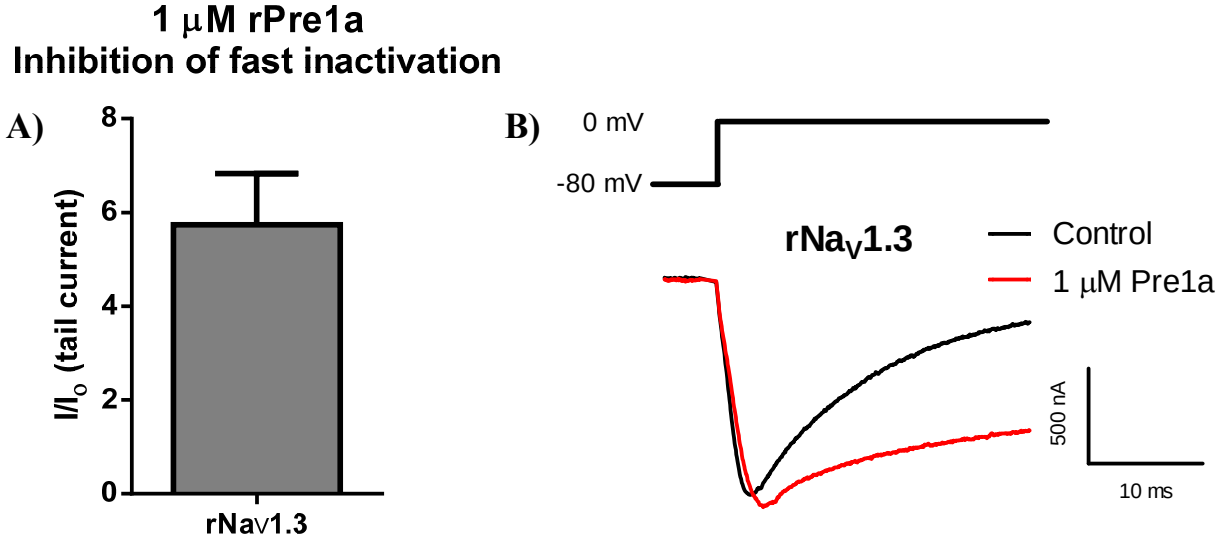

Figure 37: TEVC rPre1a inhibition of inactivation on Na$_V$1.3.

A) Inhibition of fast inactivation of rNa$_V$1.3 expressed in oocytes with 1 µM rPre1a, as measured by TEVC; n=5. Baseline inactivated current is equivalent to 0. Sample current trace for Na$_V$1.3 (B) shows inhibition of fast inactivation of late current with 1 µM rPre1a (red) after depolarization to 0 mV from a holding potential of -80 mV. Control current is shown in black.

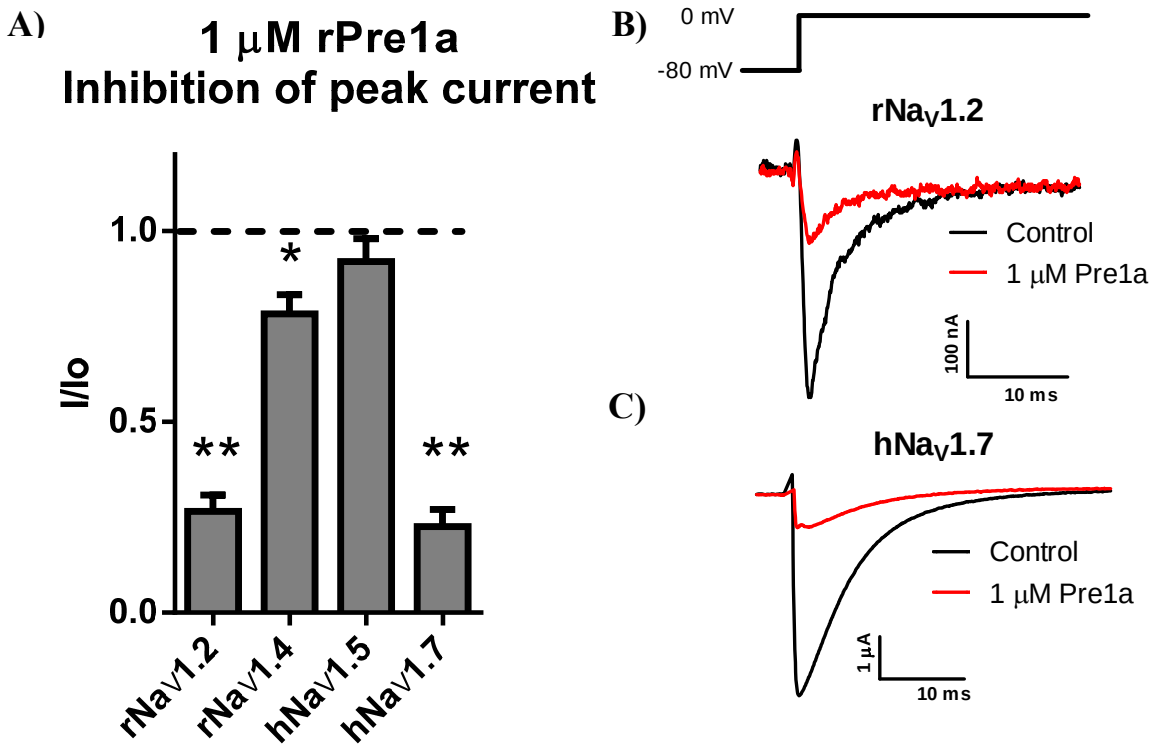

Figure 38: TEVC rPre1a inhibitory effects on Na_V channels.

A) Inhibition of Na_V peak current with 1 μM rPre1a against four separate rat or human Na_V isoforms expressed in oocytes, as measured by TEVC; $n \geq 3$ for each. The dotted line represents baseline current. Significant inhibition of the neuronal $rNa_V1.2$ and $hNa_V1.7$ is observed ($p < 0.001$). $rNa_V1.4$ is significantly inhibited to a lesser extent ($p < 0.05$). Example current traces for $rNa_V1.2$ (B) and $hNa_V1.7$ (C) showing inhibition of peak current with 1 μM rPre1a (red) after depolarization to 0 mV from a holding potential of -80 mV. Control currents are shown in black.

TRTX-rPre1a demonstrated an equipotent concentration-dependent effect when tested on both $rNa_V1.2$ and $hNa_V1.7$ using TEVC methods (Figure 39). The IC_{50} of TRTX-rPre1a is sub-micromolar a both channels: $rNa_V1.2$ with 290 nM and $hNa_V1.7$ with 340 nM. Concentration-response curves were also attempted on the FLIPR^{Tetra} platform using the Membrane Potential fluorescence kit with stably transfected, single Na_V channel expressing cell lines. As each cell line was unique to the channel it expressed, each required a separate assay. Aside from the cells used all variables were kept consistent with the exception of $rNa_V1.3$, where the concentration of veratridine used for depolarization was decreased to a submaximal concentration of 5 μM to allow for the observation of a potentiating

response. Assays were limited to available cell lines. Both $rNa_V1.6$ (IC_{50} = 6.4 µM) and $rNa_V1.7$ (IC_{50} = 7.5 µM) exhibited a concentration-dependent response to TRTX-rPre1a (Figure 40). Comparing the $Na_V1.7$ response between TEVC and FLIPR methods reveals a 22-fold difference in potency for the latter method. A range of TRTX-rPre1a concentrations were also tested on both $rNa_V1.3$ and $hNa_V1.4$ stably expressing cell lines using the same FLIPR methods. No effect of the peptide was observed in $hNa_V1.4$ in this assay up to 30 µM rPre1a. In the case of $rNa_V1.3$, analysis of the raw data for each well indicated an "all-or-nothing" maximal response with no concentration dependence, rendering an assay measuring an agonist response impractical.

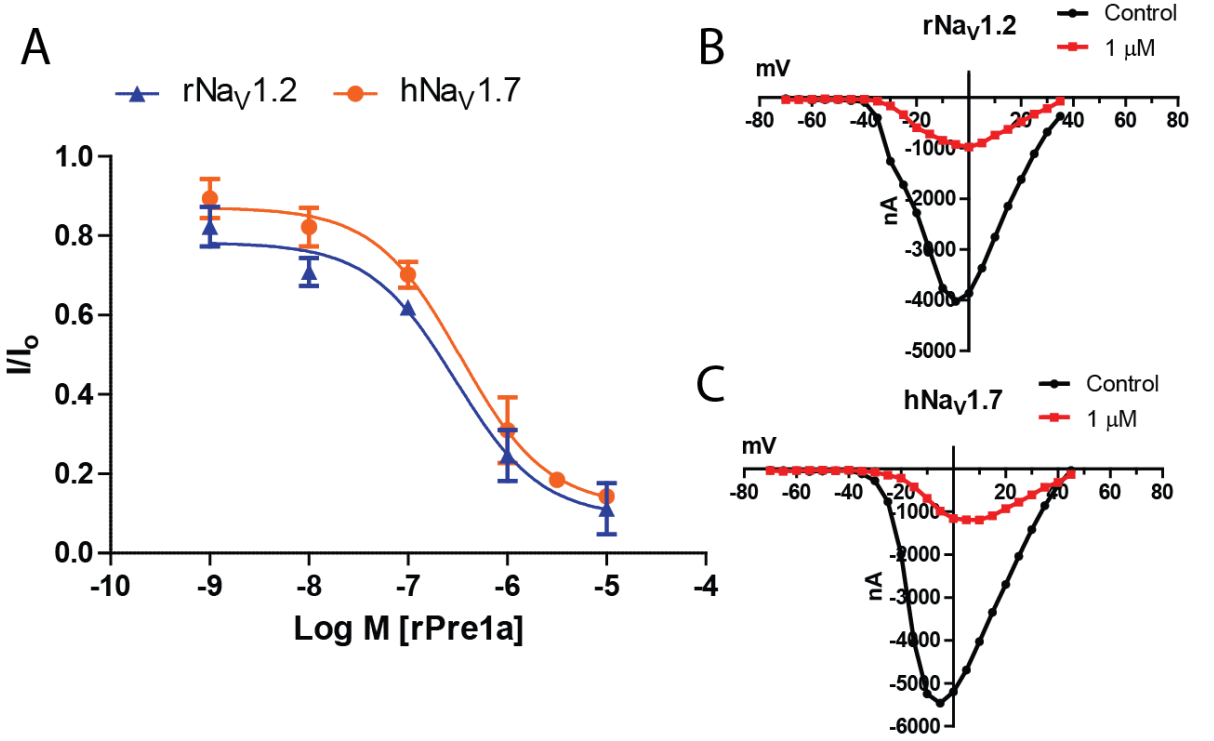

Figure 39: TEVC concentration response of rPre1a.

A) Equipotent inhibition of current for both $rNa_V1.2$ (IC_{50} = 0.29 µM) and $hNa_V1.7$ (IC_{50} = 0.34 µM); n ≥ 3 for each data point. Example IV-curves for both B) $rNa_V1.2$ and C) $hNa_V1.7$ after addition of 1 µM rPre1a.

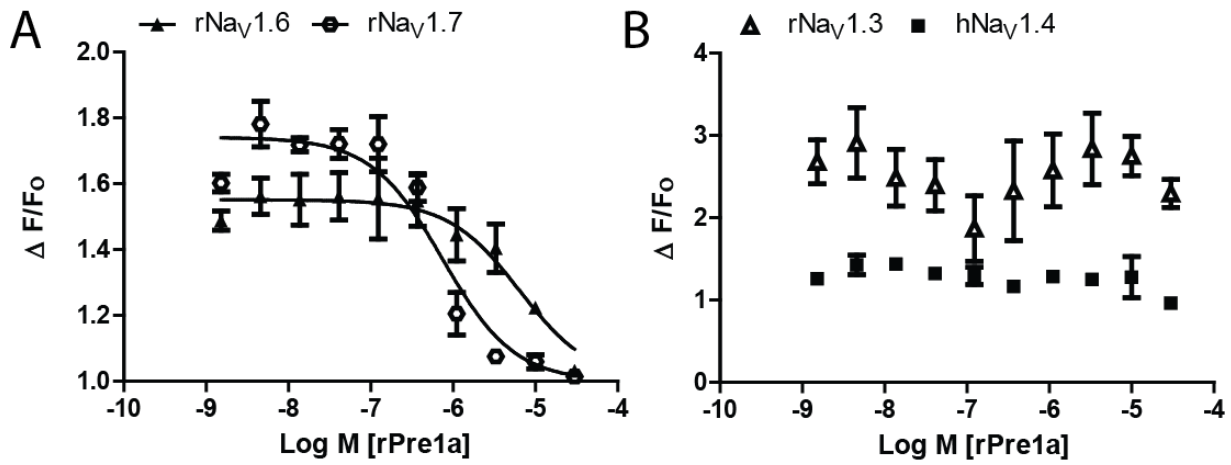

Figure 40: FLIPR membrane potential concentration response of rPre1a.

rPre1a tested on stably transfected cell lines A) expressing either rNa$_V$1.6 (IC$_{50}$ = 6.4 µM) or rNa$_V$1.7 (IC$_{50}$ = 7.5 µM. B) Neither rNa$_V$1.3 nor hNa$_V$1.4 resulted in a measurable fluorescent response after addition of rPre1a.

3.6 Structure of rPre1a

The development of an efficient bacterial expression system allowed the production of uniformly $^{13}C/^{15}N$-labelled TRTX-rPre1a for structure determination using heteronuclear NMR. The NMR data clearly indicated the presence of multiple stable conformations. Here we have chosen to characterize the most abundant form. Backbone assignments were fully completed using the $^{1}H_N$, ^{15}N, $^{13}C_\alpha$, $^{13}C_\beta$, ^{13}C resonance assignments for the toxin obtained from analysis of amide proton strips in 3D HNCACB, CBCA(CO)NH, and HNCO spectra. Full peak assignment lists can be found in Appendix E. Unfortunately, backbone RMSD values did not converge sufficiently to obtain a high resolution structure. Side chain ^{1}H and ^{13}C chemical shifts were obtained primarily from 3D H(CC)(CO)NH-TOCSY and (H)CC(CO)NH-TOCSY spectra, respectively. However, this pair of triple resonance experiments did not provide enough resolution for complete assignment of side chain ^{1}H-^{13}C connectivities, so some of the side chain ^{1}H resonances could not be unambiguously assigned. Therefore, a high resolution solution structure showing side chain positions could not be determined due to insufficient constraints. However, some secondary structure could be determined using the data available.

Secondary structure prediction analysis was run using TALOS software using the chemical shifts of backbone atoms (Figure 41). Two β-sheet formations were predicted for residues C_4-L_5 and Y_{22}-K_{23}. Analysis of the ^{13}C-NOESY strips confirmed the common ICK-motif disulfide folding pattern typical of many Na_V channel modulating spider venoms (Figure 42). Typical ICK connectivity involves six cysteine residues bound in a I-IV, II-V, III-VI pattern. $^{13}C_\alpha$ and $^{13}C_\beta$ carbons of connecting cysteine residues can be visualized in corresponding strips, denoting a close proximity in 3-dimensional space consistent with disulfide bonds between the Cys side chains.

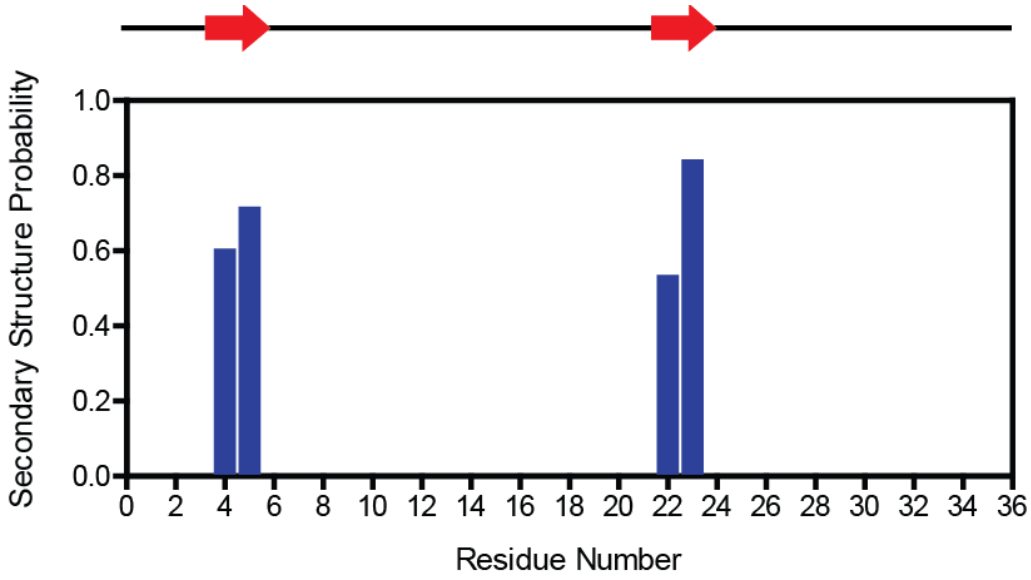

Figure 41: Secondary structure predictions of rPre1a as calculated by TALOS. *β-sheet predictions are denoted by red arrows.*

The ^{15}N-HSQC NMR data collected for TRTX-rPre1a also aided in the further characterization of its conformational heterogeneity. The ^{15}N-HSQC spectrum revealed one major and two minor conformers in solution as demonstrated by a series of smaller peaks (chemical shift perturbations of certain residues) (Figure 43). It was possible to assign the backbone of the two minor isoforms thus identifying which residues are moving in the minor isoforms (See Appendix F for figure showing the CBCA(CO)NH strips). It was previously discussed that the possibility for the observed heterogeneity was due to *cis-trans* isomerization around or near proline residues, of which there are two in TRTX-Pre1a. However, the residues in close sequence proximity to either P_{12} (S_{11}, K_{13}) and P_{19} (C_{18}, N_{20}) did not appear to exhibit chemical shift perturbations related to conformational heterogeneity. It should be noted that Pro is not visible on the ^{15}N-HSQC spectra due to its lack of amide protons.

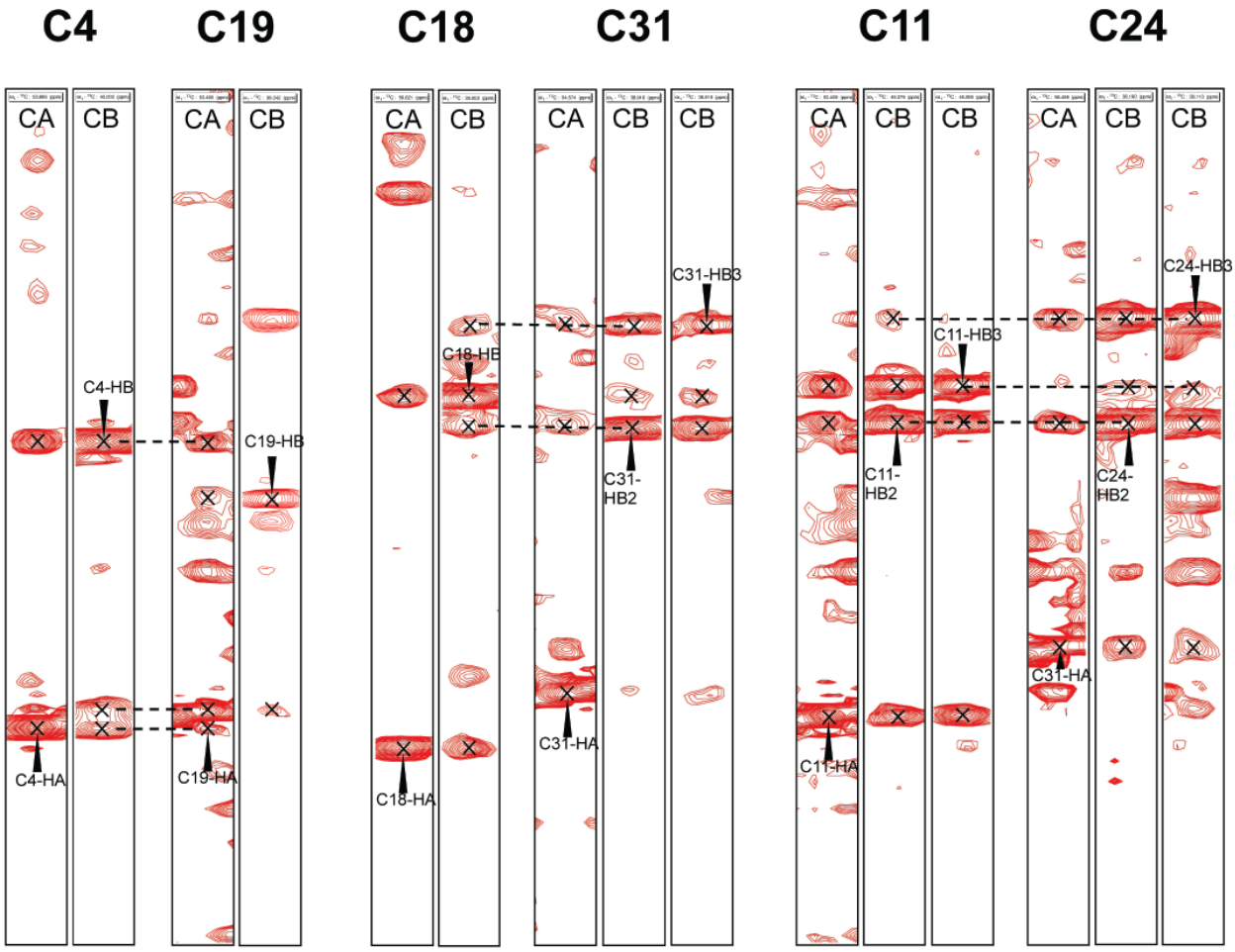

Figure 42: CBCA(CO)NH strips of the cysteine residues paired up as disulfide partners.

The connectivity of Cys residues corresponds to a typical ICK arrangement.

The residues that demonstrated the greatest chemical shift perturbations were C_4, L_5, G_6, W_7, F_8 and R_{10}, all of which occur in the Loop 1 region. G_6 represents an excellent visual example of relative conformational populations as directly related to peak intensity in the ^{15}N-HSQC. As seen in the insert of Figure 43, the major peak represents the major conformation in solution, while the two minor peaks represent 45% and 20% of the major form, respectively. This information coupled with the homology model strongly implicates the Loop 1 regions involvement with the apparent conformational heterogeneity of TRTX-Pre1a.

Finally, the homology model of TRTX-Pre1a was aligned with the backbone of the solution structure to determine the models quality (Figure 44). The solution structure appears quite similar to the homology model. However, deviations do occur with the positioning of the C-terminal tail.

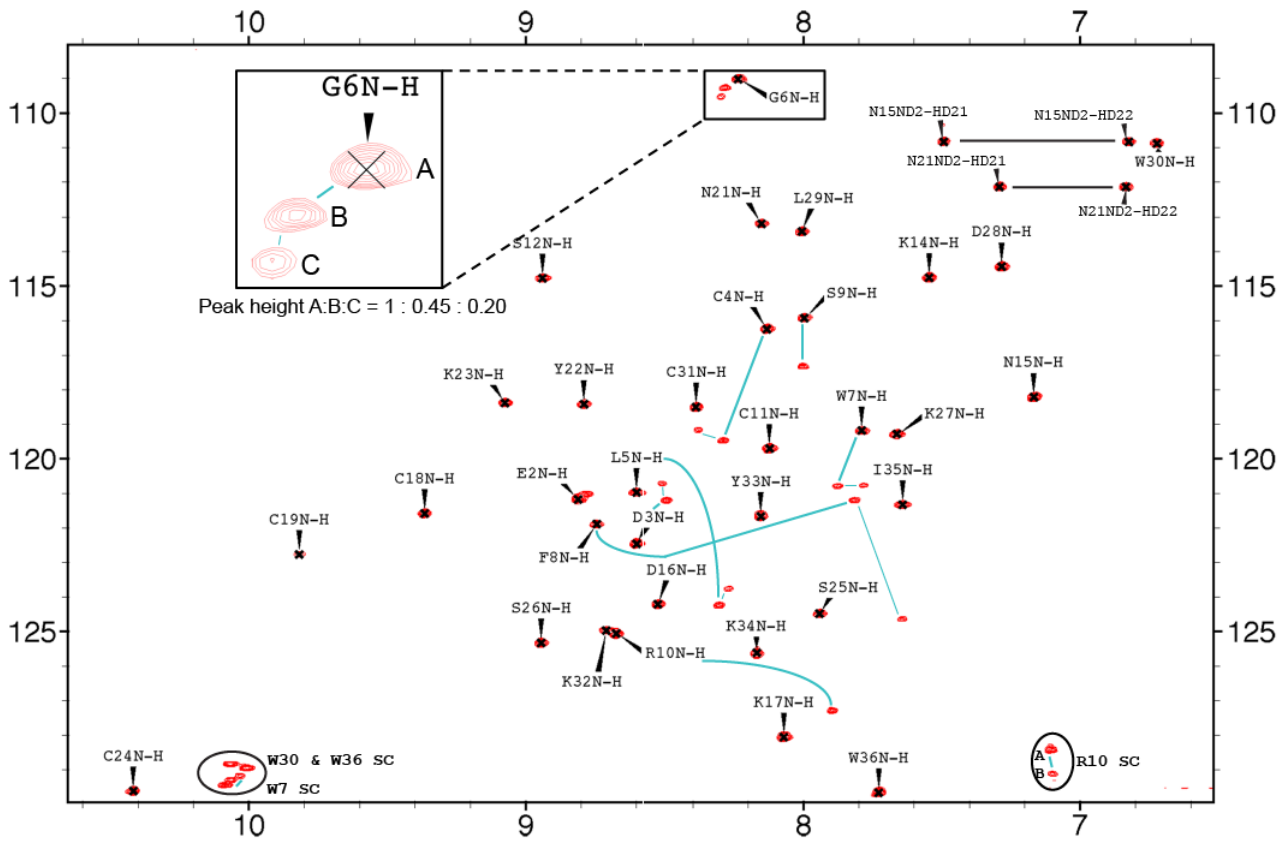

Figure 43: TRTX-rPre1a ^{15}N-HSQC. *Multiple conformational states are visible through peak shifting of a few residues, with Gly_6 highlighted as an example. The peak height intensities of Gly_6 reflect the relative proportions of each form of the peptide in solution (A:B:C/1:0.45:0.2). Peak shifts of other residues are traced by blue line. Asp_{15} and Asp_{21} side chain groups are labeled.*

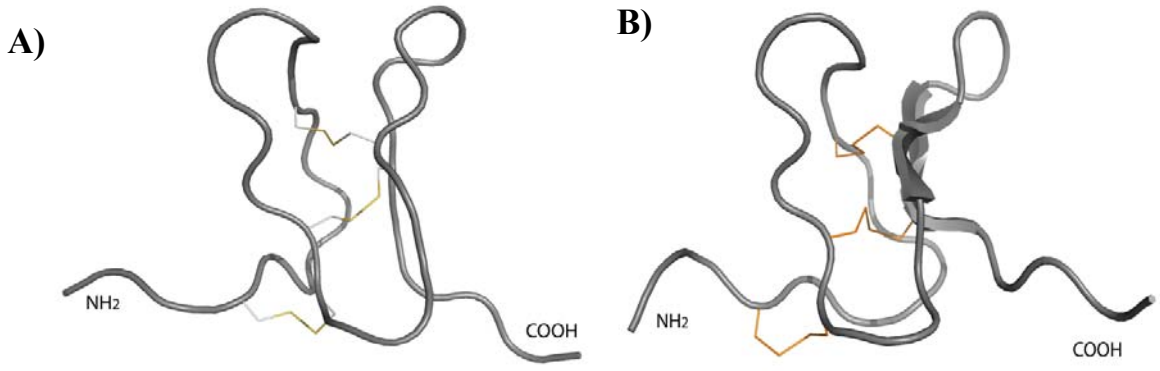

Figure 44: A backbone comparison of the TRTX-rPre1a solution structure and homology model. *A) The dominant solution structure is represented in a single backbone structure. B) A comparison to the TRTX-rPre1a homology model.*

4. Discussion

Spider venoms have been instrumental in defining novel modes of action of and sites of functional regulation on Na_V channels, demonstrating an ability to target extracellular loops around the S1-S4 voltage sensor region and act as gating modifier toxins[34, 78, 532]. The discovery of TRTX-Pre1a highlights the very interesting functional modulatory capabilities of spider venom peptides and, potentially, many other classes of venom peptides that share the structural conformation of the ICK motif. Although the inhibitory mode of action was not fully determined through functional studies, evidence suggests that TRTX-Pre1a could work as a gating modifier toxin. The mode of action can be inferred from i) structural aspects such as the amphipathic hydrophobic face common among gating modifier toxins, ii) a high sequence similarity to related ICK-motif peptides with voltage-gated ion channel gating modifier properties (Table 3)[533], and most importantly iii) the functional role this peptide has on $Na_V1.3$ through inhibiting inactivation, which in and of itself has been defined as a mechanism of voltage sensor trapping [215, 248]. In order to conclusively determine the mode of action as a gating modifier, one or more experiments can be conducted. Displacement of a radiolabelled ligand known to bind the Na_V voltage sensor by titration of TRTX-Pre1a would suggest equivalent or overlapping binding sites. Mutagenesis of voltage sensor or loop regions of the $Na_V1.2$ or $Na_V1.7$ channels known to bind gating modifier toxins, with a subsequent drop in activity for TRTX-Pre1a, would be a similar method of determination through active site association[34, 215]. An electrophysiological assessment could also be carried out that measures the voltage-dependence of activation, with a positive shift indicating gating modifier activity. However, experimental data remains to be completed in order to confirm this hypothesis.

4.1 Recombinant expression

Bacterial recombinant expression has been seen as a cost-effective and reliable alternative to producing peptides synthetically, potentially yielding milligrams of soluble, folded, mature peptide in a few liters of liquid medium[289]. The method used in this thesis for expressing recombinant TRTX-Pre1a was successful in producing high yields, with approximately 5 mg of mature, properly folded toxin produced per liter of LB medium. Recombinant expression also allowed the efficient production of uniform $^{13}C/^{15}N$ labeled peptide for NMR structural elucidation. The pLIC vector was chosen as a suitable candidate because of its production of a N-terminally fused maltose binding protein (MBP) and

periplasmic localization sequence[511]. The MBP protein acts as a solubility chaperone, limiting the occurrence of inclusion bodies that form from insoluble product. MBP has been show to be "uncommonly effective" at promoting peptide solubility when compared to other commonly used fusion proteins, such as glutathione S-transferase, and thioredoxin[534]. The exact mechanism of how and why MBP is so effective is not entirely known, although the periplasmic localization is known to aid folding. MBP itself is thought to have an "intrinsic" property of solubility, but endogenous chaperones within *E. coli* have also recently been demonstrated to mediate proper folding of the mature peptide[535].

The cytoplasm of both eukaryotic and prokaryotic organisms is known be a reducing environment, not conducive to proper disulfide bond formation[536]. Eukaryotic organisms create an environment to properly fold peptides within an organelle called the endoplasmic reticulum (ER). Prokaryotic organisms lack an ER. However, gram-negative bacteria such as *E. coli* have a periplasmic space that exists between the inner and outer membrane. Not only is this space considered non-reducing, multiple disulfide bond isomerases and other chaperones have been found within the periplasm, making it a specialized region within the cell for post-translational folding[537]. The *MalE* periplasmic localization sequence on the pLIC vector promotes the fusion protein to be shuttled to the bacterial periplasm post-production, where environmental conditions are more conducive to native folding [538].

The pLIC vector is completed with the addition of a TEV recognition site for cleavage of mature toxin from the fusion construct and an N-terminal His_6 tag for immobilized-metal affinity chromatography (IMAC) with NiNTA resin. The TEV cleavage recognition site requires an optimal signal sequence of ENLYFQ/S. Although TEV cleavage has been shown to work effectively when the C-terminal Ser is replaced by multiple other residues[539], it was our observation that Ser was necessary to induce repeatable, full cleavage of the mature toxin from the MBP fusion protein. However, cleavage between the Gln and Ser leaves a N-terminal Ser residue as an artifact of cleavage on the mature toxin. This did not appear to have an effect on the function of this peptide as compared with the native peptide of the synthesized native sequence.

In summary, the recombinant expression system efficiently produced milligrams of soluble, properly folded peptide in a reproducible, cost-effective manner.

4.2 Activity

Many of the Na_V modulating spider venoms toxins so far discovered conform to an ICK motif and act as gating modifier toxins, targeting extracellular loops around the S1-S4 voltage sensor region in DI-DIV[34, 78, 532]. As discussed in Chapter 1, these regions have been segmented into neurotoxin receptor site 3 and site 4 as originally defined by α-scorpion toxin and β-scorpion toxin binding, respectively. Site 3 toxins are voltage-dependent inhibitors of inactivation that bind in a state-dependent manner, trapping the voltage sensor in an open, hyperexcitability conformation[231]. Likewise, site 4 modulating peptides produce hyperexcitability by shifting the voltage-dependence of activation to a hyperpolarized potential, resulting in activation at sub-threshold potentials[188, 254, 540]. A few spider venom peptides have been found to bind to the same loop regions comprising site 4 but result in inhibition of current, or in some cases may occupy an undescribed binding region altogether.

One of those venom peptides that may define a new site for gating modifier peptides is β/ω-TRTX-Tp2a (ProTx-II)[251, 541]. Initial results using point mutations of specific extracellular loop amino acids of $hNa_V1.5$ concluded that Tp2a does not bind to any extracellular region, but instead binds to a transmembrane helical region[542]. The amphipathic structure of Tp2a, caused by its hydrophobic face composed of Loop 1 residues, was shown to contribute to lipid binding[542]. This functional property was seen previously with other spider toxins and presented as a hypothesis of a lipid submerged binding site[532]. An exploration of Na_V specificity found Tp2a to be 100-fold more selective to $Na_V1.7$ than other isoforms, which is interesting because $Na_V1.7$ possesses a unique residue on the C-terminal portion of DIIS3[541]. Position 813 is a Phe, whereas all other Na_V subtypes have a Gly or Ser ($Na_V1.6$). Mutation of Phe813 to a Gly or Ser resulted in 100-fold reduced Tp2a sensitivity relative to other Na_V subtype activity[541]. However, mutating the equivalent Gly839 residue in $Na_V1.2$ to Phe did not significantly increase sensitivity to Tp2a, suggesting that the interaction of Tp2a is more complex and the Phe in this position is the only residue necessary to confer high affinity of Tp2a[541] [34]. Results focusing on larger regions of the voltage sensor domain further support the S3-S4 segments as targets for Tp2a high affinity binding, and suggest that Tp2a may actually bind (at least partially) to extracellular S3-S4 loop regions[34]. Using chimeric expression of the $rNa_V1.2$ voltage sensor "paddle" regions – composed of the C-terminal S3, N-terminal S4 regions, and the S3-S4 extracellular linker – spliced into $K_V2.1$ domains, Tp2a was shown to inhibit activation by interacting with DI, DII, and DIV[34]. This finding was somewhat surprising given the presumed role of DIV in

inactivation as suggested by the authors. Based on the findings of this research, Bosmans et al. proposed that for a toxin to alter inactivation it must exclusively interact with the voltage sensor paddle of DIV and "any additional interactions with the other paddles will alter channel opening"[34]. This is an interesting finding that may give clues as to how Pre1a is able to alter the pharmacology of different Na_V isoforms in two distinct ways. If this hypothesis is followed, the interaction of Pre1a with the individual domains of $Na_V1.3$ should be explored, specifically whether it binds DIV without interacting with the other three domains of this isoform. However, the authors comment that there is high variability when dealing with specific toxins and receptor interfaces, and there is no "general lock-and-key mechanism" to define a standard[34].

As stated previously in Chapter 1, μ-TRTX-Hh2a (huwentoxin-IV) has been shown to interact with neurotoxin receptor site 4 and because of its high affinity for $Na_V1.7$, has become a popular candidate for intensive toxin profiling and Na_V selectivity characterization through directed mutagenesis and functional studies[243, 256, 543-545]. Both Tp2a and Hh2a have been demonstrated to inhibit activation by trapping the DII voltage sensor in the resting configuration, although HWTX-IV may selectively bind to neurotoxin site 4[243, 546]. Both of these toxins were the highlight of an extensive study to define their voltage sensor activity on $hNa_V1.7$[543]. The results of this study defined a new mode of action for Tp2a, where at concentrations above 1 μM the toxin was found to induce sustained currents through inhibition of fast inactivation in a mechanism similar to neurotoxin receptor site 3 α-scorpion toxins, as well as reflecting activity seen with Pre1a on $Na_V1.3$. This activity was found to be preferential to DIV of $Na_V1.7$ and fully independent to inhibition of activation, which like Hh2a requires the DIIS3-S4 paddle region. Unlike Pre1a, Tp2a exerts its mode of action simultaneously and is unable to fully inhibit Na_V current. These results suggest that Tp2a can bind to two different sites of the Na_V channel simultaneously. This not only calls into question the previous proposal that DIV requires an exclusive interaction to inhibit Na_V inactivation, but may also help redefine the roles of the classical view of Na_V neurotoxin receptor sites[34, 543].

Data gathered from experiments with Hh2a and Tp2a not only demonstrate unique functional promiscuity, but also give much needed insight into the mechanism of interaction with Na_V channels. Through the work described, the extracellular loops of the voltage sensor region of DII and DIV have been shown to be critical for the function of these two peptides' specific mode of action. This insight can give us ideas on how to determine the functional role of Pre1a for future studies, as Pre1a exhibits

both inhibition of activation and inhibition of fast inactivation. Hh2a has been further characterized through Ala scanning and directed mutagenesis, demonstrating the functional necessity of hydrophobic residues on Loop 1 and the C-terminal region of the toxin[547]. Residues contributing to the hydrophobic face of Pre1a exist in similar Loop 1 and C-terminal regions, suggesting that this region of Pre1a is likely to be important for its activity at Na_V channels.

As with Tp2a, a significant structural feature of gating modifier peptides is their amphipathicity, with one face composed of hydrophobic residues surrounded by polar, mostly basic residues[254, 255, 548, 549]. This structural composition is thought to aid in their observed ability to partially partition within the cellular membrane and interact with the transmembrane voltage sensor region[532]. This amphipathicity could also function to mediate interactions across different regions on the surface of the target receptor simultaneously, resulting in multi-domain binding[550]. Membrane partitioning should be included in future experiments to assess this ability in TRTX-Pre1a. Lipid model systems using 1-palmitoyl-2-oleoyl-*sn*-3-phosphatidylcholine (POPC) or of a mixture of POPC and 1-palmitoyl-2-oleoyl-*sn*-3-phosphatidylglycerol (POPG) to mimic the negative surface potential of the lipid leaflet facing the cytoplasm have been successfully tested and can be reproduced to determine if Pre1a exhibits membrane partitioning[551-553].

The functional profile of TRTX-Pre1a proved to be unique in that it not only inhibited $Na_V1.2$ and $Na_V1.7$ at sub-micromolar concentrations, but inhibited fast inactivation of $Na_V1.3$ as well. As discussed, this inhibition of inactivation has been previously noted with Tp2a [543]. However, this effect was caused simultaneously with inhibition of activation. Sequence similarity to known peptides of similar class and known mechanisms of action give hints to the possible mechanism of Pre1a activity. The observed inhibition of fast inactivation of $Na_V1.3$suggest that TRTX-Pre1a interacts with the voltage sensor as a gating modifier. A small depolarizing shift in the $V_{1/2}$ max of $Na_V1.7$ and $Na_V1.2$ was observed for Pre1a (See Appendix C for normalized I-V plots), although more experiments are needed to confirm the results and decrease the standard error.. The inhibitory effect on $Na_V1.2$ and $Na_V1.7$ still remains to be determined. If $Na_V1.3$ activity is due to a voltage sensor interaction, inhibition of activation could be via a mode of action similar to that of site 4 spider venom peptides, requiring the DIIS3-S4 paddle region. This mechanism involves voltage sensor trapping in the closed state, resulting in inhibition of current during a standard depolarization.

As to the binding sites through which it inhibits activation of $Na_V1.3$, there are several possibilities: i) it binds to site 3 in a mechanism similar to Tp2a or α-scorpion toxins ii) it binds to site 4 of $Na_V1.3$ but inhibits inactivation, not activation, or iii) it interacts with a completely novel binding site, around the voltage sensor domain or otherwise, to inhibit inactivation. As shown with Tp2a, these macromolecules are able to bind across sites, affecting multiple regions at once. Understanding the basis of the dual pharmacological action of Pre1a is an important step which requires further experimentation. Future studies to elucidate this activity could include using Na_V channels with mutations of binding sites in combination with Pre1a mutants, the development of Na_V channel chimeras similar to Bosmans referenced work, where a single domain of the Na_V channel is substituted with a K_V domain[79], and competitive binding experiments with known site 3 and site 4 toxins. Finally, the inhibitory effects of site 4 inhibitors can be reversed by strong, long-lasting positive voltage pulses, which drive the voltage sensor back into its activated conformation[246]. This experiment could be attempted as justification for site 4 interaction, although it is possible that an undefined interaction site in the voltage sensor region could be involved in the inhibitory activity of TRTX-Pre1a. More detailed examples of electrophysiology experiments are given in the final discussion. Regardless, defining the mode of action of Pre1a and its site of Na_V channel interaction across the various isoforms remains as critical steps. If TRTX-Pre1a is shown to be a gating modifier and not a pore blocker, it is proposed that it be given the prefix "β/δ" to indicate the dual activity at Na_V channels; β to indicate that it shifts the voltage-dependence of activation of $Na_V1.2$ and $Na_V1.7$, and δ to indicate inhibition of fast inactivation of $Na_V1.3$, as per King et al. [353].

4.2.1 FLIPR and TEVC discrepancy

An adaptation of the FLIPR assay developed in Chapter II was attempted using single Na_V channel expressing cell lines against TRTX-rPre1a. For the initial cell lines tested, all showed a significant decrease in potency as compared to TEVC methods tested. A direct comparison could be made with $Na_V1.7$, which has a 22-fold higher IC_{50} value while using the FLIPR platform. It is important to mention that different $Na_V1.7$ channels were used between platforms, with the human homologue of $Na_V1.7$ used for TEVC experiments and the rat homologue of $Na_V1.7$ expressed in the cell lines used for FLIPR assay. It is unlikely that such a large discrepancy would be apparent when both channels share a 92.7% sequence homology, but the possibility cannot be completely discounted[554]. Another likely scenario involves cross-platform variability due to different endpoint responses being measured

and different host cells tested (oocytes versus mammalian cells) to name a few, all contributing to the apparent discrepancy in sensitivity. As TEVC was used for initial discovery purposes, the data obtained set a precedent for activity. The FLIPR assay resulted in much lower potencies overall and TEVC was pursued as the primary means of functional characterization for further studies.

4.3 Structure

Structural heterogeneity has been observed among a few tarantula toxins affecting the voltage sensor domain on voltage-gated ion channels[524, 555, 556]. VSTX3 is a toxin affecting the voltage-gated potassium channel from archeabacteria *Aeropyrum pernix* and showed a broad rpHPLC chromatographic profile[555]. Likewise, κ-TRTX-Gr1a (hanatoxin 1) has been shown to elute as two chromatographically separated peaks in equilibrium[524, 556]. In the case of κ-TRTX-Gr1a the authors concluded that the two peaks were a chromatographic phenomenon [524]. However, for VSTX3 it was proposed that some tarantula toxins affecting the voltage sensor domain of voltage-gated ion channels might exhibit a degree of conformational heterogeneity. As mentioned previously, κ-TRTX-Gr1a exhibits the ability to interact with multiple regions of the K_V channel simultaneously. Perhaps the structural flexibility of these peptides allows them to occupy multiple binding domains and is necessary for their promiscuous function. This would be an extremely interesting phenomenon to explore, with relevant implications for rational drug design. Unfortunately, in the case of VSTX3, this phenomenon was not explored in more detail[555].

The chromatography of κ-TRTX-Gr1a appears very much like the chromatographic behavior observed for TRTX-Pre1a, as can be seen in Figure 30 and the inset of Figure 28. Therefore an experiment similar to the one conducted by Swartz and Mackinnon was carried out [524]. Purified, folded TRTX-Pre1a was injected and fractions of the dominant peak were collected. The fractions collected from the major peak were reinjected and a similar chromatographic profile with the two peaks was evident, as visualized in the inserts in Figure 30. This could be partially due to the multiple structural conformations that appear to be present in solution at room temperature. The possibility that the two visible peaks within the inset of Figure 28 originate from at least two conformational isomers of TRTX-Pre1a in solution was supported by information gained from making a homology model of the peptide and confirmed using NMR data collected to determine the solution structure of TRTX-rPre1a.

In order to gain a better understanding about the possible causes of the apparent conformational heterogeneity, a homology model of TRTX-Pre1a was made using the solution structure of β-TRTX-Ps1a. The model revealed key structural features, such as a hydrophobic face made up of five residues, W_7, F_8, Y_{22}, W_{30} and Y_{32}. This structural feature is common with many Na_V modulating, ICK motif, spider venom peptides[245] and has been hypothesized to contribute to the voltage sensor trapping mechanism of site 3 and site 4 gating modifier toxins[532]. The hydrophobic face has been theorized to allow the peptide to partition within the outer cell membrane, exposing a larger surface of interaction within the voltage sensor region[557]. The model revealed possible structural tension within the between the large aromatic residues of the hydrophobic face, hypothesized to be a product of aromatic stacking which will be discussed in detail later. To confirm the constraints and provide more evidence against the argument that this could be an artifact of the template used for modeling TRTX-Pre1a, a solution structure was attempted.

The solution structure of TRTX-rPre1a was partially solved using heteronuclear NMR methods previously described. The peptide was uniformly ^{13}C- and ^{15}N-labeled through recombinant methods, which allows for high resolution chemical shift mapping of resonances [558]. However, the backbone RMSD values did not converge sufficiently to determine a high resolution structure, nor was the assignment of the aliphatic and aromatic side chain ^{1}H and ^{13}C atoms possible to complete using the acquired TOCSY spectra. Regardless, the information available was enough to assign secondary structure. Through analysis of the Cys residues through the ^{13}C-NOESY strips, it was possible to identify disulfide bond connectivity through interproton nuclear Overhauser effect (NOE), which indicated the pairs of protons that are close to one another in space by around 6 Å. This was achieved by identifying NOEs between paired Cys residues, due to their proximity through space. The connectivity seen through this method was consistent with the standard ICK motif connectivity of I-IV, II-V, III-VI. Secondary structure of TRTX-rPre1a was predicted using TALOS software, which identified residues C_4-L_5 and Y_{22}-K_{23} as potential contributors to β-sheet formation. The standard ICK fold as mapped in Figure 5 in the introduction identifies the typical antiparallel β-sheets found in many Na_V modulating spider venom peptides. Residues C_4-L_5 represent a region on the ICK map that typically does not conform to a β-sheet on other peptides of similar class derived from spider venom[309]. Analysis of the backbone structure of TRTX-rPre1a suggests that a β-sheet in this position would not align in an antiparallel fashion (Figure 44). TALOS also did not predict a more common anti-parallel β-sheet that is known to occur in proximity to the 6^{th} Cys residue. Relying on the

homology model, a β-sheet around the 6th Cys residue would likely align in an antiparallel fashion to the Y_{22}-K_{23} β-sheets.

Although it was not possible to determine a high resolution structure, important evidence for the cause of structural heterogeneity in TRTX-Pre1a was found upon examination of the ^{15}N-HSQC spectrum. The hypothesis of *cis-trans* isomerization around the Pro amide bond was discounted a due to a lack of chemical shift perturbation in the vicinity of these residues. Perturbations were seen in residues associated with the Loop 1 region, confirming that the non-symmetrical peak observed on rpHPLC is due to structural heterogeneity under the chromatographic conditions. Furthermore, the NMR data indicates that the hydrophobic residues in this region – particularly W_7 and F_8 – are involved in the structural heterogeneity as hypothesized above. Analysis of the G_6 chemical shift perturbations indicated a presence of at least three forms of the toxin in solution.

These findings brought us back to the homology model in Figure 31 to study the Loop 1 region. Directly adjacent to the G_6 residue are two aromatic residues contributing to the hydrophobic face, W_7 and F_8. It is highly plausible that the five aromatic residues composing the hydrophobic face associate in a process known as aromatic stacking. Aromatic stacking involves non-covalent, weak interactions of ring centroids separated by a preferential distance of between 4.5-7 Å and typically results in structural stabilization, with multiple electrostatically favorable geometries possible [559]. The electrostatic component has been proposed to arise from interactions of the quadrupole moments of the aromatic rings. Two confirmations are found commonly in peptides i) π-interactions, which are side to face interactions of the ring centroid, and ii) offset stacking, which exhibits similar geometry to that of DNA base pairs [560]. Whereas β-TRTX-Ps1a and other similar toxins appear to form an ordered aromatic stack with two to three contributing residues, the association of five offset aromatic residues of TRTX-rPre1a may contribute to the shuffling of the aromatic stacks between multiple energetically favorable positions. In TRTX-Pre1a, the W_7 residue is sandwiched between a F_8 and W_{30} residue on one side and a Y_{22} and Y_{32} on the other, within 7 Å to each. This positioning is hypothesized to cause conformational fluctuations of W_7 between multiple possible aromatic stacking interactions. Complicating the issue further, both W_7 and F_8 appear directly adjacent to each other, constrained by their proximity and the structural rigidity of disulfide bonding. The strong forces of disulfide bonds associated with the ICK motif secondary structure would work in opposition to weaker, non-covalent aromatic side chain interactions [561]. It is a hypothesis of this chapter that the aromatic stacking of

TRTX-Pre1a contributes to the structural instability, with one dominant form stabilized by the peptides structural motif. The W_7A residue appears critical for this mode of action.

4.4 Summary

TRTX-Pre1a demonstrated a unique and interesting set of qualities, not yet seen with venom peptides characterized to date. Not only did Pre1a selectively inhibit neuronal Na_V peak current – including the novel pain target $Na_V1.7$ – but inhibited fast inactivation of the neuronal $Na_V1.3$ channel at sub micromolar concentrations. Further, the appearance of conformational heterogeneity was demonstrated over multiple experiments. Data suggested the Loop 1 region of Pre1a contributes to this observed structural heterogeneity. This could likely be related to opposing forces due to favorable aromatic stacking interactions, steric clashes, and structural constraints due to the covalent disulfide bonds. The contribution of Gly_6 to Loop 1 flexibility could also play a part. The role of this conformational flexibility, if any, is unknown, but it may be that it could play a role in the ability of Pre1a to exhibit two mechanisms of action at different channels.

In order to test this hypothesis, as well as examine the functional effects of Pre1a in greater detail, a mutagenesis study was undertaken and will be discussed in detail in the next chapter.

Chapter IV: Guided mutagenesis and SAR of TRTX-rPre1a

1. Introduction

The previous chapter highlighted the unique, characteristics of β/δ-TRTX-Pre1a and demonstrated an efficient method of production for this peptide that can be used as a platform to carry out structure-activity relationship studies. The ability of TRTX-Pre1a to modulate different isoforms of the Na_V receptor family with two distinct mechanisms of action can give helpful insight about how subtle changes in amino acid sequence can result in pronounced selectivity and functional changes. Not only did TRTX-Pre1a demonstrate functional characteristics not yet seen with other venom peptides, but it also exhibited conformational heterogeneity

TRTX-Pre1a shares close sequence homology to many other spider venom peptides discovered over the last decade, specifically the Na_V spider toxin Family 1[239] (Table 4). Many of these peptides already have pharmacological profiles of varying scope (from very basic nerve fiber function to in depth selectivity) that can be drawn upon to begin to understand which regions of Pre1a might contribute to its activity and subtype selectivity. Additionally, the inhibitory cysteine knot (ICK) motif apparent among these Na_V modulating peptides imparts a further commonality. The structural rigidity of the ICK motif makes these peptides of interest for therapeutic development as it imparts high levels of thermal and biological stability. In combination, these similarities can be exploited in order to learn more of how structural and sequence characteristics impart functional differences. The close structural motif of all these peptides allows a close comparison of minor amino acid differences between them.

In essence, using available data regarding known peptides of similar classes can help determine potential residues of functional importance. This chapter describes the directed mutagenesis of TRTX-rPre1a and the resulting pharmacologic and structural changes imparted by these selected mutations. Using a combination of results obtained in the last chapter coupled with information collected from various sources describing studies on homologous venom peptides, five mutants were designed and produced. These mutations focused on points of interest regarding either i) the observed structural heterogeneity of TRTX-Pre1a, hypothesized to be a result of aromatic interactions within the Loop 1

region; or ii) the observed functional necessity of individual residues found through the alignment of characterized peptides with high sequence similarity yet differing selectivity.

Table 4: Na_V modulating spider toxin alignment.

Comparative amino acid sequences of spider toxin family members with known Na_V selectivity profiles. Green equates an IC_{50} <1 μM. Red is inactive up to 10 μM. Yellow is activity >1 μM. Blue represents <1 μM agonist activity. White is no data available. Data accessed through Arachnoserver[509].

Family	Peptide	Sequence	Na_V channel activity									Ca_V	K_V
			1.1	1.2	1.3	1.4	1.5	1.6	1.7	1.8	1.9		
1	**β/δ-Pre1a**	-EDCLGWFSRCSPKNDKCCP--NYKCSSKDLW-CKYKIW						?					
	β-Ps1a	--DCLGFLWKCNPSNDKCCRP-NLVCSRKDKW-CKYQI											
	β-Cm1a	--DCLGWFKSCDPKNDKCCK--NYTCSRRDRW-CKYDL											
	β-Cm1b	--DCLGWFKSCDPKNDKCCK--NYTCSRRDRW-CKYYL											
	μ-Hhn1a	--ECLGFGKGCNPSNDQCCKSANLVCSRKHRW-CKYEI	DRG TTXs					DRG					
	μ-Hhn1b	--ECLGFGKGCNPSNDQCCKSSNLVCSRKHRW-CKYEI											
	μ-Hh2a	--ECLEIFKACNPSNDQCCKSSKLVCSRKTRW-CKYQI											
	μ/ω-Hh1a-d	--ACKGVFDACTPGKNECCP--NRVCSDKHKW-CKWKL						DRG					
2	Cj1a	--ACREWLGGCSKDAD-CCAH--LECRKKWPYHCVWDWTV											
	β/ω-Tp1a	--ECRYWLGGCSAGQT-CCKH--LVCSRRHGW-CVWDGTFS											
	β-Cm2a	^EGCRKLLGGCTIDDD-CCPH--LGCNKK-YWHCGWDGTF											
3	β/ω-Tp2a	--YCQKWMWTCDSER-KCCEGM--VC---RLW-CKKKLW											
7	β/κ-Cj1a	DGECGGFWWKCGRGKPPCCKG--YACSKTWGW-CAVEAP											
	δ-Cj1a	--ACGQFWWKCGEGKPPCCANFA--CKIGLYL-CIWSP											
	β/κ-Cj2a	--YCQKWMWTCD-SKRACCEGLR--CK---LW-CRKIIG GVDK^	DRG					DRG TTXs/TTXr					

Alanine (Ala) scanning is a commonly adopted method used to determine the functional significance of individual residues on both the structure and activity of a peptide[562, 563]. Out of the twenty standard amino acids, Ala is used because it contains a non-bulky, chemically inert methyl functional group that maintains the secondary structure preferences of many of the other amino acids while eliminating the side chain interactions. While Gly eliminates the functional side chain group completely, the replacement of the methyl group with a hydrogen atom creates added conformational flexibility that can distort a peptide's secondary structure, hence its lack of use for a residue replacement[564]. This chapter incorporates both Ala substitutions as well as substituting residues based on functional properties, in this case charge. Recombinant methods of production optimized for TRTX-rPre1a in the previous chapter were used in lieu of solid phase synthesis.

The primary aims of this chapter were as follows:

1) Identify the residue(s) responsible for the observed structural heterogeneity apparent in native TRTX-Pre1a and determine the functional effect of their mutation to alanine.

2) Focus on functional mutations of a single C-terminal residue known to impart specific $Na_V1.3$ isoform selectivity and attempt to engineer in/out higher $Na_V1.7$ selectivity for rPre1a.

3) Solve the solution structure of a single mutant affecting the conformational heterogeneity seen with the native and recombinant Pre1a and compare both structural and functional characteristics.

2. Methods

2.1 Selection of rPre1a mutants

TRTX-Pre1a has high sequence similarity to a variety of previously discovered ICK motif spider venom peptides across a range of genetic families, each with slightly differing Na_V isoform selectivity profiles (Table 3/Table 4)[251]. The close sequence homologies coupled with associated changes in activity have the potential to indicate which residues of TRTX-Pre1a contribute to selectivity and general Na_V activity. The first step was to access all known, published, and publicly available spider venom peptides on Arachnoserver [509]. Peptides were initially sorted for known biological activity towards mammalian Na_V channels. Next, peptides were sorted for structural similarity, primarily being the six cysteine framework defining the ICK motif. Peptides exhibiting an ICK secondary structure but with more than six disulfide bonds were excluded [565]. The resulting Table 4 was used to determine residues that could be targeted for mutagenesis of rPre1a.

There were two primary aims for the selection of residues for mutation. Residues were either chosen for their proximity to regions of conformational instability or for their known contribution to Na_V channel function and selectivity. The first two mutations were decided based on structural aspects of rPre1a highlighted in the previous chapter, elucidated using a combination of homology modeling based on Ps1a and NMR data. The homology model revealed the dense clustering of aromatic side

chain residues in Pre1a that form the hydrophobic face common to this peptide family. In particular, it showed that the Loop 1 residues W_7 and F_8 are positioned in between several other aromatic residues – Y_{22}, W_{30}, and Y_{33} – in a potentially conformationally unstable position. The hydrophobic face of Pre1a differs from other known spider venom peptides of the same family in that all five contributing residues are aromatic. With Ps1a there is a significant contribution of Leu in the center of the hydrophobic face[251], while Tp2a has a Met[566], both of which are less bulky, non-aromatic residues. Neither toxin shows structural heterogeneity.

A hypothesis regarding the close proximity of the hydrophobic stack of W_7 and F_8 of Pre1a as compared to F_5 and L_6 of Ps1a was explained in detail in the previous chapter. Based on this hypothesis, in this study W_7 and F_8 were independently mutated to Ala. The expected results of changing these residues to Ala would be to reduce the potential overcrowding of aromatic side chains, thereby decreasing or eliminating structural heterogeneity (Table 6). However, Trp is known to be a common protein-protein interaction "hotspot" residue, greatly contributing to receptor-ligand interactions [567]. It is therefore possible that these mutations may modify the rPre1a structure in such a way as to critically change the pharmacologic profile. It is therefore important to also assess whether these mutations affect Na_V function in any way, including the dual mechanism of action.

To address Pre1a function specifically, Table 4 was used to compare characterized peptides with high sequence similarity and known Na_V activity profiles. After careful analysis of Table 4, an interesting sequence deviation was noted, which is highlighted in Table 5. The spider venom peptides Cm1a and Cm1b differ by only a single residue at position 32. Changing the aromatic Y_{32} residue of Cm1b to a negatively charged D_{32} of Cm1a abolishes the inhibitory activity at $Na_V1.3$ while maintaining activity for all other Na_V channels tested [251]. The equivalent residue position in Pre1a is the positively charged K_{34}. Ps1a retains inhibitory activity to $Na_V1.3$ and contains a polar, uncharged Q_{34} (Table 5). With this information, it was decided to focus on three functional charge mutations of the K_{34} residue for rPre1a, substituting it for i) a hydrophobic, but less sterically hindered Ala (A) to potentially remove side chain interactions, ii) a negatively charged Asp (D) as pre the $Na_V1.3$ inactive Cm1b, and iii) a polar, uncharged Gln (Q) as per the $Na_V1.3$ inhibitor Ps1a (Table 6).

Table 5: Sequence alignment of key peptides with summary.

Spider toxin family alignment broken down to represent three structurally related peptides to Pre1a with the most interesting available functional information. Highlighted regions on the sequence correlate with Table 5.

Family	Peptide	Sequence	Nav channel activity								
			1.1	1.2	1.3	1.4	1.5	1.6	1.7	1.8	1.9
1	β/δ-Pre1a	-EDCLGWFSRCSPKNDKCCP--NYKCSSKDLWCKYKIW						?			
	β-Ps1a	--DCLGFLWKCNPSNDKCCRP-NLVCSRKDKWCKYQI									
	β-Cm1a	--DCLGWFKSCDPKNDKCCK--NYTCSRRDRWCKYDL									
	β-Cm1b	--DCLGWFKSCDPKNDKCCK--NYTCSRRDRWCKYYL									

Table 6: Summary of TRTX-rPre1a mutations

Mutation	Reasoning
W7A F8A	Based on homology model of Ps1a. Area on Loop 1 in close proximity to Gly
K34A	Hydrophobic, occupies less space than Tyr of Cm1b
K34D	Cm1a mimic, knocks down Nav1.3 activity (+) to (-) charge
K34Q	Ps1a mimic - switched residue to polar, uncharged

2.2 Production and purification of TRTX-Pre1a mutants

Recombinant expression of all mutants and the resulting purification by IMAC and rpHPLC within this chapter followed methods described in Chapter III, section 2.1-2.6.

2.3 Assessment of structural heterogeneity by rpHPLC

rpHPLC experiments at increasing temperatures to observe the effect on isomerization were carried out using a CTO-20A column oven attached to a Shimadzu LC-20AT Prominence system equipped with a SIL-20AHT autosampler and a SPD-20A dual wavelength UV/VIS detector. The instrument was equipped with a Zorbax 300SB-C18 column (Agilent; 4.6 × 150 mm; 3.5 µm particle diameter) and run on a 10-50% linear gradient buffer exchange of solvent A (H_20, 0.1% TFA) to B (90% ACN, 10% H_20, 0.1% TFA) over 20 min with a flow rate of 0.5 mL/min.

2.4 TEVC methods

Handling of oocytes, buffers used, and all recording and analysis methods were completed as previously described in Chapter III, section 2.8 and analyzed according to methods in Chapter III, section 2.10.

2.5 Structure determination by heteronuclear NMR

Lyophilized $^{13}C/^{15}N$-labeled recombinant rPre1a[W_7A] was resuspended at a final concentration of 300 µM in 300 µl 10 mM sodium phosphate buffer, pH 6.0, constituted in 95% H_2O / 5% D_2O. Subsequently sample was added to a susceptibility-matched 5 mm outer diameter microtube (Shigemi Inc., Japan).

Data were acquired at 298 K using a 900 MHz NMR spectrometer (Bruker BioSpin GmbH, Rheinstetten, Germany) equipped with a cryogenically cooled triple resonance probe. Sequence specific backbone resonance assignments were obtained using 3D CBCA(CO)NH, 3D HNCACB, 3D HNCO, 2D ^{1}H-^{15}N HSQC, 3D HBHA(CO)NH, and 4D HCC(CO)NH-TOCSY spectra, which were all acquired using non-uniform sampling and transformed using maximum entropy reconstruction with the Rowland NMR Toolkit (http://www.rowland.org/rnmrtk/toolkit.html) as described previously [515].

HSQC-NOESY (^{15}N-, ^{13}C aliphatic-, ^{13}C aromatic-) spectra were obtained using uniform sampling and processed using standard Fourier transform methods, then used for extraction of inter proton distance restraints, with a mixing time of 220 ms. Dihedral-angles were derived from TALOS chemical shift analysis [516], and the restraints range for structure calculations were set to twice the estimated S.D. NOESY spectra were manually peak picked and integrated using Sparky NMR analysis software [517]. The peak lists were then automatically assigned, distance restraints extracted, and an ensemble of structures calculated using the torsion angle dynamics package CYANA[518]. During the automated NOESY assignment/structure calculation process, CYANA assigned 95.4% of all NOESY cross-peaks (1277 out of 1338). The final structure was calculated using 450 unique distance restraints (142 intra residue NOEs, 139 sequential NOEs, 63 medium range NOEs – to residues closer than 5 amino acids away in the sequence, and 106 long range NOEs – to residues further than 5 amino acids away in the sequence). The backbone root-mean-square deviation (RMSD) was calculated to be 0.65 Å and the side-chain RMSD was 1.79 Å. Dihedral-angles (26 φ, 27 ψ) were derived from TALOS chemical shift

analysis[516], and the restraint range for structure calculations was set to twice the estimated S.D. All X-Pro peptide bonds were identified as *trans* on the basis of characteristic NOEs and the C_α and C_β chemical shifts of the Pro residues.

Table 7: Statistical analysis of rPre1a[W_7A] structures[1]

Experimental restraints[2]	
Interproton distance restraints	
Intraresidue	142
Sequential	139
Medium range (i–j < 5)	63
Long range (i–j > 5)	106
Hydrogen-bond restraints[3]	0
Disulfide-bond restraints	9
Dihedral-angle restraints (φ, ψ)	53
Total number of restraints per residue	14.2
R.m.s. deviation from mean coordinate structure (Å)	
Backbone atoms (residues 1–36)	0.65 ± 0.17
All heavy atoms (residues 1–36)	1.79 ± 0.30
Backbone atoms (residues 4–34)	0.34 ± 0.08
All heavy atoms (residues 4–34)	1.45 ± 0.26
Stereochemical quality[4]	
Residues in most favoured Ramachandran region (%)	85.9 ± 2.78
Ramachandran outliers (%)	0 ± 0
Unfavourable sidechain rotamers (%)	12.8 ± 4.9
Clashscore, all atoms[5]	0 ± 0
Overall MolProbity score	1.95 ± 0.14

[1]All statistics are given as mean ± S.D.

[2]Only structurally relevant restraints, as defined by CYANA, are included.

[3]Two restraints were used per hydrogen bond.

[4]According to MolProbity (http://molprobity.biochem.duke.edu)

[5]Defined as the number of steric overlaps >0.4 Å per thousand atoms

3. Results

3.1 Purified TRTX-rPre1a mutants

All five mutants of TRTX-rPre1a were successfully cleaved from their fusion protein and purified in milligram yields. Mass was confirmed by MALDI-TOF MS and purity was confirmed using analytical rpHPLC methods previously described. In reversed-phase chromatography, retention time of a peptide is directly related to its hydrophobicity [568]. A comparison of rpHPLC traces for each mutant showed shifts in retention times that reflect changes in hydrophobic surface properties (Figure 45). Both W_7A and F_8A resulted in a leftward shift of retention time as compared to native rPre1a, signifying a decrease in hydrophobic properties. This would be expected for each case, as a large hydrophobic side chain was substituted for one much smaller and presumably less surface exposed. Of the two mutations, W_7A showed the greatest shift from the native peptide. In contrast, all three Lys mutations resulted in only a slight right-shift in retention time as compared to TRTX-rPre1a, signifying a slight increase in hydrophobicity. All three Lys mutations co-eluted at the same retention time.

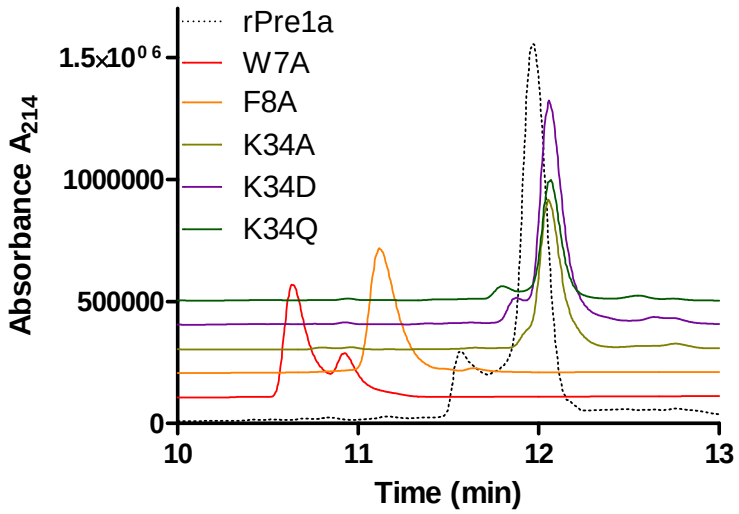

Figure 45: rpHPLC comparison of retention times of rPre1a with mutants.

An interesting point to note is the minor peak visible with TRTX-Pre1a is also apparent in an equivalent position on both the K_{34}D and K_{34}Q mutations (Figure 45). The W_7A mutation also exhibits a minor peak, however the position of the major and minor peaks is reversed as compared to TRTX-rPre1a such that the minor peak is now eluting at a later retention time (i.e. more hydrophobic). The most interesting point to note is the lack of a minor peak with F_8A. Apparently, this mutation was

successful in eliminating the structural heterogeneity apparent with the native TRTX-Pre1a. However, additional experiments are necessary to confirm this result.

3.2 Conformational flexibility of rPre1a mutations

It was clearly demonstrated within Chapter III that TRTX-Pre1a exhibits conformational heterogeneity. This property was observed first by rpHPLC in the form of a minor peak shown to by a conformer and then confirmed by analysis of the ^{15}N-HSQC of rPre1a. Similar to TRTX-Pre1a, the $K_{34}D$, W_7A, and to a lesser extent $K_{34}Q$ mutations exhibited minor peaks suggestive of multiple structural conformations. The minor peak and leading tail for each was assessed using MALDI-TOF MS, with all regions yielded equivalent mass to the major peak, confirming they are structural isoforms rather than impurities. As a secondary test, an experiment was set up to study how the equilibrium between the two peaks from TRTX-Pre1a would be influenced by elevated temperatures.

The rotational energy barrier between *cis*- and *trans*-isomers, *cis-trans* isomerization has been proven to be a slow process at room temperature [523]. Bearing this in mind, elevating the temperature speeds up the *cis-trans* isomerization of a peptide and shifts the equilibrium towards a single form. Although *cis-trans* isomerization has been discounted as an explanation for the structural heterogeneity of TRTX-Pre1a, the same concept of temperature dependence can be applied to other modes of conformational heterogeneity proposed for this peptide. For example, movement of aromatic residues has been proposed in Chapter III to be the primary force contributing to the conformational heterogeneity of TRTX-Pre1a. Therefore rpHPLC analysis of TRTX-Pre1a and mutations were carried out a room temperature (25°C) and 55°C to monitor the changes in peak shape (Figure 46).

TRTX-Pre1a was tested alongside $K_{34}D$ and W_7A. F_8A was included to confirm its apparent conformational homogeneity using differing temperature conditions. Retention time is known to decrease with an increase in temperature, which was seen for each peptide tested[569]. Further, for each sample tested at 55°C a single peak was resolved. As expected, this result indicates that the slow interconversion between multiple conformational species that is evident from the retention data at 25°C occurred at a faster rate than the chromatographic separation time, converging into a single species. This data provides additional evidence for conformational heterogeneity apparent even in the K_{34} and W_7 mutations. The results seen for F_8A demonstrate that this mutation has eliminated the structural

heterogeneity seen with TRTX-Pre1a and the other mutations. The next step was to determine whether the mutations have affected functional activity at Na_V channels and answer the question of whether structural heterogeneity is necessary for any of the functional effects of TRTX-Pre1a.

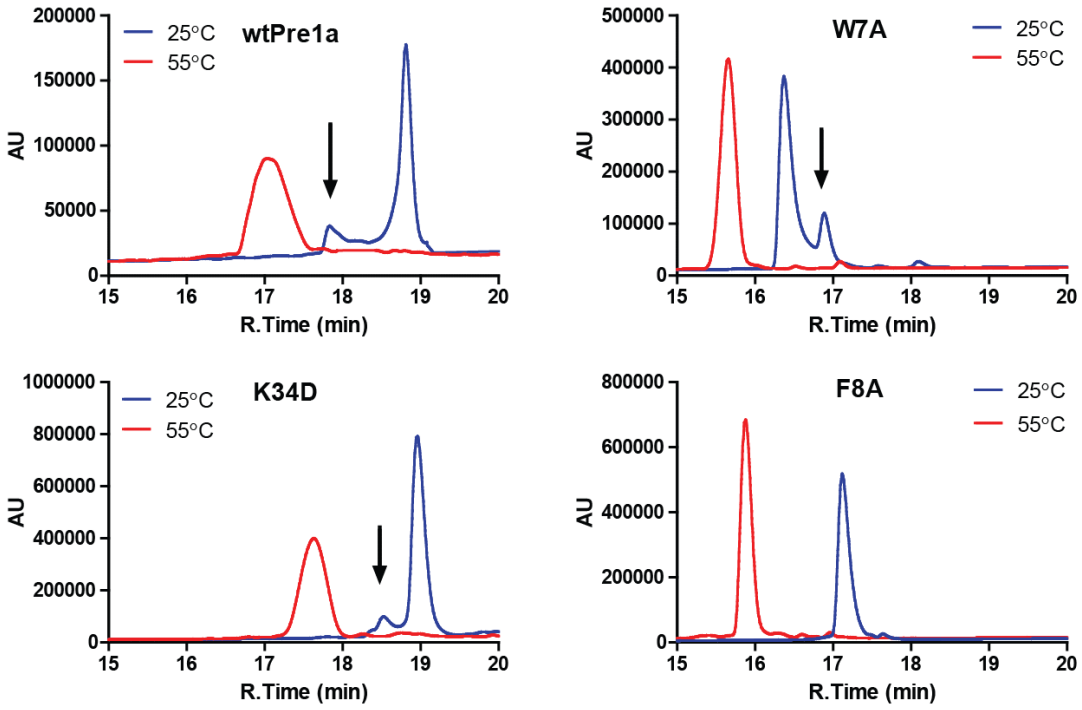

Figure 46: rpHPLC experiment using heated column.

An increase in temperature to 55°C (red) demonstrated that rPre1a and mutations present a single peak, suggesting the multiple peaks visible at 25°C (blue) are due to multiple conformational states. F_8A appears to be an exception, exhibiting one visible, sharp peak state at both temperatures tested.

3.3 Functional activity as measured by TEVC methods

Once purified, each of the five mutations were tested on *X. laevis* oocytes injected with rat (r) or human (h) Na_V channel RNA and measured with two-electrode voltage clamp (TEVC) methods. 1 µM concentrations of each mutant were tested against all available Na_V channel isoforms, including $rNa_V1.2$, $rNa_V1.3$, $rNa_V1.4$, $hNa_V1.5$ and $hNa_V1.7$ (Figure 47/Figure 48). Mutations either increased or decreased the activity as compared to the wild-type, but did not result in an apparent change in the mechanism of action (e.g., inhibition of peak current versus inhibition of fast inactivation), nor did the

kinetics of activation change at the concentration used. No mutations tested had any effect on either $rNa_V1.4$ or $hNa_V1.5$ up to 1 μM. The only mutation that appeared to have no effect on activity compared to wild type rPre1a was F_8A (Figure 49). This is a significant result, as F_8A was also the only mutation to exhibit a single conformation as tested on rpHPLC (Figure 46). On the contrary, 1 μM W_7A resulted in an almost complete loss of $rNa_V1.2$ and $hNa_V1.7$ inhibitory activity and $rNa_V1.3$ inhibition of fast inactivation (Figure 49).

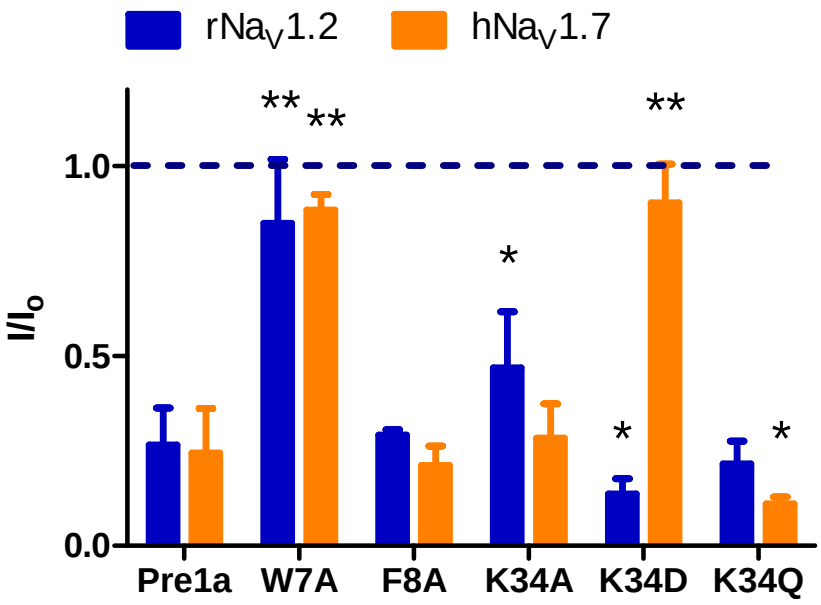

Figure 47: Inhibition of $rNa_V1.2$ and $hNa_V1.7$ by rPre1a mutants.

*Comparison of $rNa_V1.2$ and $hNa_V1.7$ inhibition from baseline (dotted line) across 1 μM rPre1a mutants as tested by TEVC methods. $n \geq 3$ for all experiments. Example I-T plots can be found in Appendix B. Significance was determined by ANOVA, denoted with * for >0.05 or ** for >0.001.*

The three K_{34} mutations resulted in activity profiles that revealed how charged residues can greatly impact the efficacy of a peptide ligand, as well as which Na_V channels may be more susceptible to ionic interactions. $K_{34}A$ replaced the positively charged long carbon side chain of Lys with a hydrophobic Ala, greatly reducing the side chain chemical space while abolishing the charge. This resulted in no significant change in rPre1a activity as tested on $rNa_V1.3$ and $hNa_V1.7$, but did result in a

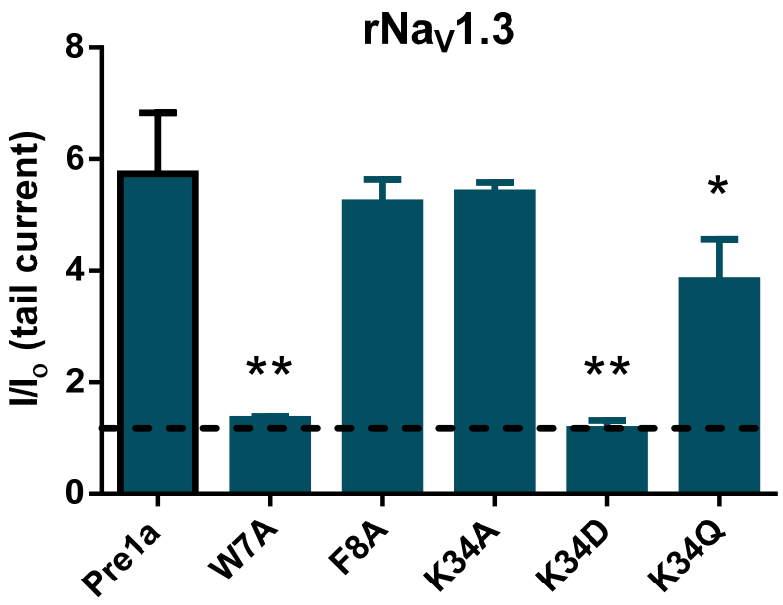

Figure 48: TEVC rPre1a inhibition of inactivation on $Na_V1.3$.

*Comparison of $rNa_V1.3$ inhibition of fast inactivation across 1 μM rPre1a mutants as tested by TEVC methods. The results are expressed as fold increase in magnitude of the late current, calculated by dividing the late current amplitude in the presence of peptide by the control late current. n ≥ 3 for all experiments. Example I-T plots can be found in Appendix B. Control response = 1 (dotted line). Significance was determined by ANOVA, denoted with a * for >0.05 or ** for >0.001.*

reasonable (~2-fold) loss of activity at $rNa_V1.2$ (Figure 47). $K_{34}Q$ replaced the Lys with an uncharged, polar side chain occupying a similar chemical space. This resulted in a slight decrease in activity for $rNa_V1.3$ (Figure 48). However, there was an almost a 2-fold increase in activity for $hNa_V1.7$. This was the only mutation that significantly increased activity for $hNa_V1.7$.

As mentioned in section 2.1 of this chapter, $K_{34}D$ was designed as a mimic of β-Cm1a – which has no activity at $Na_V1.3$ – resulting in a single residue charge shift from positive to negative. As was hoped, this single mutation essentially abolished activity against $rNa_V1.3$ at 1 μM, demonstrating the importance of this reside position for interaction with this Na_V isoform. The $K_{34}D$ mutation unfortunately also dramatically decreased the activity of Pre1a at $hNa_V1.7$ using a 1 μM concentration,

resulting in approximately 10% inhibition rather than 80%, as was seen with the wild-type. Surprisingly, the rNa$_V$1.2 activity of K$_{34}$D was increased 2-fold over native rPre1a. With these results combined with the inactivity at rNa$_V$1.4 and hNa$_V$1.5, it suggests that rPre1a[K$_{34}$D] could be a highly selective inhibitor of Na$_V$1.2. However, its activity at Na$_V$1.1, Na$_V$1.6, and Na$_V$1.8 remain to be tested.

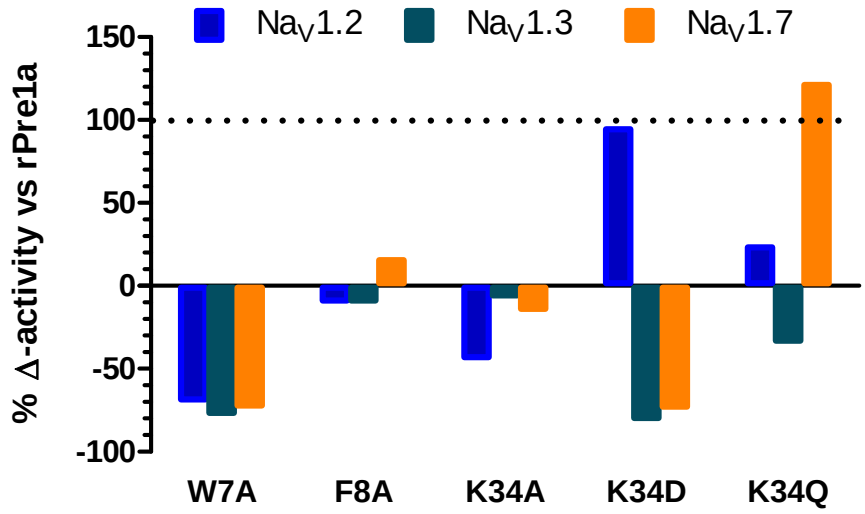

Figure 49: Percent change in activity as compared to rPre1a[wt].
Normalized averaged results for each mutation were compared to their respective rPre1a results, repeated for three Na$_V$ subtypes. Negative values represent a decrease in activity. Positive values represent an increase in activity.

3.4 Solution structure of rPre1a[W$_7$A]

The W$_7$A mutation of rPre1a was selected for NMR structural elucidation due to its central position among the hydrophobic face, seen in Figure 31 of the previous chapter. Despite the appearance of a minor peak in the rpHPLC trace indicating a second structural isoform, the ^{15}N-HSQC of rPre1a[W$_7$A] showed only a single conformation in aqueous solution. The appearance of a minor, more hydrophobic isoform in the rpHPLC trace could be due to the more hydrophobic conditions used with rpHPLC (i.e. 25-30% organic solvent when the peptide elutes), which would allow the appearance of the hydrophobic minor form. As there is no organic solvent in the aqueous buffer used with NMR, it seems the conditions are less favorable for the minor isoform seen in rpHPLC. Coupled with the high yields

of rPre1a[W_7A] from recombinant expression, it was decided to focus on solving the solution structure for this peptide. At the time, only limited pharmacology data was available to influence the decision.

Figure 50: Overlay of 20 backbone structures for rPre1a[W_7A].

The structure of the W_7A mutant was well defined, even in the tail regions. Disulfide bonds in typical ICK motif arrangement are highlighted in yellow.

The solution structure for the rPre1a[W_7A] was successfully solved using heteronuclear NMR experiments on recombinantly expressed $^{13}C/^{15}N$-labelled peptide (Figure 50). Backbone assignments were fully completed using the $^{1}H_N$, ^{15}N, $^{13}C_\alpha$, $^{13}C_\beta$, ^{13}C resonance assignments for the toxin obtained from analysis of amide proton strips in 3D HNCACB, CBCA(CO)NH, and HNCO spectra. The full peak lists can be found in Appendix E. Side chain ^{1}H and ^{13}C chemical shifts were obtained primarily from using a 4D HCC(CO)NH-TOCSY experiment, which has the advantage of providing side chain ^{1}H-^{13}C connectivities[570]. Additional aliphatic side chain assignments as well as aromatic side chain assignments were derived from 3D ^{15}N- and ^{13}C-edited NOESY-HSQC spectra. The NMR data indicated a single stable fold in solution and the rPre1a[W_7A] structure was therefore more precisely determined than the original rPre1a solution structure (backbone RMSD of 0.34 ± 0.08 Å for C_4-K_{34}) (summarized in Table 7). CYANA[518] was used for automated NOESY assignment and structure calculation. 200 structures were calculated from random starting conformations, then the 20 conformers with highest stereochemical quality as judged by MolProbity[571] were selected to represent the solution structure of rPre1a[W_7A].

As demonstrated previously with rPre1a, the structure of rPre1a[W_7A] exhibits a standard ICK motif, with four inter-cysteine loops bounded by N- and C-terminal “tails” (Figure 50). The dominant secondary structural features are two β-sheets involving residues Y_{22}-C_{24} and C_{31}-Y_{33} (Figure 51). Previous prediction by TALOS for rPre1a secondary structure resulted in slight differences, although

positively predicting the β-sheet at Y_{22}. A β-sheet at C_4 was predicted, while the C_{31} β-sheet was not. However, the two β-sheets typically seen with ICK peptides were clearly defined in the final structure (Figure 51).

The position of the W_7A mutation can clearly be seen as a central position between aromatic residues composing the hydrophobic face (Figure 52). The space-filling model highlights the gap, or cleft, left by the absence of the large aromatic Trp.

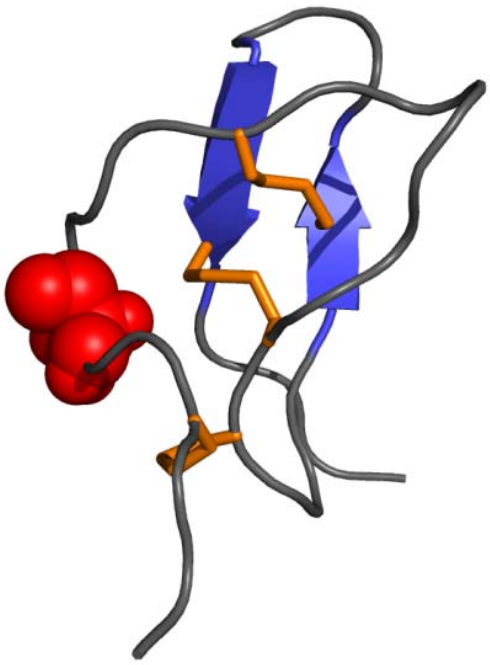

Figure 51: Cartoon representation of rPre1a[W_7A].

W_7A mutation is highlighted in red. Disulphide bonds are in yellow. β-sheets are in blue

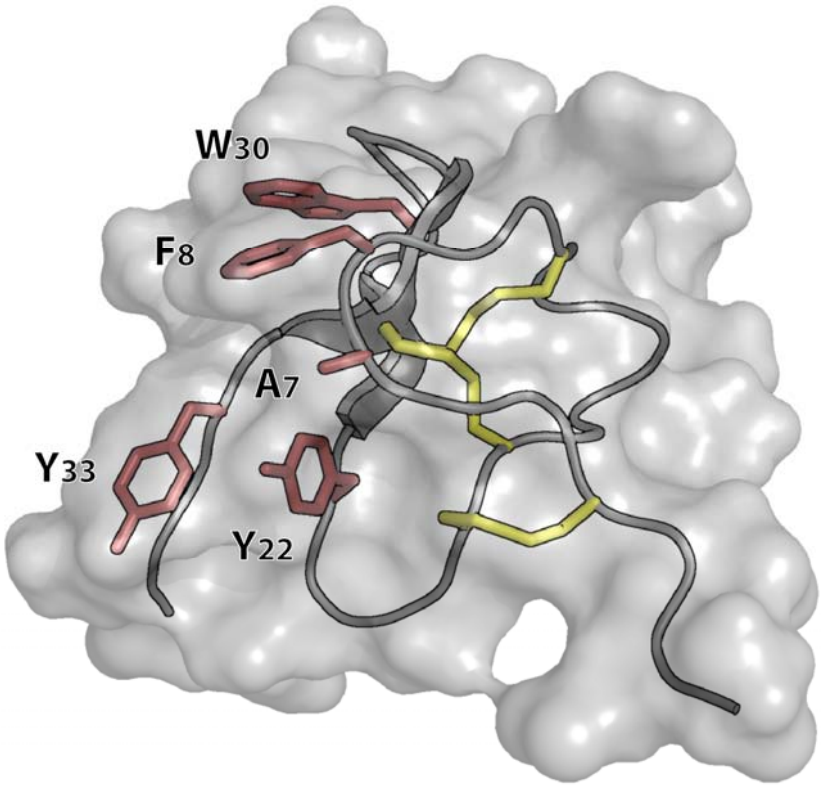

Figure 52: Space filling model of rPre1a[W_7A].

Aromatic residues contributing to the hydrophobic face are in red.

3.4.1 Comparison of rPre1a[W_7A]to rPre1a[wt]

In order to determine the effects of the W_7A mutation on structure, the changes in ^{15}N and ^{1}H chemical shifts of the ^{15}N-HSQC were compared between rPre1a[wt] and rPre1a[W_7A]. The ^{15}N-HSQC of W_7A does not exhibit the peak shifting associated with conformational heterogeneity as seen with the HSQC of rPre1a[wt] (Figure 53). Major chemical shift changes between rPre1a and W_7A can be seen to occur at residues F_8 and Y_{33}. To quantitatively express changes in the chemical shifts of the individual amide pairs, a compound chemical shift change (in ppm) was defined as the weighted change in the δ-value, using the equation below:

$$\Delta\delta_{\text{weighted}} = \sqrt{(0.154 \times \Delta\delta N)^2 + (\Delta\delta H)^2}$$

The chemical shift scaling factor, Rscale, was determined from the ratio of the average variances to be 0.154[572]. The results of the quantitative measurements of the change in weighted chemical shifts were plotted in Figure 54. The plot confirms that the largest changes occurred around residues F_8 and Y_{33}, both of which contribute to the hydrophobic face and aromatic stack, while the vast majority of the peaks overlay with the wild type peptide, confirming that the rPre1a[W_7A] is correctly folded.

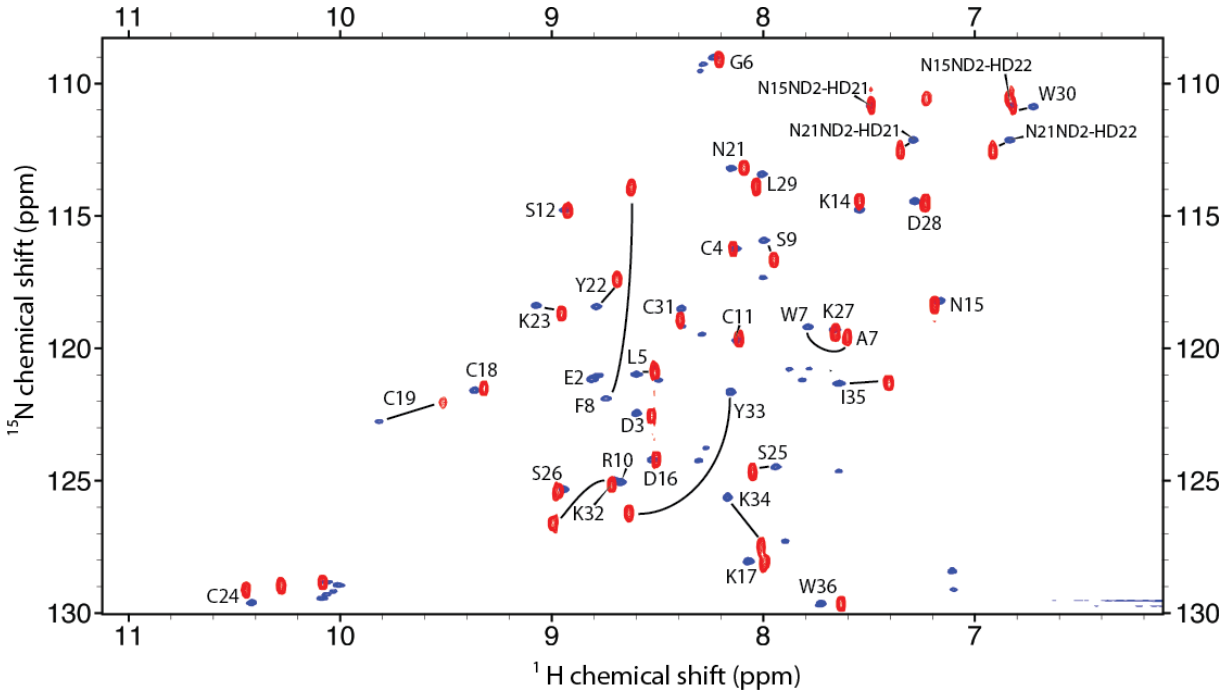

Figure 53: Overlay ^{15}N-HSQC of rPre1a[wt] (blue) with rPre1a[W_7A] (red). *Chemical shifts are traced by black lines. Asp_{15} and Asp_{21} side chain groups are also labeled.*

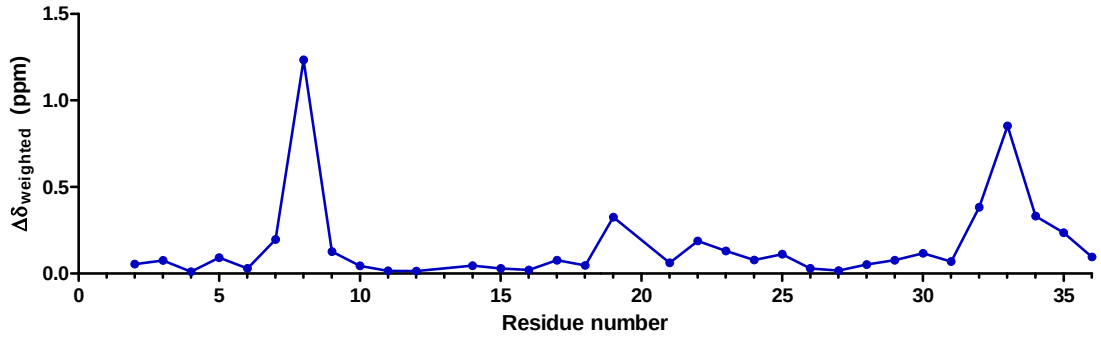

Figure 54: Weighted ^{15}N-HSQC chemical shift difference of ^{1}H and ^{15}N of rPre1a[wt] and rPre1a[W_7A]. *Large deviations are seen at F_8 and Y_{33}, which is consistent with the ^{15}N-HSQC overlay.*

This same ^{15}N-HSQC comparison was completed for each mutation to confirm proper folding and check for major structural distortions. Each peptide was ^{15}N-labeled through recombinant expression methods and the resulting ^{15}N-HSQC was compared to that of rPre1a[wt]. A collection of the K_{34} mutant ^{15}N-HSQC plots overlaid with rPre1a[wt] can be found in Appendix D. Retention times of newly expressed mutants were checked against confirmed ^{15}N-labeled retention times and corresponding peaks were isolated for pharmacologic testing.

The ^{15}N-HSQC of W_7A was compared to that of F_8A to identify regions of structural deviations caused by these mutations (Figure 55). Although F_8A peaks were not picked and assigned, some inferences can be made using the rPre1a[wt] ^{15}N-HSQC, due to their similarities. The spectrum of F_8A appears more similar to that of rPre1a[wt] than W_7A, without exhibiting the structural heterogeneity identified by peak shifts as seen with rPre1a[wt] (Figure 56). There was also no major deviation of peaks from that of rPre1a[wt], indicating correct folding and minimal structural perturbation experienced by this mutation.

.

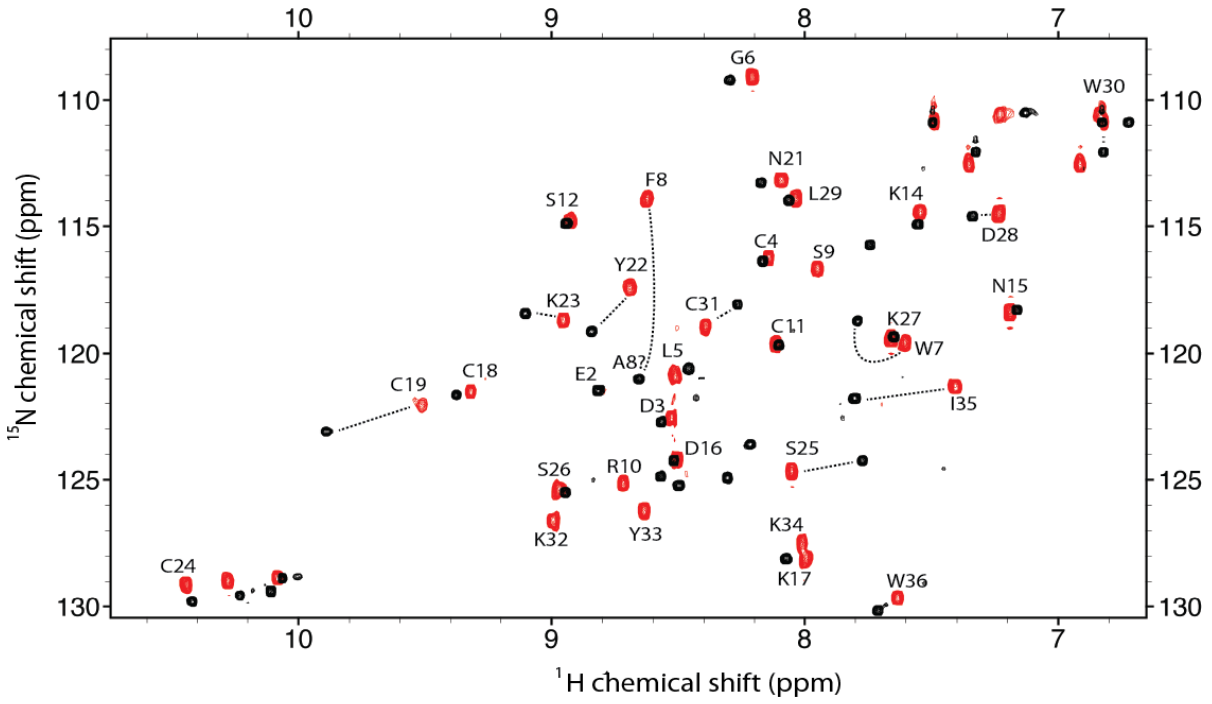

Figure 55: Overlay ^{15}N-HSQC of rPre1a[W_7A] (red) with rPre1a[F_8A] (black). *Only rPre1a[W_7A] peaks are labeled as peaks were not picked for rPre1a[F_8A].*

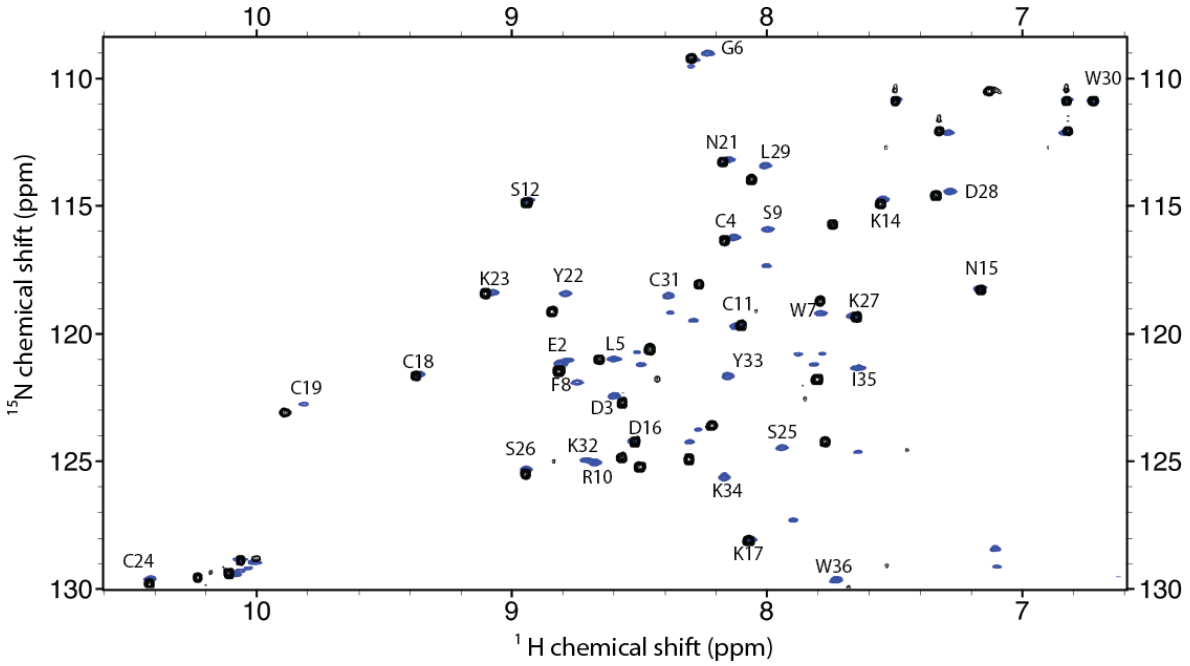

Figure 56: Overlay ^{15}N-HSQC of rPre1a[F$_8$A] (black) with rPre1a[wt] (blue). *Only rPre1a[wt] peaks are labeled as peaks were not picked for rPre1a[F$_8$A], peaks can be inferred from the rPre1a[wt]. Peak shifting and structural heterogeneity is not seen with rPre1a[F$_8$A].*

4. Discussion

This chapter described the directed mutagenesis of β/δ-TRTX-rPre1a and resulting structure-function changes, as well as elucidated the solution structure of a single mutant, rPre1a[W$_7$A]. Mutations were chosen based on a combination of structural information gained from experiments conducted in Chapter III and identification of a critical C-terminal Lys residue after comparison of sequence similarity to spider venom peptides with known Na$_V$ subtype selectivity. In this chapter, we have successfully engineered rPre1a for enhanced Na$_V$ selectivity to Na$_V$1.2 and Na$_V$1.7. We have also solved the solution structure of a mutant version of the rPre1a with reduced activity, which will give valuable insights into structural aspects contributing to activity.

Despite the relatively large number of Na$_V$ modulating spider venom peptides so far discovered and the high interest in discovering and developing subtype selective modulators there have been few SAR studies reported, with only one focusing on Na$_V$1.7. The majority of research in the public domain involves full Ala scans of a peptide with a focus on activity at a single Na$_V$ isoform, such as the case of

β/ω-TRTX-Tp2a (protoxin-II) and β-TRTX-Cj1a (jingzhaotoxin-III) tested on $Na_V1.5$ [245, 542]. Another example is β-hexatoxin-Mg1a (Magi-5), tested for potency changes at $Na_V1.2$ [254]. Of these, only Tp2a exhibits a slight sequence similarity to the Family 1 Na_V spider venom peptides, which includes β/δ-TRTX-Pre1a (Table 4). The most detailed SAR study is also the most recently published. This study involved not only a full Ala scan of μ-TRTX-Hhn2a (huwentoxin 4), but also followed up with directed mutagenesis of individual residues shown to be important form the scan [547]. This study focused solely on engineering the peptide's potency on $Na_V1.7$. However, as Hhn2a shares a high sequence similarity to Pre1a (Table 4), the results presented are directly relevant to the results observed with rPre1a mutations, as will be explained below. Taken together, this collection of published work demonstrates the novelty and scope of the work presented within this chapter, as it is to date the only directed engineering of a spider venom peptide in terms of both its potency and selectivity at different Na_V channel isoforms as well as identifying the molecular basis of its structural stability.

4.1 Functional aspects of K_{34} mutagenesis

Mutations of the single K_{34} residue – based on both side chain length and charge – resulted in significant pharmacologic changes from the native rPre1a, with the two non-alanine mutations resulting in an increase in selectivity to different Na_V isoforms. All mutations retained rPre1a's relative inactivity against $rNa_V1.4$ and $hNa_v1.5$. Changing the positively charged, long carbon chain Lys to a small hydrophobic Ala residue ($K_{34}A$) does not appear to substantially alter Na_V channel activity or selectivity as compared to rPre1a[wt]. The replacement of a positive charge at this position with a polar, neutral Gln ($K_{34}Q$) resulted in an approximate 30% decrease in $rNa_V1.3$ inhibition of fast inactivation compared to rPre1a[wt]. However, this same mutation increased $hNa_V1.7$ inhibition of peak current by over 2-fold as compared to rPre1a[wt] resulting in favorable net improvement of $hNa_V1.7$ to $rNa_V1.3$ selectivity. However, activity at $rNa_V1.2$ did not significantly change from that of rPre1a[wt], thus limiting its potential as a $Na_V1.7$ selective therapeutic lead. It is important to note that the highly homologous Hh2a and Ps1a both have a Gln (Q) at this position and are potent Nav1.7 inhibitors [543]. In the recent SAR study for Hh2a mentioned above, a change of $Q_{34}A$ also resulted in no change of potency for $hNa_V1.7$, further supporting the lack of effect of an Ala mutation in this position on Pre1a. However, the results of the Hh2a study demonstrate the limitations with Ala scanning, as this residue was not followed up with further mutations due the observed lack of effect,

even though this chapter has demonstrated the importance of K_{34} for both function and selectivity to Na_V channels.

A shift from a positive to negative charge with the $K_{34}D$ mutation also resulted in an increase of selectivity for a single Na_V channel. The natural single mutation from Y to D at this position in Cm1b and Cm1a, respectively, is sufficient to ablate the potent $Na_V1.3$ activity of Cm1b. This impressive effect was the inspiration for making the $K_{34}D$ mutation of Pre1a. As was hoped the rPre1a[$K_{34}D$] mutation eliminated $rNa_V1.3$ activity. Unfortunately, inhibition of peak $hNa_V1.7$ current was also dramatically decreased by this mutation. However, $rNa_V1.2$ inhibitory activity increased 2-fold as compared to rPre1a. These two mutations highlight the ability to manipulate selectivity towards one Na_V isoforms through a single residue change and give promise that more potent and selective Na_V modulators can be rationally designed.

An interesting observation to note is that the affinity to the Na_V isoforms tested can be dictated by a single residue on the C-terminal tail. Considering $K_{34}D$, this substitution of a negatively charged residue at the K_{34} position eliminates all functional activity for both $Na_V1.3$ and $Na_V1.7$. Although we had hoped to tailor activity to $Na_V1.7$ with this mutation, it was equally exciting to reveal the impressive $Na_V1.2$ selectivity imparted by this mutation. Future studies should include determining the full selectivity profile for rPre1a[$K_{34}D$]. If it is found to be inactive at $Na_V1.1$, $Na_V1.6$ and $Na_V1.8$ this would represent the first known highly selective inhibitor of $Na_V1.2$. As such, rPre1a[$K_{34}D$] could be an efficient research tool to determine the physiological and/or pathophysiological role of $Na_V1.2$ using acute pharmacologic intervention, thus avoiding possible confounding results due to *in vivo* receptor compensation as can occur with genetic knock-out of a channel. Further, as $Na_V1.2$ has been implicated in a wide variety of epilepsy disorders – many of which exhibit gain-of-function, excitatory phenotypes – it is reasonable to assume a selective $Na_V1.2$ inhibitor could undergo further development for use as a therapeutic for relevant epileptic conditions [175, 573]. Recently, some of the *SCN2A* mutations leading to epileptic conditions have even been linked to the development of autism [574].

While $K_{34}Q$ did not demonstrate the dramatic effects of $K_{34}D$, it did increase the functional inhibition of $Na_V1.7$ peak current. The structure for rPre1a[W_7A] reveals another Lys residue in close association with K_{34}, at position 22 on Loop 3. It would be of interest for future work to perform a similar mutagenesis experiment on this mutant – as well as create double-mutants of these Lys residues – in

order to further explore the effects of residue charge and size within this region. In combination with the recent work to improve the $Na_V1.7$ potency of Hh2a by Revell et al., this mutation sets a precedence for engineering in selectivity to a specific Na_V channel [547].

4.2 Function and structure of W_7 and F_8 mutations

The mutations of W_7A and F_8A were chosen primarily because they represented two large, hydrophobic residues, directly adjacent on the rPre1a sequence on the Loop 1 region. In Chapter III of this thesis, the ^{15}N-HSQC spectra of rPre1a revealed that residues of the Loop 1 region experienced three noticeable chemical shifts within the same spectra. The noticeable movement of residues within this region was therefore hypothesized to contribute to the conformational heterogeneity of rPre1a. Further, the central position of W_7 on the hydrophobic face is typically occupied by a non-aromatic, hydrophobic residue, such as a Met for Tp2a, a Lys for Ps1a, and an Ile for Hh2a. It was our hypothesis that the presence of two large aromatic residues in Loop 1, as seen with Pre1a, creates tension between the five bulky aromatic residues of the hydrophobic face.

The W_7A mutation was chosen for NMR structural elucidation due to its central position within the hydrophobic face, high yields of correctly folded peptide from recombinant expression, and a ^{15}N-HSQC spectrum that exhibited a single conformation in aqueous solution. It was only after structural elucidation that the functional data was obtained, demonstrating an almost complete loss of function for all Na_V isoforms tested. Despite this, solving the structure of an inactive mutant gives insight into the function of the specific mutated residue, as was demonstrated in an SAR experiment with μ-TRTX-Hhn1b [575]. As suggested by Li et. al., if the mutation causes major structural perturbations, it can be inferred that the structural deformity is contributing to the loss of function. However, if the structure remains relatively intact – as was the case for W_7A – then it is likely that the residue directly contributes to receptor interaction [575]. The loss of activity observed with W_7A could be attributed to the contribution of the Trp to protein-protein interaction “hotspots”, which was mentioned previously [567]. However, an more in-depth publication that intricately detailed the development and use of hotspot prediction software suggests that Trp is only a low level contributor as a hotspot residue [576]. Although this data was based primarily on macro-proteins, it was recently confirmed to be the case in peptide-protein interactions, as well [577]. However, these results do not discount that W_7 could contribute to a binding face, such as the highly conserved hydrophobic face. Further experiments are

needed to confirm the role of W_7 towards function at this position. As the precise role of the hydrophobic face is yet to be determined, experiments could include mutagenesis of other residues within the hydrophobic stack, functional mutations of W_7, identifying the precise binding site of rPre1a on Na_V channels, and determining if W_7 is involved in pairwise interactions with the Na_V channel protein..

In contrast to W_7A, the F_8A mutation resulted in no change of activity for any Na_V isoform tested, as compared to rPre1a[wt], yet resulted in the abolition of any detectable conformational heterogeneity. The solvophobic environment inherent with rpHPLC experiments at room temperature and 55°C resolved a single, sharp peak. Likewise, the ^{15}N-HSQC overlaid closely with that of rPre1a[wt], suggesting proper folding, no structural perturbation, and a single conformational isomer. These results suggest that conformational heterogeneity is not necessary for the activity of rPre1a[wt]. However, it does not discount the possibility that rPre1a could occupy multiple interaction sites on the Na_V channel, as is the case with κ-Gr1a [578].

The hypothesis regarding aromatic stacking in the hydrophobic face was proposed within Chapter III. Aromatic residues within 4.5-7 Å have a tendency to form aromatic stacks, with multiple electrostatically favorable geometries possible in peptides [560]. The higher precision of the rPre1a[W_7A] ensemble allows additional structural features to be recognized. This is especially apparent with the positioning of residues involved with the hydrophobic face. A 9 Å spacing can be viewed between the F_8-W_{30} residue pairs and the two Y_{22} -Y_{33} residue pairs in Figure 52 [579]. This large space creates an unfavorable conformation for aromatic interactions between these two pairs of aromatic residues [561]. However, each of the pairs mentioned would still be able to form aromatic interactions between each other, creating localized stability. With the addition of the W_7 residue, it can be hypothesized that the aromatic ring of Trp might “flip” between energetically favorable positions in the offset aromatic pairs. With the F_8A mutation, the removal of one of the external forces on W_7 strengthens the formation of a single aromatic position, resulting in a single conformer. However, to confirm this hypothesis, further mutagenesis and the structural elucidation of these analogs – especially F_8A – is required.

4.3 Summary and future prospects

In lieu of determining the precise Na_V binding domain through experiments involving Na_V channel point mutations, Na_V chimeras, or competitive binding with Pre1a, it is difficult to make assertions on the precise mechanism of ligand interaction. Regardless, the results presented in this chapter give positive insight into the functional role of individual key residues for Pre1a and related venom peptides, as well as demonstrating an ability to manipulate structural heterogeneity. The results also demonstrate a proof of concept for the engineering of selectivity towards specific Na_V isoforms. This data can be used to guide future projects, such as guiding the selection of residues for a more complete mutagenesis or indentifying residues between the Na_V channel isoforms involved in ionic ligand binding.

Chapter V: Conclusion

The continual progression of new technologies expands our ability to discover and isolate new compounds from natural sources previously overlooked; such is the case for animal venoms. As the tools for novel ligand discovery progress they fill databases with new molecular scaffolds and their corresponding pharmacologic data. To realize the full potential of the knowledge base we are building, utilization of this data needs to progress as well. This thesis describes the successful development and functional application of cell-based assays for the purpose of discovering and isolating Na_V modulating peptides from crude venom. It then goes on to describe the in depth characterization of a single Na_V modulating spider venom peptide demonstrating unique functional characteristics. This included guided mutagenesis of key residues through utilization of available data regarding peptides of a similar family. The experiments presented here successfully demonstrated a proof-of-concept for engineering selectivity towards specific Na_V isoforms, with implications for therapeutic design and development of venom peptides.

Although multiple functional assays using whole cells in microtiter format were developed, one assay in particular was carried forward to be used as a general screen of crude venoms. The choice was based on a few relevant factors, regarding the throughput of the assay and the robustness of response. The FLIPR^{Tetra} instrument was critical in this decision, as it was able to measure a fluorescence response over all wells simultaneously, whereas the Envision instrument was a single-well reader. The FLIPR^{Tetra} is able to read multiple fluorescent dyes, of which two were used to monitor either Na_V depolarization induced Ca^{2+} influx or changes in the membrane potential. Aside from cell plating and compound preparation, the assay itself was completed within a time course of minutes, with the instrument capable of compound addition while simultaneously measuring the response. This not only gave us the ability to test our cone snail crude venoms, but venoms available from multiple other organisms through collaborative work.

Out of this crude venom screening, a very potent Na_V excitatory peptide was discovered, isolated, and sequenced. Belonging to the poorly classified group of δ-conotoxins, the discovery of δ-MVIA gave us an opportunity to attempt to further characterize the Na_V neurotoxin receptor site 6. However, the extreme hydrophobic properties exhibited by this peptide made the production unattainable with

methods attempted for both SPPS and recombinant expression. Unfortunately, as no more *C. magus* specimens were available, this project was left until better methods for handling highly hydrophobic peptides could be developed. Future directions should include attempting recombinant expression in different organisms, such as the eukaryotic yeast *Pischia pastoris*, which may possess a more favorable environment for the expression of hydrophobic, disulfide rich peptides [580]. Fusion protein technology is also advancing rapidly [581-583], as is the possibility of co-expression with enzyme catalysts and isomerases that can aid proper folding and expression [289].

The discovery of TRTX-Pre1a and resulting characterization was in stark contrast to the difficulties experienced with the production of δ-MVIA. Pre1a, originally isolated from *P. reduncus* crude spider venom by Dr. Lachlan Rash, was produced successfully using bacterial recombinant expression methods. These methods allowed the production of enough recombinant peptide for all pharmacology experiments as well as providing a means for efficient, uniform isotopic labeling for structural elucidation. Pre1a presented a unique pharmacologic profile unlike any venom peptide described to date. Sub-micromolar inhibition of peak current was recorded for both $rNa_V1.2$ and $hNa_V1.7$, while potent inhibition of fast inactivation was observed at $rNa_V1.3$. A lack of activity at $rNa_V1.4$ and $hNa_V1.5$ demonstrated a preference for neuronal Na_V subtypes, as well. Further, Pre1a exhibited structural heterogeneity with multiple conformational states in solution, observable with both rpHPLC and the ^{15}N-HSQC spectrum from heteronuclear NMR. To date, this phenomenon has only been reported for two spider venom peptides, of which neither study had attempted to identify the cause. In this study, we have made progress in attempting to describe the structural heterogeneity for rPre1a, identifying the Loop 1 region as a zone of flexibility through analysis of the ^{15}N-HSQC chemical shifts. A homology model revealed an atypically close interaction of five aromatic residues (W_7, F_8, Y_{22}, W_{30}, and Y_{33}) composing a hydrophobic face, where most other similar peptides characterized have less aromatics spaced by less bulky hydrophobic residues, such as Leu or Met..

Of the five residues identified to contribute to the hydrophobic face, F_8 and W_7 were chosen for Ala substitution due to their adjacent proximity in sequence and location on the flexible Loop 1. The F_8A mutation eliminated observed structural heterogeneity while maintaining function equivalent to the wild type rPre1a. In contrast, the W_7A mutation – directly adjacent to F_8 but located more centrally on the hydrophobic face – successfully eliminated all tested Na_V function while improving structural stability as compared to rPre1a[wt]. These results demonstrated the necessity of a single residue (W_7)

for direct, non-selective Na_V channel interaction and also revealed that the structural heterogeneity of Pre1a is not necessary for either of its observed modes of activity or isoform selectivity.

Pre1a belongs to a relatively large family of Na_V modulating spider venom peptides with varying subtype selectivity. Residues that may contribute to their selectivity could be postulated by comparing peptides with the highest sequence similarity yet different selectivity for Na_V channel subtypes. Despite the large number of partially characterized spider venom peptides in the literature, and full alanine scans of several of these peptides, the experimental approach used here (rational design based on existing knowledge) had not yet been implemented for these peptides. A single residue at position 34 on the C-terminal tail was identified for its potential role in $Na_V1.3$ selectivity and was subjected to rational mutagenesis involving both standard Ala substitution and replacement of amino acids with specific functional side chains. Of the three K_{34} mutations, two resulted in increased Na_V isoforms selectivity. $K_{34}Q$ increased the potency to $Na_V1.7$ while slightly decreasing potency to $Na_V1.3$ as compared to Pre1a[wt]. However, this mutation did not improve on global selectivity, as $Na_V1.2$ potency remained unchanged from the wild type. Even so, the information gained from this mutant forms a foundation for combining with other point mutations to further improve the selectivity of Pre1a. $K_{34}D$ significantly decreased activity at both $Na_V1.3$ and $Na_V1.7$, but increased the potency to $Na_V1.2$ by 2-fold. The rational mutagenesis of K_{34} and the resulting enhanced selectivity profiles sets a precedence for the utilization of publicly available information for the purpose of identifying key residues contributing to selectivity and function on specific ion channels and their isoforms.

This thesis does not represent a complete story of Pre1a, but presents initial findings of a story that is currently ongoing. Aspects of this peptide are still needed to better understand its unique functional role. This will aid in the understanding of Na_V-ligand interactions and how these can be incorporated into the development of molecular tools and therapeutics. There is no shortage of experiments yet to be completed. Exploring the binding site of Pre1a is of particular importance. Classical competitive binding experiments can be completed using radiolabelled peptides with known binding sites. Identifying the Na_V domains involved in Pre1a binding can be accomplished using chimeric K_V channels with a single Na_V domain substituted in. As Kv channels are homotetramers, any one of their domains can be substituted with any one of the domains of a Na_V channel and remain functional. This method has been used to successfully determine the domain of Ps1a binding[34]. Once narrowed to a

specific binding region, these results can help infer what residues of the Na_V channel itself can be mutated and functionally tested with Pre1a to observe a change in activity.

Concerning function, voltage dependence of steady-state inactivation of Pre1a should be tested on $Na_V1.2$ and $Na_V1.7$ using a standard double-pulse protocol, in which a 20 ms depolarizing test potential of 0 mV follows a 500 ms prepulse at potentials that range from -130 to -10 mV with a 10 mV increment[243]. Another experiment of interest tests voltage-dependence of reversal of inhibition by using a very strong depolarized conditioning potential (+100 to +240 mV) of varying length of time, or of standard time and varying potential, before a standard test depolarization to 0 mV. The test peak current (Y-axis) is compared to conditioning duration (X-axis) and gives functional information on whether the toxin binds to the voltage sensor region. Strong depolarization before a test pulse is thought to inhibit binding to the voltage sensor region by "pushing off" the toxin, so a loss of activity would be apparent over greater lengths of time[243, 255]. To test the voltage dependence of late currents for $Na_V1.3$, the voltage can be varied after a standard 0 mV depolarization. Subsequent step to voltages ranging from −100 to −30 mV are then applied for an equivalent length of time to monitor their effects on inactivation[584]. Recovery from inactivation can be tested by administering standard depolarizing pulse potentials separated by increasing time intervals.

Depending on the results of Pre1a, these experiments may also be applied to the mutants to observe possible changes in their mode of action. In regards to the mutations of Pre1a, full concentration dependence curves of each active mutant on $Na_V1.2$, $Na_V1.3$, and $Na_V1.7$ is still needed for EC_{50} and IC_{50} values. Shifts of peak current under varying concentrations will also be apparent. Further mutagenesis of Pre1a using the information gained within this thesis and from new research will yield more information about the structural aspects of Pre1a and how they contribute to function. Specifically, focusing on the Loop 1 region and the Lys residues that seem to form a cluster are of interest as these have been shown to contribute strongly to selectivity and potency.

In conclusion, this thesis has produced an improved means of isolating Na_V channel modulators and contributed significantly to our understanding of the precise molecular details governing the structure and function of β/δ-TRTX-Pre1a. Moreover, it has uncovered several important considerations not only for future experimentation but also for future drug design. It is hoped that this information provides a

useful starting point for the further rational design and engineering of β/δ-TRTX-Pre1a analogs with high value as research tools and possible therapeutic leads for a broad range of neurological conditions.

Appendix A: δ-MVIA recombinant expression

1. Methods

1.1 Vector design for recombinant expression

Vector design was performed as previously described in Chapter III, section 2.1. However, the synthetic gene was codon optimized and ordered through EZBiolab (Carmel, IN, USA) due to regulation restraints with GeneArt in Germany.

In addition, a change had to be made to the original construct. The TEV cleavage recognition site requires an optimal signal sequence (ENLYFQ/S) to separate the peptide toxin at its N-terminus from the associated tags. The initial construct was designed for cleavage to occur between a Gln and Ser residue, leaving a residual Ser at the N-terminus of the peptide. Cleavage can occur between a number of residues in place of Ser - such as Asp, as is found at the N-terminal of δ-MVIA - so the addition of a Ser was not deemed necessary in the initial construct design[539]. However, a post-optimization change in the TEV enzyme resulted in an inability to cleave at Asp. Therefore, a mutational insertion of Ser at the N-terminal of the δ-MVIA sequence was needed. Primers were designed using PrimerX software for regions flanking the δ-MVIA sequence within the pLIC vector (Figure 57).

```
Forward:    5'  GAAAACCTGTACTTCCAAAGCGATGGCTGCTATAATGC    3'
Reverse:    5'  GCATTATAGCAGCCATCGCTTTGGAAGTACAGGTTTTC    3'
```

Figure 57: Primer set for N-terminal Ser addition to δ-MVIA gene on the pLIC construct.

Mutagenesis was performed using a QuickChange II Site Directed Mutagenesis Kit (Agilent, CA, USA) and confirmed by sequencing with the designed primers as templates (Australian Genome Research Facility). The sequenced pLIC-δ-Ser-MVIA construct was transformed into Top10 chemically competent *E. coli* (Invitrogen, CA) for large-scale vector preparation and BL21ΔE3 (Invitrogen, CA) for recombinant expression. Both transformants were stored as glycerol stocks (25% glycerol / 75% LB medium) at -80°C.

A second vector encoding a lysozyme fusion protein was also designed in parallel. The lysozyme sequence used was derived from chicken egg-white lysozyme (PDB: 1LSG_A) and codon optimized for bacterial expression[585]. The crystallization of chicken egg-white lysozyme has been well characterized and has great potential for acting as a crystallization chaperone, as is the case with recent publications[586-588]. The purpose was to express δ-MVIA as a mature fusion protein and crystallize the entire product, yielding a new method for structural elucidation of venom peptides, as no venom toxin has been characterized by this method to date. A N-terminal His_{10} affinity tag and a TEV cleavage site between the lysozyme and mature toxin sequence was designed into the construct. The designed fusion protein gene was synthesized and cloned into a pET11a expression vector, then sequenced by the UQ Protein Expression Facility (Australia). The sequenced pET11a-Lys-MVIA construct was transformed into Top10 chemically competent *E. coli* (Invitrogen, CA) for large-scale vector preparation and BL21ΔE3 (Invitrogen, CA) for recombinant expression. Both transformants were stored as glycerol stocks (25% glycerol / 75% LB medium) at -80°C.

1.2 Bacterial recombinant expression and purification

Recombinant expression of δ-MVIA and the resulting purification by IMAC and rpHPLC followed methods developed in Chapter III, section 2.1-2.5.

2. Recombinant expression results

After multiple failed synthesis attempts by collaborators, δ-MVIA was successfully expressed as an inducible 47 kDa fusion protein using methods proven in both Chapters III and IV (Figure 58). The fusion protein was also able to be purified through IMAC methods, yielding a band detectable by Western blot using an anti-His antibody (Figure 59). Unfortunately, the purified sample was unable to be cleaved or stored for any period of time without crashing out of solution. Post-cleavage using standard TEV protease methods resulted in undetectable levels of mature toxin. Isolation of the entire fusion protein was attempted, as well. However, there was no way to check for proper folding as the MBP protein dominated the molecule. Storage at 4°C, -20°C, and -80°C all resulted in the sample becoming a precipitate upon thawing. Quick buffer exchange and immediate assay as a fusion protein

was attempted post purification with irreproducible results. It was the recommendation of the supervisory committee to move on from this project.

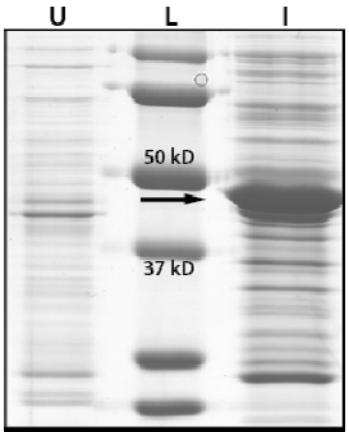

Figure 58: SDS-PAGE of inducible expression of MBP-MVIA. *Positive induction of 100 mL LB culture of pLIC-S-MVIA. U = uninduced; L = molecular weight ladder (BioRad); I = induced with 1 mM IPTG.*

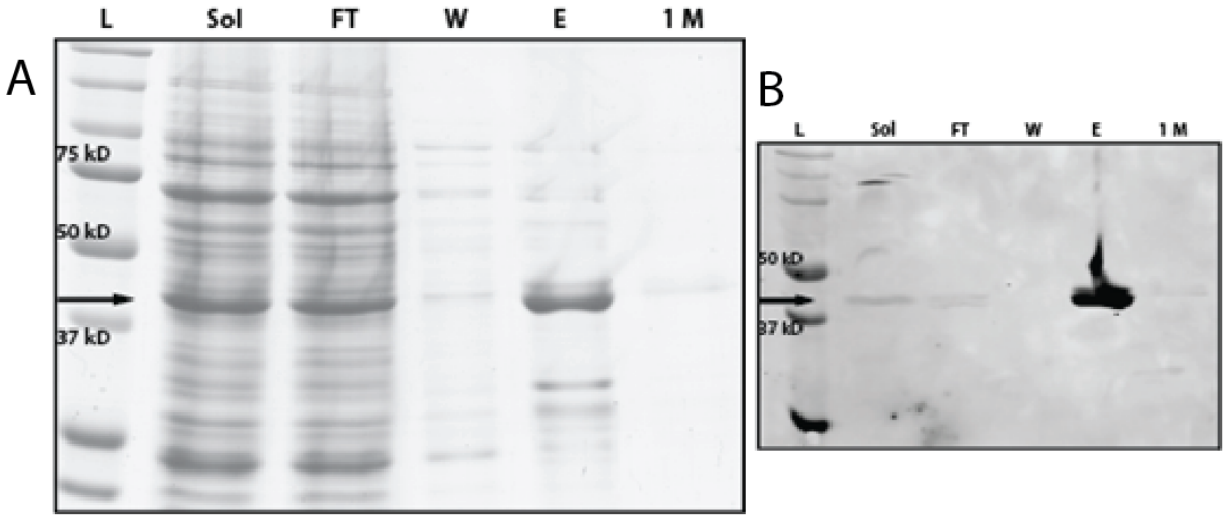

Figure 59: SDS-PAGE of δ-MVIA IMAC purification. *A) Coomassie stain; B) Western of NiNTA purification from 2L LB expression of pLIC-S-MVIA, induced with 1 mM IPTG, 16°C, 20 h. Sol = soluble lysate; FT = NiNTA flowthrough; W = 15 mM immidazole wash; E = 250 mM immidazole elution; final column wash of 1 M immidazole to check for residual binding.*

The attempt was also made to express δ-MVIA with a custom designed lysozyme fusion construct for co-crystallization studies. Although expression occurred for all tested conditions, no soluble protein was detected (Figure 60).

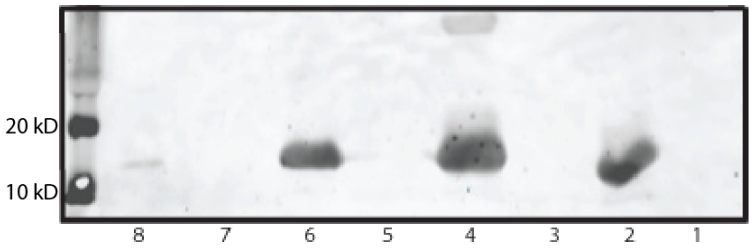

Figure 60: Western of MVIA-Lysozyme test expression. *The mature fusion protein yields a 12 kDa band. 1) Uninduced cell pellet (Insoluble fraction); 2) Uninduced cell lysate (soluble fraction); 3) 16 °C pellet; 4) 16 °C lysate; 5) 25 °C pellet; 6) 25 °C lysate; 7) 37 °C pellet; 8) 37 °C lysate.*

Appendix B: I-T plots of Pre1a and K34Q addition to rNa$_V$1.2, rNa$_V$1.3, and hNa$_V$1.7

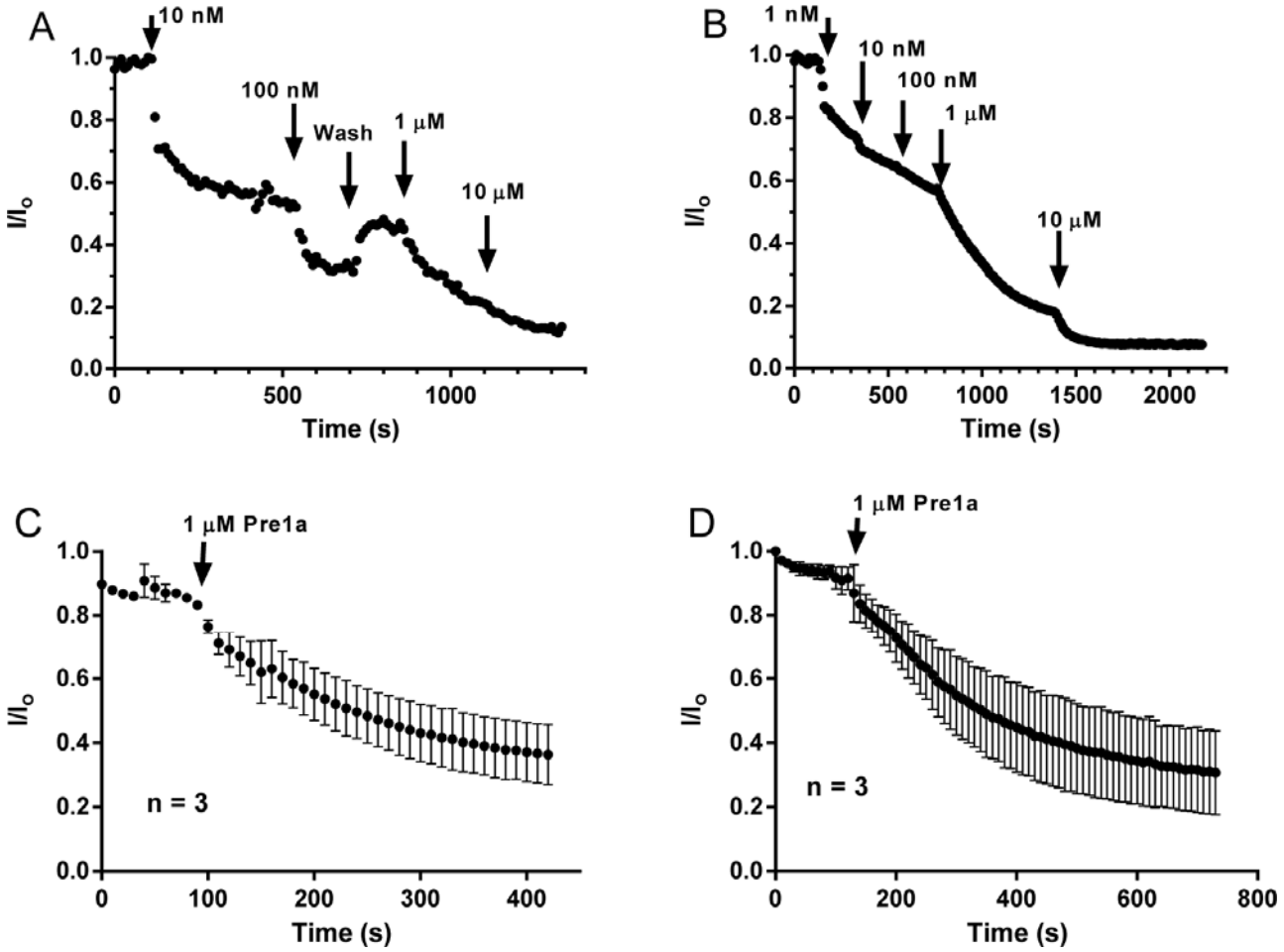

Figure 61: I-T plots Pre1a inhibition of rNa$_V$1.2 and hNa$_V$1.7. *Concentration dependent inhibition of Pre1a on A) rNa$_V$1.2 and B) hNa$_V$1.7 expressed in oocytes. 1 μM Pre1a addition resulted in inhibition of peak current for C) rNa$_V$1.2 and D) hNa$_V$1.7.* n *is representative of data obtained from separate oocytes.I-V plots were taken before the first addition and after reaching steady-state inhibition of final addition of peptide (Appendix C).*

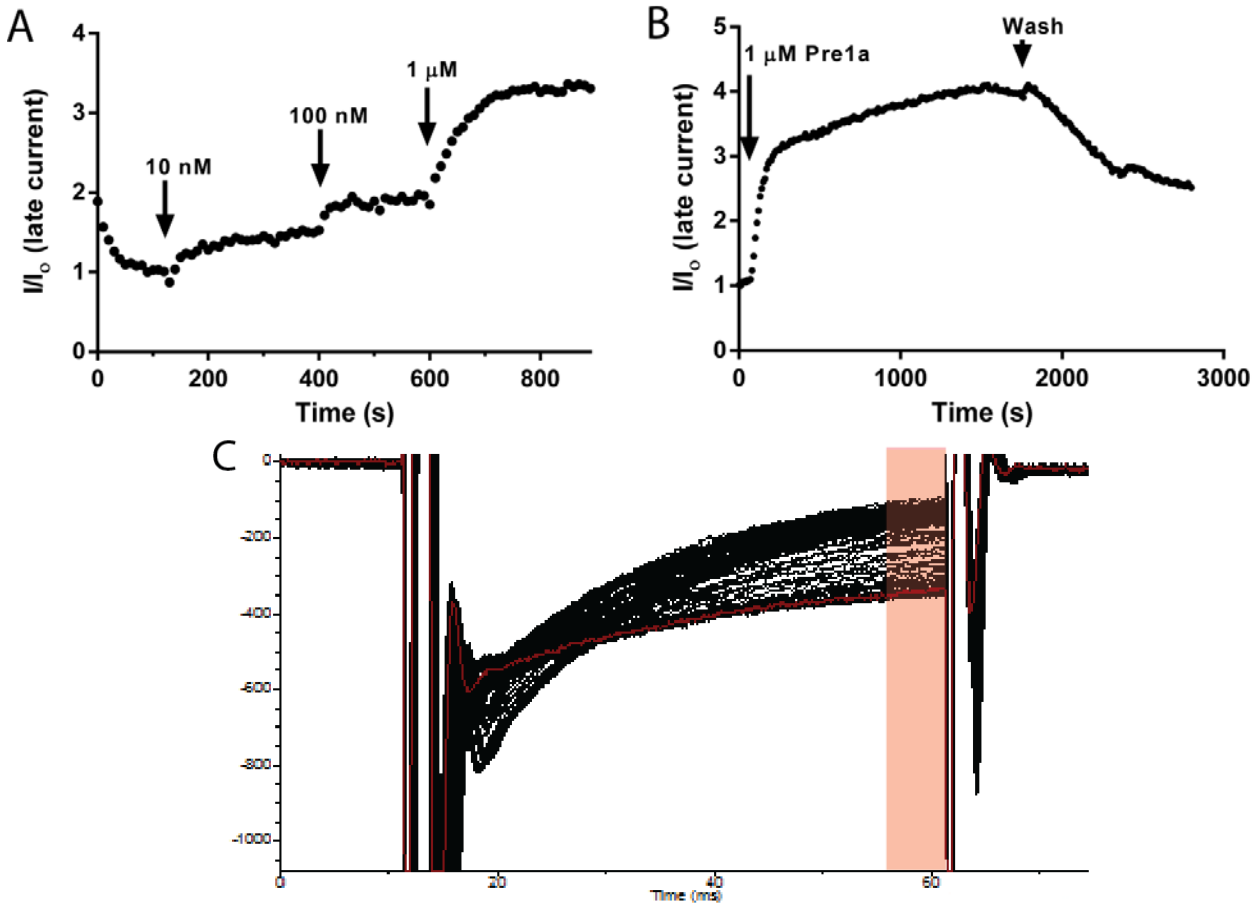

Figure 62: I-T plot of Pre1a inhibition of inactivation of rNa$_V$1.3. *A) Concentration dependent and B) 1 µM additions of Pre1a to rNa$_V$1.3 expressing oocytes. Data points represent late current (late current) values, C) highlighted in red. Pre1a activity was partially reversible with extended saline wash, as seen in B). I-V plots were taken before the first addition and after reaching steady-state activity of final addition of peptide (Appendix C).*

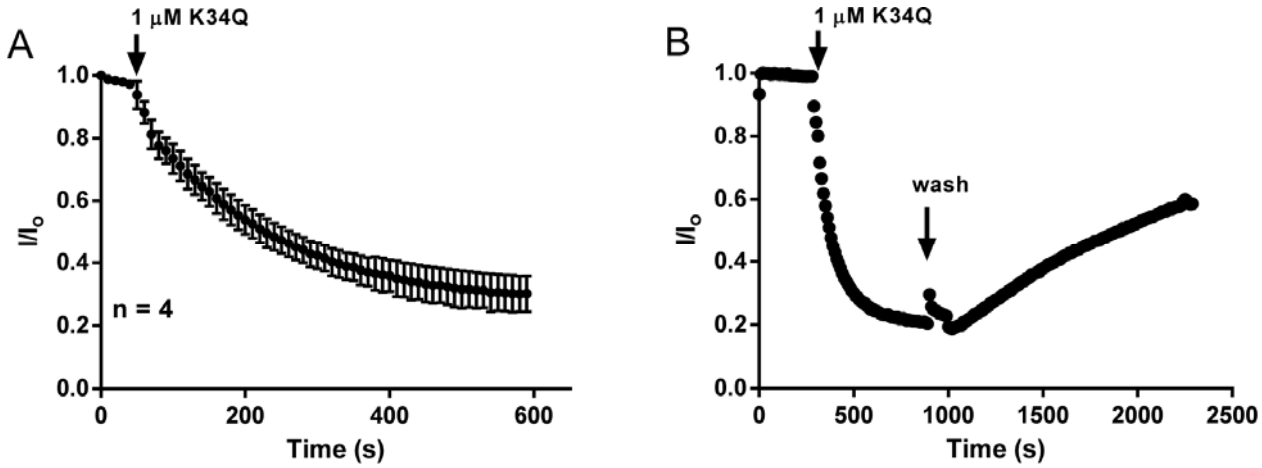

Figure 63: I-T plots for Pre1a[K_{34}Q] inhibition of rNa_V1.2 and hNa_V1.7 and washout.

1 μM addition of Pre1a[K_{34}Q] resulted in inhibition of peak current for both A) rNa_V1.2 and B) hNa_V1.7 expressed in oocytes. B) Partial reversal of hNa_V1.7 inhibition can be seen with extended wash. I-V plots were for taken for Pre1a[K_{34}Q] and all other mutations before the first addition and after reaching steady-state inhibition of final addition of peptide (Appendix C).

Appendix C: I-V relationships and steady-state activation of $Na_V1.2$ and $Na_V1.7$

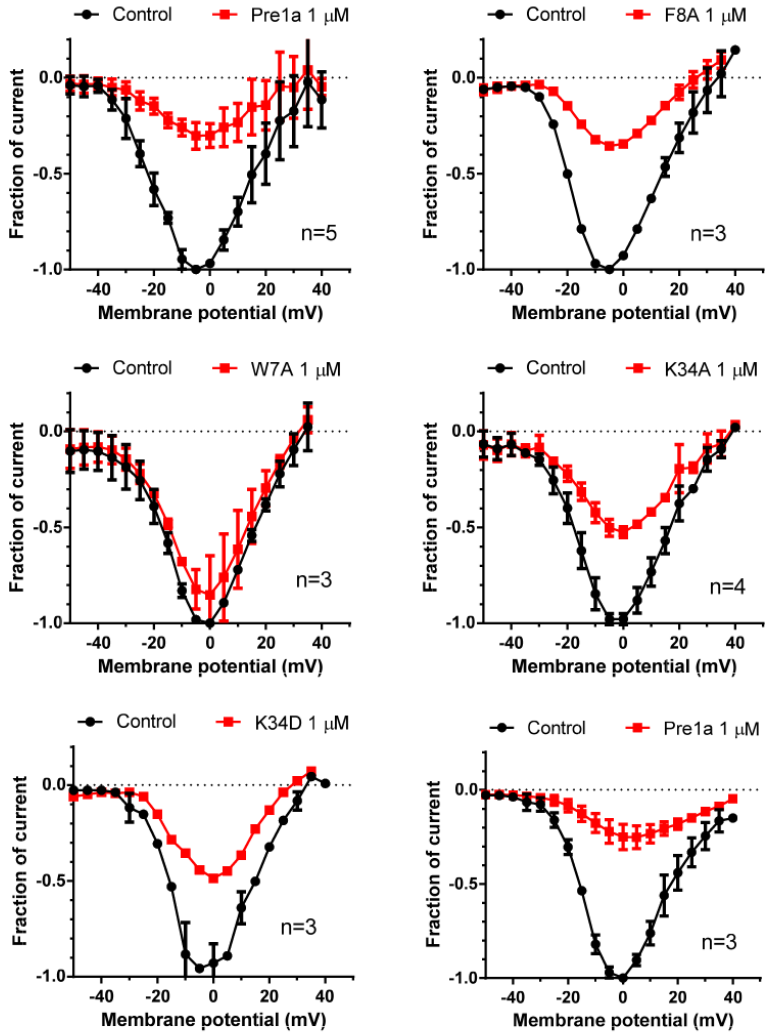

Figure 64: rNav1.2 I-V relationship curves. *Pre1a and each mutant analyzed at 1 μM on* ***rNa**$_V$1.2 expressed in oocytes. Data was normalized to peak current.* n *represents the number of individual oocytes tested.*

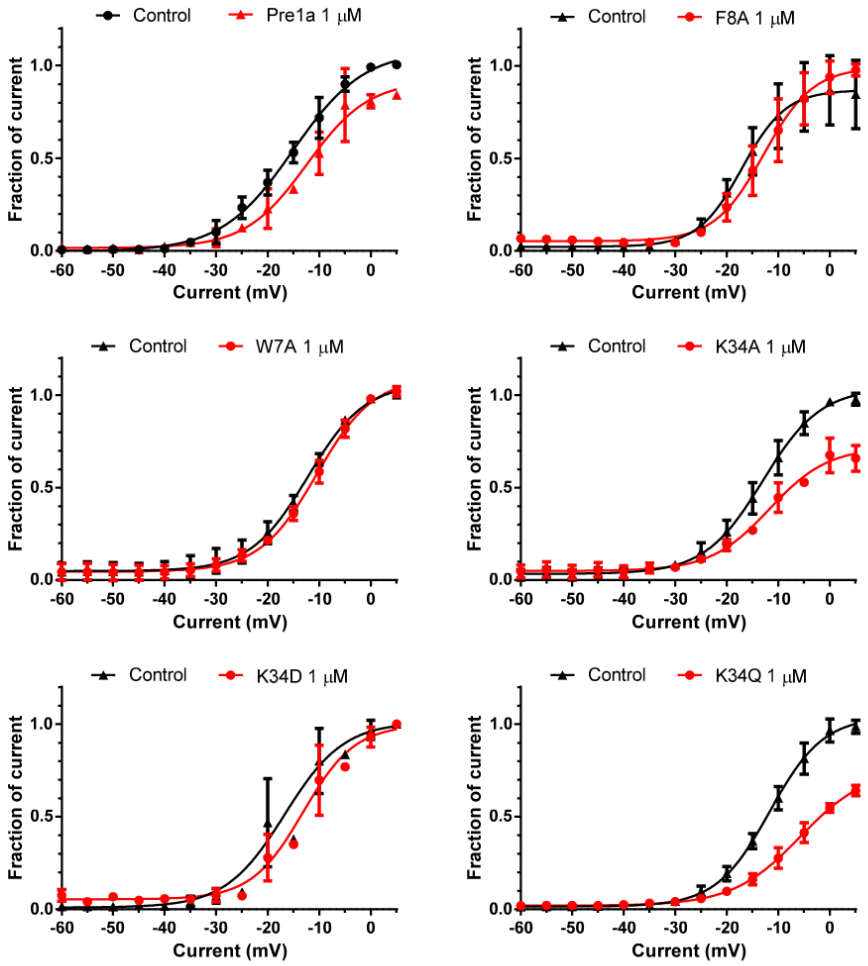

Figure 65: Steady-state activation of rNa$_V$1.2. *Steady-state activation of rNa$_V$1.2 was analyzed using the equation G(V) = I/(V − V$_{rev}$), where I, V, and V$_{rev}$ represent inward current elicited as described for the I-V plot in Figure 61, test potential, and reversal potential, respectively.*

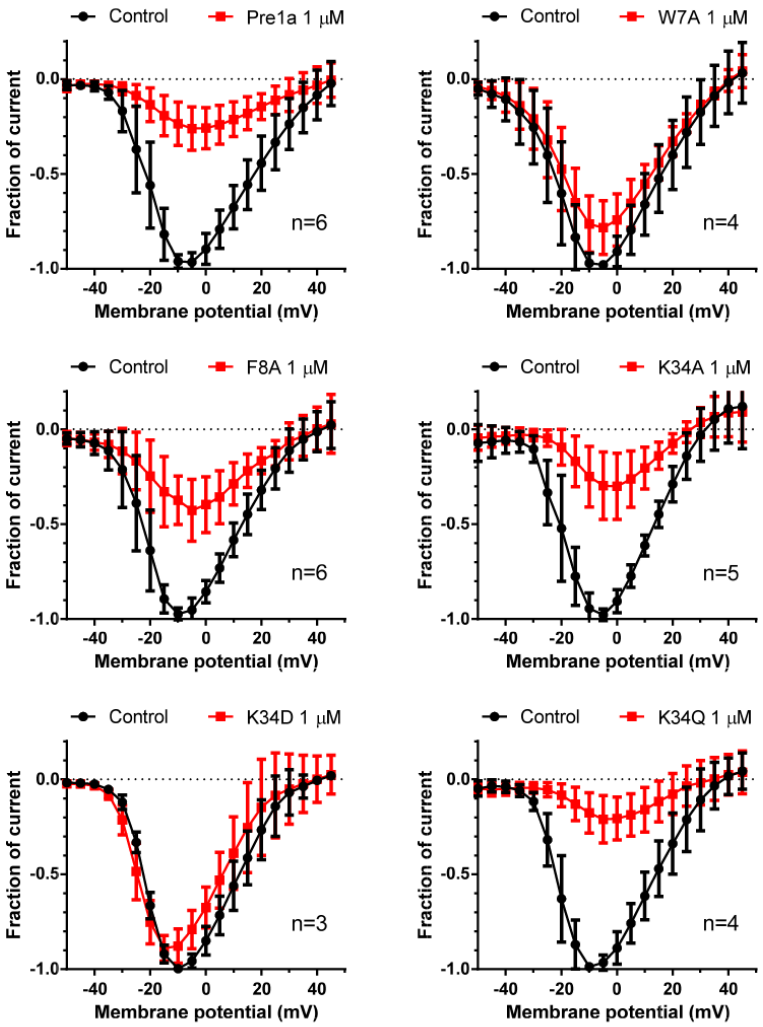

Figure 66: hNav1.7 IV-relationship curves. *Pre1a and each mutant analyzed at 1 μM on hNa$_V$1.7 expressed in oocytes. Data was normalized to peak current.* n *represents the number of oocytes tested.*

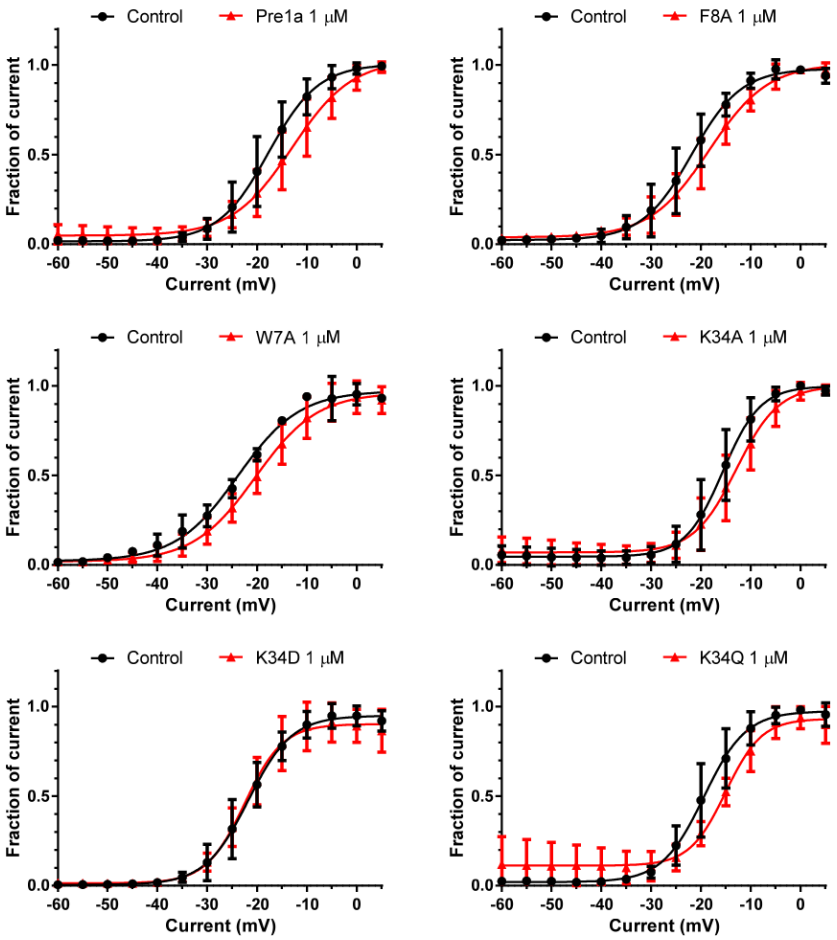

Figure 67: Steady-state activation of hNa$_V$1.7. *Steady-state activation of rNa$_V$1.2 was analyzed using the equation G(V) = I/(V − V$_{rev}$), where I, V, and V$_{rev}$ represent inward current elicited as described for the IV plot in Figure 63, test potential, and reversal potential, respectively.*

Appendix D: ^{15}N-HSQC comparisons of rPre1a[wt] vs K_{34} mutants

Each representation shows the ^{15}N-HSQC of each mutant overlaid with the ^{15}N-HSQC of wild-type rPre1a. No major deviations with Cys residues could be seen, suggesting proper folding of each peptide. Peaks were not assigned for any of the following mutants, so all labeling is specific to the rPre1a[wt] HSQC.

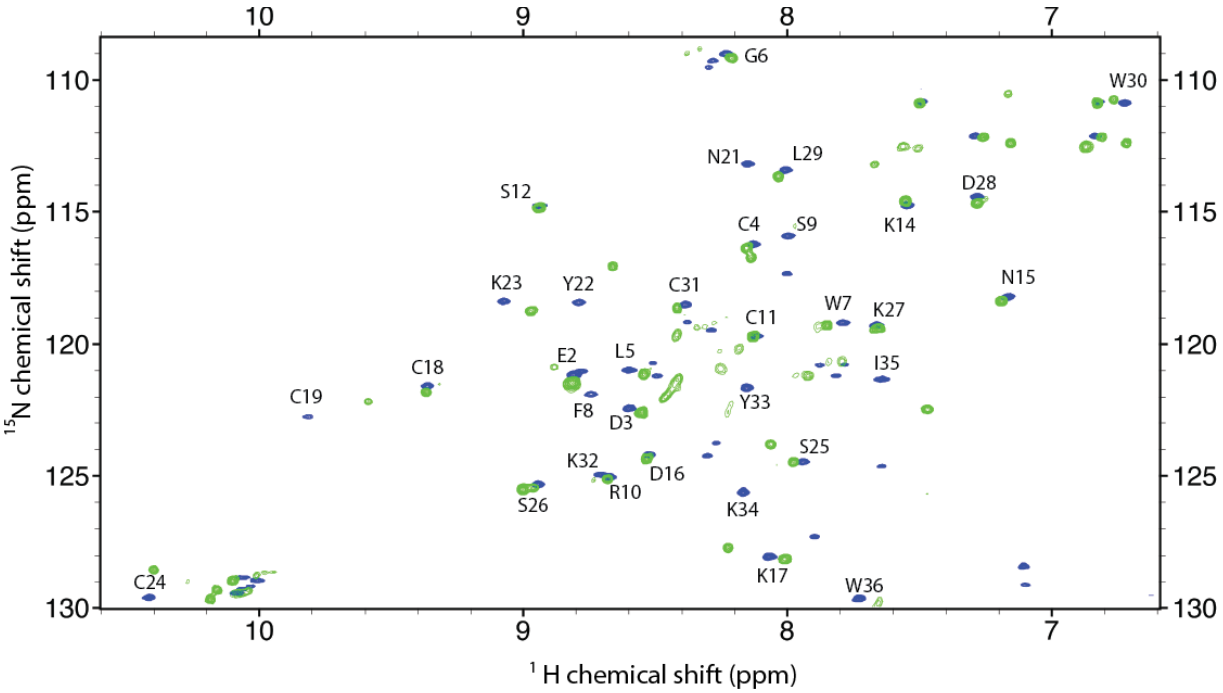

Figure 68: Overlay ^{15}N-HSQC of rPre1a[wt] (blue) and rPre1a[K_{34}Q] (green).

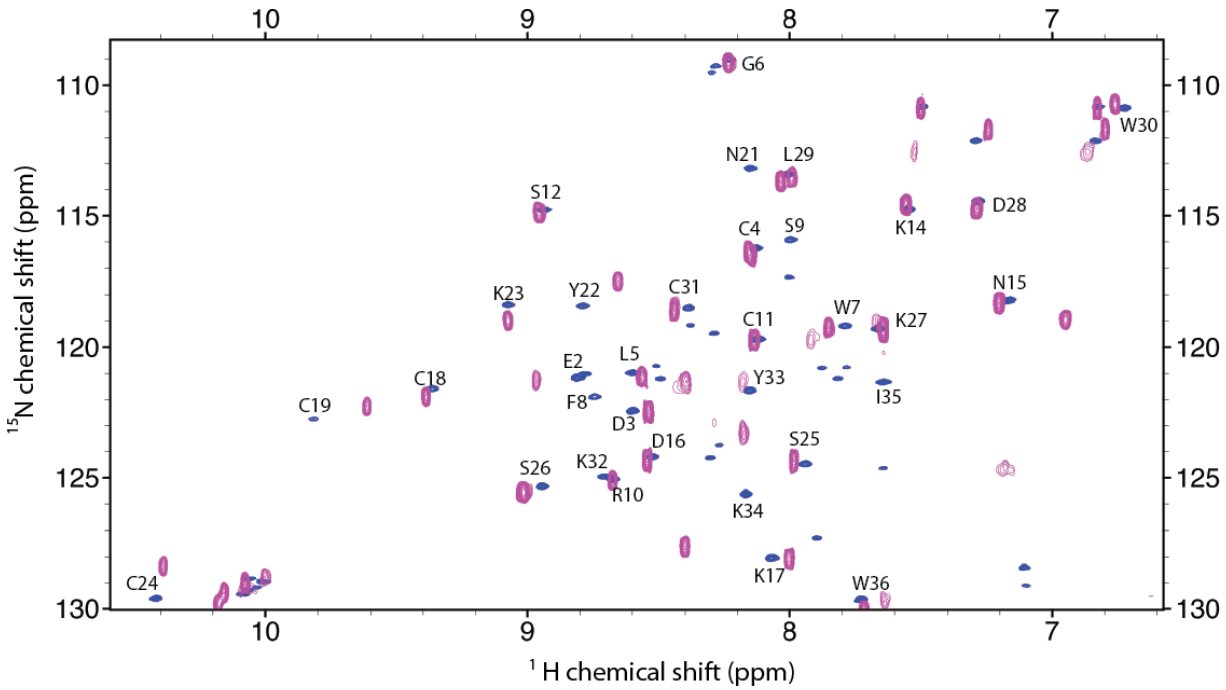

Figure 69: Overlay ^{15}N-HSQC of rPre1a[wt] (blue) and rPre1a[K_{34}D] (purple).

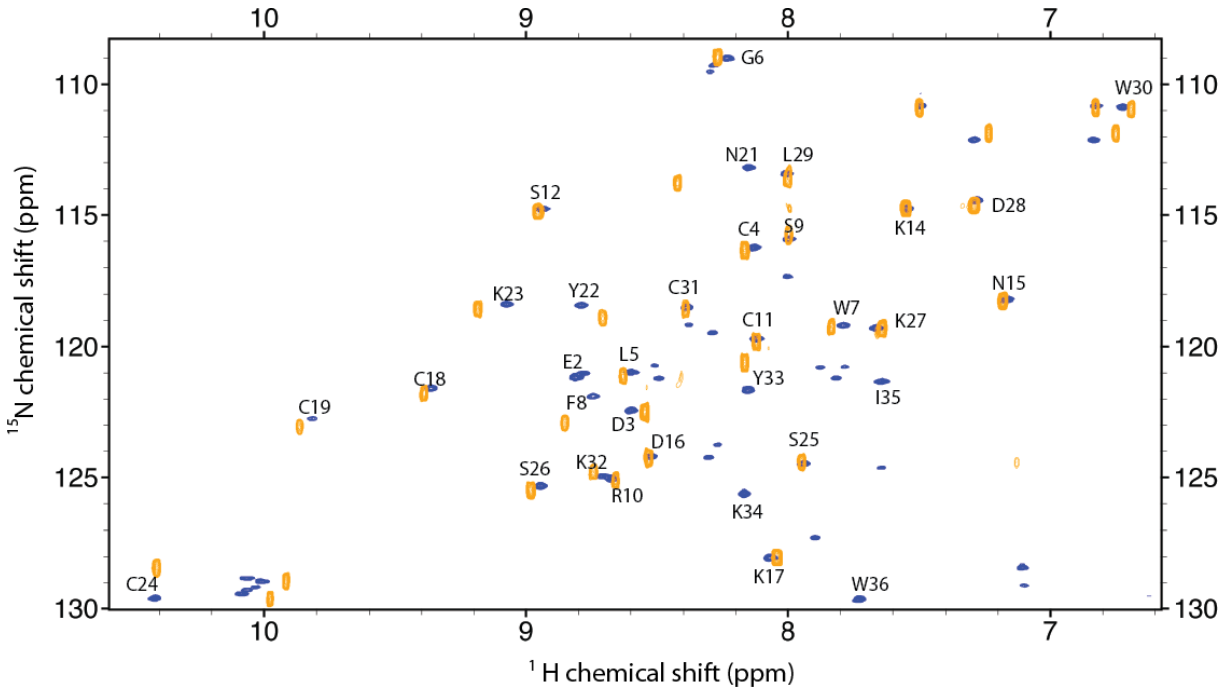

Figure 70: Overlay ^{15}N-HSQC of rPre1a[wt] (blue) and rPre1a[K_{34}A] (yellow).

Appendix E: Chemical shift lists for rPre1a[wt] and rPre1a[W_7A]

rPre1a[wt]					rPre1a[W_7A]				
Residue	**Atom**	**Nuc**	**Shift**	**SDev**	**Residue**	**Atom**	**Nuc**	**Shift**	**SDev**
S1	C	13C	170.659	0	S1	C	13C	169.892	0
S1	CA	13C	57.432	0	S1	CA	13C	57.511	0.005
S1	CB	13C	63.241	0	S1	CB	13C	63.161	0.015
S1	HA	1H	4.093	0.001	S1	HA	1H	4.138	0.003
S1	QB	1H	3.964	0	S1	QB	1H	3.977	0.002
E2	C	13C	175.719	0	E2	C	13C	174.885	0
E2	CA	13C	56.318	0.011	E2	CA	13C	56.301	0
E2	CB	13C	30.565	0.019	E2	CB	13C	30.518	0.071
E2	CG	13C	36.266	0	E2	CG	13C	36.205	0.029
E2	H	1H	8.809	0.004	E2	H	1H	8.793	0.002
E2	HA	1H	4.434	0.004	E2	HA	1H	4.417	0.006
E2	HB2	1H	2.142	0.003	E2	HB2	1H	2.121	0.004
E2	HB3	1H	1.966	0.002	E2	HB3	1H	1.935	0.004
E2	MG	1H	2.296	0.001	E2	N	15N	121.504	0.007
E2	N	15N	121.215	0.042	E2	QG	1H	2.279	0.001
D3	CA	13C	54.142	0.011	D3	C	13C	174.551	0
D3	CB	13C	41.078	0.009	D3	CB	13C	41.017	0.03
D3	H	1H	8.597	0.002	D3	H	1H	8.535	0.003
D3	HA	1H	4.692	0.001	D3	HA	1H	4.667	0.004
D3	HB2	1H	2.744	0.003	D3	HB2	1H	2.722	0.002
D3	HB3	1H	2.603	0.002	D3	HB3	1H	2.577	0.006
D3	N	15N	122.467	0	D3	N	15N	122.579	0.031
C4	C	13C	173.068	0	C4	C	13C	171.993	0
C4	CA	13C	54.145	0.013	C4	CA	13C	54.027	0
C4	CB	13C	43.215	0.012	C4	CB	13C	43.58	0.045
C4	H	1H	8.155	0.002	C4	H	1H	8.149	0.004
C4	HA	1H	4.927	0.003	C4	HA	1H	4.869	0.009
C4	MB	1H	3.252	0.001	C4	HB2	1H	3.244	0.003
C4	N	15N	116.255	0.036	C4	HB3	1H	3.156	0.001
L5	C	13C	174.976	0	C4	N	15N	116.298	0.023
L5	CA	13C	54.209	0.017	L5	C	13C	173.719	0
L5	CB	13C	43.312	0.071	L5	CA	13C	54.256	0.042
L5	CD1	13C	21.915	0	L5	CB	13C	43.386	0.037
L5	CD2	13C	26.24	0	L5	CD1	13C	26.337	0
L5	CG	13C	26.436	0	L5	CD2	13C	21.992	0
L5	H	1H	8.599	0.003	L5	CG	13C	25.945	0.002

L5	HA	1H	4.431	0.008		L5	H	1H	8.517	0.003
L5	HB2	1H	1.793	0.002		L5	HA	1H	4.374	0.004
L5	HB3	1H	1.501	0.002		L5	HB2	1H	1.739	0.003
L5	HG	1H	1.613	0.001		L5	HB3	1H	1.43	0.003
L5	MD1	1H	0.866	0		L5	HG	1H	1.576	0.002
L5	MD2	1H	0.974	0.002		L5	MD1	1H	0.944	0.001
L5	N	15N	120.984	0.007		L5	MD2	1H	0.847	0.008
G6	C	13C	173.072	0		L5	N	15N	120.874	0.029
G6	CA	13C	42.796	0.026		G6	C	13C	172.186	0
G6	H	1H	8.239	0.005		G6	CA	13C	42.79	0.059
G6	HA2	1H	3.881	0.011		G6	H	1H	8.214	0.004
G6	HA3	1H	3.586	0.003		G6	HA2	1H	3.659	0.003
G6	N	15N	108.991	0.023		G6	HA3	1H	3.443	0.006
W7	C	13C	177.322	0		G6	N	15N	109.079	0.005
W7	CA	13C	58.027	0.079		A7	C	13C	177.284	0
W7	CB	13C	29.212	0.098		A7	CA	13C	53.541	0.042
W7	H	1H	7.789	0.001		A7	CB	13C	18.983	0.009
W7	HA	1H	3.548	0.011		A7	H	1H	7.609	0.004
W7	HB2	1H	3.047	0.01		A7	HA	1H	3.045	0.002
W7	HB3	1H	2.833	0.009		A7	MB	1H	0.971	0.001
W7	N	15N	119.174	0.024		A7	N	15N	119.572	0.008
F8	C	13C	175.082	0		F8	C	13C	173.69	0
F8	CA	13C	60.151	0.048		F8	CA	13C	60.177	0.021
F8	CB	13C	37.092	0.051		F8	CB	13C	35.692	0.042
F8	H	1H	8.742	0.004		F8	CD1	13C	131.54	0
F8	HA	1H	3.456	0.011		F8	CE1	13C	131.22	0
F8	HB2	1H	2.728	0.006		F8	CZ	13C	129.487	0
F8	HB3	1H	2.127	0.005		F8	H	1H	8.63	0.003
F8	N	15N	121.912	0.021		F8	HA	1H	3.575	0.002
S9	C	13C	174.323	0		F8	HB2	1H	3.092	0.004
S9	CA	13C	59.482	0		F8	HB3	1H	2.845	0.005
S9	CB	13C	64.442	0.062		F8	HZ	1H	7.281	0
S9	H	1H	7.997	0.005		F8	N	15N	113.92	0.014
S9	HA	1H	4.422	0.001		F8	QD	1H	6.303	0.001
S9	HB2	1H	3.877	0.002		F8	QE	1H	7.232	0
S9	HB3	1H	3.824	0		S9	C	13C	173.186	0
S9	N	15N	115.915	0.027		S9	CA	13C	59.534	0.046
R10	C	13C	175.927	0		S9	CB	13C	64.653	0.046
R10	CA	13C	56.346	0.047		S9	H	1H	7.957	0.004
R10	CB	13C	29.487	0.029		S9	HA	1H	4.473	0.005

R10	CD	13C	42.717	0		S9	N	15N	116.697	0.013
R10	CG	13C	26.806	0.047		S9	QB	1H	3.826	0.008
R10	H	1H	8.671	0.002		R10	C	13C	174.838	0
R10	HA	1H	4.866	0.009		R10	CA	13C	56.625	0
R10	HD2	1H	3.378	0		R10	CB	13C	29.607	0.017
R10	HD3	1H	3.314	0.002		R10	CD	13C	42.837	0
R10	HG2	1H	1.841	0.002		R10	CG	13C	27.029	0.051
R10	HG3	1H	1.751	0		R10	H	1H	8.724	0.003
R10	MB	1H	1.895	0.002		R10	HA	1H	4.929	0.004
R10	N	15N	125.042	0.013		R10	HD2	1H	3.431	0.006
C11	C	13C	171.682	0		R10	HD3	1H	3.398	0.01
C11	CA	13C	53.69	0.066		R10	HG2	1H	1.897	0.006
C11	CB	13C	45.599	0.07		R10	HG3	1H	1.787	0.007
C11	H	1H	8.123	0.003		R10	N	15N	125.153	0.005
C11	HA	1H	4.853	0.001		R10	QB	1H	1.925	0.004
C11	HB2	1H	3.139	0.003		C11	C	13C	170.698	0
C11	HB3	1H	2.924	0.003		C11	CA	13C	53.805	0
C11	N	15N	119.683	0.009		C11	CB	13C	45.408	0.014
S12	CA	13C	52.826	0		C11	H	1H	8.121	0.003
S12	CB	13C	64.908	0.091		C11	HA	1H	4.867	0.006
S12	H	1H	8.939	0.008		C11	HB2	1H	3.14	0.004
S12	HA	1H	5.077	0.001		C11	HB3	1H	2.886	0.005
S12	HB2	1H	3.829	0.001		C11	N	15N	119.632	0.014
S12	HB3	1H	3.699	0.002		S12	CA	13C	52.964	0
S12	N	15N	114.775	0.005		S12	CB	13C	65.096	0.018
P13	C	13C	176.979	0		S12	H	1H	8.932	0.005
P13	CA	13C	64.338	0		S12	HA	1H	5.069	0.001
P13	CB	13C	32.093	0.084		S12	HB2	1H	3.827	0.004
P13	CD	13C	51.262	0.074		S12	HB3	1H	3.696	0
P13	CG	13C	27.81	0.029		S12	N	15N	114.79	0.009
P13	HA	1H	4.017	0.003		P13	C	13C	175.993	0
P13	HB2	1H	2.166	0.001		P13	CA	13C	64.432	0.053
P13	HB3	1H	1.931	0.001		P13	CB	13C	32.137	0.025
P13	HD2	1H	3.848	0.007		P13	CD	13C	51.272	0.061
P13	HD3	1H	3.772	0.001		P13	CG	13C	27.908	0.048
P13	HG2	1H	2	0.001		P13	HA	1H	4.006	0.006
P13	HG3	1H	1.634	0.001		P13	HB2	1H	2.196	0.003
K14	C	13C	176.134	0		P13	HB3	1H	1.909	0.002
K14	CA	13C	56.935	0		P13	HD2	1H	3.846	0.005
K14	CB	13C	32.322	0.053		P13	HD3	1H	3.776	0

K14	CD	13C	28.904	0.037		P13	HG2	1H	1.995	0.002
K14	CE	13C	42.114	0		P13	HG3	1H	1.606	0.01
K14	CG	13C	25.029	0.028		K14	C	13C	175.117	0
K14	H	1H	7.545	0.003		K14	CA	13C	56.925	0.038
K14	HA	1H	4.179	0.008		K14	CB	13C	32.534	0.044
K14	HB2	1H	1.807	0		K14	CD	13C	28.923	0.067
K14	HB3	1H	1.625	0		K14	CE	13C	41.788	0
K14	HD2	1H	1.646	0.001		K14	CG	13C	25.001	0.052
K14	HD3	1H	1.59	0.001		K14	H	1H	7.55	0.003
K14	HG2	1H	1.405	0.009		K14	HA	1H	4.175	0
K14	HG3	1H	1.329	0.001		K14	HB2	1H	1.796	0.006
K14	ME	1H	2.956	0		K14	HB3	1H	1.617	0.002
K14	N	15N	114.749	0.015		K14	N	15N	114.438	0.021
N15	C	13C	173.59	0		K14	QD	1H	1.575	0
N15	CA	13C	52.55	0.045		K14	QE	1H	2.948	0.001
N15	CB	13C	38.115	0.086		K14	QG	1H	1.376	0.001
N15	H	1H	7.169	0.002		N15	C	13C	172.586	0
N15	HA	1H	4.714	0.008		N15	CA	13C	52.854	0
N15	HB2	1H	2.692	0.005		N15	CB	13C	38.069	0.019
N15	HB3	1H	2.58	0.003		N15	H	1H	7.196	0.004
N15	HD21	1H	7.492	0.003		N15	HA	1H	4.696	0.006
N15	HD22	1H	6.829	0		N15	HB2	1H	2.682	0.005
N15	N	15N	118.224	0.027		N15	HB3	1H	2.558	0.007
N15	ND2	15N	110.828	0.003		N15	HD21	1H	7.496	0.001
D16	C	13C	177.379	0		N15	HD22	1H	6.83	0.002
D16	CA	13C	55.376	0		N15	N	15N	118.352	0.011
D16	CB	13C	41.359	0.089		N15	ND2	15N	110.835	0.03
D16	H	1H	8.524	0.002		D16	C	13C	176.411	0
D16	HA	1H	4.374	0.006		D16	CA	13C	55.531	0.01
D16	HB2	1H	3.031	0.004		D16	CB	13C	41.48	0.041
D16	HB3	1H	2.515	0.003		D16	H	1H	8.509	0.002
D16	N	15N	124.217	0.031		D16	HA	1H	4.34	0.009
K17	C	13C	177.146	0		D16	HB2	1H	3.022	0.009
K17	CA	13C	54.251	0.021		D16	HB3	1H	2.505	0.002
K17	CB	13C	31.224	0.025		D16	N	15N	124.183	0.013
K17	CD	13C	28.589	0		K17	C	13C	176.038	0
K17	CE	13C	42.238	0		K17	CA	13C	54.467	0.067
K17	CG	13C	24.557	0.046		K17	CB	13C	31.338	0.036
K17	H	1H	8.071	0.004		K17	CE	13C	42.125	0.041
K17	HA	1H	4.659	0.005		K17	CG	13C	24.499	0.009

K17	HB2	1H	2.393	0.002		K17	H	1H	8.002	0.004
K17	HB3	1H	1.613	0.002		K17	HA	1H	4.65	0.009
K17	HE2	1H	2.971	0.001		K17	HB2	1H	2.371	0.003
K17	HE3	1H	2.899	0.005		K17	HB3	1H	1.579	0.002
K17	HG2	1H	1.511	0.005		K17	HE2	1H	2.956	0
K17	HG3	1H	1.406	0.002		K17	HE3	1H	2.895	0.004
K17	MD	1H	1.643	0		K17	HG2	1H	1.488	0.004
K17	N	15N	128.048	0.023		K17	HG3	1H	1.386	0.002
C18	C	13C	175.735	0		K17	N	15N	128.081	0.014
C18	CA	13C	56.889	0		K17	QD	1H	1.628	0.005
C18	CB	13C	39.257	0		C18	C	13C	174.582	0
C18	H	1H	9.367	0.006		C18	CA	13C	57.024	0.027
C18	HA	1H	5.041	0.001		C18	CB	13C	39.294	0.036
C18	MB	1H	2.98	0.011		C18	H	1H	9.326	0.002
C18	N	15N	121.582	0.015		C18	HA	1H	4.975	0.002
C19	CA	13C	53.747	0		C18	HB2	1H	2.944	0.004
C19	CB	13C	38.497	0.087		C18	HB3	1H	2.88	0.001
C19	H	1H	9.818	0.013		C18	N	15N	121.544	0.027
C19	HA	1H	4.819	0		C19	CB	13C	38.762	0.017
C19	HB2	1H	3.585	0.004		C19	H	1H	9.515	0.003
C19	HB3	1H	2.534	0.003		C19	HA	1H	4.742	0
C19	N	15N	122.814	0.051		C19	HB2	1H	3.504	0.002
P20	C	13C	176.69	0		C19	HB3	1H	2.375	0.002
P20	CA	13C	65.457	0		C19	N	15N	122.064	0.007
P20	CB	13C	31.833	0.017		P20	C	13C	175.723	0
P20	CD	13C	50.816	0.022		P20	CA	13C	65.208	0.032
P20	CG	13C	27.791	0.045		P20	CB	13C	31.901	0.037
P20	HA	1H	4.269	0.001		P20	CD	13C	50.767	0.027
P20	HB2	1H	2.34	0.002		P20	CG	13C	27.92	0.005
P20	HB3	1H	1.821	0.001		P20	HA	1H	4.112	0.003
P20	HD2	1H	4.002	0.001		P20	HB2	1H	2.274	0.002
P20	HD3	1H	3.719	0.001		P20	HB3	1H	1.76	0.002
P20	HG2	1H	2.13	0		P20	HD2	1H	3.973	0.011
P20	HG3	1H	2.044	0.002		P20	HD3	1H	3.678	0.006
N21	C	13C	173.28	0		P20	HG2	1H	2.125	0.001
N21	CA	13C	55.141	0		P20	HG3	1H	2.008	0
N21	CB	13C	37.132	0		N21	C	13C	171.514	0
N21	H	1H	8.152	0.01		N21	CA	13C	55.699	0
N21	HA	1H	4.302	0.003		N21	CB	13C	37.357	0
N21	HD21	1H	7.293	0		N21	H	1H	8.096	0.004

N21	HD22	1H	6.836	0.001		N21	HA	1H	4.119	0.003
N21	MB	1H	2.474	0.005		N21	N	15N	113.149	0.018
N21	N	15N	113.209	0.005		N21	QB	1H	2.537	0.005
N21	ND2	15N	112.113	0.001		Y22	C	13C	172.996	0
Y22	C	13C	173.825	0		Y22	CA	13C	56.673	0.085
Y22	CA	13C	55.985	0.057		Y22	CB	13C	42.008	0.025
Y22	CB	13C	42.015	0.049		Y22	CD1	13C	132.485	0
Y22	H	1H	8.788	0.006		Y22	CE1	13C	117.919	0
Y22	HA	1H	5.245	0.004		Y22	H	1H	8.697	0.003
Y22	HB2	1H	3.142	0.001		Y22	HA	1H	4.947	0.007
Y22	HB3	1H	2.784	0.003		Y22	HB2	1H	3.258	0.004
Y22	N	15N	118.434	0.018		Y22	HB3	1H	2.46	0.008
K23	C	13C	176.021	0		Y22	N	15N	117.389	0.009
K23	CA	13C	54.775	0		Y22	QD	1H	6.657	0.002
K23	CB	13C	37.046	0.008		Y22	QE	1H	6.662	0.002
K23	CD	13C	29.249	0		K23	C	13C	175.088	0
K23	CE	13C	42.205	0		K23	CB	13C	37.089	0.072
K23	CG	13C	24.756	0.001		K23	CD	13C	28.994	0.008
K23	H	1H	9.074	0.004		K23	CE	13C	42.36	0
K23	HA	1H	4.611	0		K23	CG	13C	24.982	0.025
K23	HG2	1H	1.403	0.001		K23	H	1H	8.96	0.002
K23	HG3	1H	1.329	0		K23	HA	1H	4.66	0.007
K23	MB	1H	1.628	0.004		K23	HB2	1H	1.651	0.002
K23	MD	1H	1.676	0.001		K23	HB3	1H	1.591	0.002
K23	ME	1H	2.991	0.002		K23	HD2	1H	1.652	0.002
K23	N	15N	118.371	0.002		K23	HD3	1H	1.629	0
C24	C	13C	174.447	0		K23	HG2	1H	1.402	0.002
C24	CA	13C	56.71	0.012		K23	HG3	1H	1.31	0.003
C24	CB	13C	38.427	0.096		K23	N	15N	118.693	0.005
C24	H	1H	10.418	0.009		K23	QE	1H	2.962	0.004
C24	HA	1H	4.457	0.005		C24	C	13C	173.357	0
C24	HB2	1H	3.144	0.006		C24	CA	13C	56.627	0.054
C24	HB3	1H	2.53	0.002		C24	CB	13C	38.442	0.063
C24	N	15N	129.565	0.004		C24	H	1H	10.45	0.003
S25	C	13C	176.005	0		C24	HA	1H	4.455	0.004
S25	CA	13C	57.186	0		C24	HB2	1H	3.067	0.004
S25	CB	13C	63.639	0.006		C24	HB3	1H	2.526	0.008
S25	H	1H	7.94	0.004		C24	N	15N	129.112	0.011
S25	HA	1H	4.487	0.007		S25	C	13C	175.099	0
S25	HB2	1H	4.003	0.003		S25	CA	13C	57.147	0.042

S25	HB3	1H	3.835	0		S25	CB	13C	63.765	0.081
S25	N	15N	124.487	0.025		S25	H	1H	8.056	0.002
S26	C	13C	174.233	0		S25	HA	1H	4.519	0.002
S26	CA	13C	61.049	0		S25	HB2	1H	4.092	0.009
S26	CB	13C	62.567	0		S25	HB3	1H	3.891	0.008
S26	H	1H	8.943	0.003		S25	N	15N	124.651	0.014
S26	HA	1H	4.005	0.007		S26	C	13C	173.225	0
S26	HB2	1H	3.942	0		S26	CA	13C	61.323	0
S26	HB3	1H	3.856	0		S26	CB	13C	62.563	0.013
S26	N	15N	125.324	0.024		S26	H	1H	8.976	0.003
K27	C	13C	176.834	0		S26	HA	1H	4.009	0.005
K27	CA	13C	57.225	0		S26	HB2	1H	3.942	0.003
K27	CB	13C	33.369	0.025		S26	HB3	1H	3.855	0.002
K27	CG	13C	24.524	0		S26	N	15N	125.423	0.073
K27	H	1H	7.661	0.003		K27	C	13C	175.77	0
K27	HA	1H	4.189	0.003		K27	CA	13C	57.612	0.11
K27	HB2	1H	1.684	0.002		K27	CB	13C	33.45	0.031
K27	HB3	1H	1.527	0.001		K27	CG	13C	24.501	0.014
K27	HG2	1H	1.341	0.001		K27	H	1H	7.665	0.003
K27	HG3	1H	1.268	0.002		K27	HA	1H	4.179	0.004
K27	ME	1H	2.961	0.001		K27	HB2	1H	1.677	0.004
K27	N	15N	119.27	0.016		K27	HB3	1H	1.521	0.004
D28	C	13C	174.317	0		K27	HD2	1H	1.607	0
D28	CA	13C	54.686	0		K27	HD3	1H	1.358	0
D28	CB	13C	41.494	0.028		K27	HG2	1H	1.321	0.002
D28	H	1H	7.28	0.003		K27	HG3	1H	1.243	0.003
D28	HA	1H	4.304	0		K27	N	15N	119.394	0.03
D28	HB2	1H	1.358	0		K27	QE	1H	2.953	0.001
D28	HB3	1H	1.326	0		D28	C	13C	173.321	0
D28	N	15N	114.442	0.017		D28	CA	13C	54.651	0.026
L29	C	13C	176.066	0		D28	CB	13C	41.522	0.011
L29	CA	13C	55.864	0.127		D28	H	1H	7.238	0.003
L29	CB	13C	37.223	0.063		D28	HA	1H	4.234	0.007
L29	CD1	13C	25.477	0.086		D28	HB2	1H	1.263	0.003
L29	CD2	13C	23.464	0		D28	HB3	1H	1.022	0.001
L29	CG	13C	27.237	0.053		D28	N	15N	114.542	0.04
L29	H	1H	8.006	0.002		L29	C	13C	175.112	0
L29	HA	1H	3.871	0.013		L29	CA	13C	55.61	0.046
L29	HB2	1H	2.029	0.003		L29	CB	13C	37.504	0.007
L29	HB3	1H	1.899	0.006		L29	CD1	13C	25.467	0

L29	HG	1H	1.316	0.007		L29	CD2	13C	23.493	0
L29	MD1	1H	0.889	0.008		L29	CG	13C	26.827	0.128
L29	MD2	1H	0.88	0.001		L29	H	1H	8.039	0.002
L29	N	15N	113.436	0.028		L29	HA	1H	3.909	0.002
W30	C	13C	178.068	0		L29	HB2	1H	2.034	0.009
W30	CA	13C	55.363	0.025		L29	HB3	1H	1.893	0.005
W30	CB	13C	31.864	0.032		L29	HG	1H	1.343	0.007
W30	H	1H	6.72	0.002		L29	MD1	1H	0.899	0.008
W30	HA	1H	5.686	0.004		L29	MD2	1H	0.881	0.005
W30	HB2	1H	2.882	0.003		L29	N	15N	113.903	0.013
W30	HB3	1H	2.486	0.003		W30	C	13C	177.328	0
W30	N	15N	110.838	0.002		W30	CA	13C	55.009	0
C31	C	13C	174.33	0		W30	CB	13C	31.66	0
C31	CA	13C	54.847	0		W30	CD1	13C	125.402	0
C31	CB	13C	39.176	0.023		W30	CE3	13C	121.466	0
C31	H	1H	8.386	0.002		W30	CH2	13C	124.934	0
C31	HA	1H	4.718	0		W30	CZ2	13C	114.181	0
C31	HB2	1H	3.171	0.002		W30	CZ3	13C	122.009	0
C31	HB3	1H	2.561	0.006		W30	H	1H	6.84	0.003
C31	N	15N	118.497	0.013		W30	HA	1H	5.802	0.002
K32	C	13C	175.228	0		W30	HB2	1H	3.147	0
K32	CA	13C	55.081	0.035		W30	HB3	1H	2.702	0.002
K32	CB	13C	35.787	0.038		W30	HD1	1H	6.917	0.002
K32	CD	13C	29.567	0.017		W30	HE1	1H	10.28	0.003
K32	CG	13C	25.486	0.016		W30	HE3	1H	7.525	0
K32	H	1H	8.708	0.002		W30	HH2	1H	7.229	0.004
K32	HA	1H	4.927	0.002		W30	HZ2	1H	7.521	0.001
K32	HB2	1H	2.109	0.004		W30	HZ3	1H	7.163	0.002
K32	HB3	1H	1.903	0.005		W30	N	15N	110.597	0.035
K32	HD2	1H	1.744	0.002		W30	NE1	15N	128.965	0
K32	HD3	1H	1.698	0.001		C31	C	13C	173.546	0
K32	HG2	1H	1.548	0.002		C31	CB	13C	38.953	0.025
K32	HG3	1H	1.432	0.002		C31	H	1H	8.397	0.003
K32	N	15N	124.965	0.002		C31	HA	1H	4.691	0.004
Y33	C	13C	176.539	0		C31	HB2	1H	3.009	0.002
Y33	CA	13C	59.636	0		C31	HB3	1H	2.505	0.005
Y33	CB	13C	38.402	0.069		C31	N	15N	118.911	0.021
Y33	H	1H	8.16	0.01		K32	C	13C	174.473	0
Y33	HA	1H	4.258	0		K32	CB	13C	29.666	0.048
Y33	HB2	1H	2.948	0.005		K32	CE	13C	42.098	0.018

Y33	HB3	1H	2.637	0.005	K32	CG	13C	25.408	0.053
Y33	N	15N	121.663	0.006	K32	H	1H	8.998	0.003
K34	C	13C	174.818	0	K32	HA	1H	4.817	0.003
K34	CA	13C	57.193	0	K32	HB2	1H	2.055	0.001
K34	CB	13C	32.856	0.002	K32	HB3	1H	1.808	0.004
K34	CD	13C	29.413	0.07	K32	HD2	1H	1.801	0.002
K34	CE	13C	41.585	0.05	K32	HD3	1H	1.62	0.001
K34	CG	13C	25.1	0	K32	HE2	1H	3.069	0.008
K34	H	1H	8.17	0.004	K32	HE3	1H	2.979	0.004
K34	HA	1H	3.899	0.001	K32	HG2	1H	1.662	0.002
K34	HB2	1H	1.422	0.001	K32	HG3	1H	1.593	0.001
K34	HB3	1H	1.352	0.002	K32	N	15N	126.63	0.007
K34	HD2	1H	1.437	0.001	Y33	C	13C	175.057	0
K34	HD3	1H	1.383	0.001	Y33	CA	13C	59.1	0.03
K34	HE2	1H	2.725	0.001	Y33	CB	13C	38.389	0.015
K34	HE3	1H	2.622	0.001	Y33	CD1	13C	132.998	0
K34	MG	1H	0.915	0.001	Y33	CE1	13C	117.923	0
K34	N	15N	125.608	0	Y33	H	1H	8.639	0.004
I35	C	13C	175.036	0	Y33	HA	1H	3.861	0.001
I35	CA	13C	60.845	0.033	Y33	N	15N	126.24	0.008
I35	CB	13C	38.686	0.084	Y33	QB	1H	2.748	0.003
I35	CD1	13C	12.809	0	Y33	QD	1H	6.659	0.002
I35	CG1	13C	26.984	0.046	Y33	QE	1H	6.659	0.002
I35	CG2	13C	17.457	0	K34	C	13C	173.383	0
I35	H	1H	7.643	0.003	K34	CA	13C	56.979	0.019
I35	HA	1H	4.07	0.004	K34	CB	13C	32.985	0
I35	HB	1H	1.763	0.007	K34	CD	13C	29.331	0.095
I35	HG12	1H	1.337	0.007	K34	CE	13C	41.913	0
I35	HG13	1H	1.055	0.004	K34	CG	13C	24.783	0.056
I35	MD1	1H	0.827	0	K34	H	1H	8.015	0.003
I35	MG2	1H	0.826	0.005	K34	HA	1H	3.87	0.004
I35	N	15N	121.316	0.023	K34	HB2	1H	1.339	0.003
W36	CA	13C	58.461	0	K34	HB3	1H	1.309	0.001
W36	CB	13C	30.149	0.049	K34	HD2	1H	1.396	0.008
W36	H	1H	7.716	0.011	K34	HD3	1H	1.32	0.002
W36	HA	1H	4.48	0.006	K34	HE2	1H	2.616	0
W36	HB2	1H	3.324	0.001	K34	HE3	1H	2.672	0.003
W36	HB3	1H	3.164	0.001	K34	HG2	1H	0.899	0.003
W36	N	15N	129.657	0	K34	HG3	1H	0.832	0.004
					K34	N	15N	127.575	0.089

	I35	C	13C	174.074	0
	I35	CA	13C	61.104	0.024
	I35	CB	13C	38.605	0.035
	I35	CD1	13C	12.916	0.083
	I35	CG1	13C	27.126	0.071
	I35	CG2	13C	17.503	0.007
	I35	H	1H	7.412	0.004
	I35	HA	1H	3.983	0.009
	I35	HB	1H	1.721	0.006
	I35	HG12	1H	1.298	0.011
	I35	HG13	1H	1.01	0.003
	I35	MD1	1H	0.815	0.005
	I35	MG2	1H	0.781	0.007
	I35	N	15N	121.321	0.02
	W36	CA	13C	58.548	0.034
	W36	CB	13C	30.181	0.042
	W36	CD1	13C	126.784	0
	W36	CE3	13C	122.075	0
	W36	CH2	13C	124.507	0
	W36	CZ2	13C	114.827	0
	W36	CZ3	13C	122.028	0
	W36	H	1H	7.634	0.003
	W36	HA	1H	4.473	0.004
	W36	HB2	1H	3.289	0.002
	W36	HB3	1H	3.156	0.002
	W36	HD1	1H	7.21	0
	W36	HE1	1H	10.092	0.001
	W36	HE3	1H	7.66	0.001
	W36	HH2	1H	7.21	0.002
	W36	HZ2	1H	7.484	0.002
	W36	HZ3	1H	7.129	0.002
	W36	N	15N	129.671	0.014
	W36	NE1	15N	128.851	0

Appendix F: Revealing minor isoforms of Pre1a

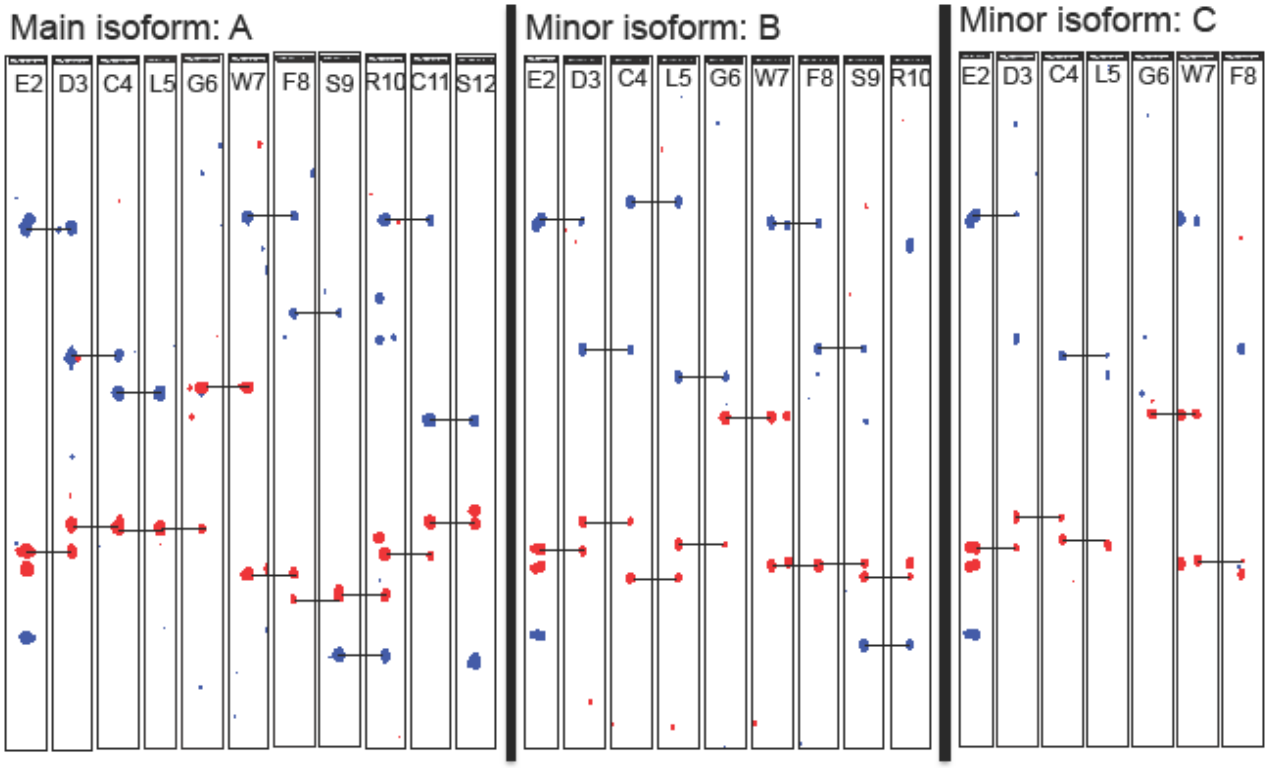

Figure 71: CBCA(CO)NH strips for rPre1a structure. *Two minor isoforms could be partially assigned using the CBCA(CO)NH strips pulled from the ^{15}N-HSQC for rPre1a.*

VI References

1. Solecki, R.S., *Shanidar IV, a Neanderthal Flower Burial in Northern Iraq.* Science, 1975. **190**(4217): p. 880-881.
2. Lev, E., *Traditional healing with animals (zootherapy): medieval to present-day Levantine practice.* Journal of Ethnopharmacology, 2003. **85**(1): p. 107-118.
3. Dutertre, S. and R.J. Lewis, *Use of Venom Peptides to Probe Ion Channel Structure and Function.* Journal of Biological Chemistry, 2010. **285**(18): p. 13315-13320.
4. Terlau, H. and B.M. Olivera, *Conus venoms: a rich source of novel ion channel-targeted peptides.* Physiol Rev, 2004. **84**(1): p. 41-68.
5. Catterall, W.A., et al., *The Hodgkin-Huxley Heritage: From Channels to Circuits.* The Journal of Neuroscience, 2012. **32**(41): p. 14064-14073.
6. Hille, B., *Ion channels of excitable membranes*. 3rd ed. 2001, Sunderland, Mass.: Sinauer. xviii, 814 p.
7. Sontheimer, H., *Voltage-dependent ion channels in glial cells.* Glia, 1994. **11**(2): p. 156-172.
8. Kaupp, U.B. and R. Seifert, *Cyclic Nucleotide-Gated Ion Channels.* Physiological Reviews, 2002. **82**(3): p. 769-824.
9. Clapham, D.E., L.W. Runnels, and C. Strubing, *The trp ion channel family.* Nat Rev Neurosci, 2001. **2**(6): p. 387-396.
10. Leung, Y.K., et al., *Cyclic Nucleotide-Gated Channels Contribute to Thromboxane A2-Induced Contraction of Rat Small Mesenteric Arteries.* PLoS One, 2010. **5**(6): p. e11098.
11. Hardie, R.C. and P. Raghu, *Visual transduction in Drosophila.* Nature, 2001. **413**(6852): p. 186-93.
12. Jan, L.Y. and Y.N. Jan, *Tracing the roots of ion channels.* Cell, 1992. **69**(5): p. 715-8.
13. Chakrapani, S., et al., *Structural Dynamics of an Isolated Voltage-Sensor Domain in a Lipid Bilayer.* Structure (London, England : 1993), 2008. **16**(3): p. 398-409.
14. Liebeskind, B.J., D.M. Hillis, and H.H. Zakon, *Evolution of sodium channels predates the origin of nervous systems in animals.* Proceedings of the National Academy of Sciences, 2011. **108**(22): p. 9154-9159.
15. Plummer, N.W. and M.H. Meisler, *Evolution and diversity of mammalian sodium channel genes.* Genomics, 1999. **57**(2): p. 323-31.
16. Lopreato, G.F., et al., *Evolution and divergence of sodium channel genes in vertebrates.* Proceedings of the National Academy of Sciences, 2001. **98**(13): p. 7588-7592.
17. Ohno, S., *Evolution by gene duplication*. 1970: Springer-Verlag.
18. Catterall, W.A., A.L. Goldin, and S.G. Waxman, *International Union of Pharmacology. XLVII. Nomenclature and Structure-Function Relationships of Voltage-Gated Sodium Channels.* Pharmacological Reviews, 2005. **57**(4): p. 397-409.
19. Catterall, W.A., Goldin, A.L., Waxman, S.G. *Voltage-gated sodium channels, introductory chapter*. IUPHAR Database 2012 13/08/2012 22/10/2012]; Available from: http://www.iuphar-db.org/DATABASE/FamilyIntroductionForward?familyId=82.
20. Roy, M.L. and T. Narahashi, *Differential properties of tetrodotoxin-sensitive and tetrodotoxin-resistant sodium channels in rat dorsal root ganglion neurons.* J Neurosci, 1992. **12**(6): p. 2104-11.
21. Hains, B.C., et al., *Upregulation of sodium channel Nav1.3 and functional involvement in neuronal hyperexcitability associated with central neuropathic pain after spinal cord injury.* J Neurosci, 2003. **23**(26): p. 8881-92.

22. Maingret, F., et al., *Inflammatory mediators increase Nav1.9 current and excitability in nociceptors through a coincident detection mechanism.* J Gen Physiol, 2008. **131**(3): p. 211-25.
23. Shah, B.S., et al., *Developmental expression of the novel voltage-gated sodium channel auxiliary subunit beta3, in rat CNS.* J Physiol, 2001. **534**(Pt 3): p. 763-76.
24. Thimmapaya, R., et al., *Distribution and functional characterization of human Nav1.3 splice variants.* Eur J Neurosci, 2005. **22**(1): p. 1-9.
25. Novak, A., et al., *Gene Duplications and Evolution of Vertebrate Voltage-Gated Sodium Channels.* Journal of Molecular Evolution, 2006. **63**(2): p. 208-221.
26. Meisler, M.H., et al., *Sodium Channels and Neurological Disease: Insights from Scn8a Mutations in the Mouse.* The Neuroscientist, 2001. **7**(2): p. 136-145.
27. Zakon, H.H., *Adaptive evolution of voltage-gated sodium channels: The first 800 million years.* Proceedings of the National Academy of Sciences, 2012. **109**(Supplement 1): p. 10619-10625.
28. Jost, M.C., et al., *Toxin-resistant sodium channels: parallel adaptive evolution across a complete gene family.* Molecular biology and evolution, 2008. **25**(6): p. 1016-1024.
29. Catterall, W.A., *From ionic currents to molecular mechanisms: the structure and function of voltage-gated sodium channels.* Neuron, 2000. **26**(1): p. 13-25.
30. Yu, F.H., et al., *Sodium channel beta4, a new disulfide-linked auxiliary subunit with similarity to beta2.* J Neurosci, 2003. **23**(20): p. 7577-85.
31. Messner, D.J. and W.A. Catterall, *The sodium channel from rat brain. Separation and characterization of subunits.* Journal of Biological Chemistry, 1985. **260**(19): p. 10597-10604.
32. Vijayaragavan, K., et al., *Role of auxiliary beta1-, beta2-, and beta3-subunits and their interaction with Na(v)1.8 voltage-gated sodium channel.* Biochem Biophys Res Commun, 2004. **319**(2): p. 531-40.
33. Lipkind, G.M. and H.A. Fozzard, *A structural model of the tetrodotoxin and saxitoxin binding site of the Na+ channel.* Biophys J, 1994. **66**(1): p. 1-13.
34. Bosmans, F., M.F. Martin-Eauclaire, and K.J. Swartz, *Deconstructing voltage sensor function and pharmacology in sodium channels.* Nature, 2008. **456**(7219): p. 202-8.
35. Catterall, W.A., *Structure and Modulation of Na+ and Ca2+ Channels.* Annals of the New York Academy of Sciences, 1993. **707**(1): p. 1-19.
36. Heinemann, S.H., H. Terlau, and K. Imoto, *Molecular basis for pharmacological differences between brain and cardiac sodium channels.* Pflugers Arch, 1992. **422**(1): p. 90-2.
37. Satin, J., et al., *A mutant of TTX-resistant cardiac sodium channels with TTX-sensitive properties.* Science, 1992. **256**(5060): p. 1202-5.
38. Noda, M., et al., *A single point mutation confers tetrodotoxin and saxitoxin insensitivity on the sodium channel II.* FEBS Letters, 1989. **259**(1): p. 213-216.
39. Terlau, H., et al., *Mapping the site of block by tetrodotoxin and saxitoxin of sodium channel II.* FEBS Lett, 1991. **293**(1-2): p. 93-6.
40. Heinemann, S.H., et al., *Calcium channel characteristics conferred on the sodium channel by single mutations.* Nature, 1992. **356**(6368): p. 441-3.
41. Favre, I., E. Moczydlowski, and L. Schild, *On the structural basis for ionic selectivity among Na+, K+, and Ca2+ in the voltage-gated sodium channel.* Biophys J, 1996. **71**(6): p. 3110-25.
42. Chiamvimonvat, N., et al., *Control of ion flux and selectivity by negatively charged residues in the outer mouth of rat sodium channels.* J Physiol, 1996. **491 (Pt 1)**: p. 51-9.
43. Fozzard, H.A. and G.M. Lipkind, *The tetrodotoxin binding site is within the outer vestibule of the sodium channel.* Mar Drugs, 2010. **8**(2): p. 219-34.
44. Lipkind, G.M. and H.A. Fozzard, *Molecular Model of Anticonvulsant Drug Binding to the Voltage-Gated Sodium Channel Inner Pore.* Molecular Pharmacology, 2010.

45. Payandeh, J., et al., *Crystal structure of a voltage-gated sodium channel in two potentially inactivated states.* Nature, 2012. **486**(7401): p. 135-139.
46. Payandeh, J., et al., *The crystal structure of a voltage-gated sodium channel.* Nature, 2011. **475**(7356): p. 353-358.
47. Long, S.B., E.B. Campbell, and R. MacKinnon, *Crystal Structure of a Mammalian Voltage-Dependent Shaker Family K+ Channel.* Science, 2005. **309**(5736): p. 897-903.
48. Long, S.B., et al., *Atomic structure of a voltage-dependent K^+ channel in a lipid membrane-like environment.* Nature, 2007. **450**(7168): p. 376-382.
49. Treptow, W. and M. Tarek, *Environment of the Gating Charges in the Kv1.2 Shaker Potassium Channel.* Biophysical journal, 2006. **90**(9): p. L64-L66.
50. Jogini, V. and B. Roux, *Dynamics of the Kv1.2 Voltage-Gated K+ Channel in a Membrane Environment.* Biophysical journal, 2007. **93**(9): p. 3070-3082.
51. Pathak, M.M., et al., *Closing In on the Resting State of the Shaker K+ Channel.* Neuron, 2007. **56**(1): p. 124-140.
52. Delemotte, L., et al., *Intermediate states of the Kv1.2 voltage sensor from atomistic molecular dynamics simulations.* Proceedings of the National Academy of Sciences, 2011. **108**(15): p. 6109-6114.
53. Henrion, U., et al., *Tracking a complete voltage-sensor cycle with metal-ion bridges.* Proceedings of the National Academy of Sciences, 2012. **109**(22): p. 8552-8557.
54. Jensen, M.Ø., et al., *Mechanism of Voltage Gating in Potassium Channels.* Science, 2012. **336**(6078): p. 229-233.
55. Carnevale, V., W. Treptow, and M.L. Klein, *Sodium Ion Binding Sites and Hydration in the Lumen of a Bacterial Ion Channel from Molecular Dynamics Simulations.* The Journal of Physical Chemistry Letters, 2011. **2**(19): p. 2504-2508.
56. Ulbricht, W., *Sodium Channel Inactivation: Molecular Determinants and Modulation.* Physiol. Rev., 2005. **85**(4): p. 1271-1301.
57. Stuhmer, W., et al., *Structural parts involved in activation and inactivation of the sodium channel.* Nature, 1989. **339**(6226): p. 597-603.
58. Vassilev, P., T. Scheuer, and W. Catterall, *Inhibition of inactivation of single sodium channels by a site-directed antibody.* Proc Natl Acad Sci USA, 1989. **86**: p. 8147 - 8151.
59. West, J.W., et al., *A cluster of hydrophobic amino acid residues required for fast Na(+)-channel inactivation.* Proc Natl Acad Sci U S A, 1992. **89**(22): p. 10910-4.
60. Eaholtz, G., W.N. Zagotta, and W.A. Catterall, *Kinetic analysis of block of open sodium channels by a peptide containing the isoleucine, phenylalanine, and methionine (IFM) motif from the inactivation gate.* J Gen Physiol, 1998. **111**(1): p. 75-82.
61. Rohl, C.A., et al., *Solution Structure of the Sodium Channel Inactivation Gate.* Biochemistry, 1998. **38**(3): p. 855-861.
62. Motoike, H.K., et al., *The Na+ channel inactivation gate is a molecular complex: a novel role of the COOH-terminal domain.* J Gen Physiol, 2004. **123**(2): p. 155-65.
63. Vedantham, V. and S.C. Cannon, *Slow inactivation does not affect movement of the fast inactivation gate in voltage-gated Na+ channels.* J Gen Physiol, 1998. **111**(1): p. 83-93.
64. Featherstone, D.E., J.E. Richmond, and P.C. Ruben, *Interaction between fast and slow inactivation in Skm1 sodium channels.* Biophys J, 1996. **71**(6): p. 3098-109.
65. Ruff, R.L., L. Simoncini, and W. Stuhmer, *Slow sodium channel inactivation in mammalian muscle: a possible role in regulating excitability.* Muscle Nerve, 1988. **11**(5): p. 502-10.
66. Hayward, L.J., G.M. Sandoval, and S.C. Cannon, *Defective slow inactivation of sodium channels contributes to familial periodic paralysis.* Neurology, 1999. **52**(7): p. 1447-53.

67. Alekov, A.K., et al., *Enhanced inactivation and acceleration of activation of the sodium channel associated with epilepsy in man.* Eur J Neurosci, 2001. **13**(11): p. 2171-6.
68. Veldkamp, M.W., et al., *Two distinct congenital arrhythmias evoked by a multidysfunctional Na(+) channel.* Circ Res, 2000. **86**(9): p. E91-7.
69. Wang, D.W., et al., *Clinical, genetic, and biophysical characterization of SCN5A mutations associated with atrioventricular conduction block.* Circulation, 2002. **105**(3): p. 341-6.
70. Groenewegen, W.A., et al., *A novel LQT3 mutation implicates the human cardiac sodium channel domain IVS6 in inactivation kinetics.* Cardiovasc Res, 2003. **57**(4): p. 1072-8.
71. Richmond, J.E., et al., *Slow inactivation in human cardiac sodium channels.* Biophys J, 1998. **74**(6): p. 2945-52.
72. Wang, S.Y. and G.K. Wang, *A mutation in segment I-S6 alters slow inactivation of sodium channels.* Biophys J, 1997. **72**(4): p. 1633-40.
73. Vilin, Y.Y., et al., *Structural determinants of slow inactivation in human cardiac and skeletal muscle sodium channels.* Biophys J, 1999. **77**(3): p. 1384-93.
74. Xiong, W., et al., *A conserved ring of charge in mammalian Na+ channels: a molecular regulator of the outer pore conformation during slow inactivation.* J Physiol, 2006. **576**(Pt 3): p. 739-54.
75. Tikhonov, D.B. and B.S. Zhorov, *Sodium channels: ionic model of slow inactivation and state-dependent drug binding.* Biophys J, 2007. **93**(5): p. 1557-70.
76. Noda, M., et al., *Primary structure of Electrophorus electricus sodium channel deduced from cDNA sequence.* Nature, 1984. **312**(5990): p. 121-7.
77. Sheets, M.F., et al., *The Na channel voltage sensor associated with inactivation is localized to the external charged residues of domain IV, S4.* Biophys J, 1999. **77**(2): p. 747-57.
78. Chanda, B. and F. Bezanilla, *Tracking voltage-dependent conformational changes in skeletal muscle sodium channel during activation.* J Gen Physiol, 2002. **120**(5): p. 629-45.
79. Bosmans, F. and K.J. Swartz, *Targeting voltage sensors in sodium channels with spider toxins.* Trends in Pharmacological Sciences, 2010. **31**(4): p. 175-182.
80. Wang, J., et al., *Mapping the receptor site for α-scorpion toxins on a Na+ channel voltage sensor.* Proceedings of the National Academy of Sciences, 2011. **108**(37): p. 15426-15431.
81. Armstrong, C.M., *Sodium channels and gating currents.* Physiol Rev, 1981. **61**(3): p. 644-83.
82. Catterall, W., *Voltage-dependent gating of sodium channels: correlating structure and function.* Trends Neurosci, 1986. **9**: p. 7 - 10.
83. Capes, D.L., et al., *Gating transitions in the selectivity filter region of a sodium channel are coupled to the domain IV voltage sensor.* Proceedings of the National Academy of Sciences, 2012. **109**(7): p. 2648-2653.
84. DeCaen, P.G., et al., *Sequential formation of ion pairs during activation of a sodium channel voltage sensor.* Proc Natl Acad Sci U S A, 2009. **106**(52): p. 22498-503.
85. DeCaen, P.G., et al., *Disulfide locking a sodium channel voltage sensor reveals ion pair formation during activation.* Proc Natl Acad Sci U S A, 2008. **105**(39): p. 15142-7.
86. Bezanilla, F., *The voltage sensor in voltage-dependent ion channels.* Physiol Rev, 2000. **80**(2): p. 555-92.
87. Brackenbury, W.J., M.B. Djamgoz, and L.L. Isom, *An emerging role for voltage-gated Na+ channels in cellular migration: regulation of central nervous system development and potentiation of invasive cancers.* Neuroscientist, 2008. **14**(6): p. 571-83.
88. Qin, N., et al., *Molecular cloning and functional expression of the human sodium channel beta1B subunit, a novel splicing variant of the beta1 subunit.* Eur J Biochem, 2003. **270**(23): p. 4762-70.

89. Brackenbury, W.J. and L.L. Isom, *Voltage-gated Na+ channels: potential for beta subunits as therapeutic targets.* Expert Opin Ther Targets, 2008. **12**(9): p. 1191-203.
90. Patino, G.A. and L.L. Isom, *Electrophysiology and beyond: Multiple roles of Na+ channel [beta] subunits in development and disease.* Neuroscience Letters. **486**(2): p. 53-59.
91. Morgan, K., et al., *beta3: An additional auxiliary subunit of the voltage-sensitive sodium channel that modulates channel gating with distinct kinetics.* Proceedings of the National Academy of Sciences of the United States of America, 2000. **97**(5): p. 2308-2313.
92. Isom, L.L., et al., *Structure and function of the [beta]2 subunit of brain sodium channels, a transmembrane glycoprotein with a CAM motif.* Cell, 1995. **83**(3): p. 433-442.
93. Isom, L., et al., *Primary structure and functional expression of the beta 1 subunit of the rat brain sodium channel.* Science, 1992. **256**(5058): p. 839-842.
94. Kim, D.Y., et al., *Presenilin/gamma-secretase-mediated cleavage of the voltage-gated sodium channel beta2-subunit regulates cell adhesion and migration.* J Biol Chem, 2005. **280**(24): p. 23251-61.
95. Davis, T.H., C. Chen, and L.L. Isom, *Sodium channel beta1 subunits promote neurite outgrowth in cerebellar granule neurons.* J Biol Chem, 2004. **279**(49): p. 51424-32.
96. Chioni, A.M., et al., *A novel adhesion molecule in human breast cancer cells: voltage-gated Na+ channel beta1 subunit.* Int J Biochem Cell Biol, 2009. **41**(5): p. 1216-27.
97. Watanabe, H., et al., *Sodium channel beta1 subunit mutations associated with Brugada syndrome and cardiac conduction disease in humans.* The Journal of Clinical Investigation, 2008. **118**(6): p. 2260-2268.
98. Scheffer, I.E., et al., *Temporal lobe epilepsy and GEFS+ phenotypes associated with SCN1B mutations.* Brain, 2007. **130**(Pt 1): p. 100-9.
99. Wallace, R., et al., *Febrile seizures and generalized epilepsy associated with a mutation in the Na+-channel beta1 subunit gene SCN1B.* Nat Genet, 1998. **19**: p. 366 - 370.
100. Aman, T.K., et al., *Regulation of Persistent Na Current by Interactions between {beta} Subunits of Voltage-Gated Na Channels.* J. Neurosci., 2009. **29**(7): p. 2027-2042.
101. Dib-Hajj, S.D., J.A. Black, and S.G. Waxman, *Voltage-Gated Sodium Channels: Therapeutic Targets for Pain.* Pain Medicine, 2009. **10**(7): p. 1260-1269.
102. Waxman, S.G., *Mechanisms of Disease: sodium channels and neuroprotection in multiple sclerosis[mdash]current status.* Nat Clin Pract Neuro, 2008. **4**(3): p. 159-169.
103. Tfelt-Hansen, J., et al., *Inherited cardiac diseases caused by mutations in the Nav1.5 sodium channel.* J Cardiovasc Electrophysiol, 2010. **21**(1): p. 107-15.
104. Leterrier, C., et al., *Voltage-gated sodium channel organization in neurons: Protein interactions and trafficking pathways.* Neurosci Lett, 2010.
105. Fraser, S.P., et al., *Voltage-gated sodium channel expression and potentiation of human breast cancer metastasis.* Clin Cancer Res, 2005. **11**(15): p. 5381-9.
106. Wood, J.N., *Recent advances in understanding molecular mechanisms of primary afferent activation.* Gut, 2004. **53 Suppl 2**: p. ii9-12.
107. Julius, D. and A.I. Basbaum, *Molecular mechanisms of nociception.* Nature, 2001. **413**(6852): p. 203-10.
108. Cummins, T.R., et al., *Voltage-clamp and current-clamp recordings from mammalian DRG neurons.* Nat Protoc, 2009. **4**(8): p. 1103-12.
109. Wall, P.D. and M. Devor, *The effect of peripheral nerve injury on dorsal root potentials and on transmission of afferent signals into the spinal cord.* Brain Res, 1981. **209**(1): p. 95-111.

110. Abdulla, F.A. and P.A. Smith, *Changes in Na(+) channel currents of rat dorsal root ganglion neurons following axotomy and axotomy-induced autotomy.* J Neurophysiol, 2002. **88**(5): p. 2518-29.
111. Zhang, J.M., et al., *Axotomy increases the excitability of dorsal root ganglion cells with unmyelinated axons.* J Neurophysiol, 1997. **78**(5): p. 2790-4.
112. Matzner, O. and M. Devor, *Hyperexcitability at sites of nerve injury depends on voltage-sensitive Na+ channels.* J Neurophysiol, 1994. **72**(1): p. 349-59.
113. Devor, M., P.D. Wall, and N. Catalan, *Systemic lidocaine silences ectopic neuroma and DRG discharge without blocking nerve conduction.* Pain, 1992. **48**(2): p. 261-8.
114. Rizzo, M.A., *Successful treatment of painful traumatic mononeuropathy with carbamazepine: insights into a possible molecular pain mechanism.* J Neurol Sci, 1997. **152**(1): p. 103-6.
115. Omana-Zapata, I., et al., *Tetrodotoxin inhibits neuropathic ectopic activity in neuromas, dorsal root ganglia and dorsal horn neurons.* Pain, 1997. **72**(1-2): p. 41-9.
116. Waxman, S.G., J.D. Kocsis, and J.A. Black, *Type III sodium channel mRNA is expressed in embryonic but not adult spinal sensory neurons, and is reexpressed following axotomy.* J Neurophysiol, 1994. **72**(1): p. 466-70.
117. Kim, C.H., et al., *The changes in expression of three subtypes of TTX sensitive sodium channels in sensory neurons after spinal nerve ligation.* Brain Res Mol Brain Res, 2001. **95**(1-2): p. 153-61.
118. Cummins, T.R., et al., *Nav1.3 sodium channels: rapid repriming and slow closed-state inactivation display quantitative differences after expression in a mammalian cell line and in spinal sensory neurons.* J Neurosci, 2001. **21**(16): p. 5952-61.
119. Dib-Hajj, S., et al., *Down-regulation of transcripts for Na channel alpha-SNS in spinal sensory neurons following axotomy.* Proc Natl Acad Sci U S A, 1996. **93**(25): p. 14950-4.
120. Hains, B.C., et al., *Altered sodium channel expression in second-order spinal sensory neurons contributes to pain after peripheral nerve injury.* J Neurosci, 2004. **24**(20): p. 4832-9.
121. Hains, B.C., C.Y. Saab, and S.G. Waxman, *Changes in electrophysiological properties and sodium channel Nav1.3 expression in thalamic neurons after spinal cord injury.* Brain, 2005. **128**(Pt 10): p. 2359-71.
122. Nassar, M.A., et al., *Nerve injury induces robust allodynia and ectopic discharges in Nav1.3 null mutant mice.* Mol Pain, 2006. **2**: p. 33.
123. Lindia, J.A., et al., *Relationship between sodium channel NaV1.3 expression and neuropathic pain behavior in rats.* Pain, 2005. **117**(1-2): p. 145-53.
124. Dib-Hajj, S.D., et al., *Voltage-gated sodium channels in pain states: role in pathophysiology and targets for treatment.* Brain Res Rev, 2009. **60**(1): p. 65-83.
125. Holland, K.D., et al., *Mutation of sodium channel SCN3A in a patient with cryptogenic pediatric partial epilepsy.* Neurosci Lett, 2008. **433**(1): p. 65-70.
126. Guo, F., et al., *Voltage-gated sodium channel Nav1.1, Nav1.3 and beta1 subunit were up-regulated in the hippocampus of spontaneously epileptic rat.* Brain Res Bull, 2008. **75**(1): p. 179-87.
127. Toledo-Aral, J.J., et al., *Identification of PN1, a predominant voltage-dependent sodium channel expressed principally in peripheral neurons.* Proc Natl Acad Sci U S A, 1997. **94**(4): p. 1527-32.
128. Felts, P.A., et al., *Sodium channel alpha-subunit mRNAs I, II, III, NaG, Na6 and hNE (PN1): different expression patterns in developing rat nervous system.* Brain Res Mol Brain Res, 1997. **45**(1): p. 71-82.

129. Klugbauer, N., et al., *Structure and functional expression of a new member of the tetrodotoxin-sensitive voltage-activated sodium channel family from human neuroendocrine cells.* EMBO J, 1995. **14**(6): p. 1084-90.
130. Sangameswaran, L., et al., *A novel tetrodotoxin-sensitive, voltage-gated sodium channel expressed in rat and human dorsal root ganglia.* J Biol Chem, 1997. **272**(23): p. 14805-9.
131. Cummins, T.R., J.R. Howe, and S.G. Waxman, *Slow closed-state inactivation: a novel mechanism underlying ramp currents in cells expressing the hNE/PN1 sodium channel.* J Neurosci, 1998. **18**(23): p. 9607-19.
132. Cummins, T.R., P.L. Sheets, and S.G. Waxman, *The roles of sodium channels in nociception: Implications for mechanisms of pain.* Pain, 2007. **131**(3): p. 243-57.
133. Herzog, R.I., et al., *Distinct repriming and closed-state inactivation kinetics of Nav1.6 and Nav1.7 sodium channels in mouse spinal sensory neurons.* J Physiol, 2003. **551**(Pt 3): p. 741-50.
134. Shields, S.D., et al., *Sodium channel Na(v)1.7 is essential for lowering heat pain threshold after burn injury.* J Neurosci, 2012. **32**(32): p. 10819-32.
135. Sage, D., et al., *Na(v)1.7 and Na(v)1.3 are the only tetrodotoxin-sensitive sodium channels expressed by the adult guinea pig enteric nervous system.* J Comp Neurol, 2007. **504**(4): p. 363-78.
136. Ahn, H.S., et al., *Nav1.7 is the predominant sodium channel in rodent olfactory sensory neurons.* Mol Pain, 2011. **7**: p. 32.
137. Rupasinghe, D.B., et al., *Localization of Nav 1.7 in the normal and injured rodent olfactory system indicates a critical role in olfaction, pheromone sensing and immune function.* Channels (Austin), 2012. **6**(2): p. 103-10.
138. Kwong, K., et al., *Voltage-gated sodium channels in nociceptive versus non-nociceptive nodose vagal sensory neurons innervating guinea pig lungs.* J Physiol, 2008. **586**(5): p. 1321-36.
139. Saleh, S., et al., *Electrophysiological and molecular identification of voltage-gated sodium channels in murine vascular myocytes.* J Physiol, 2005. **568**(Pt 1): p. 155-69.
140. Djouhri, L., et al., *Sensory and electrophysiological properties of guinea-pig sensory neurones expressing Nav 1.7 (PN1) Na+ channel alpha subunit protein.* J Physiol, 2003. **546**(Pt 2): p. 565-76.
141. Persson, A.K., et al., *Nav1.7 accumulates and co-localizes with phosphorylated ERK1/2 within transected axons in early experimental neuromas.* Exp Neurol, 2011. **230**(2): p. 273-9.
142. Diss, J.K., et al., *A potential novel marker for human prostate cancer: voltage-gated sodium channel expression in vivo.* Prostate Cancer Prostatic Dis, 2005. **8**(3): p. 266-73.
143. Hoffman, J.F., et al., *Tetrodotoxin-sensitive Na+ channels and muscarinic and purinergic receptors identified in human erythroid progenitor cells and red blood cell ghosts.* Proc Natl Acad Sci U S A, 2004. **101**(33): p. 12370-4.
144. Kis-Toth, K., et al., *Voltage-gated sodium channel Nav1.7 maintains the membrane potential and regulates the activation and chemokine-induced migration of a monocyte-derived dendritic cell subset.* J Immunol, 2011. **187**(3): p. 1273-80.
145. Black, J., et al., *Expression of Nav1.7 in DRG neurons extends from peripheral terminals in the skin to central preterminal branches and terminals in the dorsal horn.* Molecular Pain, 2012. **8**(1): p. 1-11.
146. Fertleman, C.R., et al., *SCN9A mutations in paroxysmal extreme pain disorder: allelic variants underlie distinct channel defects and phenotypes.* Neuron, 2006. **52**(5): p. 767-74.
147. Waxman, S.G. and S.D. Dib-Hajj, *Erythromelalgia: a hereditary pain syndrome enters the molecular era.* Ann Neurol, 2005. **57**(6): p. 785-8.

148. Cox, J.J., et al., *An SCN9A channelopathy causes congenital inability to experience pain.* Nature, 2006. **444**(7121): p. 894-8.
149. Goldberg, Y.P., et al., *Loss-of-function mutations in the Nav1.7 gene underlie congenital indifference to pain in multiple human populations.* Clin Genet, 2007. **71**(4): p. 311-9.
150. Fischer, T.Z. and S.G. Waxman, *Familial pain syndromes from mutations of the $Na_v1.7$ sodium channel.* Ann N Y Acad Sci, 2010. **1184**: p. 196-207.
151. Black, J.A., et al., *Changes in the expression of tetrodotoxin-sensitive sodium channels within dorsal root ganglia neurons in inflammatory pain.* Pain, 2004. **108**(3): p. 237-47.
152. Toledo-Aral, J.J., et al., *A single pulse of nerve growth factor triggers long-term neuronal excitability through sodium channel gene induction.* Neuron, 1995. **14**(3): p. 607-11.
153. Theile, J.W. and T.R. Cummins, *Recent developments regarding voltage-gated sodium channel blockers for the treatment of inherited and acquired neuropathic pain syndromes.* Frontiers in Pharmacology, 2011. **2**.
154. Zakrzewska, J., et al., *Novel design for a phase IIa placebo-controlled, double-blind randomized withdrawal study to evaluate the safety and efficacy of CNV1014802 in patients with trigeminal neuralgia.* Trials, 2013. **14**(1): p. 402.
155. Goldberg, Y.P., et al., *Treatment of Nav1.7-mediated pain in inherited erythromelalgia using a novel sodium channel blocker.* Pain, 2012. **153**(1): p. 80-85.
156. London, C., et al., *Imidazopyridines: A novel class of hNav1.7 channel blockers.* Bioorganic & Medicinal Chemistry Letters, 2008. **18**(5): p. 1696-1701.
157. Hoyt, S.B., et al., *Benzazepinone Nav1.7 blockers: potential treatments for neuropathic pain.* Bioorg Med Chem Lett, 2007. **17**(22): p. 6172-7.
158. Bregman, H., et al., *The discovery of aminopyrazines as novel, potent Nav1.7 antagonists: Hit-to-lead identification and SAR.* Bioorganic & Medicinal Chemistry Letters, 2012. **22**(5): p. 2033-2042.
159. Kers, I., et al., *Structure and activity relationship in the (S)-N-chroman-3-ylcarboxamide series of voltage-gated sodium channel blockers.* Bioorganic & Medicinal Chemistry Letters, 2012. **22**(17): p. 5618-5624.
160. Platt, D. and R. Griggs, *Skeletal muscle channelopathies: new insights into the periodic paralyses and nondystrophic myotonias.* Curr Opin Neurol, 2009. **22**(5): p. 524-31.
161. Camerino, D.C., et al., *Chapter 4 Therapeutic Approaches to Ion Channel Diseases*, in *Advances in Genetics*. 2008, Academic Press. p. 81-145.
162. Davies, N.P. and M.G. Hanna, *Neurological channelopathies: diagnosis and therapy in the new millennium.* Ann Med, 1999. **31**(6): p. 406-20.
163. Heatwole, C.R. and R.T. Moxley Iii, *The Nondystrophic Myotonias.* Neurotherapeutics, 2007. **4**(2): p. 238-251.
164. Wang, Q., et al., *Cardiac sodium channel mutations in patients with long QT syndrome, an inherited cardiac arrhythmia.* Hum Mol Genet, 1995. **4**(9): p. 1603-7.
165. Lei, M., C.L. Huang, and Y. Zhang, *Genetic Na+ channelopathies and sinus node dysfunction.* Prog Biophys Mol Biol, 2008. **98**(2-3): p. 171-8.
166. Chen, Q., et al., *Genetic basis and molecular mechanism for idiopathic ventricular fibrillation.* Nature, 1998. **392**(6673): p. 293-6.
167. Priori, S.G., C. Napolitano, and A. Vicentini, *Inherited arrhythmia syndromes: applying the molecular biology and genetic to the clinical management.* J Interv Card Electrophysiol, 2003. **9**(2): p. 93-101.
168. Milne, J.R., et al., *Class 1 antiarrhythmic drugs-Characteristic electrocardiographs differences when assessed by atrial and ventricular pacing.* European Heart Journal, 1984. **5**(2): p. 99-107.

169. Rang, H.P., Dale, M.M., Ritter, J.M., Flower, R., *Rang & Dale's Pharmacology*. 6 ed. Pharmacology, 2007, Edinburgh: Churchill Livingstone.
170. Singh, B.N., *Current Antiarrhythmic Drugs.* Journal of Cardiovascular Electrophysiology, 1999. **10**(2): p. 283-301.
171. Lossin, C., *A catalog of SCN1A variants.* Brain Dev, 2009. **31**(2): p. 114-30.
172. Harkin, L.A., et al., *The spectrum of SCN1A-related infantile epileptic encephalopathies.* Brain, 2007. **130**(Pt 3): p. 843-52.
173. Estacion, M., et al., *A sodium channel mutation linked to epilepsy increases ramp and persistent current of Nav1.3 and induces hyperexcitability in hippocampal neurons.* Experimental Neurology, 2010. **224**(2): p. 362-368.
174. Blumenfeld, H., et al., *Role of hippocampal sodium channel Nav1.6 in kindling epileptogenesis.* Epilepsia, 2009. **50**(1): p. 44-55.
175. Meisler, M.H., J.E. O'Brien, and L.M. Sharkey, *Sodium channel gene family: epilepsy mutations, gene interactions and modifier effects.* J Physiol, 2010. **588**(Pt 11): p. 1841-8.
176. Van Gassen, K.L.I., et al., *Hippocampal Navβ3 expression in patients with temporal lobe epilepsy.* Epilepsia, 2009. **50**(4): p. 957-962.
177. Ragsdale, D.S., *How do mutant Nav1.1 sodium channels cause epilepsy?* Brain Res Rev, 2008. **58**(1): p. 149-59.
178. Catterall, W.A., F. Kalume, and J.C. Oakley, *NaV1.1 channels and epilepsy.* J Physiol, 2010. **588**(Pt 11): p. 1849-59.
179. Rogawski, M.A. and W. Loscher, *The neurobiology of antiepileptic drugs.* Nat Rev Neurosci, 2004. **5**(7): p. 553-64.
180. Ragsdale, D.S., et al., *Common molecular determinants of local anesthetic, antiarrhythmic, and anticonvulsant block of voltage-gated Na+ channels.* Proc Natl Acad Sci U S A, 1996. **93**(17): p. 9270-5.
181. Smith, M.R., et al., *Functional analysis of the mouse Scn8a sodium channel.* J Neurosci, 1998. **18**(16): p. 6093-102.
182. Wingerd, J.S., I. Vetter, and R.J. Lewis, *Voltage-Gated Sodium Channels as Therapeutic Targets*, in *Therapeutic Targets*. 2012, John Wiley & Sons, Inc. p. 63-122.
183. Catterall, W.A., *Neurotoxins that act on voltage-sensitive sodium channels in excitable membranes.* Annu Rev Pharmacol Toxicol, 1980. **20**: p. 15-43.
184. Catterall, W.A. and M. Risk, *Toxin T4(6) from Ptychodiscus brevis (formerly Gymnodinium breve) enhances activation of voltage-sensitive sodium channels by veratridine.* Mol Pharmacol, 1981. **19**(2): p. 345-8.
185. Poli, M., T. Mende, and D. Baden, *Brevetoxins, unique activators of voltage-sensitive sodium channels, bind to specific sites in rat brain synaptosomes.* Mol Pharmacol, 1986. **30**(2): p. 129-135.
186. Fainzilber, M., et al., *A new neurotoxin receptor site on sodium channels is identified by a conotoxin that affects sodium channel inactivation in molluscs and acts as an antagonist in rat brain.* Journal of Biological Chemistry, 1994. **269**(4): p. 2574-2580.
187. Catterall, W.A., *Neurotoxins that Act on Voltage-Sensitive Sodium Channels in Excitable Membranes.* Annual Review of Pharmacology and Toxicology, 1980. **20**(1): p. 15-43.
188. Corzo, G., et al., *Distinct primary structures of the major peptide toxins from the venom of the spider Macrothele gigas that bind to sites 3 and 4 in the sodium channel.* FEBS Lett, 2003. **547**(1-3): p. 43-50.
189. Tedford, H.W., et al., *Australian funnel-web spiders: master insecticide chemists.* Toxicon, 2004. **43**(5): p. 601-18.

190. Nicholson, G.M., *Insect-selective spider toxins targeting voltage-gated sodium channels.* Toxicon, 2007. **49**(4): p. 490-512.
191. Catterall, W.A. and D.A. Beneski, *Interaction of polypeptide neurotoxins with a receptor site associated with voltage-sensitive sodium channels.* J Supramol Struct, 1980. **14**(3): p. 295-303.
192. Cestele, S. and W.A. Catterall, *Molecular mechanisms of neurotoxin action on voltage-gated sodium channels.* Biochimie, 2000. **82**(9-10): p. 883-92.
193. Hille, B., *The receptor for tetrodotoxin and saxitoxin. A structural hypothesis.* Biophys J, 1975. **15**(6): p. 615-9.
194. Narahashi, T., *Tetrodotoxin: a brief history.* Proc Jpn Acad Ser B Phys Biol Sci, 2008. **84**(5): p. 147-54.
195. Noda, M., et al., *A single point mutation confers tetrodotoxin and saxitoxin insensitivity on the sodium channel II.* FEBS Lett, 1989. **259**(1): p. 213-6.
196. Ohizumi, Y., et al., *Specific inhibition of [3H] saxitoxin binding to skeletal muscle sodium channels by geographutoxin II, a polypeptide channel blocker.* J Biol Chem, 1986. **261**(14): p. 6149-52.
197. Yanagawa, Y., T. Abe, and M. Satake, *Blockade of [3H]lysine-tetrodotoxin binding to sodium channel proteins by conotoxin GIII.* Neurosci Lett, 1986. **64**(1): p. 7-12.
198. Dudley, S.C., Jr., et al., *A mu-conotoxin-insensitive Na+ channel mutant: possible localization of a binding site at the outer vestibule.* Biophys J, 1995. **69**(5): p. 1657-65.
199. Sato, K., et al., *Active site of mu-conotoxin GIIIA, a peptide blocker of muscle sodium channels.* Journal of Biological Chemistry, 1991. **266**(26): p. 16989-16991.
200. Zhang, M.M., et al., *Synergistic and antagonistic interactions between tetrodotoxin and mu-conotoxin in blocking voltage-gated sodium channels.* Channels (Austin), 2009. **3**(1): p. 32-8.
201. Catterall, W.A., *Membrane potential-dependent binding of scorpion toxin to the action potential Na+ ionophore. Studies with a toxin derivative prepared by lactoperoxidase-catalyzed iodination.* J Biol Chem, 1977. **252**(23): p. 8660-8.
202. Catterall, W.A., *Activation of the action potential Na+ ionophore by neurotoxins. An allosteric model.* J Biol Chem, 1977. **252**(23): p. 8669-76.
203. Brown, G.B., *Batrachotoxin: a window on the allosteric nature of the voltage-sensitive sodium channel.* Int. Rev. Neurobiol, 1988. **29**: p. 77-116.
204. Jansen, S.A., et al., *Grayanotoxin poisoning: 'mad honey disease' and beyond.* Cardiovasc Toxicol, 2012. **12**(3): p. 208-15.
205. Gutser, U.T., et al., *Mode of antinociceptive and toxic action of alkaloids of Aconitum spec.* Naunyn Schmiedebergs Arch Pharmacol, 1998. **357**(1): p. 39-48.
206. Ulbricht, W., *Effects of veratridine on sodium currents and fluxes.* Rev Physiol Biochem Pharmacol, 1998. **133**: p. 1-54.
207. Kimura, T., et al., *On site of action of grayanotoxin in domain 4 segment 6 of rat skeletal muscle sodium channel.* FEBS Lett, 2000. **465**(1): p. 18-22.
208. Pereira, A., et al., *Hoiamide a, a sodium channel activator of unusual architecture from a consortium of two papua new Guinea cyanobacteria.* Chem Biol, 2009. **16**(8): p. 893-906.
209. Cao, Z., W. Gerwick, and T. Murray, *Antillatoxin is a sodium channel activator that displays unique efficacy in heterologously expressed rNav1.2, rNav1.4 and rNav1.5 alpha subunits.* BMC Neuroscience, 2010. **11**(1): p. 154.
210. Correa, A.M., F. Bezanilla, and R. Latorre, *Gating kinetics of batrachotoxin-modified Na+ channels in the squid giant axon. Voltage and temperature effects.* Biophys J, 1992. **61**(5): p. 1332-52.

211. Correa, A.M., R. Latorre, and F. Bezanilla, *Ion permeation in normal and batrachotoxin-modified Na+ channels in the squid giant axon.* The Journal of General Physiology, 1991. **97**(3): p. 605-625.
212. Wang, S.-Y., et al., *How Batrachotoxin Modifies the Sodium Channel Permeation Pathway: Computer Modeling and Site-Directed Mutagenesis.* Molecular Pharmacology, 2006. **69**(3): p. 788-795.
213. Trainer, V.L., G.B. Brown, and W.A. Catterall, *Site of covalent labeling by a photoreactive batrachotoxin derivative near transmembrane segment IS6 of the sodium channel alpha subunit.* J Biol Chem, 1996. **271**(19): p. 11261-7.
214. Linford, N.J., et al., *Interaction of batrachotoxin with the local anesthetic receptor site in transmembrane segment IVS6 of the voltage-gated sodium channel.* Proc Natl Acad Sci U S A, 1998. **95**(23): p. 13947-52.
215. Catterall, W.A., et al., *Voltage-gated ion channels and gating modifier toxins.* Toxicon, 2007. **49**(2): p. 124-41.
216. Du, Y., et al., *Identification of new batrachotoxin-sensing residues in segment IIIS6 of the sodium channel.* J Biol Chem, 2011. **286**(15): p. 13151-60.
217. Li, H.-L., D. Hadid, and D.S. Ragsdale, *The Batrachotoxin Receptor on the Voltage-Gated Sodium Channel is Guarded by the Channel Activation Gate.* Molecular Pharmacology, 2002. **61**(4): p. 905-912.
218. Ameri, A. and T. Simmet, *Interaction of the structurally related Aconitum alkaloids, aconitine and 6-benzyolheteratisine, in the rat hippocampus.* European Journal of Pharmacology, 1999. **386**(2–3): p. 187-194.
219. Wright, S.N., *Irreversible block of human heart (hH1) sodium channels by the plant alkaloid lappaconitine.* Mol Pharmacol, 2001. **59**(2): p. 183-92.
220. Wang, G.K. and S.Y. Wang, *Veratridine block of rat skeletal muscle Nav1.4 sodium channels in the inner vestibule.* J Physiol, 2003. **548**(Pt 3): p. 667-75.
221. Martin, C., et al., *Identification and properties of voltage-sensitive sodium channels in smooth muscle cells from pregnant rat myometrium.* Molecular Pharmacology, 1990. **38**(5): p. 667-673.
222. Rando, T.A., *Rapid and slow gating of veratridine-modified sodium channels in frog myelinated nerve.* J Gen Physiol, 1989. **93**(1): p. 43-65.
223. Sutro, J.B., *Kinetics of veratridine action on Na channels of skeletal muscle.* J Gen Physiol, 1986. **87**(1): p. 1-24.
224. Barnes, S. and B. Hille, *Veratridine modifies open sodium channels.* J Gen Physiol, 1988. **91**(3): p. 421-43.
225. Zhu, H.-L., et al., *Actions of veratridine on tetrodotoxin-sensitive voltage-gated Na+ currents, NaV1.6, in murine vas deferens myocytes.* British Journal of Pharmacology, 2009. **157**(8): p. 1483-1493.
226. Couraud, F., et al., *Two types of scorpion receptor sites, one related to the activation, the other to the inactivation of the action potential sodium channel.* Toxicon, 1982. **20**(1): p. 9-16.
227. Jover, E., F. Couraud, and H. Rochat, *Two types of scorpion neurotoxins characterized by their binding to two separate receptor sites on rat brain synaptosomes.* Biochemical and Biophysical Research Communications, 1980. **95**(4): p. 1607-1614.
228. Bergman, C., et al., *Decreased rate of sodium conductance inactivation in the node of Ranvier induced by a polypeptide toxin from sea anemone.* Biochim Biophys Acta, 1976. **455**(1): p. 173-84.

229. Catterall, W.A., *Binding of scorpion toxin to receptor sites associated with sodium channels in frog muscle. Correlation of voltage-dependent binding with activation.* J Gen Physiol, 1979. **74**(3): p. 375-91.
230. Nicholson, G.M., M.J. Little, and L.C. Birinyi-Strachan, *Structure and function of [delta]-atracotoxins: lethal neurotoxins targeting the voltage-gated sodium channel.* Toxicon, 2004. **43**(5): p. 587-599.
231. Rogers, J.C., et al., *Molecular determinants of high affinity binding of alpha-scorpion toxin and sea anemone toxin in the S3-S4 extracellular loop in domain IV of the Na+ channel alpha subunit.* J Biol Chem, 1996. **271**(27): p. 15950-62.
232. Campos, F.V., F.I. Coronas, and P.S. Beirao, *Voltage-dependent displacement of the scorpion toxin Ts3 from sodium channels and its implication on the control of inactivation.* Br J Pharmacol, 2004. **142**(7): p. 1115-22.
233. Thomsen, W.J. and W.A. Catterall, *Localization of the receptor site for alpha-scorpion toxins by antibody mapping: implications for sodium channel topology.* Proceedings of the National Academy of Sciences, 1989. **86**(24): p. 10161-10165.
234. Tejedor, F.J. and W.A. Catterall, *Site of covalent attachment of alpha-scorpion toxin derivatives in domain I of the sodium channel alpha subunit.* Proc Natl Acad Sci U S A, 1988. **85**(22): p. 8742-6.
235. Leipold, E., et al., *Combinatorial Interaction of Scorpion Toxins Lqh-2, Lqh-3, and LqhÎ±IT with Sodium Channel Receptor Sites-3.* Molecular Pharmacology, 2004. **65**(3): p. 685-691.
236. Campos, F.V., et al., *Alpha-scorpion toxin impairs a conformational change that leads to fast inactivation of muscle sodium channels.* J Gen Physiol, 2008. **132**(2): p. 251-63.
237. Sheets, M.F. and D.A. Hanck, *Voltage-dependent open-state inactivation of cardiac sodium channels: gating current studies with Anthopleurin-A toxin.* J Gen Physiol, 1995. **106**(4): p. 617-40.
238. Wang, G.K. and G.R. Strichartz, *Purification and physiological characterization of neurotoxins from venoms of the scorpions centruroides sculpturatus and leiurus quinquestriatus.* Mol Pharmacol, 1983. **23**(2): p. 519-33.
239. Klint, J.K., et al., *Spider-venom peptides that target voltage-gated sodium channels: Pharmacological tools and potential therapeutic leads.* Toxicon, 2012. **60**(4): p. 478-491.
240. Jaimovich, E., et al., *Centruroides toxin, a selective blocker of surface Na+ channels in skeletal muscle: voltage-clamp analysis and biochemical characterization of the receptor.* Proc Natl Acad Sci U S A, 1982. **79**(12): p. 3896-900.
241. Jonas, P., et al., *Toxin gamma of the scorpion Tityus serrulatus modifies both activation and inactivation of sodium permeability of nerve membrane.* Pflugers Arch, 1986. **407**(1): p. 92-9.
242. Cestèle, S., et al., *Voltage Sensor–Trapping: Enhanced Activation of Sodium Channels by β-Scorpion Toxin Bound to the S3–S4 Loop in Domain II.* Neuron, 1998. **21**(4): p. 919-931.
243. Xiao, Y., et al., *Tarantula huwentoxin-IV inhibits neuronal sodium channels by binding to receptor site 4 and trapping the domain ii voltage sensor in the closed configuration.* J Biol Chem, 2008. **283**(40): p. 27300-13.
244. Xiao, Y., et al., *Jingzhaotoxin-III, a novel spider toxin inhibiting activation of voltage-gated sodium channel in rat cardiac myocytes.* J Biol Chem, 2004. **279**(25): p. 26220-6.
245. Rong, M., et al., *Molecular basis of the tarantula toxin jingzhaotoxin-III (β-TRTX-Cj1α) interacting with voltage sensors in sodium channel subtype Nav1.5.* The FASEB Journal, 2011. **25**(9): p. 3177-3185.
246. Sokolov, S., et al., *Inhibition of Sodium Channel Gating by Trapping the Domain II Voltage Sensor with Protoxin II.* Molecular Pharmacology, 2008. **73**(3): p. 1020-1028.

247. Marcotte, P., et al., *Effects of Tityus serrulatus scorpion toxin gamma on voltage-gated Na+ channels.* Circ Res, 1997. **80**(3): p. 363-9.
248. Cestele, S., et al., *Neutralization of gating charges in domain II of the sodium channel alpha subunit enhances voltage-sensor trapping by a beta-scorpion toxin.* J Gen Physiol, 2001. **118**(3): p. 291-302.
249. Cestele, S., et al., *Structure and function of the voltage sensor of sodium channels probed by a beta-scorpion toxin.* J Biol Chem, 2006. **281**(30): p. 21332-44.
250. Leipold, E., et al., *Subtype specificity of scorpion beta-toxin Tz1 interaction with voltage-gated sodium channels is determined by the pore loop of domain 3.* Mol Pharmacol, 2006. **70**(1): p. 340-7.
251. Bosmans, F., et al., *Four novel tarantula toxins as selective modulators of voltage-gated sodium channel subtypes.* Mol Pharmacol, 2006. **69**(2): p. 419-29.
252. Adams, M.E., *Agatoxins: ion channel specific toxins from the American funnel web spider, Agelenopsis aperta.* Toxicon, 2004. **43**(5): p. 509-25.
253. Possani, L.D., et al., *Scorpion toxins specific for Na+-channels.* European Journal of Biochemistry, 1999. **264**(2): p. 287-300.
254. Corzo, G., et al., *Solution structure and alanine scan of a spider toxin that affects the activation of mammalian voltage-gated sodium channels.* J Biol Chem, 2007. **282**(7): p. 4643-52.
255. Liu, Z., et al., *Structure and Function of Hainantoxin-III, a Selective Antagonist of Neuronal Tetrodotoxin-sensitive Voltage-gated Sodium Channels Isolated from the Chinese Bird Spider Ornithoctonus hainana.* Journal of Biological Chemistry, 2013. **288**(28): p. 20392-20403.
256. Xiao, Y., et al., *Common Molecular Determinants of Tarantula Huwentoxin-IV Inhibition of Na+ Channel Voltage Sensors in Domains II and IV.* Journal of Biological Chemistry, 2011. **286**(31): p. 27301-27310.
257. Deng, M., et al., *Jingzhaotoxin-IX, a novel gating modifier of both sodium and potassium channels from Chinese tarantula Chilobrachys jingzhao.* Neuropharmacology, 2009. **57**(2): p. 77-87.
258. Zeng, X., et al., *Isolation and characterization of Jingzhaotoxin-V, a novel neurotoxin from the venom of the spider Chilobrachys jingzhao.* Toxicon, 2007. **49**(3): p. 388-399.
259. Liao, Z., et al., *Solution structure and functional characterization of jingzhaotoxin-XI: a novel gating modifier of both potassium and sodium channels.* Biochemistry, 2006. **45**(51): p. 15591-600.
260. Peng, K., X.-D. Chen, and S.-P. Liang, *The effect of Huwentoxin-I on Ca2+ channels in differentiated NG108-15 cells, a patch-clamp study.* Toxicon, 2001. **39**(4): p. 491-498.
261. Swartz, K.J., *Tarantula toxins interacting with voltage sensors in potassium channels.* Toxicon, 2007. **49**(2): p. 213-30.
262. Zorn, S., et al., *The μO-conotoxin MrVIA inhibits voltage-gated sodium channels by associating with domain-3.* FEBS Letters, 2006. **580**(5): p. 1360-1364.
263. Leipold, E., et al., *μO-Conotoxins Inhibit NaV Channels by Interfering with their Voltage Sensors in Domain-2.* Channels, 2007. **1**(4): p. 253-262.
264. Wang, L., et al., *Identification and characterization of a novel O-superfamily conotoxin from Conus litteratus.* J Pept Sci, 2008. **14**(10): p. 1077-83.
265. Pi, C., et al., *Soluble expression, purification and functional identification of a disulfide-rich conotoxin derived from Conus litteratus.* Journal of Biotechnology, 2007. **128**(1): p. 184-193.
266. Vetter, I., et al., *Isolation, characterization and total regioselective synthesis of the novel muO-conotoxin MfVIA from Conus magnificus that targets voltage-gated sodium channels.* Biochem Pharmacol, 2012. **84**(4): p. 540-8.

267. Benoit, E., A.M. Legrand, and J.M. Dubois, *Effects of ciguatoxin on current and voltage clamped frog myelinated nerve fibre.* Toxicon, 1986. **24**(4): p. 357-64.
268. Huang, J.M., C.H. Wu, and D.G. Baden, *Depolarizing action of a red-tide dinoflagellate brevetoxin on axonal membranes.* J Pharmacol Exp Ther, 1984. **229**(2): p. 615-21.
269. Lombet, A., J.N. Bidard, and M. Lazdunski, *Ciguatoxin and brevetoxins share a common receptor site on the neuronal voltage-dependent Na+ channel.* FEBS Lett, 1987. **219**(2): p. 355-9.
270. Trainer, V.L., D.G. Baden, and W.A. Catterall, *Identification of peptide components of the brevetoxin receptor site of rat brain sodium channels.* J Biol Chem, 1994. **269**(31): p. 19904-9.
271. Pérez, S., et al., *A Comparative Study of the Effect of Ciguatoxins on Voltage-Dependent Na+ and K+ Channels in Cerebellar Neurons.* Chemical Research in Toxicology, 2011. **24**(4): p. 587-596.
272. Baden, D.G., et al., *Natural and derivative brevetoxins: historical background, multiplicity, and effects.* Environ Health Perspect, 2005. **113**(5): p. 621-5.
273. Fainzilber, M., et al., *A new conotoxin affecting sodium current inactivation interacts with the delta-conotoxin receptor site.* J Biol Chem, 1995. **270**(3): p. 1123-9.
274. Sudarslal, S., et al., *Sodium channel modulating activity in a [delta]-conotoxin from an Indian marine snail.* FEBS Letters, 2003. **553**(1-2): p. 209-212.
275. Barbier, J., et al., *A delta-conotoxin from Conus ermineus venom inhibits inactivation in vertebrate neuronal Na+ channels but not in skeletal and cardiac muscles.* J Biol Chem, 2004. **279**(6): p. 4680-5.
276. Sarma, S.P., et al., *Solution Structure of δ-Am2766: A Highly Hydrophobic δ-Conotoxin from Conus amadis That Inhibits Inactivation of Neuronal Voltage-Gated Sodium Channels.* Chemistry & Biodiversity, 2005. **2**(4): p. 535-556.
277. Volpon, L., et al., *NMR Solution Structures of delta-Conotoxin EVIA from Conus ermineus That Selectively Acts on Vertebrate Neuronal Na+ Channels.* Journal of Biological Chemistry, 2004. **279**(20): p. 21356-21366.
278. Hasson, A., et al., *Alteration of sodium currents by new peptide toxins from the venom of a molluscivorous Conus snail.* Eur J Neurosci, 1993. **5**(1): p. 56-64.
279. Leipold, E., et al., *Molecular interaction of delta-conotoxins with voltage-gated sodium channels.* FEBS Lett, 2005. **579**(18): p. 3881-4.
280. Lewis, R.J. and M.L. Garcia, *Therapeutic potential of venom peptides.* Nat Rev Drug Discov, 2003. **2**(10): p. 790-802.
281. Sollod, B.L., et al., *Were arachnids the first to use combinatorial peptide libraries?* Peptides, 2005. **26**(1): p. 131-9.
282. Escoubas, P. and L. Rash, *Tarantulas: eight-legged pharmacists and combinatorial chemists.* Toxicon, 2004. **43**(5): p. 555-74.
283. Billen, B., F. Bosmans, and J. Tytgat, *Animal peptides targeting voltage-activated sodium channels.* Curr Pharm Des, 2008. **14**(24): p. 2492-502.
284. Matsumura, M., G. Signor, and B.W. Matthews, *Substantial increase of protein stability by multiple disulphide bonds.* Nature, 1989. **342**(6247): p. 291-293.
285. Olivera, B.M., *Conus peptides: biodiversity-based discovery and exogenomics.* J Biol Chem, 2006. **281**(42): p. 31173-7.
286. Escoubas, P. and G.F. King, *Venomics as a drug discovery platform.* Expert Review of Proteomics, 2009. **6**(3): p. 221-224.
287. Menez, A., R. Stocklin, and D. Mebs, *'Venomics' or : The venomous systems genome project.* Toxicon, 2006. **47**(3): p. 255-9.

288. Anangi, R., et al., *Recombinant Expression of Margatoxin and Agitoxin-2 in Pichia pastoris: An Efficient Method for Production of $K_V1.3$ Channel Blockers.* PLoS One, 2012. **7**(12): p. e52965.
289. de Marco, A., *Strategies for successful recombinant expression of disulfide bond-dependent proteins in Escherichia coli.* Microbial Cell Factories, 2009. **8**(1): p. 26.
290. Mobli, M., et al., *A non-uniformly sampled 4D HCC (CO) NH-TOCSY experiment processed using maximum entropy for rapid protein sidechain assignment.* Journal of Magnetic Resonance, 2010. **204**(1): p. 160-164.
291. Wagstaff, J.L., M.J. Howard, and R.A. Williamson, *Production of recombinant isotopically labelled peptide by fusion to an insoluble partner protein: generation of integrin alphavbeta6 binding peptides for NMR.* Mol Biosyst, 2010. **6**(12): p. 2380-5.
292. Lax, R., *The Future of Peptide Development in the Pharmaceutical Industry.* PharManufacturing: The International Peptide Review, 2010: p. 10-15.
293. Edwards, C.M.B., M.A. Cohen, and S.R. Bloom, *Peptides as drugs.* QJM, 1999. **92**(1): p. 1-4.
294. Casewell, N.R., et al., *Complex cocktails: the evolutionary novelty of venoms.* Trends in ecology & evolution (Personal edition), 2013. **28**(4): p. 219-229.
295. Kordis, D. and F. Gubensek, *Adaptive evolution of animal toxin multigene families.* Gene, 2000. **261**(1): p. 43-52.
296. Mouhat, S.p., et al., *Diversity of folds in animal toxins acting on ion channels.* Biochem. J., 2004. **378**(3): p. 717-726.
297. Whittington, C.M., et al., *Defensins and the convergent evolution of platypus and reptile venom genes.* Genome Research, 2008. **18**(6): p. 986-994.
298. Gao, B., et al., *Functional evolution of scorpion venom peptides with an inhibitor cystine knot fold.* Bioscience reports, 2013. **33**(3): p. 513-527.
299. Pauletti, G.M., et al., *Improvement of oral peptide bioavailability: Peptidomimetics and prodrug strategies.* Advanced Drug Delivery Reviews, 1997. **27**(2–3): p. 235-256.
300. Reinwarth, M., et al., *Chemical Synthesis, Backbone Cyclization and Oxidative Folding of Cystine-knot Peptides — Promising Scaffolds for Applications in Drug Design.* Molecules, 2012. **17**(11): p. 12533-12552.
301. Jia, X., et al., *Semienzymatic Cyclization of Disulfide-rich Peptides Using Sortase A.* Journal of Biological Chemistry, 2014.
302. de Araujo, A.D., et al., *Selenoether oxytocin analogues have analgesic properties in a mouse model of chronic abdominal pain.* Nature Communications, 2014. **5**.
303. Giannis, A. and T. Kolter, *Peptidomimetics for Receptor Ligands—Discovery, Development, and Medical Perspectives.* Angewandte Chemie International Edition in English, 1993. **32**(9): p. 1244-1267.
304. Kharb, R., et al., *Journal of Chemical and Pharmaceutical Research.* J. Chem, 2011. **3**(6): p. 173-186.
305. Reichert, J., *Development Trends for Peptide Therapeutics*. 2010, PEPTIDE THERAPEUTICS FOUNDATION.
306. Kaspar, A.A. and J.M. Reichert, *Future directions for peptide therapeutics development.* Drug Discovery Today, 2013. **18**(17–18): p. 807-817.
307. Pallaghy, P.K., et al., *A common structural motif incorporating a cystine knot and a triple-stranded β-sheet in toxic and inhibitory polypeptides.* Protein Science, 1994. **3**(10): p. 1833-1839.

308. Norton, R.S. and P.K. Pallaghy, *The cystine knot structure of ion channel toxins and related polypeptides.* Toxicon : official journal of the International Society on Toxinology, 1998. **36**(11): p. 1573-1583.
309. Saez, N.J., et al., *Spider-Venom Peptides as Therapeutics.* Toxins, 2010. **2**(12): p. 2851-2871.
310. Wang, X.H., et al., *Discovery and characterization of a family of insecticidal neurotoxins with a rare vicinal disulfide bridge.* Nature Structural Biology, 2000. **7**(6): p. 505-513.
311. Smith, J.J., et al., *Unique scorpion toxin with a putative ancestral fold provides insight into evolution of the inhibitor cystine knot motif.* Proceedings of the National Academy of Sciences, 2011. **108**(26): p. 10478-10483.
312. Mislow, K. and C. Liang, *Knotted Structures in Chemistry, Biochemistry, and Molecular Biology.* Croatica Chemica Acta, 1996. **69**(4): p. 1385-1403.
313. Craik, D.J., N.L. Daly, and C. Waine, *The cystine knot motif in toxins and implications for drug design.* Toxicon, 2001. **39**(1): p. 43-60.
314. Benham, C.J. and M.S. Jafri, *Disulfide bonding patterns and protein topologies.* Protein Science, 1993. **2**(1): p. 41-54.
315. Colgrave, M.L. and D.J. Craik, *Thermal, Chemical, and Enzymatic Stability of the Cyclotide Kalata B1: The Importance of the Cyclic Cystine Knot†.* Biochemistry, 2004. **43**(20): p. 5965-5975.
316. Clark, R.J., et al., *The Engineering of an Orally Active Conotoxin for the Treatment of Neuropathic Pain.* Angewandte Chemie International Edition, 2010. **49**(37): p. 6545-6548.
317. Filmer, R.M., *A Catalogue of Nomenclature and Taxonomy in the Living Conidae, 1758-1998*. 2001: Backhuys.
318. Kohn, A.J., *Diversity, utilization of resources, and adaptive radiation in shallow-water marine invertebrates of tropical oceanic islands.* Limnology and Oceanography 1971. **16**(2): p. 332-348.
319. Muttenthaler, M., et al., *Abundance and diversity of Conus species (Gastropoda: Conidae) at the northern tip of New Ireland province of Papua New Guinea.* Nautilus, 2012. **126**(2): p. 47-56.
320. Olivera, B.M., *E.E. Just Lecture, 1996. Conus venom peptides, receptor and ion channel targets, and drug design: 50 million years of neuropharmacology.* Mol Biol Cell, 1997. **8**(11): p. 2101-9.
321. Terlau, H., et al., *Strategy for rapid immobilization of prey by a fish-hunting marine snail.* Nature, 1996. **381**(6578): p. 148-51.
322. Olivera, B.M., *CONUS VENOM PEPTIDES: Reflections from the Biology of Clades and Species.* Annual Review of Ecology and Systematics, 2002. **33**(1): p. 25-47.
323. Olivera, B.M. and R.W. Teichert, *Diversity of the neurotoxic Conus peptides: a model for concerted pharmacological discovery.* Mol Interv, 2007. **7**(5): p. 251-60.
324. Olivera, B.M., et al., *Diversity of Conus neuropeptides.* Science, 1990. **249**(4966): p. 257-63.
325. Davis, J., A. Jones, and R.J. Lewis, *Remarkable inter- and intra-species complexity of conotoxins revealed by LC/MS.* Peptides, 2009. **30**(7): p. 1222-7.
326. Duda, T.F. and S.R. Palumbi, *Molecular genetics of ecological diversification: Duplication and rapid evolution of toxin genes of the venomous gastropod Conus.* Proceedings of the National Academy of Sciences, 1999. **96**(12): p. 6820-6823.
327. Han, T.S., et al., *Conus venoms - a rich source of peptide-based therapeutics.* Curr Pharm Des, 2008. **14**(24): p. 2462-79.
328. Olivera, B.M. and R.W. Teichert, *Diversity of the Neurotoxic Conus Peptides: A Model for Concerted Pharmacological Discovery.* Mol. Interv., 2007. **7**(5): p. 251-260.

329. Yuan, D.D., et al., *New conotoxins define the novel I3-superfamily.* Peptides, 2009. **30**(5): p. 861-5.
330. Luo, S., et al., *A Novel Inhibitor of α9α10 Nicotinic Acetylcholine Receptors from Conus vexillum Delineates a New Conotoxin Superfamily.* PLoS One, 2013. **8**(1): p. e54648.
331. Zhangsun, D., et al., *Novel O-superfamily conotoxins identified by cDNA cloning from three vermivorous Conus species.* Chem Biol Drug Des, 2006. **68**(5): p. 256-65.
332. Peng, C., et al., *Identification of a novel class of conotoxins defined as V-conotoxins with a unique cysteine pattern and signal peptide sequence.* Peptides, 2008. **29**(6): p. 985-991.
333. Knapp, O., J.R. McArthur, and D.J. Adams, *Conotoxins Targeting Neuronal Voltage-Gated Sodium Channel Subtypes: Potential Analgesics?* Toxins, 2012. **4**(11): p. 1236-1260.
334. Jimenez, E.C., et al., *Novel excitatory Conus peptides define a new conotoxin superfamily.* J Neurochem, 2003. **85**(3): p. 610-21.
335. Fiedler, B., et al., *Specificity, affinity and efficacy of iota-conotoxin RXIA, an agonist of voltage-gated sodium channels Na(V)1.2, 1.6 and 1.7.* Biochem Pharmacol, 2008. **75**(12): p. 2334-44.
336. Buczek, O., et al., *Characterization of D-amino-acid-containing excitatory conotoxins and redefinition of the I-conotoxin superfamily.* FEBS J, 2005. **272**(16): p. 4178-88.
337. Lewis, R.J., et al., *Isolation and Structure-Activity of μ-Conotoxin TIIIA, A Potent Inhibitor of Tetrodotoxin-Sensitive Voltage-Gated Sodium Channels.* Mol Pharmacol, 2007. **71**(3): p. 676-685.
338. Yao, S., et al., *Structure, dynamics, and selectivity of the sodium channel blocker mu-conotoxin SIIIA.* Biochemistry, 2008. **47**(41): p. 10940-9.
339. Spence, I., et al., *Characterization of the neurotoxic constituents of Conus geographus (L) venom.* Life Sciences, 1977. **21**(12): p. 1759-1769.
340. Li, R.A., et al., *Molecular Basis of Isoform-specific μ-Conotoxin Block of Cardiac, Skeletal Muscle, and Brain Na+ Channels.* Journal of Biological Chemistry, 2003. **278**(10): p. 8717-8724.
341. Shon, K.J., et al., *mu-Conotoxin PIIIA, a new peptide for discriminating among tetrodotoxin-sensitive Na channel subtypes.* J Neurosci, 1998. **18**(12): p. 4473-81.
342. Zhang, M.M., et al., *Structural and functional diversities among mu-conotoxins targeting TTX-resistant sodium channels.* Biochemistry, 2006. **45**(11): p. 3723-32.
343. Wilson, M.J., et al., *mu-Conotoxins that differentially block sodium channels NaV1.1 through 1.8 identify those responsible for action potentials in sciatic nerve.* Proc Natl Acad Sci U S A, 2011. **108**(25): p. 10302-7.
344. Favreau, P., et al., *A novel micro-conopeptide, CnIIIC, exerts potent and preferential inhibition of NaV1.2/1.4 channels and blocks neuronal nicotinic acetylcholine receptors.* Br J Pharmacol, 2012. **166**(5): p. 1654-68.
345. Green, B.R., et al., *Conotoxins containing nonnatural backbone spacers: cladistic-based design, chemical synthesis, and improved analgesic activity.* Chem Biol, 2007. **14**(4): p. 399-407.
346. Zhang, M.M., et al., *Structure/function characterization of micro-conotoxin KIIIA, an analgesic, nearly irreversible blocker of mammalian neuronal sodium channels.* J Biol Chem, 2007. **282**(42): p. 30699-706.
347. West, P.J., G. Bulaj, and D. Yoshikami, *Effects of δ-Conotoxins PVIA and SVIE on Sodium Channels in the Amphibian Sympathetic Nervous System.* Journal of Neurophysiology, 2005. **94**(6): p. 3916-3924.

348. Vetter, I. and R. J. Lewis, *Therapeutic Potential of Cone Snail Venom Peptides (Conopeptides).* Current Topics in Medicinal Chemistry, 2012. **12**(14): p. 1546-1552.
349. Platnick, N.I., *The World Spider Catalog, version 13.0*. 2012, American Museum of Natural History

350. Escoubas, P., B. Sollod, and G.F. King, *Venom landscapes: mining the complexity of spider venoms via a combined cDNA and mass spectrometric approach.* Toxicon, 2006. **47**(6): p. 650-63.
351. Pimenta, A.M., et al., *Electrospray ionization quadrupole time-of-flight and matrix-assisted laser desorption/ionization tandem time-of-flight mass spectrometric analyses to solve micro-heterogeneity in post-translationally modified peptides from Phoneutria nigriventer (Aranea, Ctenidae) venom.* Rapid Commun Mass Spectrom, 2005. **19**(1): p. 31-7.
352. Norton, R.S. and P.K. Pallaghy, *The cystine knot structure of ion channel toxins and related polypeptides.* Toxicon, 1998. **36**(11): p. 1573-83.
353. King, G.F., et al., *A rational nomenclature for naming peptide toxins from spiders and other venomous animals.* Toxicon, 2008. **52**(2): p. 264-76.
354. Mantegazza, M., et al., *Voltage-gated sodium channels as therapeutic targets in epilepsy and other neurological disorders.* Lancet Neurol. **9**(4): p. 413-24.
355. Tarnawa, I., H. Bolcskei, and P. Kocsis, *Blockers of voltage-gated sodium channels for the treatment of central nervous system diseases.* Recent Pat CNS Drug Discov, 2007. **2**(1): p. 57-78.
356. Zuliani, V., et al., *Recent advances in the medicinal chemistry of sodium channel blockers and their therapeutic potential.* Curr Top Med Chem, 2009. **9**(4): p. 396-415.
357. McElroy, S.L., et al., *Role of antiepileptic drugs in the management of eating disorders.* CNS Drugs, 2009. **23**(2): p. 139-56.
358. Lenkey, N., et al., *Classification of drugs based on properties of sodium channel inhibition: a comparative automated patch-clamp study.* PLoS One. **5**(12): p. e15568.
359. Cho, M.J. and R. Juliano, *Macromolecular versus smallmolecule therapeutics: drug discovery, development and clinical considerations.* Trends in Biotechnology, 1996. **14**(5): p. 153-158.
360. Nicholson, G. and R. Lewis, *Ciguatoxins: Cyclic Polyether Modulators of Voltage-gated Iion Channel Function.* Marine Drugs, 2006. **4**(3): p. 82-118.
361. Zimmermann, K., et al., *Sensory neuron sodium channel Nav1.8 is essential for pain at low temperatures.* Nature, 2007. **447**(7146): p. 855-8.
362. Zhang, J.H., T.D. Chung, and K.R. Oldenburg, *A Simple Statistical Parameter for Use in Evaluation and Validation of High Throughput Screening Assays.* J Biomol Screen, 1999. **4**(2): p. 67-73.
363. Vetter, I., et al., *Characterisation of Nav types endogenously expressed in human SH-SY5Y neuroblastoma cells.* Biochemical Pharmacology, 2012. **83**(11): p. 1562-1571.
364. Tabarean, I.V. and T. Narahashi, *Kinetics of Modulation of Tetrodotoxin-Sensitive and Tetrodotoxin-Resistant Sodium Channels by Tetramethrin and Deltamethrin.* Journal of Pharmacology and Experimental Therapeutics, 2001. **299**(3): p. 988-997.
365. Davies, T.G.E., et al., *DDT, pyrethrins, pyrethroids and insect sodium channels.* IUBMB Life, 2007. **59**(3): p. 151-162.
366. Choi, J.-S. and D.M. Soderlund, *Structure-activity relationships for the action of 11 pyrethroid insecticides on rat Nav1.8 sodium channels expressed in Xenopus oocytes.* Toxicology and Applied Pharmacology, 2006. **211**(3): p. 233-244.

367. Dekker, L.V., et al., *Analysis of human Nav1.8 expressed in SH-SY5Y neuroblastoma cells.* Eur J Pharmacol, 2005. **528**(1-3): p. 52-8.
368. Yamaoka, K., et al., *Synthetic ciguatoxins selectively activate Nav1.8-derived chimeric sodium channels expressed in HEK293 cells.* J Biol Chem, 2009. **284**(12): p. 7597-605.
369. Chevrier P Fau - Vijayaragavan, K., M. Vijayaragavan K Fau - Chahine, and M. Chahine, *Differential modulation of Nav1.7 and Nav1.8 peripheral nerve sodium channels by the local anesthetic lidocaine.* (0007-1188 (Print)).
370. Leffler, A., et al., *Use-dependent block by lidocaine but not amitriptyline is more pronounced in tetrodotoxin (TTX)-Resistant Nav1.8 than in TTX-sensitive Na+ channels.* J Pharmacol Exp Ther, 2007. **320**(1): p. 354-64.
371. Ekberg, J., et al., *muO-conotoxin MrVIB selectively blocks Nav1.8 sensory neuron specific sodium channels and chronic pain behavior without motor deficits.* Proc Natl Acad Sci U S A, 2006. **103**(45): p. 17030-5.
372. Daly, N.L., et al., *Structures of μO-conotoxins from Conus marmoreus: INHIBITORS OF TETRODOTOXIN (TTX)-SENSITIVE AND TTX-RESISTANT SODIUM CHANNELS IN MAMMALIAN SENSORY NEURONS.* Journal of Biological Chemistry, 2004. **279**(24): p. 25774-25782.
373. Fainzilber, M., et al., *New Sodium Channel-Blocking Conotoxins Also Affect Calcium Currents in Lymnaea Neurons.* Biochemistry, 1995. **34**(16): p. 5364-5371.
374. Benjamin, E.R., et al., *State-Dependent Compound Inhibition of Nav1.2 Sodium Channels Using the FLIPR Vm Dye: On-Target and Off-Target Effects of Diverse Pharmacological Agents.* Journal of Biomolecular Screening, 2006. **11**(1): p. 29-39.
375. Sheets, M.F. and D.A. Hanck, *Molecular Action of Lidocaine on the Voltage Sensors of Sodium Channels.* The Journal of General Physiology, 2003. **121**(2): p. 163-175.
376. Cummins, T.R., *Setting up for the block: the mechanism underlying lidocaine's use-dependent inhibition of sodium channels.* The Journal of Physiology, 2007. **582**(1): p. 11.
377. Manger, R.L., et al., *Detection of sodium channel toxins: directed cytotoxicity assays of purified ciguatoxins, brevetoxins, saxitoxins, and seafood extracts.* J AOAC Int, 1995. **78**(2): p. 521-7.
378. Poli, M.A., T.J. Mende, and D.G. Baden, *Brevetoxins, unique activators of voltage-sensitive sodium channels, bind to specific sites in rat brain synaptosomes.* Mol Pharmacol, 1986. **30**(2): p. 129-35.
379. Kaas, Q., et al., *ConoServer: updated content, knowledge, and discovery tools in the conopeptide database.* Nucleic Acids Res, 2012. **40**(Database issue): p. D325-30.
380. Bulaj, G., et al., *Delta-conotoxin structure/function through a cladistic analysis.* Biochemistry, 2001. **40**(44): p. 13201-8.
381. Dunlop, J., et al., *High-throughput electrophysiology: an emerging paradigm for ion-channel screening and physiology.* Nat Rev Drug Discov, 2008. **7**(4): p. 358-68.
382. Stein, R.L., *High-throughput screening in academia: the Harvard experience.* J Biomol Screen, 2003. **8**(6): p. 615-9.
383. Xu, J., et al., *Ion-channel assay technologies: quo vadis?* Drug Discov Today, 2001. **6**(24): p. 1278-1287.
384. Wu, G., *Functional Ion Channel Assays*, in *Assay Development*. 2010, John Wiley & Sons, Inc. p. 239-264.
385. Macarrón, R. and R. Hertzberg, *Design and Implementation of High Throughput Screening Assays.* Molecular Biotechnology, 2011. **47**(3): p. 270-285.
386. González, J.E., J. Worley, and F. Van Goor, *Ion Channel Assays Using Fluorescent Probes*, in *Protein Science Encyclopedia*. 2008, Wiley-VCH Verlag GmbH & Co. KGaA.

387. Chambers, C., et al., *Measuring intracellular calcium fluxes in high throughput mode.* Comb Chem High Throughput Screen, 2003. **6**(4): p. 355-62.
388. Lodish, H., et al., *Intracellular ion environment and membrane electric potential*, in *Molecular Cell Biology*. 2000, W. H. Freeman: New York.
389. Fermini, B., *Recent Advances in Ion Channel Screening Technologies*, in *Topics in Medicinal Chemistry*. 2008, Springer. p. 1-25.
390. Clare, J.J., et al., *Voltage-gated sodium channels as therapeutic targets.* Drug Discov Today, 2000. **5**(11): p. 506-520.
391. Trivedi, S., et al., *Cellular HTS assays for pharmacological characterization of Na(V)1.7 modulators.* Assay Drug Dev Technol, 2008. **6**(2): p. 167-79.
392. Benjamin, E.R., et al., *State-dependent compound inhibition of Nav1.2 sodium channels using the FLIPR Vm dye: on-target and off-target effects of diverse pharmacological agents.* J Biomol Screen, 2006. **11**(1): p. 29-39.
393. Gallacher, S. and T.H. Birkbeck, *A tissue culture assay for direct detection of sodium channel blocking toxins in bacterial culture supernates.* FEMS Microbiol Lett, 1992. **71**(1): p. 101-7.
394. Kenakin, T., *New concepts in drug discovery: collateral efficacy and permissive antagonism.* Nature Reviews Drug Discovery, 2005. **4**(11): p. 919-927.
395. Sink, R., et al., *False positives in the early stages of drug discovery.* Curr Med Chem, 2010. **17**(34): p. 4231-55.
396. Bradley, E., et al., *The Cardiac Sodium Current, NaV1.5, is Functionally Expressed in Rabbit Bronchial Smooth Muscle Cells.* American Journal of Physiology - Cell Physiology, 2013.
397. Bennett, P.B., et al., *On the Molecular Nature of the Lidocaine Receptor of Cardiac Na+ Channels : Modification of Block by Alterations in the α-Subunit III-IV Interdomain.* Circulation Research, 1995. **77**(3): p. 584-592.
398. Scholz, A., et al., *Complex Blockade of TTX-Resistant Na+ Currents by Lidocaine and Bupivacaine Reduce Firing Frequency in DRG Neurons.* Journal of Neurophysiology, 1998. **79**(4): p. 1746-1754.
399. Johnston, P.A. and P.A. Johnston, *Cellular platforms for HTS: three case studies.* Drug Discovery Today, 2002. **7**(6): p. 353-363.
400. Hayflick, L., *The limited in vitro lifetime of human diploid cell strains.* Experimental Cell Research, 1965. **37**(3): p. 614-636.
401. Olovnikov, A.M., *Telomeres, telomerase, and aging: origin of the theory.* Exp Gerontol, 1996. **31**(4): p. 443-8.
402. MacDonald, K.P.A., et al., *Olfactory neuronal cell lines generated by retroviral insertion of the n-myc oncogene display different developmental phenotypes.* Journal of Neuroscience Research, 1996. **45**(3): p. 237-247.
403. Carney, S.A., et al., *Immortalization of human uterine leiomyoma and myometrial cell lines after induction of telomerase activity: molecular and phenotypic characteristics.* Laboratory investigation, 2002. **82**(6): p. 719-728.
404. Rassoulzadegan, M., et al., *Expression of the large T protein of polyoma virus promotes the establishment in culture of "normal" rodent fibroblast cell lines.* Proc Natl Acad Sci U S A, 1983. **80**(14): p. 4354-8.
405. Choi, J.S., et al., *Alternative splicing may contribute to time-dependent manifestation of inherited erythromelalgia.* Brain, 2010. **133**(Pt 6): p. 1823-35.
406. Biedler, J.L., et al., *Multiple Neurotransmitter Synthesis by Human Neuroblastoma Cell Lines and Clones.* Cancer Research, 1978. **38**(11 Part 1): p. 3751-3757.

407. Lukas, R.J., S.A. Norman, and L. Lucero, *Characterization of Nicotinic Acetylcholine Receptors Expressed by Cells of the SH-SY5Y Human Neuroblastoma Clonal Line.* Molecular and Cellular Neuroscience, 1993. **4**(1): p. 1-12.
408. Peng, X., et al., *Human alpha 7 acetylcholine receptor: cloning of the alpha 7 subunit from the SH-SY5Y cell line and determination of pharmacological properties of native receptors and functional alpha 7 homomers expressed in Xenopus oocytes.* Molecular Pharmacology, 1994. **45**(3): p. 546-554.
409. Park, J.H., et al., *High expression of large-conductance Ca2+-activated K+ channel in the CD133+ subpopulation of SH-SY5Y neuroblastoma cells.* Biochemical and Biophysical Research Communications, 2010. **396**(3): p. 637-642.
410. Friederich, P., et al., *Biophysical Properties of Kv3.1 Channels in SH-SY5Y Human Neuroblastoma Cells.* Receptors and Channels, 2003. **9**(6): p. 387-396.
411. Reeve, H.L., P.F.T. Vaughan, and C. Peers, *Calcium Channel Currents in Undifferentiated Human Neuroblastoma (SH-SY5Y) Cells: Actions and Possible Interactions of Dihydropyridines and ω-Conotoxin.* European Journal of Neuroscience, 1994. **6**(6): p. 943-952.
412. Xiong, Q.-J., et al., *Acid-sensing ion channels contribute to the increase in vesicular release from SH-SY5Y cells stimulated by extracellular protons.* American Journal of Physiology - Cell Physiology, 2012. **303**(4): p. C376-C384.
413. Long, Y.-S., et al., *Identification of the promoter region and the 5'-untranslated exons of the human voltage-gated sodium channel Nav1.1 gene (SCN1A) and enhancement of gene expression by the 5'-untranslated exons.* Journal of Neuroscience Research, 2008. **86**(15): p. 3375-3381.
414. Diss, J.K.J., et al., *Identification and characterization of the promoter region of the Nav1.7 voltage-gated sodium channel gene (SCN9A).* Molecular and Cellular Neuroscience, 2008. **37**(3): p. 537-547.
415. Toselli, M., P. Tosetti, and V. Taglietti, *Functional changes in sodium conductances in the human neuroblastoma cell line SH-SY5Y during in vitro differentiation.* Journal of Neurophysiology, 1996. **76**(6): p. 3920-3927.
416. Urbano, F.J. and W. Buño, *Neurotrophin regulation of sodium and calcium channels in human neuroblastoma cells.* Neuroscience, 2000. **96**(2): p. 439-443.
417. Bollimuntha, S., et al., *TRPC1-mediated Inhibition of 1-Methyl-4-phenylpyridinium Ion Neurotoxicity in Human SH-SY5Y Neuroblastoma Cells.* Journal of Biological Chemistry, 2005. **280**(3): p. 2132-2140.
418. Wang, X.-J. and J.-X. Xu, *Salvianic acid A protects human neuroblastoma SH-SY5Y cells against MPP+-induced cytotoxicity.* Neuroscience Research, 2005. **51**(2): p. 129-138.
419. Kim, S.-S., et al., *Neuroprotective effects of 3,5-dicaffeoylquinic acid on hydrogen peroxide-induced cell death in SH-SY5Y cells.* Phytotherapy Research, 2005. **19**(3): p. 243-245.
420. Wang, X.-J. and J.-X. Xu, *Possible involvement of Ca2+ signaling in rotenone-induced apoptosis in human neuroblastoma SH-SY5Y cells.* Neuroscience Letters, 2005. **376**(2): p. 127-132.
421. Repetto, G., A. del Peso, and J.L. Zurita, *Neutral red uptake assay for the estimation of cell viability/cytotoxicity.* Nat Protoc, 2008. **3**(7): p. 1125-31.
422. Sousa, S.R., et al., *Expression and Pharmacology of Endogenous Cav Channels in SH-SY5Y Human Neuroblastoma Cells.* PLoS One, 2013. **8**(3): p. e59293.
423. Vetter, I., *Development and Optimization of FLIPR High Throughput Calcium Assays for Ion Channels and GPCRs*, in *Calcium Signaling*, M.S. Islam, Editor. 2012, Springer Netherlands. p. 45-82.

424. Jellett, J.F., et al., *Paralytic shellfish poison (saxitoxin family) bioassays: automated endpoint determination and standardization of the in vitro tissue culture bioassay, and comparison with the standard mouse bioassay.* Toxicon, 1992. **30**(10): p. 1143-56.
425. Leung, Y.-M., et al., *Osthol is a Use-Dependent Blocker of Voltage-Gated Na+ Channels in Mouse Neuroblastoma N2A Cells.* Planta Med, 2010. **76**(EFirst): p. 34-40.
426. Leung, Y.-M., et al., *Diphenidol inhibited sodium currents and produced spinal anesthesia.* Neuropharmacology, 2010. **58**(7): p. 1147-1152.
427. Kuo, C.-S., et al., *Apocynum venetum leaf aqueous extract inhibits voltage-gated sodium channels of mouse neuroblastoma N2A cells.* Journal of Ethnopharmacology, 2011. **136**(1): p. 149-155.
428. Lou, J.-Y., et al., *Fibroblast growth factor 14 is an intracellular modulator of voltage-gated sodium channels.* The Journal of Physiology, 2005. **569**(1): p. 179-193.
429. Carpaneto, A., et al., *Chloride channels activated by hypotonicity in N2A neuroblastoma cell line.* Exp Brain Res, 1999. **124**(2): p. 193-9.
430. Hoffmann, A. and D.R. Cool, *Angiotensin II Receptor Types 1A, 1B, and 2 in Murine Neuroblastoma Neuro-2a Cells.* Journal of Receptors and Signal Transduction, 2003. **23**(1): p. 111-121.
431. Gómez-Villafuertes, R., et al., *Ca2+/calmodulin-dependent kinase II signalling cascade mediates P2X7 receptor-dependent inhibition of neuritogenesis in neuroblastoma cells.* FEBS Journal, 2009. **276**(18): p. 5307-5325.
432. Chen, C.-C. and W.-C. Chen, *P2Y Receptor Linked to Phospholipase C: Stimulation of Neuro 2A Cells by UTP and ATP and Possible Regulation by Protein Kinase C Subtype ε.* Journal of Neurochemistry, 1997. **69**(4): p. 1409-1416.
433. Koenig, J.A., J.M. Edwardson, and P.P.A. Humphrey, *Somatostatin receptors in Neuro2A neuroblastoma cells: operational characteristics.* British Journal of Pharmacology, 1997. **120**(1): p. 45-51.
434. Leung, Y.-M., et al., *Voltage-gated K+ channels play a role in cAMP-stimulated neuritogenesis in mouse neuroblastoma N2A cells.* Journal of Cellular Physiology, 2011. **226**(4): p. 1090-1098.
435. Greene, L.A. and A.S. Tischler, *Establishment of a noradrenergic clonal line of rat adrenal pheochromocytoma cells which respond to nerve growth factor.* Proc Natl Acad Sci U S A, 1976. **73**(7): p. 2424-8.
436. Furukawa, K., et al., *Effects of nerve growth factor and cAMP on expression of acetylcholine receptor in PC12 cells.* Neurosci Res, 1991. **12**(3): p. 459-62.
437. Dichter, M.A., A.S. Tischler, and L.A. Greene, *Nerve growth factor-induced increase in electrical excitability and acetylcholine sensitivity of a rat pheochromocytoma cell line.* Nature, 1977. **268**(5620): p. 501-4.
438. Inoue, N. and H. Hatanaka, *Nerve growth factor induces specific enkephalin binding sites in a nerve cell line.* Journal of Biological Chemistry, 1982. **257**(16): p. 9238-9241.
439. Kozlowski, M.R., M.P. Rosser, and E. Hall, *Identification of 3H-bradykinin binding sites in PC-12 cells and brain.* Neuropeptides, 1988. **12**(4): p. 207-211.
440. Nardone, J., et al., *Identification of a B2 bradykinin receptor expressed by PC12 pheochromocytoma cells.* Proceedings of the National Academy of Sciences, 1994. **91**(10): p. 4412-4416.
441. Furukawa, K., et al., *Expression of 5-HT3 receptors in PC12 cells treated with NGF and 8-Br-cAMP.* Journal of Neurophysiology, 1992. **67**(4): p. 812-819.

442. Usowicz, M.M., et al., *Differential expression by nerve growth factor of two types of Ca2+ channels in rat phaeochromocytoma cell lines.* The Journal of Physiology, 1990. **426**(1): p. 95-116.
443. Plummer, M.R., D.E. Logothetis, and P. Hess, *Elementary properties and pharmacological sensitivities of calcium channels in mammalian peripheral neurons.* Neuron, 1989. **2**(5): p. 1453-1463.
444. Grantham, C.J., M.J. Main, and M.B. Cannell, *Fluspirilene block of N-type calcium current in NGF-differentiated PC12 cells.* Br J Pharmacol, 1994. **111**(2): p. 483-8.
445. Chu, X.-P., et al., *Proton-Gated Channels in PC12 Cells.* Journal of Neurophysiology, 2002. **87**(5): p. 2555-2561.
446. Conforti, L. and D. Millhorn, *Oxygen-sensitive Ion Channels in Pheochromocytoma (PC12) Cells*, in *Hypoxic Pulmonary Vasoconstriction*, J.J. Yuan, Editor. 2004, Springer US. p. 389-399.
447. Pollock, J.D., M. Krempin, and B. Rudy, *Differential effects of NGF, FGF, EGF, cAMP, and dexamethasone on neurite outgrowth and sodium channel expression in PC12 cells.* J Neurosci, 1990. **10**(8): p. 2626-37.
448. Kalman, D., et al., *Nerve growth factor acts through cAMP-dependent protein kinase to increase the number of sodium channels in PC12 cells.* Neuron, 1990. **4**(3): p. 355-366.
449. Rudy, B., et al., *Nerve growth factor increases the number of functional Na channels and induces TTX-resistant Na channels in PC12 pheochromocytoma cells.* J Neurosci, 1987. **7**(6): p. 1613-25.
450. D'Arcangelo, G., et al., *Neuronal growth factor regulation of two different sodium channel types through distinct signal transduction pathways.* The Journal of Cell Biology, 1993. **122**(4): p. 915-921.
451. Chen, W., et al., *Immortalization and characterization of a nociceptive dorsal root ganglion sensory neuronal line.* Journal of the Peripheral Nervous System, 2007. **12**(2): p. 121-130.
452. Wood, J.N., et al., *Novel Cell Lines Display Properties of Nociceptive Sensory Neurons.* Proceedings of the Royal Society of London. Series B: Biological Sciences, 1990. **241**(1302): p. 187-194.
453. Wu, G., et al., *Chronic opioid treatment of neuroblastoma x dorsal root ganglion neuron hybrid F11 cells results in elevated GM1 ganglioside and cyclic adenosine monophosphate levels and onset of naloxone-evoked decreases in membrane K+ currents.* J Neurosci Res, 1995. **42**(4): p. 493-503.
454. Platika, D., et al., *Neuronal traits of clonal cell lines derived by fusion of dorsal root ganglia neurons with neuroblastoma cells.* Proceedings of the National Academy of Sciences, 1985. **82**(10): p. 3499-3503.
455. Tojima, T., et al., *Acquisition of neuronal proteins during differentiation of NG108-15 cells.* Neurosci Res, 2000. **37**(2): p. 153-61.
456. Hamprecht, B., *Structural, electrophysiological, biochemical, and pharmacological properties of neuroblastoma-glioma cell hybrids in cell culture.* Int Rev Cytol, 1977. **49**: p. 99-170.
457. Li, Y., et al., *Cell-Specific Expression and Lipopolysaccharide-Induced Regulation of Tumor Necrosis Factor α (TNFα) and TNF Receptors in Rat Dorsal Root Ganglion.* The Journal of Neuroscience, 2004. **24**(43): p. 9623-9631.
458. Jow, F., et al., *Validation of DRG-like F11 cells for evaluation of KCNQ/M-channel modulators.* Assay Drug Dev Technol, 2006. **4**(1): p. 49-56.
459. Pollard, C.E., *A volume-sensitive Cl− conductance in a mouse neuroblastoma × rat dorsal root ganglion cell line (F11).* Brain Research, 1993. **614**(1–2): p. 178-184.

460. Fan, S.F., K.F. Shen, and S.M. Crain, *μ and δ opioid agonists at low concentrations decrease voltage-dependent K+ currents in F11 neuroblastoma × DRG neuron hybrid cells via cholera toxin-sensitive receptors.* Brain Research, 1993. **605**(2): p. 214-220.
461. Fan, S.-f. and S.M. Crain, *Dual regulation by μ, δ and κ opioid receptor agonists of K+ conductance of DRG neurons and neuroblastoma × DRG neuron hybrid F11 cells.* Brain Research, 1995. **696**(1–2): p. 97-105.
462. Gaudioso, C., et al., *Menthol pain relief through cumulative inactivation of voltage-gated sodium channels.* Pain, 2012. **153**(2): p. 473-484.
463. Nakanishi, M., et al., *Acid Activation of Trpv1 Leads to an Up-Regulation of Calcitonin Gene-related Peptide Expression in Dorsal Root Ganglion Neurons via the CaMK-CREB Cascade: A Potential Mechanism of Inflammatory Pain.* Molecular Biology of the Cell, 2010. **21**(15): p. 2568-2577.
464. John, V.H., et al., *Heterologous expression and functional analysis of rat NaV1.8 (SNS) voltage-gated sodium channels in the dorsal root ganglion neuroblastoma cell line ND7–23.* Neuropharmacology, 2004. **46**(3): p. 425-438.
465. John, V.H., et al., *Heterologous expression and functional analysis of rat Nav1.8 (SNS) voltage-gated sodium channels in the dorsal root ganglion neuroblastoma cell line ND7-23.* Neuropharmacology, 2004. **46**(3): p. 425-38.
466. Yang, T., et al., *Blocking Scn10a Channels in Heart Reduces Late Sodium Current and Is Antiarrhythmic.* Circulation Research, 2012. **111**(3): p. 322-332.
467. Herold, K.F., et al., *Isoflurane inhibits the tetrodotoxin-resistant voltage-gated sodium channel Nav1.8.* Anesthesiology, 2009. **111**(3): p. 591-599.
468. O'Brien, J.E., et al., *Interaction of Voltage-gated Sodium Channel Nav1.6 (SCN8A) with Microtubule-associated Protein Map1b.* Journal of Biological Chemistry, 2012. **287**(22): p. 18459-18466.
469. Klee, W.A. and M. Nirenberg, *A Neuroblastoma × Glioma Hybrid Cell Line with Morphine Receptors.* Proceedings of the National Academy of Sciences, 1974. **71**(9): p. 3474-3477.
470. Ghahary, A. and K.W. Cheng, *Identification and characterization of the beta-adrenergic receptor on neuroblastoma × glioma hybrid NG108-15 cells.* Cellular and Molecular Neurobiology, 1990. **10**(3): p. 337-350.
471. Neijt, H., et al., *Characterisation of 5-HT3 recognition sites in membranes of NG 108-15 neuroblastoma-glioma cells with [3H]ICS 205-930.* Naunyn-Schmiedeberg's Archives of Pharmacology, 1988. **337**(5): p. 493-499.
472. McGee, R., Jr., M.P. Sansom, and P.R. Usherwood, *Characterization of a delayed rectifier K+ channel in NG108-15 neuroblastomaX glioma cells: Gating kinetics and the effects of enrichment of membrane phospholipids with arachidonic acid.* The Journal of Membrane Biology, 1988. **102**(1): p. 21-34.
473. Yokoyama, S., et al., *Potassium channels from NG108-15 neuroblastoma-glioma hybrid cells. Primary structure and functional expression from cDNAs.* FEBS Lett, 1989. **259**(1): p. 37-42.
474. Meves, H., *Inactivation of the ERG current in NG108-15 cells.* Biochemical and Biophysical Research Communications, 1999. **263**(2): p. 510-515.
475. Yokoyama, S., et al., *B2 Bradykinin Receptors in NG108-15 Cells: cDNA Cloning and Functional Expression.* Biochemical and Biophysical Research Communications, 1994. **200**(1): p. 634-641.
476. Bodewei, R., et al., *Sodium and calcium currents in neuroblastoma x glioma hybrid cells before and after morphological differentiation by dibutyryl cyclic AMP.* Gen Physiol Biophys, 1985. **4**(2): p. 113-27.

477. Kawaguchi, A., et al., *Enhancement of Sodium Current in NG108-15 Cells during Neural Differentiation is Mainly due to an Increase in NaV1.7 Expression.* Neurochemical Research, 2007. **32**(9): p. 1469-1475.
478. Liu, J., et al., *Voltage-gated sodium channel expression and action potential generation in differentiated NG108-15 cells.* BMC Neuroscience, 2012. **13**(1): p. 129.
479. Liu, J., et al., *Changes of calcium channel mRNA, protein and current in NG108-15 cells after cell differentiation.* Biochem Biophys Res Commun, 2012. **423**(1): p. 55-9.
480. Kovalevich, J. and D. Langford, *Considerations for the Use of SH-SY5Y Neuroblastoma Cells in Neurobiology*, in *Neuronal Cell Culture*, S. Amini and M.K. White, Editors. 2013, Humana Press. p. 9-21.
481. Gordon, D., et al., *Tissue-specific expression of the RI and RII sodium channel subtypes.* Proc Natl Acad Sci U S A, 1987. **84**(23): p. 8682-6.
482. Caldwell, J.H., et al., *Sodium channel Nav1.6 is localized at nodes of Ranvier, dendrites, and synapses.* Proceedings of the National Academy of Sciences, 2000. **97**(10): p. 5616-5620.
483. Powers, A.S.T.J.F., *Culturing Pheochromocytoma Cells.* 2004.
484. Rosario, M., et al., *The neurite outgrowth multiadaptor RhoGAP, NOMA-GAP, regulates neurite extension through SHP2 and Cdc42.* J Cell Biol, 2007. **178**(3): p. 503-16.
485. Kilian, P., et al., *Angiotensin II Type 2 Receptor Stimulation Increases the Rate of NG108–15 Cell Migration via Actin Depolymerization.* Endocrinology, 2008. **149**(6): p. 2923-2933.
486. Mosmann, T., *Rapid colorimetric assay for cellular growth and survival: application to proliferation and cytotoxicity assays.* J Immunol Methods, 1983. **65**(1-2): p. 55-63.
487. Berridge, M.V., P.M. Herst, and A.S. Tan, *Tetrazolium dyes as tools in cell biology: New insights into their cellular reduction*, in *Biotechnology Annual Review*, M.R. El-Gewely, Editor. 2005, Elsevier. p. 127-152.
488. Liu, J., et al., *Ouabain interaction with cardiac Na+/K+-ATPase initiates signal cascades independent of changes in intracellular Na+ and Ca2+ concentrations.* J Biol Chem, 2000. **275**(36): p. 27838-44.
489. Mankovitz, R., M. Buchwald, and R.M. Baker, *Isolation of ouabain-resistant human diploid fibroblasts.* Cell, 1974. **3**(3): p. 221-226.
490. Sweadner, K.J., *A third mode of ouabain signaling. Focus on "Regulation of ERK1/2 by ouabain and Na-K-ATPase-dependent energy utilization and AMPK activation in parotid acinar cells".* American Journal of Physiology - Cell Physiology, 2008. **295**(3): p. C588-C589.
491. Gao, J., et al., *Isoform-specific stimulation of cardiac Na/K pumps by nanomolar concentrations of glycosides.* J Gen Physiol, 2002. **119**(4): p. 297-312.
492. Cohen, I., J. Daut, and D. Noble, *An analysis of the actions of low concentrations of ouabain on membrane currents in Purkinje fibres.* J Physiol, 1976. **260**(1): p. 75-103.
493. Koike, T., et al., *Sodium overload through voltage-dependent Na+ channels induces necrosis and apoptosis of rat superior cervical ganglion cells in vitro.* Brain Research Bulletin, 2000. **51**(4): p. 345-355.
494. Dargent, B., et al., *Activation of voltage-dependent sodium channels in cultured cerebellar granule cells induces neurotoxicity that is not mediated by glutamate release.* Neuroscience, 1996. **73**(1): p. 209-216.
495. Soderlund, D.M., et al., *Mechanisms of pyrethroid neurotoxicity: implications for cumulative risk assessment.* Toxicology, 2002. **171**(1): p. 3-59.
496. Soderlund, D.M., *Molecular mechanisms of pyrethroid insecticide neurotoxicity: recent advances.* Arch Toxicol, 2012. **86**(2): p. 165-81.

497. Kiss, T. and O.N. Osipenko, *Effect of deltamethrin on acetylcholine-operated ionic channels in identified Helix pomatia L. neurons.* Pesticide Biochemistry and Physiology, 1991. **39**(2): p. 196-204.
498. Gee, K.R., et al., *Chemical and physiological characterization of fluo-4 Ca2+-indicator dyes.* Cell Calcium, 2000. **27**(2): p. 97-106.
499. Connor, M., A. Yoe, and G. Henderson, *The effect of nociceptin on Ca2+ channel current and intracellular Ca2+ in the SH-SY5Y human neuroblastoma cell line.* British Journal of Pharmacology, 1996. **118**(2): p. 205-207.
500. Dajas-Bailador, F.A., A.J. Mogg, and S. Wonnacott, *Intracellular Ca2+ signals evoked by stimulation of nicotinic acetylcholine receptors in SH-SY5Y cells: contribution of voltage-operated Ca2+ channels and Ca2+ stores.* Journal of Neurochemistry, 2002. **81**(3): p. 606-614.
501. Fainzilber, M., et al., *A new neurotoxin receptor site on sodium channels is identified by a conotoxin that affects sodium channel inactivation in molluscs and acts as an antagonist in rat brain.* J Biol Chem, 1994. **269**(4): p. 2574-80.
502. Xia, Z., et al., *Recombinant -Conotoxin MVIIA Possesses Strong Analgesic Activity.* BioDrugs, 2006. **20**: p. 275-281.
503. Nassar, M.A., et al., *Nociceptor-specific gene deletion reveals a major role for Nav1.7 (PN1) in acute and inflammatory pain.* Proc Natl Acad Sci U S A, 2004. **101**(34): p. 12706-11.
504. Yang, Y., et al., *Mutations in SCN9A, encoding a sodium channel alpha subunit, in patients with primary erythermalgia.* J Med Genet, 2004. **41**(3): p. 171-4.
505. Dib-Hajj, S.D., et al., *The NaV1. 7 sodium channel: from molecule to man.* Nature Reviews Neuroscience, 2012. **14**(1): p. 49-62.
506. Lam, K.S., *New aspects of natural products in drug discovery.* Trends in Microbiology, 2007. **15**(6): p. 279-289.
507. DiMasi, J.A., *New drug development in the United States from 1963 to 1999.* Clinical pharmacology and therapeutics, 2001. **69**(5): p. 286.
508. King, G.F., *Venoms as a platform for human drugs: translating toxins into therapeutics.* Expert Opinion on Biological Therapy, 2011. **11**(11): p. 1469-1484.
509. Herzig, V., et al., *ArachnoServer 2.0, an updated online resource for spider toxin sequences and structures.* Nucleic Acids Res, 2011. **39**(Database issue): p. D653-7.
510. Billen, B., et al., *Two novel sodium channel inhibitors from Heriaeus melloteei spider venom differentially interacting with mammalian channel's isoforms.* Toxicon, 2008. **52**(2): p. 309-17.
511. Cabrita, L., W. Dai, and S. Bottomley, *A family of E. coli expression vectors for laboratory scale and high throughput soluble protein production.* BMC Biotechnology, 2006. **6**(1): p. 12.
512. Fang, L., et al., *An improved strategy for high-level production of TEV protease in Escherichia coli and its purification and characterization.* Protein Expr Purif, 2007. **51**(1): p. 102-9.
513. Gill, S.C. and P.H. von Hippel, *Calculation of protein extinction coefficients from amino acid sequence data.* Analytical Biochemistry, 1989. **182**(2): p. 319-326.
514. Pace, C.N., et al., *How to measure and predict the molar absorption coefficient of a protein.* Protein Sci, 1995. **4**(11): p. 2411-23.
515. Mobli, M., et al., *An automated tool for maximum entropy reconstruction of biomolecular NMR spectra.* Nat Methods, 2007. **4**(6): p. 467-8.
516. Cornilescu, G., F. Delaglio, and A. Bax, *Protein backbone angle restraints from searching a database for chemical shift and sequence homology.* J Biomol NMR, 1999. **13**(3): p. 289-302.
517. Goddard, T.D., Kneller, D. G. , *SPARKY 3*. 30/6/2008: University of California, San Francisco.
518. Güntert, P., *Automated NMR Structure Calculation With CYANA*, in *Protein NMR Techniques*, A.K. Downing, Editor. 2004, Humana Press. p. 353-378.

519. Eswar, N., et al., *Comparative protein structure modeling using MODELLER.* Curr Protoc Protein Sci, 2007. **Chapter 2**: p. Unit 2 9.
520. King, G.F., et al., *A rational nomenclature for naming peptide toxins from spiders and other venomous animals.* Toxicon, 2008. **52**(2): p. 264-276.
521. Tong, X., et al., *Solution structure of BmKalphaIT01, an alpha-insect toxin from the venom of the Chinese scorpion Buthus martensii Karsch.* Biochemistry, 2007. **46**(40): p. 11322-30.
522. Guan, R.J., et al., *Structural mechanism governing cis and trans isomeric states and an intramolecular switch for cis/trans isomerization of a non-proline peptide bond observed in crystal structures of scorpion toxins.* Journal of Molecular Biology, 2004. **341**(5): p. 1189-204.
523. Pal, D. and P. Chakrabarti, *Cis peptide bonds in proteins: residues involved, their conformations, interactions and locations.* J Mol Biol, 1999. **294**(1): p. 271-88.
524. Swartz, K.J. and R. MacKinnon, *An inhibitor of the Kv2.1 potassium channel isolated from the venom of a Chilean tarantula.* Neuron, 1995. **15**(4): p. 941-9.
525. Salahuddin, A., *Proline peptide isomerization and protein folding.* Journal of Biosciences, 1984. **6**(4): p. 349-355.
526. Nguyen, K., M. Iskandar, and D.L. Rabenstein, *Kinetics and Equilibria of Cis/Trans Isomerization of Secondary Amide Peptide Bonds in Linear and Cyclic Peptides.* The Journal of Physical Chemistry B, 2010. **114**(9): p. 3387-3392.
527. Dalal, S., S. Balasubramanian, and L. Regan, *Transmuting alpha helices and beta sheets.* Fold Des, 1997. **2**(5): p. R71-9.
528. Bone, S., *Structural flexibility in hydrated proteins.* J Phys Chem B, 2008. **112**(32): p. 10071-5.
529. Klint, J.K., et al., *Production of Recombinant Disulfide-Rich Venom Peptides for Structural and Functional Analysis via Expression in the Periplasm of E. coli.* PLoS One, 2013. **8**(5): p. e63865.
530. Baneyx, F., *Recombinant protein expression in Escherichia coli.* Current Opinion in Biotechnology, 1999. **10**(5): p. 411-421.
531. Sorensen, H. and K. Mortensen, *Soluble expression of recombinant proteins in the cytoplasm of Escherichia coli.* Microbial Cell Factories, 2005. **4**(1): p. 1.
532. Milescu, M., et al., *Tarantula toxins interact with voltage sensors within lipid membranes.* J Gen Physiol, 2007. **130**(5): p. 497-511.
533. Bhogal, S. and K. Revett. *Animal toxins: what features differentiate pore blockers from gate modifiers?* in *Computational Intelligence Methods and Applications, 2005 ICSC Congress on*. 2005.
534. Kapust, R.B. and D.S. Waugh, *Escherichia coli maltose-binding protein is uncommonly effective at promoting the solubility of polypeptides to which it is fused.* Protein Sci, 1999. **8**(8): p. 1668-74.
535. Raran-Kurussi, S. and D.S. Waugh, *The ability to enhance the solubility of its fusion partners is an intrinsic property of maltose-binding protein but their folding is either spontaneous or chaperone-mediated.* PLoS One, 2012. **7**(11): p. e49589.
536. Hatahet, F., et al., *Disruption of reducing pathways is not essential for efficient disulfide bond formation in the cytoplasm of E. coli.* Microbial Cell Factories, 2010. **9**(1): p. 67.
537. Wülfing, C. and A. Plückthun, *Protein folding in the periplasm of Escherichia coli.* Molecular Microbiology, 1994. **12**(5): p. 685-692.
538. Depuydt, M., et al., *A periplasmic reducing system protects single cysteine residues from oxidation.* Science, 2009. **326**(5956): p. 1109-11.
539. Kapust, R.B., et al., *The P1' specificity of tobacco etch virus protease.* Biochemical and Biophysical Research Communications, 2002. **294**(5): p. 949-955.

540. Zeng, X.-Z., Q.-B. Xiao, and S.-P. Liang, *Purification and characterization of raventoxin-I and raventoxin-III, two neurotoxic peptides from the venom of the spider Macrothele raveni.* Toxicon, 2003. **41**(6): p. 651-656.
541. Schmalhofer, W.A., et al., *ProTx-II, a selective inhibitor of NaV1.7 sodium channels, blocks action potential propagation in nociceptors.* Mol Pharmacol, 2008. **74**(5): p. 1476-84.
542. Smith, J.J., et al., *Molecular interactions of the gating modifier toxin ProTx-II with NaV 1.5: implied existence of a novel toxin binding site coupled to activation.* J Biol Chem, 2007. **282**(17): p. 12687-97.
543. Xiao, Y., et al., *The Tarantula Toxins ProTx-II and Huwentoxin-IV Differentially Interact with Human Nav1.7 Voltage Sensors to Inhibit Channel Activation and Inactivation.* Molecular Pharmacology, 2010. **78**(6): p. 1124-1134.
544. Revell, J.D., et al., *Potency optimization of Huwentoxin-IV on hNav1.7: A neurotoxin TTX-S sodium-channel antagonist from the venom of the Chinese bird-eating spider Selenocosmia huwena.* Peptides, 2013. **44**(0): p. 40-46.
545. Deng, M., et al., *Synthesis and biological characterization of synthetic analogs of Huwentoxin-IV (Mu-theraphotoxin-Hh2a), a neuronal tetrodotoxin-sensitive sodium channel inhibitor.* Toxicon, 2013. **71**(0): p. 57-65.
546. Edgerton, G.B., K.M. Blumenthal, and D.A. Hanck, *Evidence for multiple effects of ProTxII on activation gating in NaV1.5.* Toxicon, 2008. **52**(3): p. 489-500.
547. Revell, J.D., et al., *Potency optimization of Huwentoxin-IV on hNa$_V$1.7: A neurotoxin TTX-S sodium-channel antagonist from the venom of the Chinese bird-eating spider Selenocosmia huwena.* Peptides, 2013. **44C**: p. 40-46.
548. Smith, J.J., et al., *Differential phospholipid binding by site 3 and site 4 toxins. Implications for structural variability between voltage-sensitive sodium channel domains.* J Biol Chem, 2005. **280**(12): p. 11127-33.
549. Phillips, L.R., et al., *Voltage-sensor activation with a tarantula toxin as cargo.* Nature, 2005. **436**(7052): p. 857-60.
550. Redaelli, E., et al., *Target Promiscuity and Heterogeneous Effects of Tarantula Venom Peptides Affecting Na+ and K+ Ion Channels.* Journal of Biological Chemistry, 2010. **285**(6): p. 4130-4142.
551. Beschiaschvili, G. and J. Seelig, *Melittin binding to mixed phosphatidylglycerol/phosphatidylcholine membranes.* Biochemistry, 1990. **29**(1): p. 52-58.
552. Seelig, A., et al., *Phospholipid Binding of Synthetic Talin Peptides Provides Evidence for an Intrinsic Membrane Anchor of Talin.* Journal of Biological Chemistry, 2000. **275**(24): p. 17954-17961.
553. Wang, J., J.R. Schnell, and J.J. Chou, *Amantadine partition and localization in phospholipid membrane: a solution NMR study.* Biochemical and Biophysical Research Communications, 2004. **324**(1): p. 212-217.
554. Consortium, T.U., *Reorganizing the protein space at the Universal Protein Resource (UniProt).* Nucleic Acids Research, 2012. **40**(D1): p. D71-D75.
555. Ruta, V. and R. MacKinnon, *Localization of the voltage-sensor toxin receptor on KvAP.* Biochemistry, 2004. **43**(31): p. 10071-9.
556. Takahashi, H., et al., *Solution structure of hanatoxin1, a gating modifier of voltage-dependent K(+) channels: common surface features of gating modifier toxins.* Journal of Molecular Biology, 2000. **297**(3): p. 771-80.
557. Lee, S.Y. and R. MacKinnon, *A membrane-access mechanism of ion channel inhibition by voltage sensor toxins from spider venom.* Nature, 2004. **430**(6996): p. 232-5.

558. Pellecchia, M., D.S. Sem, and K. Wüthrich, *NMR in drug discovery.* Nature Reviews Drug Discovery, 2002. **1**(3): p. 211-219.
559. Hunter, C.A., et al., *Aromatic interactions.* Journal of the Chemical Society, Perkin Transactions 2, 2001. **0**(5): p. 651-669.
560. Waters, M.L., *Aromatic interactions in model systems.* Current Opinion in Chemical Biology, 2002. **6**(6): p. 736-741.
561. Thomas, A., et al., *Aromatic side-chain interactions in proteins. I. Main structural features.* Proteins: Structure, Function, and Bioinformatics, 2002. **48**(4): p. 628-634.
562. Morrison, K.L. and G.A. Weiss, *Combinatorial alanine-scanning.* Current Opinion in Chemical Biology, 2001. **5**(3): p. 302-307.
563. Weiss, G.A., et al., *Rapid mapping of protein functional epitopes by combinatorial alanine scanning.* Proceedings of the National Academy of Sciences, 2000. **97**(16): p. 8950-8954.
564. Yan, B.X. and Y.Q. Sun, *Glycine Residues Provide Flexibility for Enzyme Active Sites.* Journal of Biological Chemistry, 1997. **272**(6): p. 3190-3194.
565. Gunning, S.J., et al., *Isolation of delta-missulenatoxin-Mb1a, the major vertebrate-active spider delta-toxin from the venom of Missulena bradleyi (Actinopodidae).* FEBS Lett, 2003. **554**(1-2): p. 211-8.
566. Priest, B.T., et al., *ProTx-I and ProTx-II: gating modifiers of voltage-gated sodium channels.* Toxicon, 2007. **49**(2): p. 194-201.
567. Bogan, A.A. and K.S. Thorn, *Anatomy of hot spots in protein interfaces.* Journal of Molecular Biology, 1998. **280**(1): p. 1-9.
568. Steer, D.L., et al., *Comparison of the binding of alpha-helical and beta-sheet peptides to a hydrophobic surface.* J Pept Res, 1998. **51**(6): p. 401-12.
569. Tran, J.V., et al., *Temperature effects on retention in reversed phase liquid chromatography.* Journal of Separation Science, 2001. **24**(12): p. 930-940.
570. Mobli, M., et al., *A non-uniformly sampled 4D HCC(CO)NH-TOCSY experiment processed using maximum entropy for rapid protein sidechain assignment.* Journal of Magnetic Resonance, 2010. **204**(1): p. 160-164.
571. Davis, I.W., et al., *MolProbity: all-atom contacts and structure validation for proteins and nucleic acids.* Nucleic Acids Res, 2007. **35**(Web Server issue): p. W375-83.
572. Mulder, F.A., et al., *Altered flexibility in the substrate-binding site of related native and engineered high-alkaline Bacillus subtilisins.* J Mol Biol, 1999. **292**(1): p. 111-23.
573. Shi, X., et al., *Clinical spectrum of SCN2A mutations.* Brain and Development, 2012. **34**(7): p. 541-545.
574. Sanders, S.J., et al., *De novo mutations revealed by whole-exome sequencing are strongly associated with autism.* Nature, 2012. **485**(7397): p. 237-241.
575. Li, D., et al., *Structure-Activity Relationships of Hainantoxin-IV and Structure Determination of Active and Inactive Sodium Channel Blockers.* Journal of Biological Chemistry, 2004. **279**(36): p. 37734-37740.
576. Ofran, Y. and B. Rost, *Protein–Protein Interaction Hotspots Carved into Sequences.* PLoS Comput Biol, 2007. **3**(7): p. e119.
577. London, N., D. Movshovitz-Attias, and O. Schueler-Furman, *The structural basis of peptide-protein binding strategies.* Structure, 2010. **18**(2): p. 188-199.
578. Swartz, K.J. and R. MacKinnon, *Hanatoxin Modifies the Gating of a Voltage-Dependent K+ Channel through Multiple Binding Sites.* Neuron, 1997. **18**(4): p. 665-673.
579. Burley, S. and G. Petsko, *Aromatic-aromatic interaction: a mechanism of protein structure stabilization.* Science, 1985. **229**(4708): p. 23-28.

580. Graf, A., et al., *Yeast systems biotechnology for the production of heterologous proteins.* FEMS Yeast Research, 2009. **9**(3): p. 335-348.
581. Esposito, D. and D.K. Chatterjee, *Enhancement of soluble protein expression through the use of fusion tags.* Current Opinion in Biotechnology, 2006. **17**(4): p. 353-358.
582. Ohana, R.F., et al., *HaloTag7: A genetically engineered tag that enhances bacterial expression of soluble proteins and improves protein purification.* Protein Expression and Purification, 2009. **68**(1): p. 110-120.
583. Rogov, V.V., et al., *A Universal Expression Tag for Structural and Functional Studies of Proteins.* Chembiochem, 2012. **13**(7): p. 959-963.
584. Jackson, M.B., *Whole-Cell Voltage Clamp Recording*, in *Current protocols in neuroscience*. 2001, John Wiley & Sons, Inc.
585. Donahue, J.P., et al., *Three-dimensional structure of the platelet integrin recognition segment of the fibrinogen gamma chain obtained by carrier protein-driven crystallization.* Proc Natl Acad Sci U S A, 1994. **91**(25): p. 12178-82.
586. Forsythe, E.L., E.H. Snell, and M.L. Pusey, *Crystallization of chicken egg-white lysozyme from ammonium sulfate.* Acta Crystallogr D Biol Crystallogr, 1997. **53**(Pt 6): p. 795-7.
587. Ashok, Y., R.T. Nanekar, and V.P. Jaakola, *Crystallogenesis of adenosine A(2A) receptor-T4 lysozyme fusion protein: a practical route for the structure.* Methods Enzymol, 2013. **520**: p. 175-98.
588. Zou, Y., W.I. Weis, and B.K. Kobilka, *N-terminal T4 lysozyme fusion facilitates crystallization of a G protein coupled receptor.* PLoS One, 2012. **7**(10): p. e46039.